Mechanisms by which PE21, an extract from the white willow *Salix alba*, delays chronological aging in budding yeast

Younes Medkour

A Thesis
In the Department
of
Biology

Presented in Partial Fulfillment of the Requirements
For the Degree of
Doctor of Philosophy (Biology) at
Concordia University
Montreal, Quebec, Canada

July 2019

CONCORDIA UNIVERSITY

SCHOOL OF GRADUATE STUDIES

This is to certify that the thesis prepared

By: Younes Medkour

Entitled: Mechanisms by which PE21, an extract from the white willow Salix alba, delays chronological aging in budding yeast

and submitted in partial fulfillment of the requirements for the degree of

Doctor Of Philosophy (Biology)

complies with the regulations of the University and meets the accepted standards with respect to originality and quality.

Signed by the final examining committee:

_____ Chair
Dr. Roisin O'Connor

_____ External Examiner
Dr. Dusica Maysinger

_____ External to Program
Dr. Paul Joyce

_____ Examiner
Dr. Patrick Gulick

_____ Examiner
Dr. Madoka Gray-Mitsumune

_____ Thesis Supervisor
Dr. Vladimir Titorenko

Approved by _____
Dr. Robert Weladji, Graduate Program Director

September 16, 2019

_____
Dr. Andre Roy, Dean
Faculty of Arts and Science

ABSTRACT

Mechanisms by which PE21, an extract from the white willow *Salix alba*, delays chronological aging in budding yeast

Younes Medkour, Ph.D.
Concordia University, 2019

To discover novel aging-delaying and longevity-extending chemical compounds of plant origin, we conducted a screen for plant extracts that can prolong yeast chronological lifespan. Our screen revealed six plant extracts that increase yeast chronological lifespan. One of these six plant extracts is PE21, an extract from the white willow *Salix alba*. We found that PE21 extends the longevity of chronologically aging yeast to a significantly greater extent than any of the presently known longevity-extending chemical compounds. We demonstrated that PE21 is a geroprotector which delays the onset and slows the progression of yeast chronological aging by eliciting a hormetic stress response. We showed that PE21 has the following effects on cellular processes known to define longevity in organisms across phyla: 1) PE21 amplifies mitochondrial respiration and membrane potential; 2) PE21 alters the pattern of age-related changes in the intracellular concentration of reactive oxygen species; 3) PE21 reduces oxidative damage to cellular proteins, membrane lipids, and mitochondrial and nuclear genomes; 4) PE21 enhances cell resistance to oxidative and thermal stresses; and 5) PE21 accelerates degradation of neutral lipids deposited in lipid droplets. We found that PE21 causes a remodeling of lipid metabolism in chronologically aging yeast, thereby instigating changes in the concentrations of several lipid classes. We demonstrated that such changes in the cellular lipidome initiate three mechanisms of aging delay and longevity extension. The first mechanism through which PE21 slows aging and prolongs longevity consists in its ability to decrease

the intracellular concentration of free fatty acids. This postpones an age-related onset of liponecrotic cell death promoted by excessive concentrations of free fatty acids. The second mechanism of aging delay and longevity extension by PE21 consists in its ability to decrease the concentrations of triacylglycerols and to increase the concentrations of glycerophospholipids within the endoplasmic reticulum membrane. This activates the unfolded protein response system in the endoplasmic reticulum, which then decelerates an age-related decline in protein and lipid homeostasis and slows down an aging-associated deterioration of cell resistance to stress. The third mechanism underlying aging delay and longevity extension by PE21 consists in its ability to change concentrations of some lipids in the mitochondrial membranes. This alters certain catabolic and anabolic processes in mitochondria, thus amending the pattern of aging-associated changes in several key aspects of mitochondrial functionality.

ACKNOWLEDGMENTS

I am grateful to my supervisor, Dr. Vladimir Titorenko, for providing me with the opportunity to work with him and for his guidance during the years I have spent in his laboratory. I have come so far only because of his generous and continuous support. I thank the members of my committee, Dr. Madoka Gray-Mitsumune, and Dr. Patrick Gulick, for their invaluable suggestions during my graduate research and studies. I would also like to thank the Center for Biological Applications of Mass Spectrometry (CBAMS). I thank especially Dr. Heng Jiang for his invaluable assistance and expertise with training and help in method development and instrumentation for my various uses of mass spectrometry. I would also like to thank all my lab colleagues for their cooperation and support. Finally, I would like to acknowledge the numerous undergraduate students, volunteers, summer research students, and international exchange students who made the laboratory a vibrant work environment.

DEDICATIONS

I dedicate this thesis to my father, Djamel, a retired Doctor in Energy Physics and Professor, who taught at several universities back in my home country: Algeria. My father was my first teacher, and to this day, he remains my greatest inspiration. His love for teaching is contagious, and it is because of him that I have decided to pursue the path of academia. I also dedicate this thesis to my mother, Djemaa Rahmouni, for her unconditional love and support. Throughout my graduate studies, I have faced numerous hardships in my personal life, and it is only because of her that I have made it through. Let's not forget to mention my amazing younger sisters Nadia, Kahina, and Silya. They have been proud and supportive throughout my graduate studies and more. The last person I dedicate this thesis to is my "other half" and good friend Dilan Jaunky. We have been following each other from one degree to another and competing since high school. Here, we are finishing our doctoral degrees in the same field at the same University. What's next, Dilan?

TABLE OF CONTENTS

LIST OF FIGURES

LIST OF TABLES

LIST OF ABBREVIATIONS

ACN, acetonitrile

CDP-DAG, cytidine diphosphate-diacylglycerol

CDK, cyclin-dependent kinase

CFU, colony forming units

CLS, chronological lifespan

CL, cardiolipin

CR, caloric restriction

CW, Calcofluor White M2R

DAG, diacylglycerol

DHR, Dihydrorhodamine 123

DIC, differential interference contrast

DTT, dithiothreitol

ER, the endoplasmic reticulum

ETC, electron transport chain

IAA, iodoacetamide

IMM, inner mitochondrial membrane

IMS, the intermembrane space

LCA, lithocholic bile acid

LD, lipid droplet

MAM, the mitochondria-associated membrane domain of the endoplasmic reticulum

MFQL, Molecular Fragmentation Query Language

MICOS, the mitochondrial contact site protein complex

MS, mass spectrometry

mtDNA, mitochondrial DNA

nDNA, nuclear DNA

OMM, outer mitochondrial membrane

PA, phosphatidic acid

PC, phosphatidylcholine

PG, phosphatidylglycerol

PGP, phosphatidylglycerol-phosphate

Pho85, phosphate metabolism, protein 85

PI, phosphatidylinositol

PKA, protein kinase A

POA, palmitoleic acid

PS, phosphatidylserine

PP2ACdc55, the Cdc55 protein phosphatase 2A

RCD, regulated cell death

RLS, replicative lifespan

ROS, reactive oxygen species

R123, Rhodamine 123

Snf1, sucrose non-fermenting, protein 1

TCA, tricarboxylic acid

TORC1, target of rapamycin complex 1

1 Introduction

The budding yeast *Saccharomyces cerevisiae* is amenable to thorough molecular analyses and has relatively short and easily measurable chronological and replicative lifespans [1–15]. The use of this unicellular eukaryote with a sequenced genome as a model organism in aging research has provided fundamental insights on mechanisms of cellular aging [1, 2, 5–8, 10, 12, 13, 15]. Studies in *S. cerevisiae* uncovered genes, signaling pathways and chemical compounds that postpone cellular aging in not only unicellular eukaryotes but also in evolutionarily diverse metazoans [1, 2, 5–8, 10, 12, 13, 15, 16–34]. After being discovered in yeast, these genes, signaling pathways, and chemical compounds appeared to extend healthy lifespan also in multicellular eukaryotes across phyla. It is believed therefore that the key aspects of the aging process and the mechanisms of its delay by certain genetic, dietary and pharmacological interventions have been conserved during evolution [1, 7, 8, 12, 15, 18, 20, 24, 33, 34].

There are two different ways of studying aging in *S. cerevisiae*; each of these ways investigates a different mode of yeast aging.

A so-called replicative mode of yeast aging is monitored by counting the total number of asymmetric mitotic divisions - each producing a small daughter cell - that a mother cell could undergo on the surface of a solid nutrient-rich medium before it becomes senescent [5, 35, 36]. Yeast replicative aging has long been considered to resemble aging of those cells in humans and other mammals that are able to divide mitotically; among these mitotically active cells are lymphocytes, monocytes, granulocytes, fibroblasts and some stem cell types [2, 5, 8, 35, 36]. Recent studies have revealed that many genes that modulate aging of post-mitotic cells in adults of the nematode *Caenorhabditis elegans* also influence yeast replicative aging [37–39]. Moreover, it appears that many hallmarks of aging characteristic of post-mitotic cells in humans and other mammals are also cellular hallmarks of yeast replicative aging [40]. Hence, it is conceivable that the replicative mode of yeast aging may also mirror aging of post-mitotic cells and even aging of the entire organism in nematodes, humans, and other mammals [37–40].

A so-called chronological mode of yeast aging is monitored by determining how long a yeast cell cultured in a liquid medium can retain viability after it undergoes cell cycle arrest and enters a state of quiescence [5, 41, 42]. Yeast chronological aging is believed to model aging of human and mammalian cells that lose the ability to divide mitotically; these post-mitotic cells include adipocytes, mature muscle cells and mature neurons [5, 42, 43]. The chronological mode

of yeast aging is also considered to be a simple model of organismal aging in multicellular eukaryotes [42, 44].

Although the replicative and chronological modes of aging in yeast are usually examined separately from each other, recent evidence indicates that these two modes of yeast aging most likely converge into a single aging process [45–47].

1.1 Major aspects of the aging process and mechanisms of its deceleration by pharmacological interventions are evolutionarily conserved

Aging of unicellular eukaryotes and metazoans is an intricate biological phenomenon of an age-related functional deterioration [48–51]. Such aging-associated functional decline impairs the regulation of a distinct set of cellular processes, thus making an organism more susceptible to disease and death [48–51]. Cellular processes whose progressive dysregulation has been implicated in cellular and organismal aging of eukaryotes across phyla include cell cycle regulation, quiescent state maintenance by adult stem cells, cell growth, stress response, cellular signaling, apoptosis and other modes of regulated cell death (RCD), autophagy (including mitophagy), actin organization, nuclear DNA replication, chromatin assembly and maintenance, ribosome biogenesis and protein synthesis in the cytosol and mitochondria, protein folding, proteasomal degradation of misfolded proteins, oxidative and biosynthetic metabolic pathways in mitochondria, lipid and carbohydrate metabolism, NAD^+ homeostasis, amino acid biosynthesis and degradation, and ammonium and amino acid uptake [48–74]. All these processes are controlled by a nutrient-sensing signaling network of longevity regulation that in evolutionarily distant metazoans integrates the insulin/insulin-like growth factor 1 (IGF-1) pathway, the AMP-dependent protein kinase (AMPK) pathway, the mammalian target of rapamycin complex 1 (mTORC1) pathway and the sirtuin-governed protein deacetylation module; in some organisms, this nutrient-sensing signaling network also assimilates the cAMP/protein kinase A (cAMP/PKA) pathway [1, 50, 53, 54, 75–79].

In chronologically aging *S. cerevisiae*, the nutrient-sensing signaling network of longevity regulation incorporates the TORC1, cAMP/PKA, Pkb-activating kinase homolog (PKH1/2), sucrose non-fermenting (SNF1) and autophagy (ATG) pathways [1, 5, 25, 68, 80–97]. The network also integrates the serine/threonine-specific protein kinases Sch9 (which is stimulated by the TORC1 and PKH1/2 pathways) and Rim15 (which is inhibited by the TORC1, PKA, and

PKH1/2 pathways) [1, 5, 25, 68, 80–97]. Certain chemical compounds of bacterial, fungal, plant or mammalian origin can delay chronological aging and extend the longevity of *S. cerevisiae* because they regulate the flow of information through these convergent, divergent and multiply branched signaling pathways and protein kinases. Such aging-delaying chemicals include resveratrol, rapamycin, caffeine, spermidine, myriocin, methionine sulfoxide, lithocholic acid and cryptotanshinone [1, 2, 24–26, 29, 87, 93, 98–100].

1.2 Lipids are essential contributors to replicative and chronological aging of budding yeast

Lipids are water-insoluble amphiphilic biomolecules; they are structurally diverse and generated by an intricate network of integrated metabolic pathways [101–106]. Lipids are known to play key roles in the organization and function of biological membranes, energy homeostasis, signal transduction, vesicular trafficking, organelle biogenesis, and regulated cell death [105–114]. The initial indications that lipids may also modulate the rate of cellular and organismal aging came from observations that longevity-extending mutations in the IGF-1 (insulin/insulin-like growth factor 1) and TORC1 (target of rapamycin complex 1) signaling pathways elicit an increase in the concentration of storage lipids in the nematode *Caenorhabditis elegans*, the fruit fly *Drosophila melanogaster* and the laboratory mice [115]. As outlined below, a body of evidence indicates that lipid metabolism and transport control the pace of cellular aging in the yeast *S. cerevisiae*. Several mechanisms underlying the essential roles of lipids in defining yeast longevity have emerged and are discussed in this section of the thesis.

1.2.1 Sphingolipids contributes to longevity regulation of replicatively and chronologically aging yeast

In *S. cerevisiae*, the *de novo* synthesis of sphingolipids begins in the endoplasmic reticulum (ER) where the serine palmitoyltransferase (SPT) protein complex catalyzes the condensation of a serine with palmitoyl-CoA to form 3-ketodihydrosphingosine (Figure 1.1) [116–118]. The activity of SPT in the ER can be inhibited by the amino acid antibiotic myriocin derived from certain thermophilic fungi [119, 120]. 3-ketodihydrosphingosine is transformed into dihydrosphingosine (DHS), which then undergoes conversion to phytosphingosine (PHS) in the ER; DHS and PHS are sphingoid backbone bases of all sphingolipids (Figure 1.1) [117, 121, 122].

An acyl-CoA ester of hexacosanoic fatty acid having 26 carbon atoms is then used as a fatty acid donor for the synthesis of dihydroceramide (dhCer) or phytoceramide (phytoCer) from DHS or PHS (respectively) in a reaction that is catalyzed by ceramide synthase (CerS) and confined to the ER (Figure 1.1) [122–127]. The activity of the CerS protein complex in the ER can be inhibited by mycotoxins fumonisin B1 and australifungin [128, 129]. dhCer or phytoCer are transported from the ER to the Golgi apparatus by the coat protein complex II vesicle-mediated flow as well as by the Nvj2-facilitated transfer via the ER-Golgi membrane contact sites (Figure 1.1) [130–132]. In the Golgi apparatus, a stepwise attachment of different polar groups converts dhCer and phytoCer into such complex sphingolipids as inositol-phosphorylceramide (IPC), mannosyl-inositol-phosphorylceramide (MIPC) and mannosyl-di-inositol-phosphorylceramide (M(IP)2C) (Figure 1.1) [133, 134]. The Aur1/Kei1-dependent synthesis of IPC in the Golgi apparatus can be inhibited by aureobasidin A, an antifungal cyclic peptide antibiotic [133, 135, 136]. A vesicular flow delivers these complex sphingolipids from the Golgi apparatus to the plasma membrane (PM) (Figure 1.1) [96, 101]. After being synthesized in the Golgi apparatus, these complex sphingolipids can also be used to replenish the cellular pool of ceramides. Such replenishment occurs in mitochondria and is catalyzed by Isc1, an inositol phosphosphingolipid phospholipase C which is translocated from the ER to mitochondria during the post-diauxic growth phase (Figure 1.1) [137–139]. Following DHS and PHS synthesis in the ER, these sphingoid backbone bases of sphingolipids can be used not only for ceramide synthesis in the ER but also for phosphorylation in the cytosol (Figure 1.1) [96, 140]. The products of such phosphorylation, DHS-1-phosphate, and PHS-1-phosphate (respectively), can be then converted into such non-sphingolipid molecules as ethanolamine-phosphate and aliphatic aldehydes having sixteen carbon atoms [141].

Growing evidence supports the notion that certain molecular species of long-chain sphingoid bases of sphingolipids, ceramides and/or more complex sphingolipids (which are formed from ceramides through the covalent attachment of certain polar head groups) may play essential roles in defining the rates of replicative or chronological aging in the yeast *S. cerevisiae*. Specifically, it has been demonstrated that some genetic or pharmacological interventions altering the concentrations of certain sphingolipid classes extend yeast replicative or chronological lifespan (RLS or CLS, respectively).

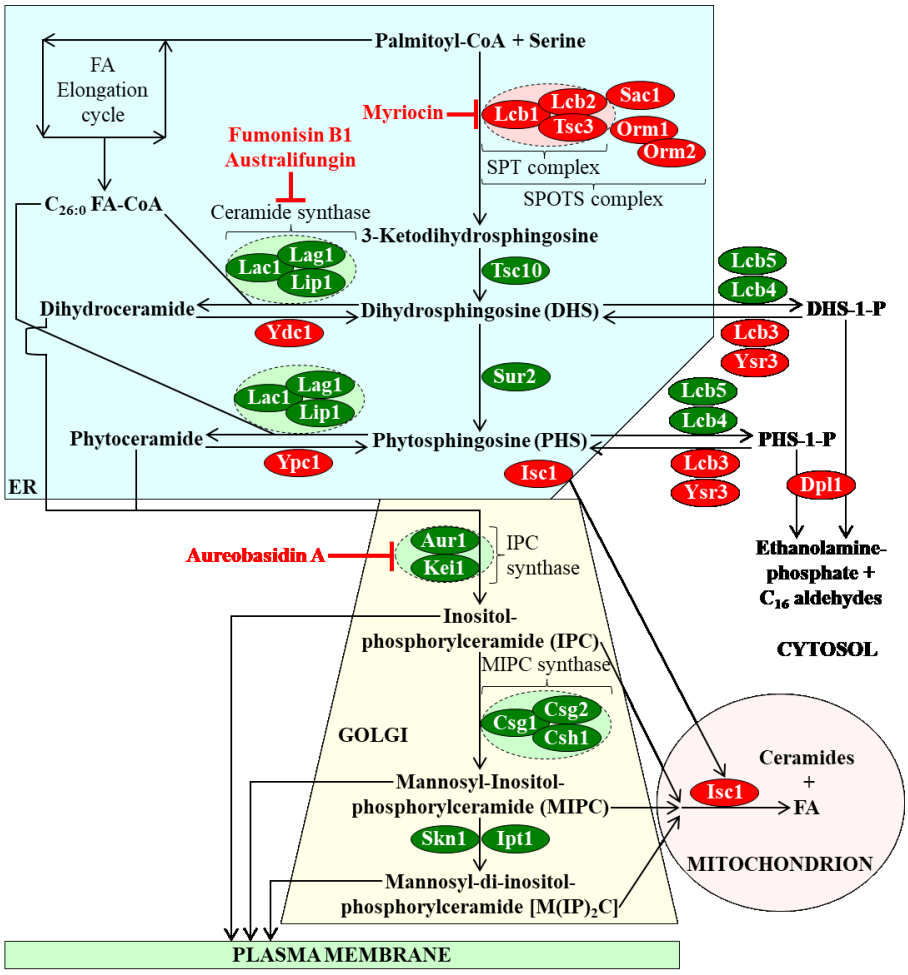

Figure 1.1. Sphingolipid metabolism in the yeast *Saccharomyces cerevisiae*. 3-ketodihydrosphingosine, dihydrosphingosine, and phytosphingosine (DHS and PHS, respectively; two sphingoid backbone bases of all sphingolipids), acyl-CoA esters of very-long-chain fatty acids (including the acyl-CoA ester of hexacosanoic fatty acid (C26:0 FA-CoA)), as well as dihydroceramide and phytoceramide are all generated in the endoplasmic reticulum (ER). After being transported from the ER to the Golgi apparatus, phytoceramide undergoes conversion into complex sphingolipids, including inositol-phosphorylceramide (IPC), mannosyl-inositol-phosphorylceramide (MIPC) and mannosyl-di-inositol-phosphorylceramide (M(IP)2C). Following IPC, MIPC and M(IP)2C synthesis in the Golgi, these complex sphingolipids can be either sorted to the plasma membrane or used to regenerate ceramides in a reaction catalyzed by Isc1 in mitochondria. After DHS and PHS are synthesized in the ER, they can undergo phosphorylation in the cytosol. Such phosphorylation yields DHS-1-phosphate and PHS-1-phosphate (respectively), which can be further catabolized into ethanolamine-phosphate and aliphatic aldehydes having sixteen carbon atoms (C16 aldehydes). Enzymes that catalyze anabolic or catabolic reactions of sphingolipid metabolism are displayed in green or red color, respectively. See text for more details. Abbreviations: Aur1, aureobasidin A resistance 1; Csg1 and Csg2, calcium-sensitive growth 1 and 2 (respectively); Csh1, CSG1/SUR1 homolog1; Dpl1, dihydrosphingosine phosphate lyase 1; ER, endoplasmic reticulum; FA, fatty acid; Ipt1, inositolphosphotransferase 1; IPC, inositol-phosphorylceramide; Isc1, inositol phosphosphingolipid phospholipase C 1; 3-KDHS, 3-ketodihydrosphingosine; Kei1, Kex2-cleavable protein essential for inositol-phosphorylceramide synthesis 1; Lac1, longevity-assurance gene cognate 1; Lag1, longevity assurance gene 1; Lip1, Lag1/Lac1 interacting protein 1; Lcb1, Lcb2, Lcb3, Lcb 4 and Lcb5, long-chain base proteins 1, 2, 3, 4 and 5 (respectively); MIPC, mannosyl-inositol-phosphorylceramide; M(IP)2C, mannosyl-di-inositol-phosphorylceramide; Npr1, nitrogen permease reactivator 1; Orm1 and Orm2, orosomucoid 1 and 2 (respectively); PM, plasma membrane; Sac1, suppressor of actin 1; SPOTS, serine palmitoyltransferase, Orm1/2 and Sac1; Sit4, suppressor of initiation of transcription 4; Slm1/2, synthetic lethal with Mss4 protein 1 or 2; SPT, serine palmitoyltransferase; Sur2, suppressor 2 of Rvs161 and rvs167 mutations; Tsc3 and Tsc10, temperature-sensitive suppressors of Csg2 mutants 3 and 10; Ydc1, yeast dihydroceramidase 1; Ypc1, yeast phytoceramidase 1; Ysr3, yeast sphingolipid resistance 3.

For example, a single-gene-deletion mutation eliminating the Lag1 subunit of CerS (Figure 1.1) extends yeast RLS [123] but not CLS [82]. Of note, a single-gene-deletion mutation

eliminating a different subunit of CerS, Lac1 (Figure 1.1), does not alter yeast RLS or CLS [142]. Two alternative explanations for the essential mechanistic role of Lag1 in yeast RLS have been proposed, namely that 1) lack of Lag1 (but not lack of Lac1) elicits a change in the concentrations of sphingosine and/or ceramide species that are critical for longevity of replicatively aging yeast; or 2) Lag1 determines yeast RLS not because of its distinct effects on sphingosine and/or ceramide concentrations but because of its known physical and functional interactions with many proteins that do not interact with Lac1 and are not related to sphingolipid metabolism [93]. The unique role of Lag1 in regulating longevity of replicatively aging yeast is underscored by the observations that both the lack of this subunit of CerS [123] and its moderate overexpression prolong yeast RLS [142], whereas its massive overexpression has an opposite effect on the RLS of *S. cerevisiae* [142]. Thus, it is conceivable that the relative level of the Lag1 subunit of CerS exhibits a non-linear dose-response effect on the concentrations of some distinct sphingosine and/or ceramide species with essential roles in yeast RLS but not in CLS. The identities of such critical species of sphingosine (DHS and/or PHS) and/or ceramide (dhCer and/or phytoCer) remain to be established, perhaps by measuring the concentrations of different sphingolipid metabolism intermediates in yeast mutant strains that exhibit the wide-range expression levels of Lag1 and have quite different RLS.

Single-gene-deletion mutations eliminating Ipt1 and/or Skn1, two inositolphosphotransferases involved in the synthesis of M(IP)2C from MIPC (Figure 1.1) [63, 64], have been shown to extend yeast CLS [82, 143]. Each of these mutations causes an accumulation of excessive amounts of MIPC and impairs the synthesis of M(IP)2C, the most abundant and complex sphingolipid in *S. cerevisiae* [144, 145]. These findings suggest that M(IP)2C may be an essential negative regulator of yeast CLS and/or MIPC may play an essential stimulatory role in regulating yeast CLS.

A single-gene-deletion mutation eliminating Isc1, an inositol phosphosphingolipid phospholipase C which hydrolyzes complex sphingolipids to produce ceramides (Figure 1.1) [137–139], has been shown to shorten yeast CLS [146]. The most prominent effects of the *isc1Δ* mutation on cellular sphingolipids include a decline in the concentrations of different molecular species of DHS and a rise in the concentrations of dhCer and phytoCer having 26 carbon atoms [147]. The CLS-shortening effect of the *isc1Δ* mutation is likely due to its demonstrated abilities to lower mitochondrial respiration, diminish catalase A activity, stimulate cellular iron

accumulation, intensify oxidative damage to cellular macromolecules, decrease cell resistance to oxidative stress, enhance programmed apoptotic cell death, and/or activate Hog1 (a mitogen-activated protein kinase (MAPK) of the high osmotic glycerol (HOG) pathway) [146–148]. Importantly, the abilities of the *isc1Δ* mutation to shorten yeast CLS, lessen mitochondrial respiration, weaken catalase A activity and decline cell resistance to oxidative stress can be partially suppressed by a single-gene-deletion mutation that eliminates any of the following four proteins: 1) Sit4, a catalytic subunit of type 2A ceramide-activated protein phosphatase and a downstream effector in the TORC1-Sit4 branch of the nutrient and stress signaling TORC1 pathway [147]; 2) Hog1 [148]; 3) Tor1, a nutrient-sensing protein kinase component of TORC1, which regulates cell growth, metabolism, stress response and longevity in response to nutrient availability and cellular stresses [149]; or 4) Sch9, a nutrient-sensing protein kinase and a downstream effector in the TORC1-Sch9 branch of the TORC1 pathway [149]. It needs to be emphasized that both the TORC1-Sit4 and TORC1-Sch9 branches are modulated not only in response to nutrient availability but also in response to concentrations of certain sphingolipid species; some of these sphingolipid species are synthesized *de novo* while others are produced by the Isc1-driven hydrolysis of complex sphingolipids [93, 96, 117, 118, 150–153]. Furthermore, the TORC1-Sit4 branch regulates some reactions of the *de novo* sphingosine and ceramide biosynthesis [154], whereas the TORC1-Sch9 branch controls the production of sphingosines, ceramides, and complex sphingolipids both biosynthetically and hydrolytically [155]. Moreover, the Sch9 protein component of the TORC1-Sch9 branch is required for the translocation of Isc1 from the ER to mitochondria during the post-diauxic growth phase [156]. These findings support the notion that the TORC1-Sit4 and TORC1-Sch9 branches, as well as Hog1 and Isc1, are linked nodes of a signaling network that integrates nutrient and sphingolipid signaling to regulate longevity of chronologically aging yeast [93, 96, 149–154, 156]. A more detailed description of this signaling network is provided below in this section and schematically depicted in Figure 1.2.

The identities of molecular species of mitochondrial membrane sphingolipids that may modulate information flow through the TORC1-Sit4/TORC1-Sch9/Hog1/Isc1 signaling nodes remain to be established. These sphingolipid species may include DHS and PHS, two sphingoid backbone bases of sphingolipids whose concentrations in yeast are gradually increased with chronological age [157]. Such age-related rise of DHS and PHS in mitochondrial membranes of chronologically aging yeast may shorten CLS by slowing mitochondrial fusion, eliciting

mitochondrial fragmentation, lowering mitochondrial respiration and electrochemical membrane potential, compromising ATP synthesis in mitochondria, and lessening the number of mitochondrial DNA copies [157].

Another convincing evidence for the essential roles of sphingolipids in yeast chronological aging has been provided by the demonstration that yeast CLS can be extended by pharmacological and genetic interventions that weaken (but do not completely stop) metabolite flow through the pathway of *de novo* sphingolipid synthesis. Such weakening of metabolite flow through sphingolipid synthesis pathway was achieved via a partial inhibition of the initial, SPT-driven step of the pathway using 1) relatively low concentrations of myriocin, an inhibitor of SPT enzymatic activity (Figure 1.1) [158]; or 2) the tetracycline-repressible promoter cassette to lower transcription of genes encoding the Lcb1 or Lcb2 subunits of the SPT protein complex (Figure 1.1) [158]. By eliciting a partial inhibition of SPT, both these CLS-extending interventions have been shown to decrease the concentrations of DHS, PHS, DHS-1-phosphate, PHS-1-phosphate, and IPC (Figure 1.1) [158]. Such decline in the abundance of sphingosine species and/or IPC is likely to be responsible for the observed abilities of both these interventions to lower protein kinase activities of Pkh1 (Pkb-activating kinase homolog protein 1) and Pkh2, two sphingolipid-activated protein kinases that phosphorylate a specific residue in the activation loop of the nutrient-sensing protein kinase Sch9 [158]. Pkh1 and Pkh2 are likely stimulated by PHS [159]. Although the Pkh1/2-Sch9 branch of a network that integrates nutrient and sphingolipid signaling is the primary target of both these interventions, myriocin treatment also elicits the following pro-longevity changes in other pathways possibly integrated into this network: 1) it weakens the pro-aging PKA (protein kinase A) pathway; 2) it attenuates the pro-aging TORC1 pathway; 3) it activates the anti-aging Snf1 (sucrose non-fermenting) pathway; and 4) it stimulates the anti-aging ATG (autophagy) pathway [90]. These effects of myriocin treatment on different nodes and hubs comprising the nutrient and sphingolipid signaling network are believed to be responsible for the global changes in the transcription of numerous nuclear genes seen in myriocin-treated yeast [90]. It is presently unclear which of the above effects of myriocin treatment on signaling and transcription are due to the decline in the abundance of sphingosine species and IPC that occurs in yeast exposed to myriocin [93]. Some of these effects could be due to the abilities of certain sphingolipid species to act in minor quantities as signaling molecules that bind to specific protein components integrated into the nutrient and sphingolipid signaling network, whereas others could be caused by the

abilities of bulk quantities of sphingolipids to influence general physical properties of cellular membranes and/or create functionally distinct membrane domains [93].

In sum, emergent evidence indicates that the metabolic pathway for the biosynthetic and hydrolytic production of sphingosines, ceramides, and complex sphingolipids is integrated into an intricate network with certain nutrient- and sphingolipid-sensing signaling pathways. This network defines yeast CLS and is schematically depicted in Figure 1.2. The nutrient and sphingolipid signaling network includes three hubs, each representing a chemical reaction (or several chemical reactions) in the sphingolipid metabolism pathway which is linked to several nodes or branches of nutrient- and sphingolipid-sensing signaling pathways.

At the SPT hub of this network, the SPT protein complex catalyzing the initial reaction of sphingolipid metabolism is inhibited by non-phosphorylated forms of the Orm1 and Orm2 proteins (Figure 1.2A) [96, 153, 160–164]. This Orm1/2-dependent inhibition of SPT can be relieved via phosphorylation of Orm1 and Orm2 by the protein kinase Npr1 of the TORC1-Sit4-Npr1 branch of the nutrient-sensing TORC1 signaling pathway; the catalytic subunit of type 2A protein phosphatase Sit4, another component of this branch, can be inhibited by TORC1 and activated by phytoCer (Figure 1.2A) [96, 148, 153, 163, 164]. Orm1 and Orm2 can also be phosphorylated (and SPT inhibition can be relieved) via partially overlapping TORC2-Ypk1/2 and Pkh1/2-Ypk1/2 signaling branches; a common component of these branches, the protein kinase Ypk1/2, phosphorylates Orm1 and Orm2 at sites that differ from sites phosphorylated by the protein kinase Npr1 of the TORC1-Sit4-Npr1 branch (Figure 1.2A) [96, 153, 162–164]. Both the TORC2-Ypk1/2 and Pkh1/2-Ypk1/2 branches are modulated by sphingolipids. The TORC2-Ypk/2 branch of the TORC2 signaling pathway is activated if a decline in the abundance of complex sphingolipids increases tension of the plasma membrane (PM); this allows the phosphatidylinositol-4,5-bisphosphate binding proteins Slm1 and Slm2 to move from the MCC (membrane compartment containing Can1)/eisosome domain of the PM to the MCT (membrane compartment containing TORC2) area of the PM, where they activate Ypk1/2 phosphorylation by the PM-associated TORC2 complex (Figure 1.2A) [96, 153, 155, 162, 165]. The Pkh1/2-Ypk1/2 branch is activated by PHS, a sphingoid base of sphingolipids which stimulates both protein components of this signaling branch (Figure 1.2A) [96, 159]. The TORC1-Sit4-Npr1-, TORC2-Ypk1/2-, and Pkh1/2-Ypk1/2-dependent phosphorylations of Orm1 and Orm2 can be offset (and SPT inhibition can be restored) by the complex between Cdc55 and Pph21/Pph22, the regulatory and catalytic subunits

(respectively) of yeast protein phosphatase 2A (PP2A) (Figure 1.2A) [96, 153, 166]. Altogether, these findings indicate that the SPT hub of the nutrient and sphingolipid signaling network is modulated by three feedback loops. One of these feedback loops acts in a negative manner (i.e. SPT is indirectly inhibited by complex sphingolipids), whereas two others are positive feedback loops (i.e. SPT is indirectly activated by PHS and phytoCer) (Figure 1.2A). It is conceivable that these three feedback loops orchestrate a delicate tuning of SPT activity in response to the availability of nutrients and the extent of cellular stress (which is exhibited in part as changes in sphingolipid concentrations), thus defining the longevity of chronologically aging yeast.

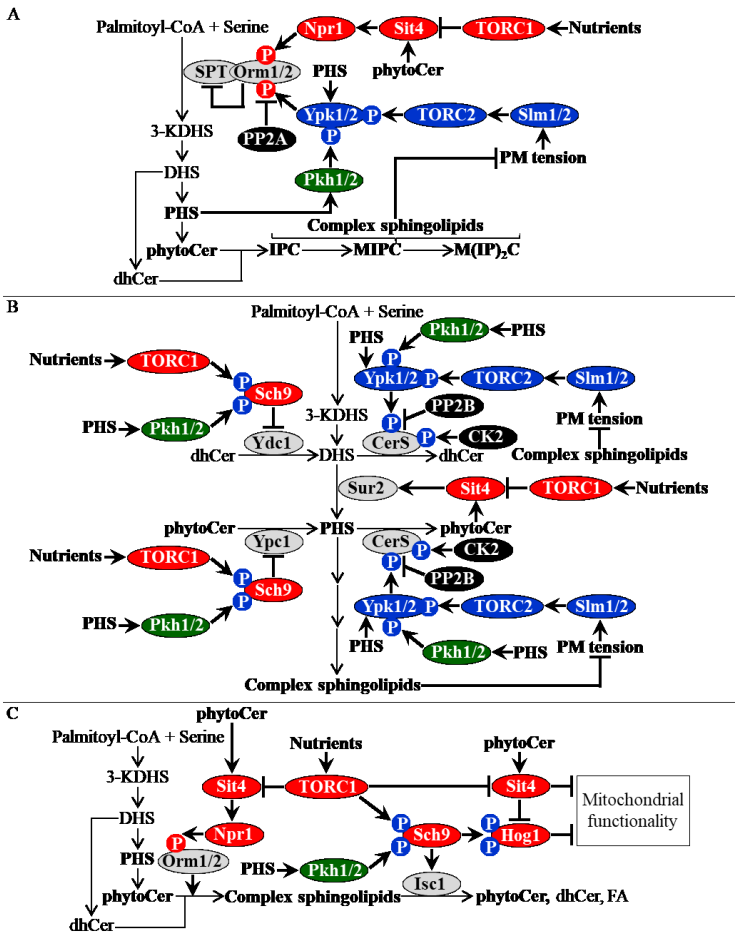

Figure 1.2. Sphingolipid metabolism, nutrient-sensing signaling, and sphingolipid-controlled signaling pathways are integrated into a network. This network includes three hubs. Each hub is a chemical reaction (or several chemical reactions) of sphingolipid metabolism linked to several nodes or branches of nutrient-sensing and sphingolipid-controlled signaling pathways. **(A)** The SPT hub of this network links the initial reaction of sphingolipid metabolism to the TORC1-Sit4-Npr1, TORC2-Ypk1/2 and Pkh1/2-Ypk1/2 branches of nutrient- and sphingolipid-dependent signaling. **(B)** The CerS/Ydc1/Ypc1/Sur2 hub of this network links reactions of sphingosine and ceramide metabolism to the TORC2-Ypk1/2, Pkh1/2-Ypk1/2, TORC1-Sch9, Pkh1/2-Sch9 and TORC1-Sit4-Npr1 branches of nutrient- and sphingolipid-dependent signaling. **(C)** Enzymes involved in the synthesis and hydrolysis of complex sphingolipids constitute a network hub linked to the TORC1-Sit4-Npr1, TORC1-Sch9 and Pkh1/2-Sch9 branches of nutrient- and sphingolipid-dependent signaling. Inhibiting or activating phosphorylations are displayed in red or blue color, respectively. See text for more details. Abbreviations: CerS, ceramide synthase; CK2, casein kinase 2; dhCer, dihydroceramide; DHS, dihydrosphingosine; FA, fatty acid; HOG, high osmotic glycerol; IPC, inositol-phosphorylceramide; Isc1, inositol phosphosphingolipid phospholipase C 1; 3-KDHS, 3-ketodihydrosphingosine; MIPC, mannosyl-inositol-phosphorylceramide; M(IP)2C, mannosyl-di-inositol-phosphorylceramide; Npr1, nitrogen permease reactivator 1; Orm1 and Orm2, orosomucoid 1 and 2 (respectively); PHS, phytosphingosine; phytoCer, phytoceramide; Pkh, Pkb-activating kinase homolog; PM, plasma membrane; PP2A, protein phosphatase type 2A; PP2B, protein phosphatase type 2B; Pkh, Pkb-activating kinase homolog; Sit4, suppressor of initiation of transcription 4; Slm1/2, synthetic lethal with Mss4 protein 1 or 2; SPT, serine palmitoyltransferase; Sur2, suppressor 2 of Rvs161 and rvs167 mutations; TOR, target of rapamycin; TORC1, TOR complex 1; TORC2, TOR complex 2; Ydc1, yeast dihydroceramidase 1; Ypc1, yeast phytoceramidase 1; Ypk1/2, yeast protein kinase 1 or 2.

Another hub of the nutrient and sphingolipid signaling network includes the CerS protein complex, ceramidases Ydc1 and Ypc1, and the sphinganine C4-hydroxylase Sur2 (Figure 1.2B). These proteins and protein complexes are involved in the synthesis of dhCer and phytoCer from DHS and PHS, hydrolysis of dhCer and phytoCer to DHS and PHS, and conversion of DHS into PHS (respectively) (Figure 1.1). At the CerS/Ydc1/Ypc1/Sur2 hub, CerS is activated in response to phosphorylation at different sites by 1) Ypk1/2, a common component of partially overlapping TORC2-Ypk1/2 and Pkh1/2-Ypk1/2 signaling branches [167, 168]; and 2) casein kinase 2 (CK2), a Ser/Thr protein kinase with many cellular functions (Figure 1.2B) [169, 170]. The TORC2-Ypk1/2 branch is attenuated by complex sphingolipids, whereas both components of the Pkh1/2-Ypk1/2 branch are activated by PHS (Figure 1.2B) [96, 153, 155, 159, 162, 165]. The TORC2-Ypk1/2 branch is also weakened by calcineurin, a Ca2+/calmodulin-regulated type 2B protein phosphatase (PP2B) which stimulates the dephosphorylation of CerS sites phosphorylated by Ypk1/2 (Figure 1.2B) [167, 168]. Ceramidases Ydc1 and Ypc1 are components of the CerS/Ydc1/Ypc1/Sur2 hub whose abundance can be decreased if the nutrient-sensing protein kinase Sch9 represses transcription of the YDC1 and YPC1 genes (Figure 1.2B) [75]. Sch9 is a common component of the partially overlapping TORC1-Sch9 and Pkh1/2-Sch9 signaling branches; it can be activated if concomitantly phosphorylated at different sites by nutrient-sensing TORC1 and PHS-dependent Pkh1/2 (Figure 1.2B) [83, 90, 94, 158, 162, 171]. The Sur2 component of the CerS/Ydc1/Ypc1/Sur2 hub can be activated by Sit4, a catalytic subunit of PP2A which can be inhibited by nutrient-sensing TORC1 and stimulated by phytoCer (Figure 1.2B) [96, 147, 153, 154, 163, 164]. Thus, the CerS/Ydc1/Ypc1/Sur2 hub of the nutrient and sphingolipid signaling network is under control of the following four feedback loops: 1) a positive feedback loop in which CerS is indirectly activated by PHS; 2) a negative feedback loop in which CerS is indirectly inhibited by complex sphingolipids; 3) a negative feedback loop in which Ydc1 and Ypc1 are indirectly inhibited by PHS; and 4) a positive feedback loop in which Sur2 is indirectly activated by phytoCer (Figure 1.2B). It is tempting to speculate that these four feedback loops allow the coordination of synthesis and breakdown of DHS, PHS, dhCer, and phytoCer in response to the intracellular nutrient and stress status, thereby being essential for regulating longevity of chronologically aging yeast.

The third hub of the nutrient and sphingolipid signaling network includes enzymes involved in the synthesis and hydrolysis of complex sphingolipids (Figure 1.2C). The synthesis of

complex sphingolipids in the Golgi apparatus is activated by phosphorylated forms of the Orm1 and Orm2 proteins; a mechanism of such activation remains unknown (Figure 1.2C) [164]. Orm1 and Orm2 are phosphorylated by the protein kinase Npr1 of the TORC1-Sit4-Npr1 signaling branch; the Sit4 component of this branch can be suppressed by nutrient-sensing TORC1 and can be stimulated by phytoCer (Figure 1.2C) [96, 154, 164]. The hydrolysis of complex sphingolipids in mitochondria is catalyzed by Isc1, whose translocation from the ER to mitochondria during the post-diauxic growth phase requires the nutrient-sensing protein kinase Sch9 [156]. The Sch9-driven stimulation of complex sphingolipids hydrolysis is under positive control of the TORC1-Sch9 and Pkh1/2-Sch9 signaling branches, as nutrient-sensing TORC1 and PHS-dependent Pkh1/2 can activate Sch9 by phosphorylating different sites of this protein (Figure 1.2C) [83, 90, 94, 158, 162, 171]. Besides their essential roles in regulating the synthesis and hydrolysis of complex sphingolipids (as well as other reactions of sphingolipid metabolism; see Figures 1.2A and 1.2B), the TORC1-Sit4 and TORC1-Sch9 branches are nodes of a signaling subnetwork that modulates mitochondrial functionality in response to nutrient status and phytoCer concentration (Figure 1.2C). This signaling subnetwork integrates the TORC1-Sit4 and TORC1-Sch9 branches with Hog1 (a MAPK which is phosphorylated by Sch9) and Isc1, thereby coordinating sphingolipid metabolism and mitochondrial function and regulating longevity of chronologically aging yeast (Figure 1.2C) [93, 96, 149–154, 156]. Together, these findings indicate that the third hub of the nutrient and sphingolipid signaling network is controlled by a positive feedback loop which indirectly activates complex sphingolipid synthesis by phytoCer, as well as by a positive feedback loop which indirectly stimulates complex sphingolipid hydrolysis by PHS (Figure 1.2C). By coordinating complex sphingolipid metabolism and mitochondrial functionality in response to the intracellular nutrient and stress status, these feedback loops are likely to play an essential role in regulating longevity of chronologically aging yeast.

1.2.2 Triacylglycerol synthesis and degradation are essential contributors to chronological aging of *S. cerevisiae*

Triacylglycerols (TAG) are uncharged (and therefore called ″neutral″) lipids synthesized in the ER and then deposited in lipid droplets (LD) [152, 172, 173]. The hydrolytic degradation of TAG stored in LD can provide free fatty acids (FFA) and diacylglycerols (DAG) to produce

energy, synthesize phospholipid and sphingolipid constituents of cellular membranes, and generate some signaling lipids [107, 152, 172–176].

The metabolic pathways of TAG synthesis and degradation in yeast cells are well known [172, 173, 175, 176]; they are schematically depicted in Figure 1.3. The *de novo* synthesis of TAG begins in the ER where two glycerol-3-phosphate/dihydroxyacetone phosphate (Gro-3-P/DHAP) acyltransferases, Sct1 and Gpt2, catalyze the formation of lysophosphatidic acid (LPA) or acyl-DHAP from fatty acyl-CoA esters (FA-CoA) and Gro-3-P or DHAP, respectively (Figure 1.3) [177, 178]. FA-CoA, which serve as co-substrates in these Sct1- and Gpt2-driven reactions, are synthesized *de novo* from acetyl-CoA by the cytosolic acetyl-CoA carboxylase Acc1 and FA synthase complex Fas1/Fas2 (Figure 1.3) [179–184]. LPA can also be formed from acyl-DHAP in an Ayr1-driven reduction reaction (Figure 1.3) [185]. The LPA acyl-transferases Slc1, Slc4, Loa1, and Ale1 catalyze the conversion of LPA to PA in an acyl CoA-dependent reaction (Figure 1.3) [186–190]. PA can then be used as a substrate in two different reactions, each yielding a distinct precursor molecule for a biosynthetic pathway that contributes to TAG formation *de novo*. One of these reactions is catalyzed by the cytidine diphosphate (CDP)-DAG synthase Cds1; this reaction converts PA to CDP-DAG, which is then used for the synthesis of the phospholipids phosphatidylserine (PS), phosphatidylcholine (PC) and phosphatidylinositol in the ER, and also of the phospholipid phosphatidylethanolamine (PE) in mitochondria (Figure 1.3) [172–176, 191]. The other reaction is catalyzed by the PA phosphatases Pah1, App1, Dpp1, and Lpp1; this reaction converts PA to DAG (Figure 1.3) [192–194]. DAG is then acylated to TAG in the following two reactions: 1) an FA-CoA-dependent reaction catalyzed by Dga1, Are1 and Are2 [195, 196]; and 2) a phospholipid (mainly PE and PC)-dependent reaction catalyzed by Lro1 (Figure 1.3) [197]. After being *de novo* synthesized in the ER, TAG are deposited in LD. To provide FFA and DAG needed to support growth and division of rapidly proliferating yeast, these TAG can undergo hydrolysis which is catalyzed by the TAG lipases Tgl1, Tgl3, Tgl4, Tgl5, and Ayr1; all these TAG lipases reside in LD (Figure 1.3) [198–202]. DAG can also be hydrolyzed, likely by Tgl3, to yield monoacylglycerols (MAG) (Figure 3) [201]. The lipolytic degradation of MAG in LD is catalyzed by the MAG lipase Yju3 (Figure 1.3) [203]. FFA generated in LD as the products of TAG, DAG, and MAG hydrolysis can be reactivated to FA-CoA by the long-chain acyl-CoA synthetases Faa1, Faa4, and Fat1, which form a complex in LD (Figure 3) [152, 204–206]. After being formed in LDs, these FA-CoA can undergo beta-oxidation in peroxisomes, which associate with LD in

rapidly proliferating yeast cells (Figure 1.3) [53, 152, 207–213]. Peroxisomal oxidation of these FA-CoA species produces acetyl-CoA, which can then be used for 1) energy production in mitochondria; and/or 2) FA-CoA formation and its subsequent utilization for the *de novo* synthesis of TAG and phospholipids in the ER (Figure 1.3) [53, 152, 175, 176, 209]. In addition, the FA-CoA and DAG species formed in LD can be used for the synthesis of membrane and signaling lipids in yeast cells that undergo rapid growth and division (Figure 1.3) [107, 152, 172, 174, 175, 214–217].

The intensities of lipid fluxes via metabolic pathways for TAG synthesis and degradation in yeast cells are modulated by different mechanisms, controlled in space and time, and altered in response to certain changes in environmental, nutritional and developmental conditions. Indeed, many reactions of TAG synthesis and degradation are catalyzed by partially redundant enzymes that have different substrate specificities (Figure 1.3); this may allow modulation of the cellular concentrations of TAG, DAG, phospholipids, and FFA under different internal and external conditions [172, 174–176]. Also, some enzymes involved in TAG synthesis (i.e. Gpt2, Ayr1, Slc1, Loa1, and Dga1), TAG hydrolysis (i.e. Tgl1 and Yju3) and FFA reactivation (i.e. Faa1, Faa4, and Fat1) in yeast cells exhibit dual localization to the ER and LD; this may also be used as a mechanism for adapting the anabolic and catabolic branches of TAG metabolism to certain changes in intracellular and extracellular conditions [152, 174–176]. In addition, the ER and LD form physical contacts and share lipid intermediates of TAG metabolism with many other cellular structures, including mitochondria, peroxisomes, vacuoles, the nucleus, the Golgi apparatus, and the PM; this allows to maintain lipid homeostasis of the entire cell under different environmental, nutritional and developmental conditions [210–213, 216–225]. Furthermore, TAG lipolysis supplies (while TAG synthesis removes) certain TAG metabolism intermediates that in yeast cells play essential roles in cell cycle progression and cytokinesis; these pathways of TAG metabolism 1) are controlled by the cyclin-dependent kinases Pho85-Pho80 and/or Cdc28 at two different cell-cycle checkpoints, and 2) modulate the intracellular concentrations of lipid species that control cell-cycle progression activities of the phosphatase PP2ACdc55 and morphogenesis checkpoint kinase Swe1 [214–216, 226–229]. Moreover, TAG synthesis in yeast cells is under the tight control by such key nutrient-sensing protein kinases as Tor1, PKA, and Snf1; this allows to sustain cellular homeostasis of lipids under different conditions of nutrient availability [152, 172, 174, 229–233].

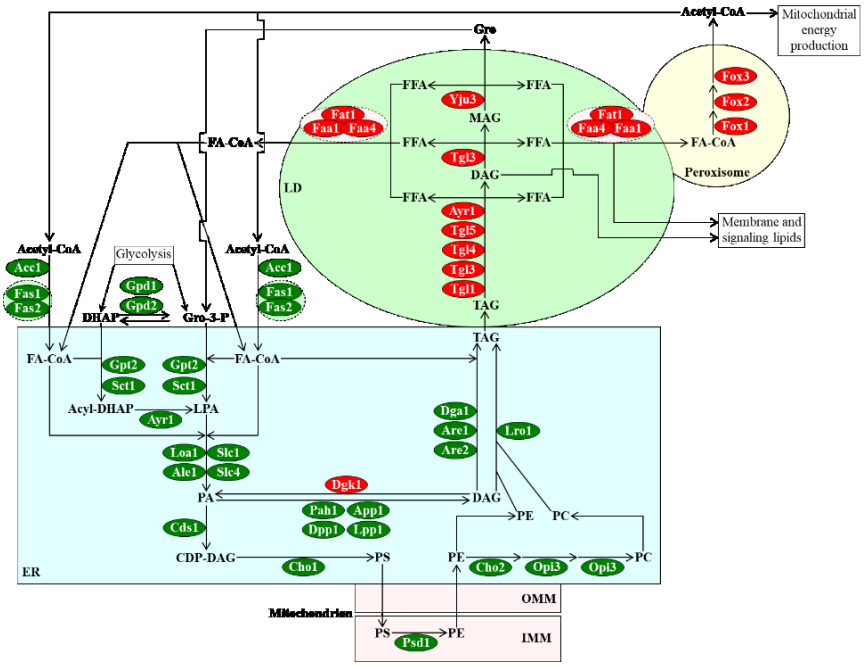

Figure 1.3. Pathways for the synthesis of phospholipids in the endoplasmic reticulum (ER) and mitochondria partially overlap with the anabolic branch of TAG (triacylglycerol) metabolism in the ER. The catabolic branch of TAG metabolism is confined to lipid droplets (LD) and peroxisomes. Enzymes that catalyze anabolic or catabolic reactions of TAG metabolism are displayed in green or red color, respectively. See text for more details. Abbreviations: Acc1, acetyl-CoA carboxylase 1; Ale1, acyltransferase for lysophosphatidylethanolamine 1; App1, actin patch protein 1; Are1/2, acyl-coenzyme A: cholesterol acyl transferase-related enzymes 1 and 2; Ayr1, acyl-dihydroxyacetone-phosphate reductase 1; CDP, cytidine diphosphate; Cds1, CDP-diacylglycerol synthase 1; Cho1/2, choline requiring 1 and 2; DAG, diacylglycerol; Dga1, diacylglycerol acyltransferase 1; Dgk1, diacylglycerol kinase 1; Dpp1, diacylglycerol pyrophosphate phosphatase 1; DHAP, dihydroxyacetone phosphate; Faa1/4, fatty acid activation 1 and 2; FA-CoA, fatty acyl-CoA ester; Fas1/2, fatty acid synthetases 1 and 2; Fat1, fatty acid transporter 1; FFA, free fatty acid; Fox1/2/3, fatty acid oxidation 1, 2 and 3; Gpd1/2, glycerol-3-phosphate dehydrogenases 1 and 2; Gpt2, glycerol-3-phosphate acyltransferase; Gro, glycerol; Gro-3-P, glycerol-3-phosphate; OMM, outer mitochondrial membrane; IMM, inner mitochondrial membrane; Loa1, lysophosphatidic acid: oleoyl-CoA acyltransferase 1; Lpp1, lipid phosphate phosphatase 1; LPA, lysophosphatidic acid; Lro1, lecithin cholesterol acyl transferase related open reading frame 1; MAG, monoacylglycerol; Opi3, overproducer of inositol 3; PA, phosphatidic acid; Pah1, phosphatidic acid phosphohydrolase 1; PC, phosphatidylcholine; PE, phosphatidylethanolamine; PS, phosphatidylserine; Psd1, phosphatidylserine decarboxylase 1; Sct1, suppressor of choline-transport mutants 1; Slc1/4, sphingolipid compensation 1 and 4; Tgl1/3/4/5, triglyceride lipases 1, 3, 4 and 5.

Given that TAG metabolism in *S. cerevisiae* is spatially and temporally integrated into many vital cellular processes confined to different cellular compartments and controlled by some key signaling pathways in response to specific changes in intracellular and extracellular conditions, it is not surprising that TAG synthesis and degradation have been shown to define the longevity of chronologically aging yeast. It seems that there are two different ways of delaying yeast chronological aging by differently altering the age-related dynamics of changes in intracellular TAG concentration. These two ways are described below.

One of these ways of aging delay has been discovered by studies of yeast cultured in a nutrient-rich liquid medium initially containing 2% glucose [234, 235]. Under this so-called non-caloric restriction (non-CR) condition yeast cells are not limited in the supply of calories [236, 237]. In non-CR yeast, the intracellular concentration of TAG is substantially increased during logarithmic (L), diauxic (D) and post-diauxic (PD) phases [159]. After entering the stationary (ST)

phase, yeast cells cultured under non-CR conditions gradually consume TAG accumulated in LD during the preceding L, D and PD phases of growth [237]. It has been found that in non-CR yeast 1) single-gene-deletion mutations eliminating the TAG lipases Tgl3 and/or Tgl4 increase TAG concentration and extend CLS; 2) a simultaneous lack of DAG acyltransferases Dga1 and Lro1 in the *dga1Δlro1Δ* mutant strain decreases TAG concentration and shortens CLS; and 3) the overexpression of the DAG acyltransferase Dga1 rises TAG concentration and prolongs CLS [234]. It was therefore concluded that an increase in the abundance of TAG seen in *tgl3Δ*, *tgl4Δ*, *tgl3Δtgl4Δ* and Dga1 overexpressing cells under non-CR conditions is responsible for the extension of their CLS [234, 235]. A ″radical sink″ mechanism may underlie the ability of increased concentration of TAG to serve as a longevity assurance factor in chronologically aging non-CR yeast (Figure 1.4) [235]. In this mechanism, an age-related accumulation of reactive oxygen species (ROS) in non-CR yeast elicits oxidative damage to different kinds of biological macromolecules, especially to unsaturated FFA which are known to be highly susceptible to such damage [235]. Genetic manipulations that increase incorporation of unsaturated FFA into TAG (i.e. the *tgl3Δ* and/or *tgl4Δ* mutations or Dga1 overexpression) may intensify the flow of these susceptible to oxidative damage unsaturated FFA into LD, where TAG are stored. This may decrease the abundance of unsaturated FFA in cellular membranes, thereby lowering the extent of age-related oxidative damage to membrane lipids and proteins (and perhaps to water-soluble macromolecules, such as proteins, DNA and RNA) and extending the CLS of non-CR yeast (Figure 1.4) [235]. Moreover, because genetic manipulations that increase the incorporation of unsaturated FFA into TAG may sequester the major target molecules of an age-related oxidative damage inside the hydrophobic core of LD, this is expected to limit the distribution of oxidative damage to water-soluble molecules outside LD and thus to prolong the CLS of non-CR yeast as well (Figure 1.4) [235]. The ″radical sink″ mechanism, which has been proposed to explain how the accumulation of bulk quantities of TAG by non-CR cells of some yeast mutants may extend CLS, provides a framework for future studies aimed at testing its validity. It remains to be established if TAG stored in LD of these long-lived mutant cells amass oxidatively damaged unsaturated FFA. Another challenge is to assess if membrane-associated and/or water-soluble macromolecules in these mutant cells exhibit a lowered extent of oxidative damage. In the future, it would be also interesting to investigate if pharmacological interventions that can extend yeast

CLS under non-CR conditions may (akin to the aging-delaying *tgl3Δ*, *tgl4Δ,* and *tgl3Δtgl4Δ* mutations or Dga1 overexpression) elicit an accumulation of excessive TAG quantities.

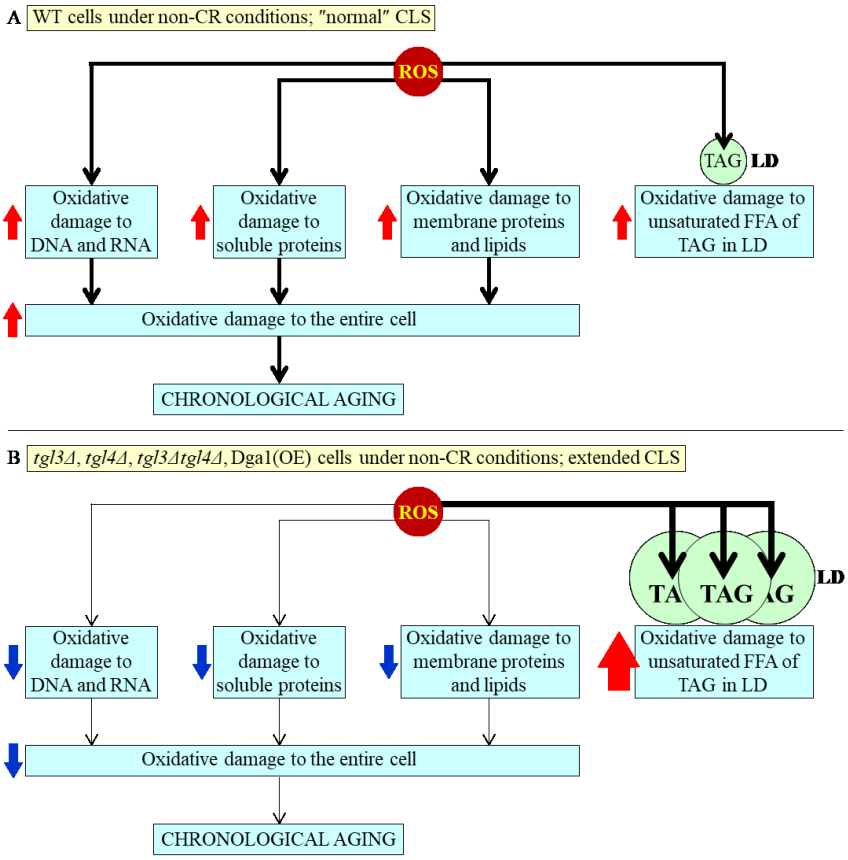

Figure 1.4. A "radical sink" mechanism may explain how the accumulation of triacylglycerols (TAG) by non-CR cells of some yeast mutants may extend yeast chronological lifespan (CLS). **(A)** An age-related accumulation of reactive oxygen species (ROS) in non-CR cells of wild-type (WT) strain elicits an oxidative damage to water-soluble molecules (i.e. DNA, RNA, proteins and metabolites) as well as to membrane proteins and lipids, and also to unsaturated free fatty acids (FFA) that are incorporated into TAG stored in lipid droplets (LD). The substantial oxidative damage to water-soluble and membrane-associated molecules elicits massive oxidative damage to the entire cell, thereby accelerating yeast chronological aging. **(B)** The *tgl3Δ*, *tgl4Δ* and *tgl3Δtgl4Δ* mutations, as well as Dga1 overexpression (OE), increase the incorporation of unsaturated FFA into TAG, thereby intensifying the flow of these unsaturated FFA (which are very susceptible to oxidative damage) into LD. This may decrease the abundance of unsaturated FFA in cellular membranes, thus lowering the extent of oxidative damage to membrane proteins and lipids as well as to water-soluble DNA, RNA, proteins, and metabolites. This, in turn, lowers the extent of oxidative damage to the entire cell and decelerates yeast chronological aging. The thickness of black arrows is proportional to the extent of oxidative damage to various molecules, the degree of oxidative damage to the entire cell or efficiency with which chronological aging is accelerated. Arrows next to the boxes showing names of affected processes denote those of them that are intensified (red arrows) or weakened (blue arrows). See text for more details.

The other way of delaying yeast chronological aging by altering the age-related dynamics of TAG has been discovered by studies of yeast placed on a CR diet; this diet was imposed by culturing *S. cerevisiae* in a nutrient-rich liquid medium initially containing 0.2% or 0.5% glucose [98, 237]. CR is a dietary intervention that delays aging not only in yeast [237] but also in multicellular eukaryotes across phyla [1, 24, 238–240]. In yeast cultured under CR conditions, the intracellular concentration of TAG is increased during L and D phases to reach a significantly lower steady-state level than that in yeast cultured under non-CR conditions [237]. CR yeast cells

completely consume TAG during the subsequent PD phase, unlike non-CR yeast cells that maintain a relatively high concentration of TAG through the entire CLS [237]. Yeast cells cultured under non-CR conditions (but not yeast cells cultured under CR conditions) amass ethanol [53, 237]. This product of glucose fermentation has been shown to decrease yeast CLS [241], however, a mechanism by which ethanol shortens the longevity of chronologically aging yeast remains unknown. Ethanol accumulated by yeast cells cultured under non-CR conditions has been shown to suppress the synthesis of Fox1, Fox2, and Fox3, all of which are the core enzymes of peroxisomal beta-oxidation of FFA [242, 243]. Because of the resulting low efficiency of FFA oxidation in peroxisomes of prematurely aging non-CR yeast cells, they accumulate FFA [237]. Moreover, it has been shown that 1) a close physical association of peroxisomes with LD promotes the lipolytic degradation of TAG within LD, thus providing bulk quantities of FFA for beta-oxidation in yeast peroxisomes [53, 207, 211, 212]; and 2) lack of peroxisomal Fox1, Fox2 or Fox3 in the *fox1Δ*, *fox2Δ* or *fox3Δ* mutant strain elicits an accumulation of electron-dense arrays of FFA (which are called ″gnarls″), as well as a deposition of bulk quantities of TAG, within yeast LD [207, 211, 212]. Based on all these findings, a mechanism has been proposed for how a CR diet may extend yeast CLS by altering the spatiotemporal dynamics of TAG synthesis in the ER, TAG lipolysis in LD and beta-oxidation of TAG-derived FFA in peroxisomes [53, 110, 237, 244–246]. This mechanism is schematically depicted in Figure 1.5. In this mechanism, yeast cells grown under non-CR conditions amass ethanol. The accumulated ethanol weakens peroxisomal oxidation of FA-CoA because it represses the synthesis of Fox1, Fox2, and Fox3 (Figure 1.5) [53, 110, 237, 244, 245]. The ensuing build-up of FA-CoA in peroxisomes creates a negative feedback loop which attenuates the transport of FA-CoA from associated LD, where these FA-CoA are formed from TAG-derived FFA. This elicits an accumulation of arrays of FFA (gnarls) within LD of non-CR yeast, thus initiating several negative feedback loops that weaken TAG lipolysis in LD, TAG transport from the ER to LD and TAG synthesis from DAG in the ER (Figure 1.5) [53, 110, 237, 244, 245]. The resulting build-up of FFA and DAG in the ER and LD shortens the CLS of non-CR yeast because these two lipid classes are known to elicit an age-related form of liponecrotic RCD (Figure 1.5) [110, 246]. Because yeast cells grown under CR conditions do not accumulate ethanol [237], they are not susceptible to liponecrotic RCD and thus live longer than non-CR yeast [53, 110, 237, 244–246]. In the above mechanism, age-related liponecrotic RCD shortens the longevity of non-CR yeast. Because proteins that execute this mode of RCD in

chronologically aging yeast have been identified [110, 246], it would be interesting to investigate if single-gene-deletion mutations eliminating these proteins can extend the longevity of yeast cultured under non-CR conditions.

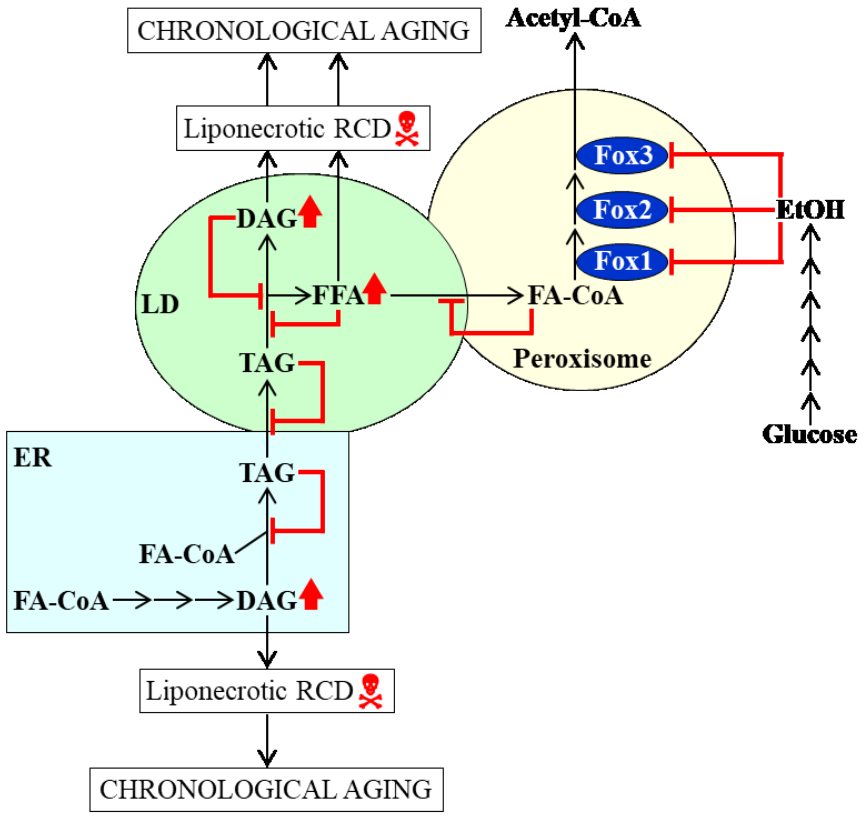

Figure 1.5. A mechanism through which a build-up of ethanol by chronologically aging yeast cells grown under non-CR conditions may shorten their longevity by altering the spatiotemporal dynamics of triacylglycerol (TAG) synthesis in the endoplasmic reticulum (ER), TAG lipolysis in lipid droplets (LD) and beta-oxidation of TAG-derived free fatty acids (FFA) in peroxisomes. Yeast cells under non-CR conditions accumulate ethanol, which then represses the synthesis of Fox1, Fox2, and Fox3. This elicits a build-up of fatty acyl-CoA esters (FA-CoA) in peroxisomes, thereby initiating several negative feedback loops that weaken TAG lipolysis in LD, TAG transport from the ER to LD and TAG synthesis from diacylglycerol (DAG) in the ER. The resulting build-up of FFA and DAG in the ER and LD shortens yeast CLS because these two lipids trigger an age-related form of liponecrotic regulated cell death (RCD). Red arrows next to the names of lipid classes denote those of them whose concentrations are increased in non-CR yeast. Inhibition bars displayed in red color signify negative feedback loops. See text for more details.

1.2.3 Mitochondrial membrane phospholipids contribute to longevity regulation in chronologically aging yeast

A high-throughput chemical genetic screen for low molecular weight chemical compounds capable of prolonging yeast CLS has identified lithocholic bile acid (LCA) as one of such geroprotectors [98]. Yeast cells do not produce LCA or other bile acids, all of which are synthesized and released into an ecosystem by animals and humans [247–250]. If LCA is added exogenously to yeast cultured in a liquid medium, this highly hydrophobic bile acid enters the yeast cell, is delivered to mitochondria, accumulates mainly in the inner mitochondrial membrane (IMM), and associates with the outer mitochondrial membrane (OMM) [251]. A body of evidence

supports the notion that LCA slows down yeast chronological aging because it instigates specific changes in the concentrations of mitochondrial membrane phospholipids [63, 91, 100, 251–257]. The data confirming that certain LCA-dependent changes in mitochondrial membrane phospholipids play essential roles in the ability of LCA to extend yeast CLS are summarized below in this section and integrated into a model presented in Figure 1.6.

After being sorted to a double membrane delimiting the mitochondrion, LCA elicits three major changes in the abundance and composition of mitochondrial membrane phospholipids. These major changes are depicted in Figure 1.6 and outlined beneath.

First change: LCA significantly increases the phospholipid/protein ratio of mitochondrial membranes; this rise in the abundance of all membrane phospholipid classes in mitochondria causes a substantial enlargement of these organelles (Figure 1.6) [251].

Second change: LCA considerably augments the relative concentration of PA, likely by activating its transfer from the ER to the OMM via mitochondria-ER contact sites and the ensuing movement of PA from the OMM via the intermembrane space (IMS) to the IMM [63, 251]. PA is a so-called ″fusogenic″ lipid class known to stimulate fusion of two or more small mitochondria into a single mitochondrion [254]. This LCA-driven increase in the relative concentration of PA causes a substantial decline in the number of mitochondria (Figure 1.6) [251].

Third change: LCA differently affects the relative concentrations of different phospholipid classes as follows: a) it causes a rise in PS, phosphatidylglycerol (PG) and PC; and b) it causes a decline in PE, cardiolipin (CL) and monolysocardiolipin (MLCL) (Figure 1.6) [63, 251]. These effects of LCA are believed to be instigated by an LCA-dependent attenuation of Psd1 and Crd1, which catalyze the conversion of PS into PE and of PG into CL (respectively) (Figure 1.6) [63, 251]. These LCA-driven changes in different phospholipids not only decrease the relative concentrations of the non-bilayer forming classes of phospholipids but also increase the relative concentrations of the bilayer forming classes of phospholipids (Figure 1.6) [63, 251]. The non-bilayer forming classes of phospholipids are known to enhance membrane curving for the IMM, whereas the bilayer forming classes of phospholipids have the opposite effect on IMM curving [114, 251, 258–260]. Because LCA elicits these divergent effects on the non-bilayer forming and bilayer forming classes of phospholipids, many cristae in mitochondria of yeast treated with LCA are disconnected from the IMM and amass within the mitochondrial matrix as flat bilayers (Figure 1.6) [100, 251, 255, 257]. Moreover, because LCA increases the phospholipid/protein ratio of

mitochondrial membranes (see above), this bile acid also raises the abundance of such disconnected cristae inside mitochondria (Figure 1.6) [100, 251, 255, 257].

Taken together, these data indicate that the LCA-driven changes in mitochondrial membrane phospholipids play a causal role in enlarging mitochondria, lessening the mitochondrial number, and increasing the abundance of mitochondrial cristae that are disconnected from the IMM and accumulate within the mitochondrial matrix as flat bilayers (Figure 1.6) [100, 251, 255, 257].

The above changes in the abundance and morphology of mitochondria in LCA-treated yeast lead to significant changes in the concentrations of many mitochondrial proteins; these mitochondrial proteins have been implicated in such longevity-defining processes as the tricarboxylic acid cycle, glyoxylate cycle, electron transport chain, amino acid synthesis, heme synthesis and attachment, iron-sulfur clusters synthesis and assembly, NADPH synthesis, ROS detoxification, protein import and folding, stress response and protection, mitochondrial division, mitochondrial DNA replication and maintenance, and synthesis and translation of mitochondrial RNA (Figure 1.6) [63, 253]. The LCA-driven changes in mitochondrial proteome of LCA-treated yeast alter the age-related chronology of several longevity-defining mitochondrial processes, including mitochondrial respiration, membrane potential preservation, ROS homeostasis maintenance and ATP synthesis (Figure 1.6) [63, 251]. These LCA-dependent alterations in mitochondrial functionality allow mitochondria to operate as signaling platforms that a) orchestrate a longevity-extending transcriptional program for many nuclear genes that are controlled by a discrete set of ten transcriptional factors, thus altering the entire cellular proteome; b) promote changes in the lipidomes of cellular organelles other than mitochondria; and c) elicit changes in the concentrations of certain water-soluble metabolites located outside of mitochondria (Figure 1.6) [100, 251, 255, 257].

In sum, the LCA-driven changes in mitochondrial membrane phospholipids trigger a cascade of downstream events that gradually lead to the development of a cellular pattern extending yeast CLS. In the future, it would be interesting to investigate mechanisms through which LCA-dependent changes in mitochondrial functionality prompt changes in membrane lipidomes and water-soluble metabolomes outside of mitochondria. Another challenge is to assess the timetable of events that, in response to LCA-driven changes in mitochondrial membrane phospholipids, lead to the development of a pro-longevity pattern of the entire yeast cell.

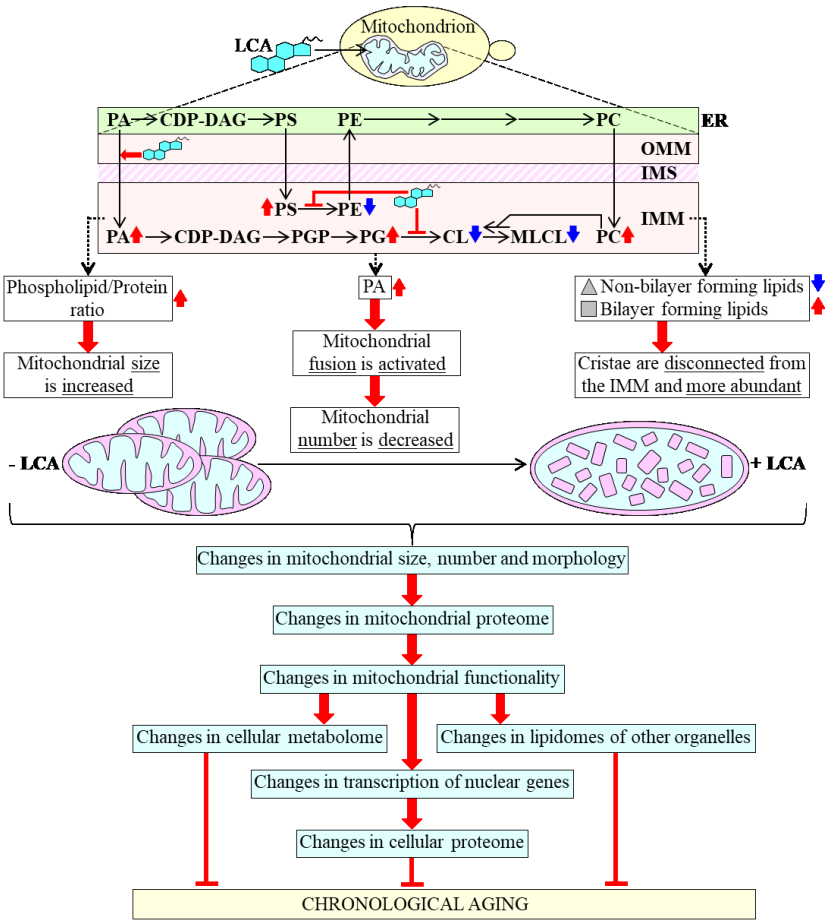

Figure 1.6. Exogenously added lithocholic bile acid (LCA) enters the yeast cell, accumulates in a double membrane delimiting the mitochondrion, and elicits major changes in the abundance and composition of mitochondrial membrane phospholipids. These changes in mitochondrial membrane phospholipids initiate a cascade of downstream events that gradually develop an anti-aging cellular pattern, thus extending the longevity of chronologically aging yeast. See text for more details. Abbreviations: CDP-DAG, cytidine diphosphate-diacylglycerol; Cl, cardiolipin; ER, endoplasmic reticulum; OMM, outer mitochondrial membrane; IMM, inner mitochondrial membrane; IMS, intermembrane space; MLCL, monolysocardiolipin; PA, phosphatidic acid; PC, phosphatidylcholine; PE, phosphatidylethanolamine; PG, phosphatidylglycerol; PS, phosphatidylserine; PGP, phosphatidylglycerol-phosphate.

1.3 Liponecrosis, an age-related mode of regulated cell death induced by excessive concentrations of FFA

Some forms of cell death are classified as ″programmed″ cell death subroutines; they involve molecular machinery dedicated to committing cellular ″suicide″ that is aimed at providing certain benefits for development and/or survival of the entire organism [261–266]. Other forms of cell death are actively driven by molecular machinery that attempt to protect cells against certain stresses (without providing benefits for organismal development and/or survival); these forms are known as ″regulated″ cell death (RCD) subroutines [261, 263]. Cells commit RCD executed by a discrete molecular machinery because 1) the capacity of a molecular machinery dedicated to cell protection against a certain kind of stress is not sufficient to maintain cell viability if the intensity of such extracellular and/or intracellular stress exceeds a threshold; and/or 2) molecular machinery driving some cellular processes that (directly or indirectly) contribute to cell protection against a certain kind of exogenous and/or endogenous stress are excessively activated, thereby generating

products of these processes in concentrations that are lethal to the cell [261, 263, 267]. *S. cerevisiae* is a model organism most commonly and productively used for studying different forms of RCD elicited by perturbations in lipid metabolism [68, 109, 112, 132, 133, 146, 147, 158, 268–289]. The detailed knowledge of mechanisms underlying the molecular pathways of various modes of lipotoxic RCD in this yeast is therefore instrumental to our understanding of many human pathologies that are causally linked to dysregulated lipid metabolism, unbalanced lipid homeostasis, lipotoxicity and lipid-induced cell death [68, 109, 112, 290–293]. Among these human pathologies are obesity, metabolic syndrome, type 2 diabetes, insulin resistance, cardiovascular diseases, hepatic steatosis, liver cirrhosis and cancer [68, 107, 290–307].

The scope of this section of the thesis is to analyze mechanisms underlying one of the modes of lipotoxic RCD. It has been discovered in the yeast *S. cerevisiae* and named ″liponecrosis″. Liponecrotic RCD can be elicited by a short-term (for 2 h) treatment of yeast cells with exogenous palmitoleic acid (POA), a 16-carbon monounsaturated fatty acid (16:1, n-7) [98, 110, 246]. The section describes cellular processes that yeast cells exposed to POA use for stress adaptation and viability maintenance. The section also evaluates mechanisms (including POA-induced oxidative stress) through which yeast cells that are exposed to POA die of liponecrosis if the capacities of cellular processes for protection against POA-imposed stress become insufficient to maintain cell viability.

1.3.1 Mechanisms through which yeast cells treated with POA can either die or mount a protective stress response to survive

A model for the mechanism of liponecrotic RCD elicited by a short-term treatment of yeast with POA and for the mechanism protecting yeast from such RCD is schematically depicted in Figure 1.7.

Yeast cells that are briefly exposed to exogenous POA use the lipid-synthesizing and lipid-transporting enzymatic machinery of the endoplasmic reticulum (ER), mitochondria, lipid droplets (LD) and the plasma membrane (PM) to incorporate this fatty acid into copious amounts of two classes of lipids [110, 112]. One of these POA-containing classes is the so-called ″neutral″ (uncharged) lipids triacylglycerols (TAG) and ergosteryl esters (EE), both of which are first produced in the ER and then deposited in LD (Figure 1.7) [53, 68, 176, 290]. The other class are POA-containing phospholipids (Figure 1.7); they include 1) phosphatidic acid (PA),

phosphatidylserine (PS), phosphatidylcholine (PC) and phosphatidylinositol (PI), all of which are synthesized only in the ER and then transferred to mitochondria through mitochondria-ER junctions and to the PM through PM-ER junctions [91, 175, 210, 213, 251, 308–311]; 2) phosphatidylethanolamine (PE), which is produced from ER-derived PS in the inner and outer mitochondrial membranes (IMM and OMM, respectively) and then transferred to the ER through mitochondria-ER junctions and from the ER to the PM through PM-ER junctions [114, 224, 308–314]; and 3) cardiolipin (CL), a signature mitochondrial phospholipid which is generated from ER-derived PA in a series of reactions confined to the IMM and OMM [224, 259, 312, 315, 316]. It needs to be emphasized that genetic interventions weakening the incorporation of exogenously added POA into POA-containing phospholipids within the ER have been shown to increase cell resistance to POA-induced liponecrotic RCD [110, 112]. Thus, such incorporation is a pro-death process essential for the commitment of yeast to liponecrotic RCD in response to treatment with exogenous POA.

After being synthesized in the ER, the bulk quantities of POA-containing phospholipids in yeast cells committed to liponecrotic RCD amass in the PM (Figure 1.7) [110, 112]. Such accumulation of POA-containing phospholipids in the PM activates the alkaline-pH- and lipid-asymmetry-responsive Rim101 signaling pathway, which orchestrates a series of endocytic internalization and trafficking events ultimately promoting transcription of the nuclear RSB1 gene [317–325]. A protein product of this gene, Rsb1, is known to regulate the bidirectional active transport of PE across the PM bilayer; specifically, Rsb1 stimulates the Lem3-driven transport of PE from the outer monolayer of the PM to its inner monolayer and slows down the Yor1-driven transport of PE in the opposite direction [324, 326–329]. These effects of Rsb1 elicit a depletion of PE in the outer monolayer of the PM, thereby markedly raising the permeability of the PM to small molecules (Figure 1.7) [110, 112]. Such an increase in the permeability of the PM to small molecules has been shown to play an essential role in committing yeast to POA-induced liponecrotic RCD (Figure 1.7) [110, 112].

The bulk quantities of POA-containing phospholipids initially synthesized in the ER of yeast cells that are committed to liponecrotic RCD accumulate not only in the PM but also in both membranes enclosing mitochondria (Figure 1.7) [110, 112]. This buildup of POA-containing phospholipids in the IMM and OMM markedly weakens mitochondrial respiratory capacity, uncouples mitochondria respiratory chain from ATP synthesis and lowers the electrochemical

potential across the IMM (Figure 1.7) [110, 112]. The resulting decline in mitochondrial functionality plays an essential role in committing yeast to POA-induced liponecrotic RCD, likely because these dysfunctional mitochondria cannot produce enough ATP to support the energy-demanding, pro-survival process of incorporating exogenous POA into neutral lipids (see text below for discussion of this pro-survival process) (Figure 1.7) [110, 112].

The buildup of POA-containing phospholipids in the IMM and OMM of yeast committed to liponecrotic RCD not only impairs mitochondrial functionality but also considerably increases the intracellular concentration of reactive oxygen species (ROS) that are produced in mitochondria as by-products of respiration (Figure 1.7) [110, 112]. This rise of ROS concentrations elicits oxidative damage to different types of molecules in two cellular locations, namely 1) to protein and lipid components of mitochondria and other cellular organelles; and 2) to proteins in the cytosol, thereby causing their unfolding and aggregation (Figure 1.7) [110, 112]. Both these types of cellular oxidative damage are essential contributing factors either to the commitment of yeast to POA-induced liponecrotic RCD or to an execution of this RCD subroutine. Specifically, a massive breakdown of numerous oxidatively damaged and dysfunctional organelles through a non-selective macroautophagic degradation (which is choreographed by the phagophore assembly-specific serine/threonine protein kinase Atg1, adapter protein Atg11 and scaffold protein Atg17 [239, 246, 330–332]) plays a crucial role in executing POA-induced liponecrotic RCD (Figure 1.7) [110, 112, 246]. Moreover, the buildup of oxidatively damaged, dysfunctional, unfolded and aggregated proteins in the cytosol of yeast cells treated with POA impairs cellular proteostasis, thus committing these cells to POA-induced liponecrotic RCD (Figure 1.7) [110, 112].

If the stress imposed by exposure to POA does not exceed a toxic threshold, yeast cells can use at least four different processes to cope with this stress and maintain viability (Figure 1.7).

One of these pro-survival cellular processes is an assimilation of POA into neutral lipids (TAG and EE), which occurs in the ER and is followed by a buildup of POA-containing neutral lipids in LDs (Figure 1.7) [110, 112, 246]. This process lowers the extreme cellular stress caused by the accumulation of POA-containing phospholipids in the PM, IMM, and OMM because it attenuates the flow of POA into the pathways for the synthesis of POA-containing phospholipids [110, 112, 246]. The assimilation of POA into neutral lipids is essential for protecting yeast from POA-induced liponecrotic RCD, as demonstrated by the finding that genetic interventions

weakening the incorporation of exogenously added POA into POA-containing neutral lipids increase the susceptibility of yeast to this subroutine of RCD [246].

Another pro-survival cellular process is the β-oxidation of POA in peroxisomes of yeast exposed to this monounsaturated free fatty acid (Figure 1.7) [98, 110, 112, 246]. Peroxisomal oxidation of POA mitigates POA-induced liponecrotic RCD because it weakens the incorporation of POA into phospholipids, thereby relieving the excessive cellular stress instigated by the buildup of POA-containing phospholipids in the PM, IMM and OMM [110, 112, 246]. In support of an essential role of peroxisomal oxidation of POA in the protection of yeast from POA-induced liponecrotic RCD, yeast strains that carry the single-gene-deletion mutations *pex5Δ* and *fox1Δ* attenuating oxidative degradation of POA in peroxisomes are more susceptible to this mode of RCD than an otherwise isogenic wild-type strain [98, 110, 112, 246].

Macromitophagy, a macroautophagic degradation of dysfunctional or damaged mitochondria, is also a pro-survival process that allows yeast to cope with the POA-induced cellular stress [110, 112, 246]. Macromitophagy protects yeast from POA-induced liponecrotic RCD because, by selectively degrading dysfunctional mitochondria, it helps to maintain a population of functionally active mitochondria that are needed to generate enough ATP to support the pro-survival process of assimilating POA into neutral lipids (Figure 1.7) [110, 112, 246]. The *atg32Δ*-dependent mutational block of macromitophagy impairs the accumulation of LD-deposited neutral lipids and sensitizes yeast to POA-induced liponecrotic RCD [246]; thus, macromitophagy plays an essential role in protecting yeast from this subroutine of RCD.

The degradation of oxidatively damaged, dysfunctional, unfolded and aggregated proteins that accumulate in the cytosol of yeast cells treated with POA is another pro-survival process in these cells; this proteolytic degradation is catalyzed by the metacaspase Yca1 and serine protease Nma111, two protein components of the caspase-dependent apoptotic RCD pathway (Figure 1.7) [57, 110, 112, 333, 334]. This Yca1- and Nma111-driven proteolysis of oxidatively damaged, dysfunctional, unfolded and aggregated proteins slows down a progression of POA-induced liponecrotic RCD because it allows to sustain efficient cellular proteostasis, thereby weakening proteostatic cellular stress (Figure 1.7) [110, 112]. In support of an essential role of such proteolysis in the protection of yeast from POA-induced liponecrotic RCD, lack of Yca1 or Nma111 increases the susceptibility of yeast to this mode of RCD [110, 112].

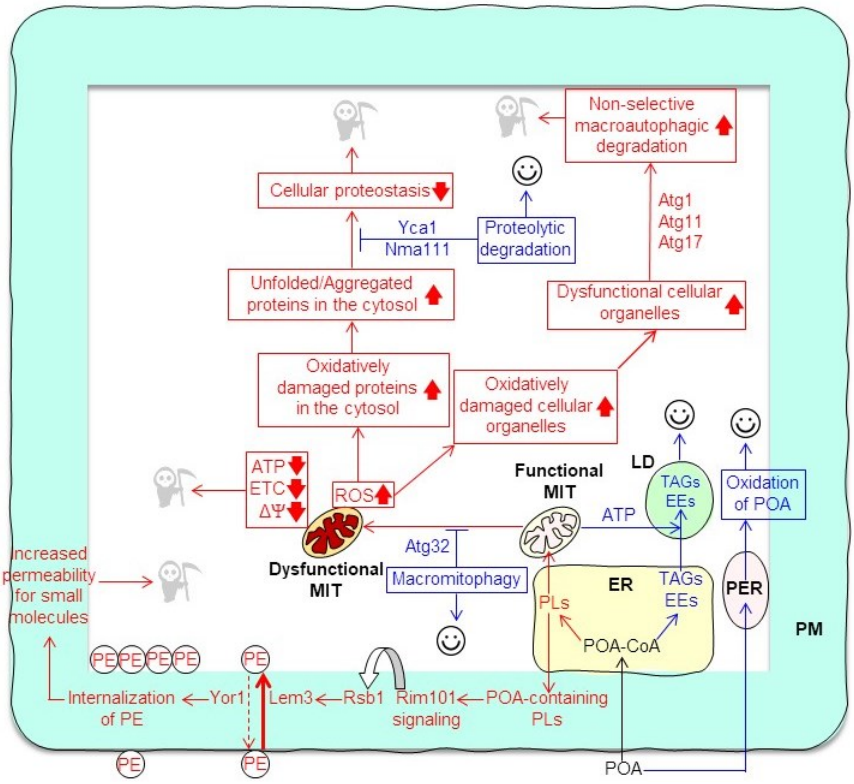

Figure 1.7. A model for how yeast cells exposed to exogenous palmitoleic acid (POA) either mount a protective stress response and survive or commit to POA-induced regulated liponecrosis and die. Yeast cells briefly exposed to POA can employ four different pro-survival processes to cope with the POA-induced cellular stress and maintain viability. These pro-survival cellular processes include the following: 1) an assimilation of POA into neutral lipids (triacylglycerols [TAG] and ergosteryl esters [EE]), in the endoplasmic reticulum (ER) and the subsequent deposition of these neutral lipids in lipid droplets (LD); 2) POA oxidation in peroxisomes (PER); 3) a macroautophagic degradation of dysfunctional or damaged mitochondria (MIT); and 4) a proteolytic degradation of oxidatively damaged, dysfunctional, unfolded and aggregated proteins that accumulate in the cytosol of yeast cells. Arrows and names displayed in blue color denote pro-survival processes, metabolites, and proteins that protect yeast from POA-induced liponecrotic regulated cell death (RCD). Yeast cells briefly treated with POA can use four different pro-death processes to commit to POA-induced liponecrotic RCD and to execute this RCD subroutine. These pro-death cellular processes include the following: 1) a buildup of POA-containing phospholipids (PLs) in the PM and the ensuing increase in the permeability of the PM to small molecules; and 2) the accumulation of POA-containing PLs in both mitochondrial membranes and the resulting decline in mitochondrial functionality, which is needed to support the pro-survival process of incorporating exogenous POA into neutral lipids; 3) a ROS-inflicted oxidative damage to mitochondria and other cellular organelles, which stimulates a non-selective macroautophagic degradation of many kinds of organelles; and 4) a ROS-imposed oxidative damage to cytosolic proteins, which impairs cellular proteostasis because it promotes an accumulation of oxidatively damaged, dysfunctional, unfolded and aggregated proteins in the cytosol. Arrows and names displayed in red color denote pro-death processes, metabolites, and proteins that commit yeast to POA-induced RCD or execute this RCD subroutine. The up or down arrows in red color denote processes or metabolites whose intensities or concentrations are increased or decreased (respectively) in yeast cells briefly exposed to exogenous POA. See text for more details. Abbreviations: ETC, mitochondrial electron transport chain; PE, phosphatidylethanolamine; PLs, phospholipids; PM, plasma membrane; ROS, reactive oxygen species; ΔΨ, the electrochemical potential across the inner mitochondrial membrane.

1.3.2 A hypothesis on mechanisms that may regulate a balance between pro-death and pro-survival processes in yeast treated with POA

As outlined in the previous section, pro-death cellular processes in yeast treated with POA are directly or indirectly due to the initial incorporation of this fatty acid into bulk quantities of POA-containing phospholipids. Two direct pro-death processes include the following: 1) the buildup of POA-containing phospholipids in the PM and the ensuing increase in the permeability

of the PM to small molecules; and 2) the accumulation of POA-containing phospholipids in both mitochondrial membranes and the resulting decline in mitochondrial functionality, which is needed to support the pro-survival process of incorporating exogenous POA into neutral lipids (Figure 1.7). Two other pro-death processes are only indirectly caused by the buildup of POA-containing phospholipids in both mitochondrial membranes because such buildup elicits a rise of the intracellular concentration of ROS initially produced in mitochondria. These indirect pro-death processes are as follows: 1) the ROS-inflicted oxidative damage to mitochondria and other cellular organelles, which stimulates a non-selective macroautophagic degradation of many kinds of organelles; and 2) the ROS-imposed oxidative damage to cytosolic proteins, which impairs cellular proteostasis because it promotes the accumulation of oxidatively damaged, dysfunctional, unfolded and aggregated proteins in the cytosol (Figure 1.7). Thus, the four pro-death processes relate because they all are initiated in response to the buildup of POA-containing phospholipids. We hypothesize that 1) the direct pro-death processes may precede in time the indirect ones; and 2) the relative contribution of each direct or indirect pro-death process into POA-induced liponecrotic RCD may be defined by the relative rates with which POA-containing phospholipids are transferred from the ER to the PM and mitochondria, mitochondria generate ROS, mitochondria and other cellular organelles undergo ROS-inflicted oxidative damage, oxidatively damaged cellular organelles are subjected to non-selective macroautophagic degradation, cytosolic proteins are oxidatively damaged by mitochondrially produced ROS, and oxidatively damaged cytosolic proteins unfold and aggregate. In our hypothesis, none of the pro-death processes may be considered as an individual pro-death pathway. In contrast, our hypothesis posits that all four pro-death processes are likely to be nodes of a branched subnetwork that integrates the flow of POA-containing phospholipids from the ER to the PM and mitochondria, mitochondrial ROS formation, the ROS-imposed oxidative damage to organelles and cytosolic proteins, the non-selective macroautophagic breakdown of different kinds of oxidatively damaged organelles, and the unfolding and aggregation of oxidatively damaged proteins in the cytosol.

Our hypothesis further suggests that pro-survival processes are likely to be nodes of the same branched subnetwork integrating the four pro-death processes. Two direct pro-survival processes relieve the extreme cellular stress by preventing the buildup of POA-containing phospholipids in the PM and mitochondria; they include the following: 1) the assimilation of POA into neutral lipids in the ER and the subsequent buildup of POA-containing neutral lipids in LDs;

and 2) peroxisomal oxidation of POA (Figure 1.7). Two indirect pro-survival processes are activated to lower the extreme cellular stress created by the buildup of POA-containing phospholipids in both mitochondrial membranes and by the resulting decline in mitochondrial functionality and rise in mitochondrially produced ROS; they are as follows: 1) the selective macroautophagic degradation of oxidatively damaged and dysfunctional mitochondria, which helps to maintain a population of functionally active mitochondria generating sufficient quantities of ATP and producing ROS in non-toxic concentrations; and 2) the Yca1- and Nma111-driven proteolysis of oxidatively damaged and aggregated cytosolic proteins, which allows to sustain efficient cellular proteostasis (Figure 1.7). Akin to pro-death processes, the four pro-survival processes relate because they are all stimulated in an attempt to relieve the extreme cellular stress that is generated (directly or indirectly) by the initial incorporation of POA into POA-containing phospholipids. Our hypothesis posits that 1) the direct pro-survival processes may occur earlier than the indirect ones; and 2) the relative contribution of each direct or indirect pro-survival process into cell protection from POA-induced liponecrosis may depend on the relative rates with which POA is assimilated into neutral lipids in the ER, POA-containing neutral lipids are transferred from the ER to LD, POA is oxidized in peroxisomes, oxidatively damaged and dysfunctional mitochondria are subjected to selective macroautophagic degradation, and oxidatively damaged and aggregated cytosolic proteins undergo proteolytic degradation.

In sum, the above hypothesis posits the following: 1) the balance between different pro-death and pro-survival processes may be regulated by their relative rates; and 2) these relative rates may be defined by the extracellular and/or intracellular concentrations of POA, nutrient availability, the metabolic state of a yeast cell, and the chronological age of a yeast cell.

1.3.3 The subnetwork of liponecrotic RCD is likely integrated into a signaling network that orchestrates different RCD modes in yeast cells

Yeast cells undergoing POA-induced liponecrotic RCD exhibit characteristic morphological and biochemical traits [110, 112, 246]. Some of these traits are unique to liponecrotic RCD, whereas other traits are shared by this and certain other modes of RCD (Table 1.1).

Table 1.1. Some of the morphological and biochemical traits characteristic of palmitoleic acid (POA)-induced liponecrotic regulated cell death (RCD) are unique to this mode of RCD, whereas other traits are shared by this mode and other (i.e. caspase-dependent apoptotic, autophagic and necrotic) RCD modes. Abbreviations: LD, lipid droplets; PM, plasma membrane; PS, phosphatidylserine.

Trait	Caspase-dependent apoptotic RCD [references]	Autophagic RCD [references]	Necrotic RCD [references]	POA-induced liponecrotic RCD [references]
Nuclear fragmentation	+ [335]	-	-	- [246]
PS externalization within the PM	+ [335]	-	-	- [246]
Role of Yca1 and Nma111	+ (pro-death role) [336, 337]	-	-	+ (pro-survival role) [110]
Excessive cytoplasmic vacuolization	-	+ [338]	-	- [246]
Massive degradation of various cellular organelles	-	+ [338]	-	+ [246]
Rupture of the PM	-	-	+ [25]	- [246]
Permeability of the PM to small molecules	-	-	+ [25]	+ [110]
Excessive accumulation of LD	-	-	-	+ [246]

While yeast cells committed to POA-induced liponecrotic RCD do not display such characteristic traits of apoptotic RCD as nuclear fragmentation and PS externalization within the PM bilayer, the metacaspase Yca1 and serine protease Nma111 play essential roles in both liponecrotic and caspase-dependent apoptotic modes of RCD [110, 112]. However, the roles of Yca1 and Nma111 play in each of these two RCD modes are quite different (Table 1.1). As mentioned above, the Yca1- and Nma111-dependent proteolysis of oxidatively damaged, dysfunctional, unfolded and aggregated proteins in the cytosol of yeast cells is a pro-survival process in POA-induced liponecrotic RCD [110, 112]. Such a pro-survival role of Yca1 in sustaining efficient cellular proteostasis is well known [339–346]. In contrast, the Yca1- and Nma111-driven degradation of various cellular proteins is an executing, pro-death process in several caspase-dependent modalities of apoptotic RCD in yeast exposed to certain exogenous stimuli [57, 333, 334, 336, 337, 347–349].

While yeast cells undergoing POA-induced liponecrotic RCD do not display such hallmark trait of autophagic RCD as extreme cytoplasmic vacuolization instigated by a buildup of double-membrane vesicles called autophagosomes [110, 112, 246], both liponecrotic and autophagic modes of RCD 1) exhibit a non-selective massive degradation of various cellular organelles; and 2) depend on the phagophore assembly-specific serine/threonine protein kinase Atg1 for executing these RCD modes (Table 1.1) [110, 246, 261, 350–352].

While yeast cells undergoing POA-induced liponecrotic RCD do not exhibit such hallmark feature of necrotic RCD as a severe fracture of the PM [110, 112, 246], both liponecrotic and necrotic modes of RCD display substantially increased permeability of the PM to small molecules (Table 1.1) [25, 109, 110, 246, 353, 354].

A trait which is unique to POA-induced liponecrotic RCD is a buildup of POA-containing neutral lipids in numerous LD, a feature that has not been reported for an apoptotic, autophagic or necrotic mode of RCD (Table 1.1) [110, 246, 261, 333, 350–353].

Because POA-induced liponecrotic RCD has several different traits in common with apoptotic, autophagic and necrotic modes of RCD, we hypothesize that the molecular subnetwork of POA-induced liponecrotic RCD is integrated into a signaling network that orchestrates different RCD modes in yeast cells. Other pathways and subnetworks integrated into this signaling network may include apoptotic, autophagic and necrotic pathways and subnetworks of RCD. In our hypothesis, the molecular subnetwork of POA-induced liponecrotic RCD only partially overlaps with apoptotic, autophagic and necrotic RCD pathways and subnetworks of the network. Our hypothesis satisfactorily explains the observed existence of several proteins that are common to liponecrotic, apoptotic, autophagic and necrotic modes of RCD [110, 112, 246]. Furthermore, as our hypothesis suggests, some of the morphological and biochemical traits characteristic of POA-induced liponecrotic RCD are shared by this mode of RCD and other (i.e. apoptotic, autophagic and necrotic) RCD modes integrated into the network [110, 112, 246]. Moreover, in agreement with our hypothesis on only a partial overlap between liponecrotic and other pathways and subnetworks of RCD, at least one trait characteristic of liponecrotic RCD is unique to this mode of RCD; this trait is the accumulation of POA-containing neutral lipids in many LD [110, 112, 246].

Our hypothesis on the existence of an RCD signaling network orchestrating different RCD scenarios in yeast cells is reminiscent of the hypothesis on the global programmed cell death (PCD)

network that has been proposed and then confirmed for mammalian cells [252, 253, 355, 356]. A systems biology platform has been developed for defining the topology of such network operating in mammalian cells; this platform employs cell biological and computational approaches for measuring and computing the effects of single and double genetic interventions on the molecular events characteristic of different PCD modes that are integrated into the network [252]. The use of such platform, possibly in combination with powerful tools of proteomic and metabolomic analyses recently applied for molecular analyses of RCD in yeast [345, 346], will allow to test our hypothesis on the global RCD signaling network in yeast and, perhaps, to dissect the architecture of such network in the near future.

1.3.4 Liponecrotic RCD may contribute to yeast chronological aging

POA-induced liponecrotic RCD is an age-related mode of RCD, as the susceptibility of a population of yeast cells to POA-induced liponecrosis increases with the chronological age of this population [63, 110, 112, 246]. Furthermore, the susceptibility of yeast cells to POA-induced liponecrotic RCD can be significantly decreased by some aging-delaying dietary and pharmacological interventions. These interventions include caloric restriction (CR) and lithocholic bile acid (LCA), each implemented at the time of cell inoculation into growth medium [53, 63, 98].

Our recent unpublished findings indicate that in yeast cultured under non-CR conditions on 1% or 2% glucose, the risk of age-related death depends not only on the POA-induced liponecrotic mode of RCD but also on ROS-induced apoptotic RCD mode. Moreover, we found that the liponecrotic and apoptotic modes of RCD have different relative contributions to age-related death of non-CR yeast at different periods of chronological lifespan (CLS). The apoptotic mode of RCD predominates during diauxic (D) phase, apoptotic and liponecrotic RCD modes equally increase the risk of death during post-diauxic (PD) phase, whereas the liponecrotic mode of RCD prevails during stationary (ST) phase of culturing under non-CR conditions (our unpublished data). The longevity-defining mode of liponecrotic RCD is elicited by the accumulation of POA and other free fatty acids in chronologically aging non-CR yeast cells that progress through PD and ST phases of culturing (our unpublished data). In contrast, the longevity-defining mode of apoptotic RCD is caused by the rapid decline of mitochondrial functionality and rise of mitochondrially generated ROS in chronologically aging non-CR yeast cells progressing

through D and PD phases of culturing (our unpublished data). CR diet, which is implemented by culturing yeast on 0.2% or 0.5% glucose, decreases the risk of age-related death by attenuating liponecrotic and apoptotic RCD modes during D, PD and ST phases; these effects of CR are due to its ability 1) to decrease free fatty acid (including POA) concentrations during PD and ST phases of culturing; and 2) to improve mitochondrial functionality and to lessen concentrations of mitochondrially generated ROS during D and PD phases of culturing (our unpublished data).

LCA is a geroprotective chemical compound that delays yeast chronological aging mainly under CR conditions [98]. LCA exhibits the following effects on yeast susceptibility to POA-induced liponecrotic RCD: 1) it decreases such susceptibility only if added to growth medium at the time of cell inoculation, during logarithmic (L) or D phase of culturing; 2) it increases such susceptibility if added during PD phase; and 3) it has no effect on such susceptibility if added during ST phase [63]. Taken together, these findings suggest that liponecrotic RCD may be an essential longevity-limiting (i.e. pro-aging) factor in chronologically ″young″ yeast, may somehow contribute to longevity extension (i.e. aging delay) in chronologically ″middle-aged″ yeast and may have no influence on longevity (i.e. on the pace of aging) of chronologically ″old″ yeast. Noteworthy, all these age-related variations in yeast susceptibility to POA-induced liponecrotic RCD coincide with age-related changes in yeast resistance to chronic oxidative, thermal and osmotic stresses [63]. In the future, it would be important to explore mechanisms that underlie the observed age-related coincidence between yeast susceptibility to POA-induced liponecrotic RCD and yeast resistance to long-term stresses. Moreover, it remains to be determined if and how the concentrations of endogenously produced free fatty acids (including POA) influence the extent of liponecrotic RCD at different stages of yeast chronological aging.

Of note, LCA decreases yeast susceptibility to the mitochondria-controlled, ROS-induced mode of apoptotic RCD if added to the growth medium at the time of cell inoculation and during L, D, PD or ST phase of culturing [63]. In yeast cultured under CR conditions, exogenous LCA enters cells, is sorted to mitochondria, amasses primarily in the IMM and also resides in the OMM, alters the concentrations of certain mitochondrial membrane phospholipids, elicits a major enlargement of mitochondria, significantly decreases mitochondrial number, prompts an intra-mitochondrial accumulation of cristae disconnected from the IMM, triggers substantial alterations in mitochondrial proteome, decreases the frequencies of deletion and point mutations in mitochondrial DNA, and leads to changes in vital aspects of mitochondrial functionality [91, 174,

251, 357]. In the future, it would be important to explore how all these aging-delaying effects of LCA are linked to yeast susceptibility to the mitochondria-controlled, ROS-induced mode of apoptotic RCD at different stages of chronological aging.

In sum, it is conceivable that liponecrotic and apoptotic modes of RCD may have different effects on yeast CLS at different periods of life. This is like the ″P″ (″big P″) and ″p″ (″small p″) modes of death in the nematode *Caenorhabditis elegans*, which define lifespan earlier or later in life (respectively) [358]. The P mode of death is manifested as a substantial enlargement of the posterior pharyngeal bulb caused by intensified pharyngeal pumping, whereas the p mode of death is due to the complete atrophy of pharynx [331].

1.3.5 Liponecrotic RCD differs from other modes of lipotoxic RCD and may be integrated into a global network of different lipotoxic RCD modes

Several exogenously added lipids [268–276], as well as different genetic [133, 146, 147, 158, 271, 275–281, 291] and pharmacological [158, 282–286] interventions that impair certain aspects of lipid metabolism, have been shown to elicit apoptotic and/or necrotic modes of lipotoxic RCD in yeast. These modes have been recently extensively reviewed [68, 109, 287, 293, 359]. In brief, yeast cells committed to POA-induced liponecrotic RCD exhibit a unique combination of morphological and biochemical traits that is not characteristic of any of these other modes of lipotoxic RCD. Moreover, some of these other modes of lipotoxic RCD differ from each other with respect to 1) structural and/or functional features of yeast committed to a particular mode of RCD; 2) classes of lipids whose concentrations are altered (or are expected to be altered) in yeast committed to a particular mode of RCD; and 3) proteins that are involved in committing to and/or executing a particular mode of RCD [68, 109, 133, 146, 147, 158, 268–286, 288, 293, 359].

Altogether, these findings can be considered as a further support of our hypothesis (which is outlined in section 1.3.3) on the possible existence of a global signaling network that integrates partially overlapping molecular pathways and subnetworks of lipotoxic RCD, each pathway and subnetwork being differently responsive to certain perturbations in diverse aspects of lipid metabolism within a yeast cell. The key challenge for the future is to explore mechanisms through which such perturbations in lipid metabolism 1) modulate individual molecular pathways and subnetworks of lipotoxic RCD; and 2) orchestrate the integration of these individual pathways and subnetworks into the global signaling network of lipotoxic RCD. To address this challenge, the

systems biology platform (which is discussed in section 1.3.3) exploited for mammalian cells [252] can be used in combination with proteomic and metabolomic analyses of molecular signatures [345, 346] characteristic of different lipotoxic RCD modes.

1.4 Some phytochemicals delay aging, extend longevity and improve health in eukaryotes across phyla

Plants use a diverse set of secondary biochemical pathways not to fulfill their primary metabolic needs in energy and biosynthetic products, but to generate many secondary metabolites called phytochemicals [360–364]. Some phytochemicals are produced not by plants, but by non-pathogenic endophytic bacteria and fungi that live within the plants [365–370].

Phytochemicals are structurally diverse chemical compounds; based on chemical nature, they can be divided into the following major classes: 1) phenolic compounds, including flavonoids, phenolic acids, hydroxycinnamic acids, lignans, tyrosol esters, stilbenoids, and alkylresorcinols; 2) terpenes, including carotenoids, monoterpenes, saponins, some modified lipid species, and triterpenoids; 3) betalains, including betacyanins and betaxanthins; 4) polysulfides; 5) organosulfur compounds; 6) indole compounds; 7) some protease inhibitors; 8) oxalic and anacardic organic acids; 9) modified purines; 10) quinones; and 11) polyamines [364, 371–376]. It is believed that plants have evolved secondary biochemical pathways for synthesizing chemically diverse phytochemicals as ecosystemic adaptations; such evolutionary adaptations are thought to increase the chances of these immobile autotrophic organisms to survive and reproduce within their natural ecological niches [360–362, 364, 377–380]. Indeed, phytochemicals are used by plants as interspecies chemical signals that can: 1) help plants to survive various environmental stresses, including UV light, heat and cold stresses, osmotic stress and high salinity, extreme pH, water deficit and dehydration, and nutrient deprivation; 2) protect plants from viral, bacterial, yeast and fungal infections; 3) defend plants from invading insects, herbivorous animals and competitor plant species; 4) provide plants with a protection from environmental pollutants; 5) attract pollinators and other symbiotes; and 6) attract the natural predators of herbivorous insects and animals [360, 361, 364, 377–393]. Moreover, phytochemicals that are produced by non-pathogenic endophytic microorganisms living within the plants can promote the survival of the host plants by protecting them from being eaten by herbivorous insects and animals as well as by defending them

from many environmental stresses and infections by pathogenic microorganisms [365, 366, 367–370, 394–399].

A body of evidence supports the notion that, in addition to being beneficial to survival and reproduction of the plants producing them, phytochemicals can delay aging, extend longevity and/or improve health in various heterotrophic organisms [364, 372–377, 380, 381, 385, 397, 400]. The scope of this section of the thesis is to discuss recent progress in understanding mechanisms underlying such aging-delaying, longevity-extending and health-improving effects of phytochemicals on heterotrophic organisms across phyla.

1.4.1 Phytochemicals delay aging and extend lifespan in evolutionarily distant heterotrophic organisms by targeting an evolutionarily conserved set of cellular processes

Table 1.2 recapitulates numerous findings on how different phytochemicals delay aging and prolong longevity in various heterotrophic organisms by modulating certain cellular processes [25, 361, 401–452]. The mechanisms by which these phytochemicals decelerate aging and extend lifespan in organisms across phyla have begun to emerge. Such mechanisms are discussed below in this section.

Table 1.2. Phytochemicals that delay aging and extend lifespan in various heterotrophic organisms and longevity-defining cellular processes that they modulate. Abbreviations: CaMK, Ca^{2+}/calmodulin-dependent protein kinase; FOXO, forkhead box protein O; HDTIC, 4-hydroxy-5-hydroxymethyl-[1,3]dioxolan-2,6'-spirane-5',6',7',8'-tetrahydro-indolizine-3'-carbaldehyde; Q3'G, quercetin 3'-O-β-D-glucopyranoside; Q3M, 3-O-β-D-glucopyranoside-(4→1)-β-D-glucopyranoside; MAPK, mitogen-activated protein kinase; NT, not tested; rDNA, ribosomal DNA; ROS, reactive oxygen species.

Phytochemical	Plant	Chemical nature	Organism exhibiting aging delay and lifespan extension	Cellular proteins and signaling pathways required	Changes caused
Acteoside	Many plants	Caffeoyl phenylethanoid glycoside (a phenolic compound)	• The fruit fly *Drosophila melanogaster* [401]	NT	NT
Allicin	*Allium sativum* (garlic)	Organosulfur compound	• Senescence-accelerated mice [402–404, 453]	NT	• Improved memory retention and acquisition [402–404, 453]
Butein	*Toxicodendron vernicifluum*	Chalconoid (a phenolic compound)	• The yeast *Saccharomyces cerevisiae* [405]	• The sirtuin Sir1 [405]	NT
Caffeic acid, rosmarinic acid	*Eucalyptus globulus*, *Salvinia molesta*	Hydroxycinnamic acids (phenolic compounds)	• The nematode *Caenorhabditis elegans* [406]	• The OSR-1/UNC-43 (CaMKII)/SEK-1 (p38 MAPK) signaling pathway[406] • The sirtuin SIR-2.1 [406] • Caffeic acid only: the DAF-16/FOXO transcription factor [406]	• Lowered susceptibility to thermal stress [406] • Decreased oxidative damage to macromolecules [406] • Reduced body size, altered lipid metabolism, delayed reproductive timing [406]
Caffeine	*Coffea* plants	Methylxanthine (a purine)	• The yeasts *Saccharomyces cerevisiae* [407] and *Schizosaccharomyces pombe* [408] • The nematode *C. elegans* [409, 410]	• In *S. cerevisiae* and *Sch. pombe*: the target of rapamycin complex 1 (TORC1) [407, 408] • In *C. elegans*: the insulin-like receptor DAF-2, transcription factor DAF-16/FOXO and transcriptional activator CBP-1 [409, 410]	• In *S. cerevisiae*: enhanced transcription of genes encoding heat-shock proteins and molecular chaperones [407] • In *Sch. pombe*: decelerated growth, G2 cell-cycle arrest, altered transcription of many nuclear genes, attenuated protein synthesis and inhibited phosphorylation of ribosomal S6 proteins [408]

					• In *C. elegans*: delayed onset of paralysis and reduced protein aggregation in nematode models of the Alzheimer's and Huntington's diseases [409, 410]
Catechin	Vascular plants	Flavan-3-ol (a phenolic compound)	• The nematode *C. elegans* [411]	• The AKT-2 serine/threonine protein kinase, MEV-1 subunit of succinate-coenzyme Q oxidoreductase in the mitochondrial electron transport chain, and nuclear hormone receptor NHR-8 [411]	• Reduced body length and susceptibility to thermal stress [411] • Elevated pumping rate [411]
Celastrol	*Tripterygium wilfordii*, *Celastrus regelii*	Triterpenoid (a terpen)	• Transgenic mouse model of amyotrophic lateral sclerosis (ALS) [412]	NT	• Decelerated weight loss, improved motor performance, increased number of neurons and delayed onset of ALS [412]
Curcumin, tetrahydrocurcumin	*Curcuma longa*	Diarylheptanoids (phenolic compounds)	• The nematode *C. elegans* [413] • The fruit fly *D. melanogaster*, including 5 different models of Alzheimer's disease [414–416]	• In *C. elegans*: the OSR-1/UNC-43 (CaMKII)/SEK-1 (p38 MAPK) signaling pathway [413] • In *C. elegans*: the sirtuin SIR-2.1 [413] • In *C. elegans*: the phosphatidylinositol 3-kinase AGE-1, transcription factor SKN-1/Nrf and MAPK kinase MEK-1 [413]	• In *C. elegans*: Reduced ROS levels, macromolecular oxidative damage, susceptibility to oxidative and thermal stresses, body length, and pumping rate [413] • In *D. melanogaster*: Decreased macromolecular oxidative damage, lowered susceptibility to oxidative stress, improved locomotor performance [414–416]
Crocin	*Crocus*, *Gardenia*	Carotenoid (a terpen)	• Dalton's lymphoma ascites bearing mice [417]	NT	• Increased hemoglobin and lymphocytes [417] • Decreased white blood cell count and neutrophils [417]
Cryptotanshinone	*Salvia miltiorrhiza*	Tanshion (a quinone)	• The yeast *S. cerevisiae* [375]	• Mitochondrial superoxide dismutase Sod2, as well as the nutrient-sensing protein kinases Tor1, Sch9 and Gcn2 [375]	• Lowered ROS levels [375]

Cyanidin	Many plants	Anthocyanidin (a phenolic compound)	• WI-38 human diploid fibroblasts [418]	NT	• Reduced oxidative damage to lipids and susceptibility to oxidative stress [418]
Diallyl trisulfide	*Allium sativum* (garlic)	A polysulfide (an organosulfide compound)	• The nematode *C. elegans* [419]	• The nicotinic acetylcholine receptor EAT-2 and transcription factor SKN-1/Nrf [419]	• Altered expression of many nuclear genes involved in metabolism and stress response [419]
Ellagic acid	Many plants	Phenolic acid (a phenolic compound)	• The nematode *C. elegans* [420]	• The nicotinic acetylcholine receptor EAT-2 [420]	• Delayed beginning of egg deposition and reduced oxidative damage to water-soluble metabolites [420]
Epigallocatechin gallate	*Camellia sinensis*	Flavan-3-ol (a phenolic compound)	• The nematode *C. elegans* [421, 422]	NT	• Lowered ROS levels, reduced susceptibility to oxidative stress, decreased oxidative damage to lipids, attenuated expression of nuclear genes encoding HSP-16, induced nuclear import of the transcription factor DAF-16/FOXO, reduced formation of Aβ deposits [421, 422]
Ferulsinaic acid	*Ferula* plants	Sesquiterpene coumarin (a terpene)	• The nematode *C. elegans* [423]	NT	• Reduced susceptibility to oxidative and thermal stresses, decreased oxidative damage to lipids, lowered formation of advanced glycation end products [423]
Fisetin	Many plants	Flavonol (a phenolic compound)	• The yeast *S. cerevisiae* [405] • The nematode *C. elegans* [425]	• In *S. cerevisiae*: The sirtuin Sir1 [405] • In *C. elegans*: Nuclear import of the transcription factor DAF-16/FOXO [425]	• In *S. cerevisiae*: NT [405] • In *C. elegans*: Lowered ROS levels, reduced susceptibility to oxidative stress, decreased oxidative damage to macromolecules, induced nuclear import of transcription factor DAF-16/FOXO [425]
Gallic acid	Many plants	Phenolic acid (a phenolic compound)	• The nematode *C. elegans* [420]	• The nicotinic acetylcholine receptor EAT-2 [420]	• Increased body length, delayed the beginning of egg deposition and reduced oxidative damage to water-soluble metabolites [420]

Glaucarubinone	*Simaroubaceae* plants	Triterpenoid (a terpen)	• The nematode *C. elegans* [426]	NT	• Increased rate of oxygen consumption and lowered levels of neutral lipids [426]
HDTIC-1, HDTIC-2	*Astragalus membranceus*	Indolizines (indole compounds)	• Human fetal lung diploid fibroblasts [427]	NT	• Improved growth and proliferation, accelerated entry from G0 or G1 phase to S phase, decreased activity of the senescence-associated-β-galactosidase, and reduced formation of advanced glycation end products [427]
Icariin, icariside II	*Epimedium* plants	Flavonol glycosides (phenolic compounds)	• The nematode *C. elegans* [428]	• The insulin-like receptor DAF-2, transcription factor DAF-16/FOXO and heat shock transcription factor HSF-1 [428]	• Reduced susceptibility to oxidative and thermal stresses, decelerated decline in age-related locomotion, delayed onset of paralysis caused by the proteotoxicity of polyQ and Aβ (1-42), enhanced transcription of the SOD-3 and HSP-12.3 genes [428]
Kaempferol	Many plants	Flavonol (a phenolic compound)	• The nematode C. elegans [425]	• Nuclear import of the transcription factor DAF-16/FOXO [425]	• Lowered ROS levels, reduced susceptibility to oxidative stress, decreased oxidative damage to macromolecules, induced nuclear import of transcription factor DAF-16/FOXO [425]
Myricetin	Many plants	Flavonol (a phenolic compound)	• The nematode *C. elegans* [429]	• Nuclear import of the transcription factor DAF-16/FOXO [429]	• Lowered ROS levels, reduced oxidative damage to proteins, induced nuclear import of transcription factor DAF-16/FOXO, enhanced transcription of the SOD-3 gene [429]
Nordihydroguaiaretic acid	*Larrea tridentata*	Lignan (a phenolic compound)	• Transgenic mouse model of ALS [430] • Male mice [431] • Rats [432] • The fruit fly *D. melanogaster* [433]	NT	• In the transgenic mouse model of ALS: reduced motor dysfunction [430] • In *D. melanogaster*: lowered rate of oxygen consumption [433]

			• Mosquitoes [434]		
Oleuropein	*Olea europaea*	Phenylethanoid (a phenolic compound)	• Human embryonic fibroblasts [435]	NT	• Lowered ROS levels, reduced oxidative damage to proteins, increased rate of proteasomal degradation of oxidatively damaged proteins, decelerated age-related decline in proteasome activity [435]
Phloridzin	Many plants	Chalconoid (a phenolic compound)	• The yeast *S. cerevisiae* [436]	• Cytosolic and mitochondrial superoxide dismutases Sod1 and Sod2 (respectively) [436]	• Lowered ROS levels, decreased susceptibility to oxidative stress, activated transcription of the *SOD1*, *SOD2* and *SIR2* genes, increased superoxide dismutase activity [436]
Quercetin, Q3'G, Q3M, isorhamnetin, tamarixetin	Many plants	Flavonols (phenolic compounds)	• The yeast *S. cerevisiae* [437] • The nematode *C. elegans* [406, 438–440, 442] • Human embryonic fibroblasts [441]	• In *C. elegans*: the insulin-like receptor DAF-2, phosphatidylinositol 3-kinase AGE-1 and nuclear import of the transcription factor DAF-16/FOXO [425, 439, 440], as well as the OSR-1/UNC-43 (CaMKII)/SEK-1 (p38 MAPK) signaling pathway [440]	• In *S. cerevisiae*: Lowered ROS levels, decreased glutathione oxidation, reduced protein carbonylation, lowered lipid peroxidation, decreased susceptibility to oxidative stress [437] • In *C. elegans*: Lowered ROS levels, reduced oxidative damage to macromolecules, enhanced anti-oxidative activities, decreased susceptibility to thermal and oxidative stresses, lowered level of neutral lipids, induced nuclear import of transcription factor DAF-16/FOXO [406, 425, 439, 440] • In human fibroblasts: Lowered activity of the senescence-associated-β-galactosidase, decreased ROS levels, reduced susceptibility to oxidative stress, increased proteasome activity [441]

Reserpine	*Rauvolfia serpentina*	Indole alkaloid (an indole compound)	• The nematode *C. elegans* [443] • The nematode *C. elegans* model of, Alzheimer's disease [444]	• TPH-1, a tryptophan hydroxylase enzyme [443].	• Reduced susceptibility to thermal stress, decelerated decline in age-related locomotion and pharyngeal pumping, delayed postembryonic development [443, 444] • The nematode *C. elegans* model of the Alzheimer's disease: delayed onset of paralysis caused by the proteotoxicity of Aβ [444]
Resveratrol	Many plants	Stilbenoid (a phenolic compound)	• The yeast *S. cerevisiae* [405] • The nematode *C. elegans* [445] • The fruit fly *D. melanogaster* [445] • The short-lived fish *Nothobranchius furzeri* [446] • The honey bee *Apis mellifera* [447] • Mice on a high-calorie diet [448]	• In *S. cerevisiae*: the sirtuin Sir1 [405] • The nematode *C. elegans*: the sirtuin SIR-2.1 [445] • The fruit fly *D. melanogaster*: the sirtuin Sir2 [445] • Mouse: SIRT1 and many other cellular targets, direct or indirect [26, 27, 400]	• In *S. cerevisiae*: reduced frequency of rDNA recombination [405] • In the nematode *C. elegans*: induced autophagy [449] • In *N. furzeri*: delayed age-related decay of locomotor activity and cognitive performances, reduced neurofibrillary degeneration in the brain [446] • In mouse: increased insulin sensitivity, increased activities of AMP-activated protein kinase (AMPK) and peroxisome proliferator-activated receptor-gamma coactivator 1α (PGC-1α), reduced levels of insulin-like growth factor-1 (IGF-I), increased number of mitochondria, altered transcription of many nuclear genes [448]
Spermidine, putrescine	Many plants	Polyamines	• The yeast *S. cerevisiae* [25] • The nematode *C. elegans* [25]	• In *S. cerevisiae*, *C. elegans* and *D. melanogaster*: autophagy [25, 450]	• In *S. cerevisiae*, *D. melanogaster* and PBMC: lowered activities of histone acetyltransferases, increased

			• The fruit fly *D. melanogaster* [25] • Human peripheral blood mononuclear cells (PBMC) [25]		histone H3 deacetylation, activated transcription of many autophagy-related genes, induced autophagy, delayed onset of age-related necrotic cell death, reduced age-related decline of locomotor activity [25] • In *D. melanogaster*: decelerated age-related decline of locomotor activity, increased level of triglycerides, altered relative levels of fatty acid species and phospholipid classes [450, 451]
Tannic acid	Many plants	Polyphenol (a phenolic compound)	• The nematode *C. elegans* [409, 420, 452]	• The mitogen-activated protein kinase SEK-1, transcription factor DAF-16/FOXO, nicotinic acetylcholine receptor EAT-2 and MEV-1 subunit of succinate-coenzyme Q oxidoreductase in the mitochondrial electron transport chain [409, 420, 452]	• Reduced body length, decreased susceptibility to thermal and oxidative stresses, lowered levels of triglycerides, enhanced antioxidant capacity [409, 420, 452]
Tyrosol	Many plants	Phenylethanoid (a phenolic compound)	• The nematode *C. elegans* [455]	• The insulin-like receptor DAF-2, transcription factor DAF-16/FOXO and heat shock transcription factor HSF-1 [455]	• Decreased susceptibility to thermal and oxidative stresses, decelerated onset of age-related decline in pharyngeal pumping, activated transcription of nuclear genes encoding several heat-shock proteins [455]

1.4.2 Aging-delaying and longevity-extending phytochemicals and heterotrophic organisms whose aging they delay and whose lifespan they extend

Aging-delaying and longevity-extending phytochemicals differ in chemical nature; they belong to various classes, including phenolic compounds [401, 405, 406, 409, 411, 413–416, 420–423, 425, 428–442, 452], terpenes [412, 417, 424, 426], polysulfides [419], organosulfur compounds [402–404, 453], indole compounds [427, 443, 444], modified purines [407–410], quinones [375] and polyamines [25] (Table 1.2). These phytochemicals delay aging and extend lifespan in such evolutionarily distant heterotrophic organisms and cultured cells as the budding yeast *Saccharomyces cerevisiae* [25, 375, 405, 407, 436, 437], the fission yeast *Schizosaccharomyces pombe* [408], the nematode *Caenorhabditis elegans* (including a transgenic model of Alzheimer's disease) [25, 329, 409–411, 413, 418–426, 428, 429, 438–440, 442–445, 452, 454], the fruit fly *Drosophila melanogaster* (including different transgenic models of Alzheimer's disease) [401, 414–416, 433, 445, 450], the honey bee *Apis mellifera* [447], mosquitoes [434], the naturally short-lived fish *Nothobranchius furzeri* [446], laboratory mice (including mice on a high-calorie diet and transgenic mice models of several age-related diseases) [402–404, 412, 417, 430, 431, 448, 453], laboratory rats [432], different lines of cultured human fibroblasts [418, 427, 435, 441], and human peripheral blood mononuclear cells [450] (Table 1.2). It needs to be emphasized that some studies revealed that several of the aging-delaying and longevity-extending phytochemicals mentioned in Table 1.2 are unable to decelerate aging and prolong lifespan in certain heterotrophic organisms; for example, such phenolic compounds as resveratrol and curcumin did not alter the lifespan in genetically heterogeneous mice [454].

1.4.3 Proteins and signaling pathways required for aging delay and longevity extension by phytochemicals

Cellular proteins and signaling pathways that are indispensable for lifespan-prolonging abilities of many longevity-extending phytochemicals have been identified (Table 1.2). They include the following proteins and pathways: 1) DAF-2, the only known receptor of the insulin/insulin-like growth factor 1 (IGF-1) signaling (IIS) pathway; this pathway defines longevity of the nematode *C. elegans* by regulating metabolism, protein homeostasis, resistance to many stresses, development and reproduction [409, 410, 428, 440, 455]; 2) the phosphatidylinositol 3-kinase AGE-1, an essential protein component of the IIS pathway in the

nematode *C. elegans* [413, 425, 438, 440]; 3) AKT-2, a serine/threonine protein kinase involved in the IIS pathway in the nematode *C. elegans* [411]; 4) SKN-1/Nrf, one of the transcription factors playing an essential role in the IIS pathway in the nematode *C. elegans* [413, 419] 5) the heat-shock factor 1 (HSF-1), a transcriptional factor involved in the IIS pathway in the nematode *C. elegans* [428, 455]; 6) the transcription factor DAF-16/FOXO and its nuclear import in the nematode *C. elegans* - this protein is a key component of the IIS pathway [406, 409, 410, 420, 425, 428, 429, 438–440, 452, 455]; 7) the OSR-1/UNC-43 (CaMKII)/SEK-1 (p38 MAPK) signaling pathway, which in the nematode *C. elegans* defines resistance to osmotic stress, arsenic, and pathogen infection [406, 413, 440]; 8) the nicotinic acetylcholine receptor EAT-2, which is essential for longevity regulation in the nematode *C. elegans* because it defines the rate of pharyngeal pumping in this organism [409, 419, 420, 452]; 9) NHR-8, a non-canonical nuclear hormone receptor which is essential for longevity regulation - likely because it defines resistance to xenobiotic stress and plays essential roles in the metabolism of cholesterol, bile acids, and neutral lipids in the nematode *C. elegans* [411]; 10) the mitogen-activated protein kinase (MAPK) kinase MEK-1, which in the nematode *C. elegans* is involved in protein synthesis and stress-induced apoptosis and defines resistance to pathogen infection and heavy metals [413]; 11) the MEV-1 subunit of succinate-coenzyme Q oxidoreductase, a component of the mitochondrial electron transport chain that defines longevity of the nematode *C. elegans* [409, 411, 420, 452]; 12) the histone acetyl transferase CBP-1, a transcriptional activator which is involved in mRNA processing and neurogenesis in the nematode *C. elegans* [409, 410]; 13) TPH-1, a tryptophan hydroxylase enzyme involved in serotonin synthesis in the nematode *C. elegans* [443]; 14) the sirtuins Sir1 in the yeast *S. cerevisiae* [405], SIR-2.1 in the nematode *C. elegans* [406, 413, 445], Sir2 in the fruit fly *D. melanogaster* [445], and SIRT1 in mice on a high-calorie diet [26, 27, 400, 448] - all of which define longevity by modulating numerous cellular processes; 15) the target of rapamycin complex 1 (TORC1), which in the yeasts *S. cerevisiae* and *Sch. pombe* controls cell metabolism, protein synthesis, resistance to many stresses, and autophagy [375, 407, 408]; 16) the nutrient-sensing protein kinases Sch9 and Gcn2, which define longevity by modulating cell cycle progression, transcription, protein synthesis, responses to various stresses, amino acid synthesis and sphingolipid synthesis in the yeast *S. cerevisiae* [375]; 17) cytosolic and mitochondrial superoxide dismutases Sod1 and Sod2 (respectively), both playing essential roles in longevity regulation by detoxifying the superoxide radical, modulating cellular respiration, and controlling

cell response to various stresses in the yeast *S. cerevisiae* [375, 436]; and 18) the non-selective autophagy pathway for degradation of various cellular organelles and macromolecules in the yeast *S. cerevisiae*, nematode *C. elegans*, and fruit fly *D. melanogaster* [25, 450, 451].

1.4.4 Processes targeted by aging-delaying and longevity-extending phytochemicals in evolutionarily distant organisms

Aging-delaying and longevity-extending phytochemicals have been shown to elicit changes in various cellular and organismal processes in organisms across phyla. These processes and organisms are outlined below and detailed in Table 1.2.

Yeasts

In the yeast *S. cerevisiae*, the changes elicited by longevity-extending phytochemicals include the following: 1) caffeine enhances transcription of genes encoding heat-shock proteins and molecular chaperones [407]; 2) cryptotanshinone reduces cellular levels of reactive oxygen species (ROS) [375]; 3) phloridzin decreases cellular levels of ROS, increases resistance to oxidative stress and superoxide dismutase activity, and activates transcription of the SOD1 (cytosolic superoxide dismutase), SOD2 (mitochondrial superoxide dismutase) and SIR2 (sirtuin) genes [436]; 4) quercetin reduces cellular levels of ROS, the efficiencies of glutathione oxidation and lipid peroxidation, the extent of protein carbonylation, and cell susceptibility to oxidative stress [437]; 5) resveratrol decreases the frequency of rDNA recombination [405]; and 6) spermidine reduces activities of histone acetyltransferases, increases the extent of histone H3 deacetylation, activates transcription of many autophagy-related genes, induces autophagy and delays onset of age-related necrotic cell death [25] (Table 1.2). In the yeast *Sch. pombe*, caffeine decelerates growth, causes cell-cycle arrest in G2, alters transcription of many nuclear genes, attenuates protein synthesis and inhibits phosphorylation of ribosomal S6 proteins [408] (Table 1.2).

The nematode *C. elegans*

In the nematode *C. elegans*, aging-delaying and longevity-extending phytochemicals cause the following changes: 1) caffeic and rosmarinic acids decrease susceptibility to thermal stress, reduce oxidative damage to macromolecules, lower body size, alter lipid metabolism and delay

reproductive timing [406]; 2) caffeine delays the onset of paralysis and reduces protein aggregation in nematode models of Alzheimer's and Huntington's diseases [409, 410]; 3) catechin lowers body length, reduces susceptibility to thermal stress, and elevates pumping rate [411]; 4) curcumin and tetrahydrocurcumin decrease cellular levels of ROS, the extent of oxidative damage to macromolecules, susceptibility to oxidative and thermal stresses, body length, and pumping rate [413]; 5) diallyl trisulfide alters expression of many nuclear genes involved in metabolism and stress response [419]; 6) ellagic acid delays the beginning of egg deposition and lowers the extent of oxidative damage to water-soluble metabolites [420]; 7) epigallocatechin gallate lowers cellular levels of ROS, reduces susceptibility to oxidative stress, decreases the extent of oxidative damage to lipids, attenuates expression of nuclear genes encoding HSP-16, enhances nuclear import of the transcription factor DAF-16/FOXO, and mitigates the formation of Aβ deposits [421, 422]; 8) ferulsinaic acid reduces susceptibility to oxidative and thermal stresses, lowers the extent of oxidative damage to lipids, and slows down the formation of advanced glycation end products [424]; 9) fisetin decreases cellular levels of ROS, lowers susceptibility to oxidative stress, reduces the extent of oxidative damage to macromolecules and stimulates nuclear import of the transcription factor DAF-16/FOXO [425]; 10) gallic acid increases body length, delays the beginning of egg deposition, and reduces the extent of oxidative damage to water-soluble metabolites [420]; 11) glaucarubinone increases the rate of oxygen consumption and reduces cellular levels of neutral lipids [426]; 12) icariin and icariside II lower susceptibility to oxidative and thermal stresses, decelerate age-related decline in locomotion, delay the onset of paralysis elicited by the proteotoxicity of polyQ and Aβ(1–42), and stimulate transcription of the SOD-3 and HSP-12.3 genes [428]; 13) kaempferol lowers cellular levels of ROS, reduces susceptibility to oxidative stress, decreases the extent of oxidative damage to macromolecules, and accelerates nuclear import of the transcription factor DAF-16/FOXO [425]; 14) myricetin decreases cellular levels of ROS, lowers the extent of oxidative damage to proteins, stimulates nuclear import of the transcription factor DAF-16/FOXO and enhances transcription of the SOD-3 gene [429]; 15) quercetin lowers cellular levels of ROS, decreases the extent of oxidative damage to macromolecules, elevates anti-oxidative activities, reduces susceptibility to thermal and oxidative stresses, reduces cellular levels of neutral lipids, and stimulates nuclear import of the transcription factor DAF-16/FOXO [406, 438–440]; 16) reserpine decreases susceptibility to thermal stress, decelerates the age-related declines in locomotion and pharyngeal pumping, and delays

postembryonic development [443, 444]; in the nematode model of Alzheimer's disease it also postpones the onset of paralysis caused by the proteotoxicity of Aβ [444]; 17) resveratrol and spermidine induce autophagy [25, 449]; 18) tannic acid decreases body length, lowers susceptibility to thermal and oxidative stresses, reduces cellular levels of triglycerides, and enhances anti-oxidant capacity [409, 420, 452]; and 19) tyrosol lowers susceptibility to thermal and oxidative stresses, decelerates the onset of an age-related decline in pharyngeal pumping, and stimulates transcription of nuclear genes encoding several heat-shock proteins [455] (Table 1.2).

The fruit fly *D. melanogaster*

In the fruit fly *D. melanogaster*, the alterations caused by aging-delaying and longevity-extending phytochemicals include the following: 1) curcumin and tetrahydrocurcumin lower the extent of macromolecular oxidative damage, reduce susceptibility to oxidative stress, and improve locomotor performance [414–416]; 2) nordihydroguaiaretic acid decreases the rate of oxygen consumption [433]; and 3) spermidine lowers susceptibility to oxidative stress, induces autophagy, decelerates age-related decline of locomotor activity, increases cellular levels of triglycerides, and alters relative levels of fatty acid species and phospholipid classes [450, 451] (Table 1.2).

The fish *Nothobranchius furzeri*

In the naturally short-lived fish *N. furzeri*, resveratrol delays age-related decay of locomotor activity and cognitive performances [446]. This phenolic phytochemical is also known to reduce neurofibrillary degeneration in the brain of *N. furzeri* [446] (Table 1.2).

Laboratory mouse

In laboratory mice (including transgenic mice models of several age-related diseases and mice on a high-calorie diet), aging-delaying and longevity-extending phytochemicals elicit the following changes: 1) allicin improves memory retention and acquisition in senescence-accelerated mice models [402–404, 453]; 2) celastrol decelerates weight loss, improves motor performance, increases the number of neurons and delays the onset of amyotrophic lateral sclerosis (ALS) in a transgenic mouse model of ALS [412]; 3) crocin increases hemoglobin and lymphocytes, and decreases white blood cell count and neutrophils in Dalton's lymphoma ascites-bearing mice [417]; 4) epicatechin reduces degeneration of aortic vessels and fat deposition,

decreases hydropic degeneration in the liver and markers of systematic inflammation, lowers levels of serum LDL cholesterol and circulating insulin-like growth factor 1, improves skeletal muscle stress output, increases concentration of hepatic glutathione and total superoxide dismutase activity, and elevates AMP-activated protein kinase activity in diabetic mice [423]; 5) nordihydroguaiaretic acid reduces motor dysfunction in a transgenic mouse model of ALS [430]; and 6) resveratrol increases insulin sensitivity, stimulates activities of AMP-activated protein kinase (AMPK) and peroxisome proliferator-activated receptor-gamma coactivator 1α (PGC-1α), lowers levels of insulin-like growth factor-1 (IGF-I), elevates the number of mitochondria, and alters transcription of many nuclear genes in mice on a high-calorie diet [448] (Table 1.2).

Cultured human cells

In cultured human cells, the alterations caused by aging-delaying and longevity-extending phytochemicals include the following: 1) cyanidin lowers oxidative damage to lipids and decreases susceptibility to oxidative stress in WI-38 human diploid fibroblasts [418]; 2) two 4-hydroxy-5-hydroxymethyl-[1,3]dioxolan-2,6'-spirane-5',6',7',8'-tetrahydro-indolizine-3'-carbaldehydes (HDTIC), HDTIC-1, and HDTIC-2 improve growth and proliferation, accelerate entry from G0 or G1 phase to S phase of the cell cycle, lower activity of the senescence-associated-β-galactosidase, and decrease formation of advanced glycation end products in human fetal lung diploid fibroblasts [427]; 3) oleuropein lowers cellular levels of ROS, reduces oxidative damage to proteins, increases the rate of proteasomal degradation of oxidatively damaged proteins, and decelerates age-related decline in proteasome activity in human embryonic fibroblasts [435]; 4) quercetin lowers the activity of the senescence-associated-β-galactosidase, decreases cellular levels of ROS, reduces susceptibility to oxidative stress, and stimulates proteasome activity in human embryonic fibroblasts [441]; and 5) spermidine lowers the extent of histone H3 acetylation in human peripheral blood mononuclear cells (PBMC) and induces autophagy in human HeLa cells [25] (Table 1.2).

1.4.5 Mechanisms of aging delay and longevity extension by phytochemicals are evolutionarily conserved

Findings described above in this section indicate that the mechanisms by which phytochemicals delay aging and extend the longevity of various heterotrophic organisms have

been conserved in the course of evolution. Indeed, longevity-extending phytochemicals increase lifespan of such evolutionarily distant organisms as yeasts, worms, flies, bees, mosquitoes, fishes, laboratory mice and laboratory rats [25, 375, 401–417, 419–426, 428–431, 433, 436, 437, 439, 440, 442–448, 450, 453, 455]; these phytochemicals also prolong the replicative lifespans of different lines of cultured human cells [25, 418, 427, 435, 441] (Table 1.2). Furthermore, the aging-delaying and lifespan-prolonging abilities of these phytochemicals rely on cellular proteins integrated into several evolutionarily conserved signaling pathways known to regulate longevity in organisms across phyla [1, 2, 5, 7, 24, 50, 55, 98, 210]. These nutrient-, energy- and stress-sensing pathways include the following: 1) the IIS pathway [406, 409–411, 413, 419, 420, 425, 428, 429, 438–440, 452, 455]; 2) the TOR pathway [375, 407, 408]; 3) the sirtuin-governed protein deacetylation module of the longevity signaling network integrating the IIS and TOR pathways [26, 27, 405, 413, 445, 448, 456]; 4) the OSR-1/UNC-43 (CaMKII)/SEK-1 (p38 MAPK) stress-responsive signaling pathway [406, 413, 440]; and 5) the non-selective autophagy pathway for degradation of various cellular organelles and macromolecules [25, 450, 451] (Table 1.2). Moreover, these aging-delaying and lifespan-prolonging phytochemicals postpone the onset of several longevity-defining cellular processes called ″the cellular and molecular hallmarks of aging″ [1, 2, 5, 24, 50, 54, 307, 457–462]. Out of the nine commonly accepted cellular and molecular hallmarks of aging [50], the aging-delaying and lifespan-prolonging phytochemicals are known to delay the development of the following seven common traits of aging in evolutionarily distant heterotrophic organisms: 1) genomic instability [405]; 2) epigenetic alterations [25]; 3) loss of proteostasis [25, 406, 407, 409, 410, 412–416, 418, 420–425, 428–430, 435, 437, 441, 444, 449, 455]; 4) deregulated nutrient sensing [406, 409, 410, 413, 425, 428, 448]; 5) mitochondrial dysfunction [375, 413, 421–423, 425, 426, 429, 433, 435, 436, 437, 441, 448]; 6) cellular senescence [402–404, 408, 427, 441, 453]; and 7) altered intercellular communication [402–404, 412, 417, 446, 450, 453] (Table 1.2).

1.5 Thesis outline and contributions of colleagues

The objective of studies described in Chapter 2 was to make a first step towards uncovering novel aging-delaying and longevity-extending chemical compounds of plant origin. To attend this objective, Paméla Dakik, Vicky Lutchman, Mélissa McAuley and myself conducted a screen for plant extracts (PEs) that can prolong yeast chronological lifespan (CLS). Our screen revealed six PEs that increase yeast CLS. One of these six PEs is PE21, an extract from the white willow *Salix alba*. I investigated various properties of PE21. I demonstrated that PE21 is a geroprotector which delays the onset and slows the progression of yeast chronological aging by eliciting a hormetic stress response. I also found that PE21 affects various longevity-defining cellular processes in chronologically aging yeast. I conducted experiments shown in Figures 2.6-2.16, 2.19 and 2.20, and prepared these figures. I also prepared figure 2.21. The experiments shown in Figures 2.1-2.5 were carried out by Paméla Dakik, Vicky Lutchman, Mélissa McAuley and me. The experiments shown in Figures 2.17 and 2.18 were carried out by me. All findings described in Chapter 2 have been published in Oncotarget. 2016; 7:16542-16566. Dr. Titorenko provided the intellectual leadership of this project. He also edited the first draft of Chapter 2 of the thesis and the entire manuscript of the above article.

Since studies described in Chapter 2 revealed that PE21 promotes rapid age-related degradation of neutral lipids deposited in LD, the objective of studies described in Chapter 3 was to determine whether PE21 may affect the abundance of other lipid classes of chronologically aging yeast under non-CR conditions. We found that, in addition to its effect on neutral lipids, PE21 alters the concentrations of several other lipid classes and that such alterations occur in an age-related manner. These findings indicated that PE21 causes a specific remodeling of lipid metabolism and transport in chronologically aging yeast. Based on the abilities of PE21 to elicit such remodeling of lipid metabolism and transport (as described in this chapter of the thesis) and to impose changes in certain cellular processes (as outlined in chapter 2 of the thesis) within yeast cultured under non-CR conditions, in Chapter 3 we put forward a hypothesis that there may be at least three different mechanisms by which PE21 delays yeast chronological aging and extends yeast CLS. Chapter 3 describes studies that confirm the existence of the first proposed mechanism underlying aging delay and longevity extension by PE21. This mechanism consists in the ability of PE21 to delay an age-related onset of liponecrotic RCD. I conducted experiments shown in Figures 3.10-3.12 and prepared these figures. I also prepared Figures 3.2-3.4. The experiments

shown in Figures 3.1 and 3.5-3.9 were performed by Karamat Mohammad, Veronika Svistkova, Paméla Dakik, Monica Enith Lozano Rodriguez and me. All findings described in Chapter 3 have been submitted for publication as a manuscript of a research paper. Titorenko provided intellectual leadership of this project. He also edited the first draft of Chapter 3 of the thesis and the above manuscript.

The objective of studies described in Chapter 4 was to make a first step towards testing our hypothesis on the second and third mechanisms of yeast longevity extension by PE21 (this hypothesis is described in Chapter 3 of the thesis). To attain this objective, we wanted to get a broader view of cellular processes that are influenced by PE21 in chronologically aging yeast. We, therefore, used quantitative mass spectrometry to compare the cellular proteomes of yeast cultured in the presence of PE21 or in its absence. We found that PE21 stimulates the establishment of a distinct cellular proteome pattern in yeast and that the efficiency with which PE21 changes this pattern is gradually increased with the chronological age of yeast cells. We then evaluated how single-gene-deletion mutations eliminating proteins that are up- or downregulated by PE21 affect the geroprotective efficiency of PE21. This evaluation supported our hypothesis on the second mechanism by which PE21 delays yeast chronological aging and extends yeast CLS. In this mechanism, PE21 stimulates the UPR^{ER} system, thereby decelerating an age-related decline in protein and lipid homeostasis and slowing down an aging-associated deterioration of cell resistance to oxidative and thermal stresses. I conducted experiments shown in Figures 4.1-4.4 and prepared these figures. The experiments shown in Figures 4.5-4.7 were carried out by Paméla Dakik, Monica Enith Lozano Rodriguez and me. All findings described in Chapter 4 have been submitted for publication as a manuscript of a research paper. Titorenko provided intellectual leadership of this project. He also edited the first draft of Chapter 4 of the thesis and the above manuscript.

The objective of studies described in Chapter 5 was to test our hypothesis on the third mechanism by which PE21 may prolong the longevity of chronologically aging yeast. This hypothesis posits that the PE21-dependent changes in the membrane lipidome of mitochondria may remodel certain processes taking place in these organelles, thus altering mitochondrial functionality and delaying yeast chronological aging. We found that PE21 causes changes in the concentrations of many mitochondrial proteins. We then examined how single-gene-deletion mutations eliminating mitochondrial proteins that are up- or downregulated by PE21 influence the

geroprotective efficiency of PE21. This examination validated our hypothesis on the third mechanism by which PE21 delays yeast chronological aging and prolongs yeast CLS. I conducted experiments shown in Figures 5.1-5.3 and prepared these figures. The experiments shown in Figures 5.4-5.6 were carried out by Paméla Dakik, Monica Enith Lozano Rodriguez and me. All findings described in Chapter 5 have been submitted for publication as a manuscript of a research paper. Titorenko provided intellectual leadership of this project. He also edited the first draft of Chapter 5 of the thesis and the above manuscript.

2 Discovery of PE21, a plant extract that delays yeast chronological aging and has different effects on longevity-defining cellular processes

2.1 Introduction

Our research is aimed at using *S. cerevisiae* as a model organism to discover chemical compounds that can slow aging and delay the onset of age-related diseases in evolutionarily distant eukaryotic organisms. Some of such geroprotective compounds have been previously revealed in natural products extracted from certain plants [29, 373, 463]. As a first step towards uncovering novel aging-delaying and longevity-extending chemical compounds of plant origin, we conducted a screen for plant extracts (PEs) that can prolong yeast chronological lifespan (CLS). Our screen revealed six PEs that increase yeast CLS. One of these six PEs is PE21, an extract from the white willow *Salix alba*. We found that PE21 extends the longevity of chronologically aging yeast to a significantly greater extent than any of the presently known longevity-extending chemical compounds. We demonstrated that PE21 decelerates yeast chronological aging by influencing a distinct set of longevity-defining cellular processes. Chapter 2 describes these findings.

2.2 Materials and methods

2.2.1 Yeast strains, media and growth conditions

The wild-type strain *Saccharomyces cerevisiae* BY4742 (*MATα his3Δ1 leu2Δ0 lys2Δ0 ura3Δ0*) from Thermo Scientific/Open Biosystems were grown in synthetic minimal YNB medium (0.67% Yeast Nitrogen Base without amino acids) initially containing 0.5% or 2% glucose, 20 mg/l *L*-histidine, 30 mg/l *L*-leucine, 30 mg/l *L*-lysine and 20 mg/l uracil. Cells were cultured at 30°C with rotational shaking at 200 rpm in Erlenmeyer flasks at a "flask volume/medium volume" ratio of 5:1.

2.2.2 CLS assay

A sample of cells was taken from a culture at a certain day following cell inoculation and PE addition into the medium. A fraction of the sample was diluted to determine the total number of cells using a hemocytometer. Another fraction of the cell sample was diluted, and serial dilutions of cells were plated in duplicate onto YPD medium (1% yeast extract, 2% peptone) containing 2%

glucose as carbon source. After 2 days of incubation at 30ºC, the number of colony-forming units (CFU) per plate was counted. The number of CFU was defined as the number of viable cells in a sample. For each culture, the percentage of viable cells was calculated as follows: (number of viable cells per ml/total number of cells per ml) × 100. The percentage of viable cells in the mid-logarithmic growth phase was set at 100%.

2.2.3 A screen for PEs that can extend yeast CLS

CLS analysis in the presence of various PEs was performed as follows. A 20% stock solution of each PE in ethanol was made on the day of adding this PE to cell cultures. For each PE, the stock solution was added to the growth medium with 2% glucose immediately following cell inoculation into the medium. The final concentration of each PE in the medium was 0.02%, 0.04%, 0.06%, 0.08%, 0.1%, 0.3%, 0.5% or 1.0% (w/v).

2.2.4 Oxygen consumption assay (cellular respiration measurement)

A sample of cells was taken from a culture at a certain time-point. Cells were pelleted by centrifugation and resuspended in 1 ml of fresh YPD (1% yeast extract, 2% peptone) medium containing 0.05% glucose. Oxygen uptake by cells was measured continuously in a 2-ml stirred chamber using a custom-designed biological oxygen monitor (Science Technical Center of Concordia University) equipped with a Clark-type oxygen electrode.

2.2.5 Live cell fluorescence microscopy for mitochondrial membrane potential measurement

The mitochondrial membrane potential ($\Delta\Psi$) was measured in live yeast by fluorescence microscopy of Rhodamine 123 (R123) staining. For R123 staining, 5×10^6 cells were harvested by centrifugation for 1 min at 21000 × g at room temperature and then resuspended in 100 µl of 50 mM sodium citrate buffer (pH 5.0) containing 2% glucose. R123 was added to a final concentration of 10 µM. Following incubation in the dark for 30 min at room temperature, the cells were washed twice in 50 mM sodium citrate buffer (pH 5.0) containing 2% glucose and then analyzed by fluorescence microscopy. Images were collected with a Zeiss Axioplan fluorescence microscope (Zeiss) mounted with a SPOT Insight 2-megapixel color mosaic digital camera (Spot Diagnostic Instruments). To evaluate the percentage of R123-positive cells, the UTHSCSA Image

Tool (Version 3.0) software was used to calculate both the total number of cells and the number of stained cells. Fluorescence of individual R123-positive cells in arbitrary units was determined by using the UTHSCSA Image Tool software (Version 3.0). In each of three independent experiments, the value of the median fluorescence was calculated by analyzing at least 800-1000 cells that were collected at each time-point. The median fluorescence values were plotted as a function of the number of days cells were cultured.

2.2.6 Live cell fluorescence microscopy for measuring the formation of reactive oxygen species (ROS)

ROS production was tested microscopically by incubating cells with Dihydrorhodamine 123 (DHR). Inside a cell, this non-fluorescent compound can be oxidized to the fluorescent chromophore Rhodamine 123 by ROS. DHR was stored in the dark at -20^{o}C as 50 µl aliquots of a 1 mg/ml solution in ethanol. The staining of cells with DHR was carried out as follows. For cell cultures with a titer of ~ 10^7 cells/ml, 100 µl was taken out of the culture to be treated. If the cell titer was lower, proportionally larger volumes were used. 6 µl of the 1 mg/ml DHR was added to each 100 µl aliquot of the culture. After a 2-h incubation in the dark at room temperature, the samples were centrifuged at 21000 × g for 5 min. Pellets were resuspended in 10 ml of PBS buffer (20 mM KH_2PO_4/KOH, pH 7.5, and 150 mM NaCl). Each sample was then supplemented with 5 µl of mounting medium, added to a microscope slide, covered with a coverslip, and sealed using nail polish. Once the slides were prepared, they were visualized under the Zeiss Axioplan fluorescence microscope mounted with a SPOT Insight 2-megapixel color mosaic digital camera. Fluorescence of individual DHR-positive cells in arbitrary units was determined by using the UTHSCSA Image Tool software (Version 3.0). In each of 3-5 independent experiments, the value of the median fluorescence was calculated by analyzing at least 800-1000 cells that were collected at each time point. The median fluorescence values were plotted as a function of the number of days cells were cultured.

2.2.7 Live cell fluorescence microscopy for examining neutral lipids deposited in lipid droplets (LDs)

BODIPY 493/503 staining for monitoring neutral lipids deposited in LDs was performed as follows. Yeast cells (10^7) were harvested by centrifugation for 1 min at 21000 × g at room

temperature. The cells in the pellet were permeabilized by treatment with 100 µL Triton X-100 for 10 mins and incubated with 10 µM BODIPY 493/503 in 20 mM Tris-HCl (pH 7.5), 150 mM NaCl for 15 min to stain LDs. Live imaging was performed on a Leica DM6000B epifluorescence microscope equipped with a high-resolution Hamamatsu Orca ER CCD camera using oil immersion and a 100X objective. Images were acquired with 20-ms exposures using PerkinElmer Volocity software. Image files were exported as TIFFs then opened in ImageJ where the percentage of cells with LDs was counted.

2.2.8 Measurement of oxidative damage to cellular proteins

Yeast cells (10^7) were harvested by centrifugation for 1 min at 21000 × g at room temperature. The cell pellet was resuspended in 1 ml of ice-cold 50 mM KH_2PO_4/KOH buffer (pH 7.5) + 1 mM EDTA. The cells were sonicated on ice, harvested by centrifugation for 5 min at 21000 × g at 4ºC and then resuspended in 200 µl of ice-cold 50 mM KH_2PO_4/KOH buffer (pH 7.5) + 1 mM EDTA. The Protein Carbonyl Assay Kit assay kit (#10005020; Cayman Chemical) was used to measure protein carbonylation (i.e. protein oxidative damage) as the amount of protein-hydrazone produced in the DNPH (2,4-dinitrophenylhydrazine) reaction at an absorbance of 360 nm.

2.2.9 Measurement of oxidative damage to cellular membrane lipids

Yeast cells (10^7) were harvested by centrifugation for 3 min at 16000 × g at room temperature. The cell pellet was washed with ice-cold ABC buffer (155 mM ammonium bicarbonate, pH 8.0) by centrifugation for 3 min at 16000 × g at 4ºC, and then resuspended in 1 ml of ice-cold ABC buffer. Glass beads (200 µl) were added, and the sample was vortexed for 5 min. Ice-cold nanopure water (1 ml) was added, and the sample was transferred to a 15-ml glass centrifuge tube. Then, 3 ml of a chloroform/methanol (17:1) mixture was added, and the sample was vortexed at 4°C for 2 h. The sample was subjected to centrifugation at 3000 × g for 5 min at room temperature to form two phases. The lower organic phase was transferred to a new 15-ml glass tube. The solvent was evaporated off under nitrogen flow or in a vacuum evaporator. The lipid film was dissolved in 100 µl of methanol/chloroform (2:1) mixture. The PeroXOquant Quantitative Peroxide Assay Kit assay kit (#23285; Thermo Scientific Pierce) was used to measure

lipid hydroperoxides as the Fe^{3+} complexes with the xylenol orange dye at an absorbance of 595 nm.

2.2.10 Measurement of the frequency of spontaneous mutations in nuclear DNA

The frequency of spontaneous point mutations in the *CAN1* gene of nuclear DNA was evaluated by measuring the frequency of mutations that caused resistance to the antibiotic canavanine. A sample of cells was removed from each culture at various time-points. Cells were plated in triplicate onto YNB (0.67% Yeast Nitrogen Base without amino acids) plates containing 2% glucose and supplemented with *L*-canavanine (50 mg/l), histidine, leucine, lysine and uracil. In addition, serial dilutions of each sample were plated in triplicate onto YPD plates containing 2% glucose for measuring the number of viable cells. The number of CFU was counted after 4 days of incubation at 30ºC. For each culture, the frequency of mutations that caused resistance to canavanine was calculated as follows: number of CFU per ml on YNB plates containing 2% glucose, *L*-canavanine (50 mg/l), histidine, leucine, lysine and uracil/number of CFU per ml on YPD plates containing 2% glucose.

2.2.11 Measurement of the frequency of spontaneous mutations in mitochondrial DNA

The frequency of spontaneous point mutations in the *rib2* and *rib3* loci of mitochondrial DNA (mtDNA) was evaluated by measuring the frequency of mtDNA mutations that caused resistance to the antibiotic erythromycin. These mutations only impair mtDNA. A sample of cells was removed from each culture at various time-points. Cells were plated in triplicate onto YPG plates containing 3% glycerol and erythromycin (1 mg/ml). In addition, serial dilutions of each sample were plated in triplicate onto YPG plates containing 3% glycerol as a carbon source for measuring the number of respiratory-competent (rho^+) cells. The number of CFU was counted after 6 days of incubation at 30ºC. For each culture, the frequency of mutations that caused resistance to erythromycin was calculated as follows: number of CFU per ml on YPG plates containing 3% glycerol and erythromycin/number of CFU per ml on YPG plates containing 3% glycerol.

2.2.12 Plating assays for the analysis of resistance to oxidative and thermal stresses

For the analysis of hydrogen peroxide (oxidative stress) resistance, serial dilutions (1:100 to $1:10^5$) of cells removed from each culture at various time-points were spotted onto two sets of plates. One set of plates contained YPD medium with 2% glucose alone, whereas the other set contained YPD medium with 2% glucose supplemented with 5 mM hydrogen peroxide. Pictures were taken after 3 days of incubation at 30°C.

For the analysis of thermal stress resistance, serial dilutions (1:100 to $1:10^5$) of cells removed from each culture at various time-points were spotted onto two sets of plates containing YPD medium with 2% glucose. One set of plates was incubated at 30°C. The other set of plates was initially incubated at 60°C for 60 min and was then transferred to 30°C. Pictures were taken after 3 days of incubation at 30°C.

2.2.13 Miscellaneous procedures

The age-specific mortality rate (qx) [465, 469], Gompertz slope or mortality rate coefficient (α) [467, 469], and mortality rate doubling time (MRDT) [467, 469] were calculated as previously described.

2.2.14 Statistical analysis

Statistical analysis was performed using Microsoft Excel's Analysis ToolPack-VBA. All data are presented as mean ± SEM. The p values for comparing the means of two groups (using an unpaired two-tailed t-test) and survival curves (using a two-tailed t-test) were calculated with the help of the GraphPad Prism statistics software.

2.3 Results and Discussion

2.3.1 A screen for PEs that can extend the longevity of chronologically aging yeast

We screened a library of PEs for extracts that can increase yeast CLS. This library includes 35 different PEs of known origin and properties (Tables 2.1 and 2.2, respectively). To perform the screen for lifespan-extending PEs, we used a robust assay for measuring yeast CLS. This assay was like the one described previously [237], but the wild-type strain BY4742 was cultured in the synthetic minimal YNB medium initially containing 2% glucose (instead of the nutrient-rich YPD medium supplemented with 0.5% glucose). Yeast cells cultured on 2% glucose are not limited in

calorie supply; these cells age chronologically under so-called non-caloric restriction (non-CR) conditions that accelerate aging in different yeast genetic backgrounds, including BY4742 [2, 5, 7].

Table 2.1. A list of plant extracts that have been used in this study. All the plant extracts were obtained from the same commercial source, Idunn Technologies.

Abbreviated name	Botanical name	Plant part used
PE1	*Echinacea purpurea*	Whole plant
PE2	*Astragalus membranaceous*	Root
PE3	*Rhodiola rosea L.*	Root
PE4	*Cimicifuga racemosa*	Root and rhizome
PE5	*Valeriana officinalis L.*	Root
PE6	*Passiflora incarnate L.*	Whole plant
PE7	*Polygonum cuspidatum*	Root and rhizome
PE8	*Ginkgo biloba*	Leaf
PE9	*Zingiber officinale Roscoe*	Rhizome
PE10	*Theobroma cacao L.*	Cacao nibs
PE11	*Camellia sinensis L. Kuntze*	Leaf
PE12	*Apium graveolens L.*	Seed
PE13	*Scutellaria baicalensis*	Root
PE14	*Euterpe oleracea*	Fruit
PE15	*Withania somnifera*	Root and leaf
PE16	*Phyllanthus emblica*	Fruit
PE17	*Camellia sinensis*	Leaf
PE18	*Pueraria lobata*	Root
PE19	*Silybum marianum*	Seed
PE20	*Eleutherococcus senticosus*	Root and stem
PE21	*Salix alba*	Bark
PE22	*Glycine max L.*	Bean
PE24	*Calendula officinalis*	Flower
PE25	*Salvia miltiorrhiza*	Root
PE27	*Panax quinquefolium*	Root
PE28	*Harpagophytum procumbens*	Root
PE29	*Olea europaea L.*	Leaf
PE30	*Gentiana lutea*	Root
PE31	*Piper nigrum*	Fruit
PE32	*Aesculus hippocastanum*	Seed
PE33	*Mallus pumila Mill.*	Fruit
PE34	*Fragaria spp.*	Fruit
PE35	*Ribes nigrum*	Leaf
PE36	*Dioscorea opposita*	Root
PE37	*Cinnamomum verum*	Bark

Table 2.2. Properties of plant extracts that have been used in this study.

Abbreviated name	Properties
PE1	Extraction solvent: ethanol (75%)/water (25%). Extract ratio: 4/1. Composition: natural extract, maltodextrin.
PE2	Extraction solvent: denatured ethanol (70%)/water (30%). Extract ratio: 10/1. Composition: natural extract (40-50%), gum arabic (50-60%).
PE3	Extraction solvent: ethanol (60-80%)/water (40-20%). Extract ratio: 15-20/1. Composition: natural extract (80-100%), maltodextrin (0-20%).
PE4	Extract ratio: 6-8/1. Composition: natural extract (28-38%), maltodextrin (60-70%), tricalcium phosphate (0-5%).
PE5	Extraction solvent: denatured ethanol/water. Extract ratio: ~ 6/1. Composition: natural extract, maltodextrin, silica (0-1%).
PE6	Extraction solvent: water (100%). Extract ratio: 4/1. Composition: natural extract, maltodextrin.
PE7	Extraction solvent: ethanol (80%)/water (20%). Extract ratio: 40/1. Composition: natural extract (90-100%), maltodextrin (0-10%).
PE8	Extraction solvent: ethanol/water. Extract ratio: 50/1. Composition: natural extract.
PE9	Extraction solvent: ethanol/water. Composition: natural extract (96%), gingerols (4%).
PE10	Natural powder/final product ratio: 2-3/1. Composition: natural powder.
PE11	Extraction solvent: ethyl acetate (90%)/water (10%). Extract ratio: 6/1. Composition: natural extract (100%).
PE12	Extraction solvent: ethanol (90%)/water (10%). Extract ratio: 8/1. Composition: natural extract, maltodextrin, modified starch, silica.
PE13	Extraction solvent: ethanol/water. Extract ratio: 4/1. Composition: natural extract.
PE14	Extraction solvent: ethanol/water. Extract ratio: 4/1. Composition: natural extract.
PE15	Extraction solvent: water. Extract ratio: 9/1. Composition: withanolide glycoside conjugates (10%), oligosaccharides (32%), free withanolides (0.5%).
PE16	Extraction solvent: water. Composition: hydrolysable tannins (>60%), including Emblicanin-A, Emblicanin-B, Punigluconin, Pedunculagin.
PE17	Composition: tea polyphenols (>90%), including epigallocatechin gallate (>40%).
PE18	Composition: flavonoids (>40%), including puerarin.
PE19	Extraction solvent: ethanol/water. Composition: silymarin (>80%).
PE20	Extraction solvent: water. Composition: eleutheroside B+E (>0.8%).
PE21	Extraction solvent: ethanol/water. Composition: salicin (>25%).
PE22	Composition: isoflavones (40%).
PE24	Composition: lutein (>5%).
PE25	Composition: tanshinones, isotanshinones, cryptotanshinone, isocryptotanshinone, dihydrotanshinone, hydroxytanshinones.

PE27	Composition: ginsenosides (10%, by HPLC-UV), quintozene-free.
PE28	Extraction solvent: ethanol/water. Extract ratio: 40/1. Composition: harpagosides (20%, by HPLC-UV).
PE29	Extraction solvent: ethanol (70%)/water (30%). Extract ratio: 5-10/1. Composition: natural extract, maltodextrin, silica (0.2%).
PE30	Composition: isogentisin (0.04%).
PE31	Extraction solvent: ethanol. Extract ratio: 10/1. Composition: piperine (>90%).
PE32	Composition: aescin (20%).
PE33	Extraction solvent: ethanol (70%)/water (30%). Extract ratio: 120-130/1. Composition: natural extract (60-70%), maltodextrin (30-40%).
PE34	Extract ratio: 5/1. Composition: natural extract, including polyphenols (>2%).
PE35	Extraction solvent: water. Composition: polyphenols (15%, by HPLC-UV).
PE36	Composition: diosgenine (>16%, by HPLC-UV).
PE37	Extraction solvent: water. Composition: polyphenols (25%, by HPLC-UV).

In our screen for longevity-extending PEs, each PE from the library was added to the growth medium at the time of cell inoculation at a final concentration in the 0.02% to 1.0% range. Some PEs from the library did not alter the mean and maximum CLS of yeast under non-CR conditions at any concentration examined; among these PEs were PE9, PE13, PE16, PE22, PE28 and PE36 (Figures 2.2 - 2.5). Many PEs from the library shortened the mean and/or maximum CLS of yeast under non-CR conditions at final concentrations ranging from 0.08% to 1.0%; among these PEs were PE1 - PE3, PE7, PE10, PE11, PE14, PE15, PE17 - PE20, PE24, PE25, PE27, PE29 - PE35 and PE37 (Figures 2.1 - 2.5). Finally, 6 of the 35 PEs from the library significantly increased both the mean and maximum CLS of yeast under non-CR conditions if added at final concentrations ranging from 0.04% to 1.0% (Figures 2.1 - 2.3). A group of these longevity-extending PEs included the following extracts: 1) 0.5% PE4 from *Cimicifuga racemose* [464]; 2) 0.5% PE5 from *Valeriana officinalis L*. [464]; 3) 1.0% PE6 from *Passiflora incarnata L*. [464]; 4) 0.3% PE8 from *Ginkgo biloba* [464]; 5) 0.1% PE12 from *Apium graveolens L*. [464]; and 6) 0.1% PE21 from *Salix alba* (Figure 2.3, Figure 2.6, Figures 2.8A and 2.8B). PE21 did not affect growth rates in logarithmic (L) and post-diauxic (PD) phases and did not influence the maximum cell density in stationary (ST) phase of yeast cultures under non-CR conditions on 2% glucose (Figure 2.9). Thus, the observed lifespan extension by PE21 is unlikely to be caused by its ability to decrease growth rate or to make yeast more resistant to toxic substances accumulated during culturing in the synthetic minimal YNB medium.

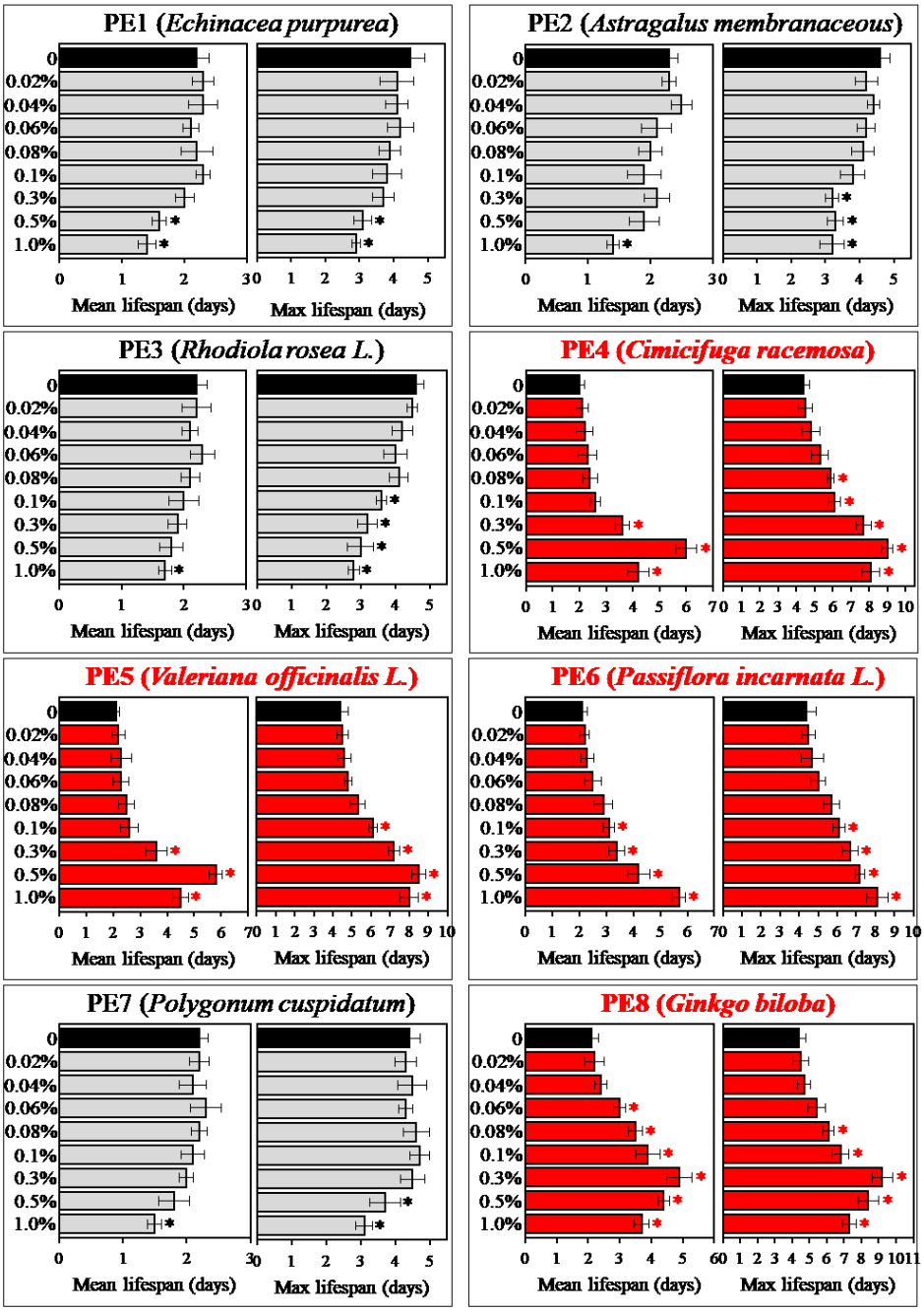

Figure 2.1. PE4, PE5, PE6 and PE8, but not PE1, PE2, PE3 or PE7, extend the CLS of WT yeast grown under non-CR conditions. WT cells were grown in synthetic minimal YNB medium initially containing 2% glucose (non-CR conditions), in the presence of a PE or in its absence. The mean and maximum lifespans of a chronologically aging WT strain cultured under non-CR conditions without a PE or with a PE added at various concentrations are shown; data are presented as means ± SEM (n = 6-21; * $p < 0.05$; the p values for comparing the means of two groups were calculated with the help of the GraphPad Prism statistics software using an unpaired two-tailed t test). Note that PE1, PE2, PE3, and PE7 can shorten the CLS of WT yeast under non-CR conditions if added at high concentrations (n = 6; * $p < 0.05$; the p values for comparing the means of two groups were calculated with the help of the GraphPad Prism statistics software using an unpaired two-tailed t test).

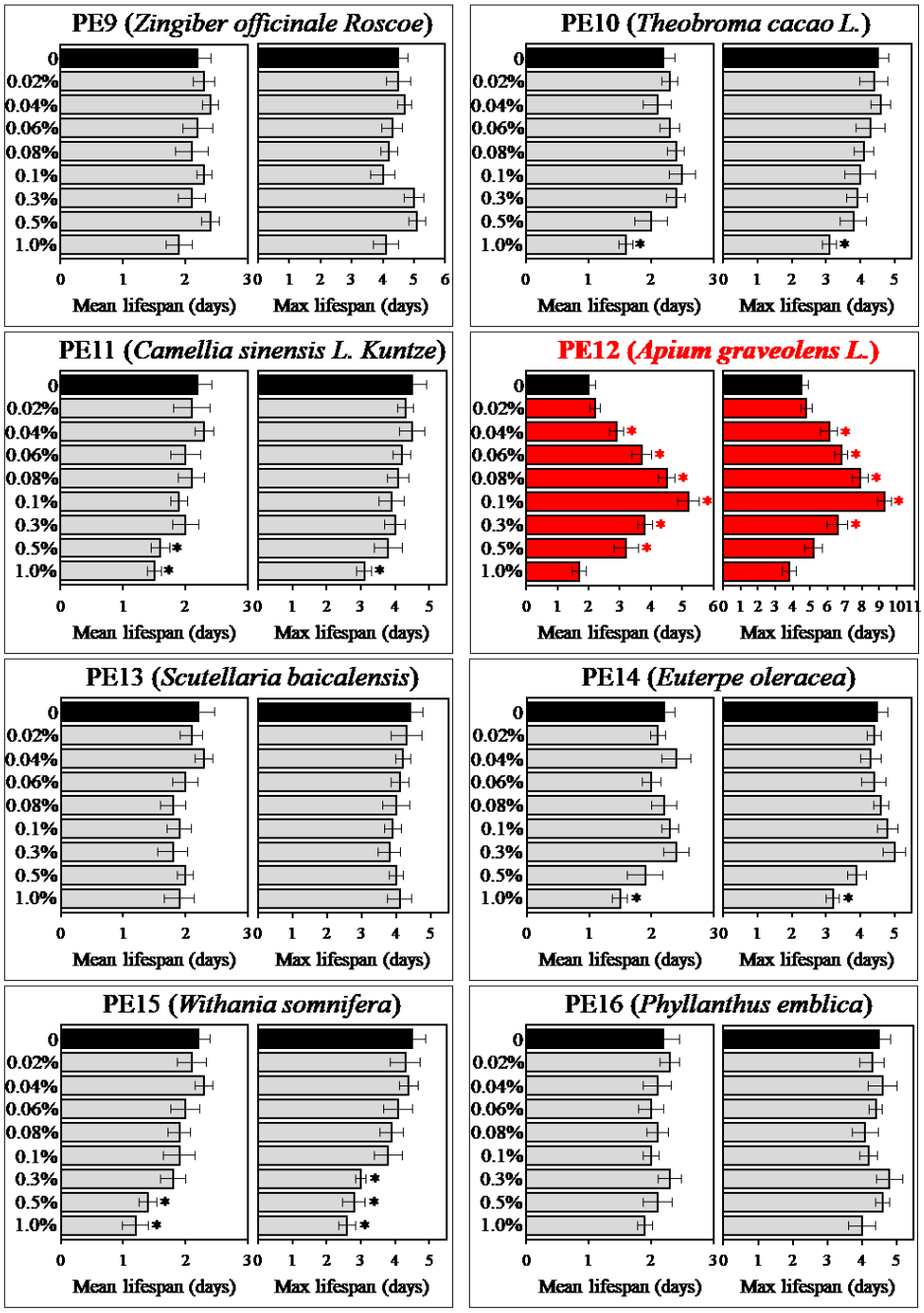

Figure 2.2. PE12, but not PE9, PE10, PE11, PE13, PE14, PE15 or PE16, extends the CLS of WT yeast grown under non-CR conditions. WT cells were grown in synthetic minimal YNB medium initially containing 2% glucose (non-CR conditions), in the presence of a PE or in its absence. The mean and maximum lifespans of a chronologically aging WT strain cultured under non-CR conditions without a PE or with a PE added at various concentrations are shown; data are presented as means ± SEM (n = 6-29; * $p < 0.05$; the p values for comparing the means of two groups were calculated with the help of the GraphPad Prism statistics software using an unpaired two-tailed t test). Note that PE10, PE11, PE14, and PE15 can shorten the CLS of WT yeast under non-CR conditions if added at high concentrations (n = 6; * $p < 0.05$; the p values for comparing the means of two groups were calculated with the help of the GraphPad Prism statistics software using an unpaired two-tailed t test).

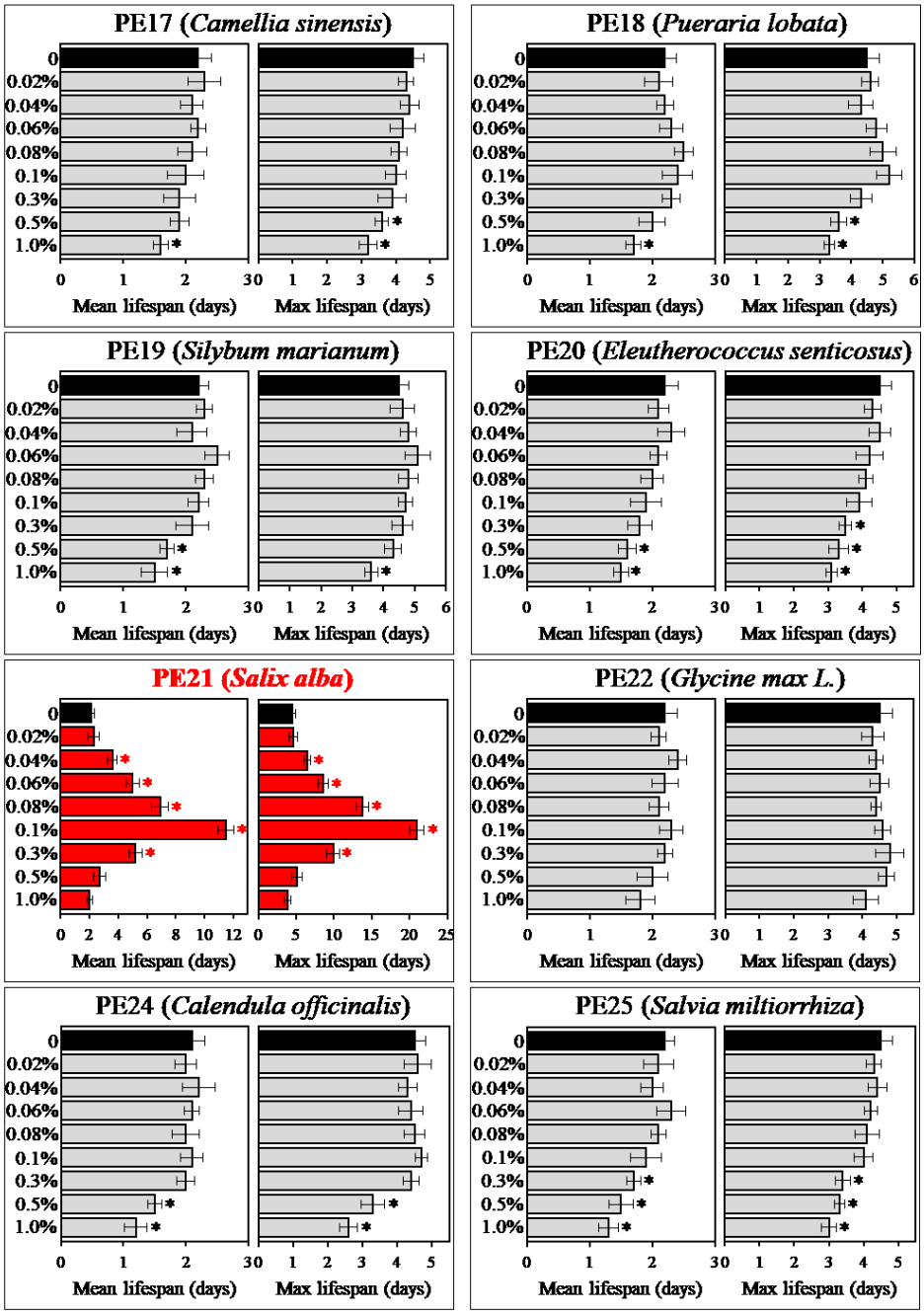

Figure 2.3. PE21, but not PE17, PE18, PE19, PE20, PE22, PE24 or PE25, extends the CLS of WT yeast grown under non-CR conditions. WT cells were grown in synthetic minimal YNB medium initially containing 2% glucose (non-CR conditions), in the presence of a PE or in its absence. The mean and maximum lifespans of a chronologically aging WT strain cultured under non-CR conditions without a PE or with a PE added at various concentrations are shown; data are presented as means ± SEM (n = 6-35; * $p < 0.05$; the p values for comparing the means of two groups were calculated with the help of the GraphPad Prism statistics software using an unpaired two-tailed *t* test). Note that PE17, PE18, PE19, PE20, PE24 and PE25 can shorten the CLS of WT yeast under non-CR conditions if added at high concentrations (n = 6; * $p < 0.05$; the *p* values for comparing the means of two groups were calculated with the help of the GraphPad Prism statistics software using an unpaired two-tailed *t* test).

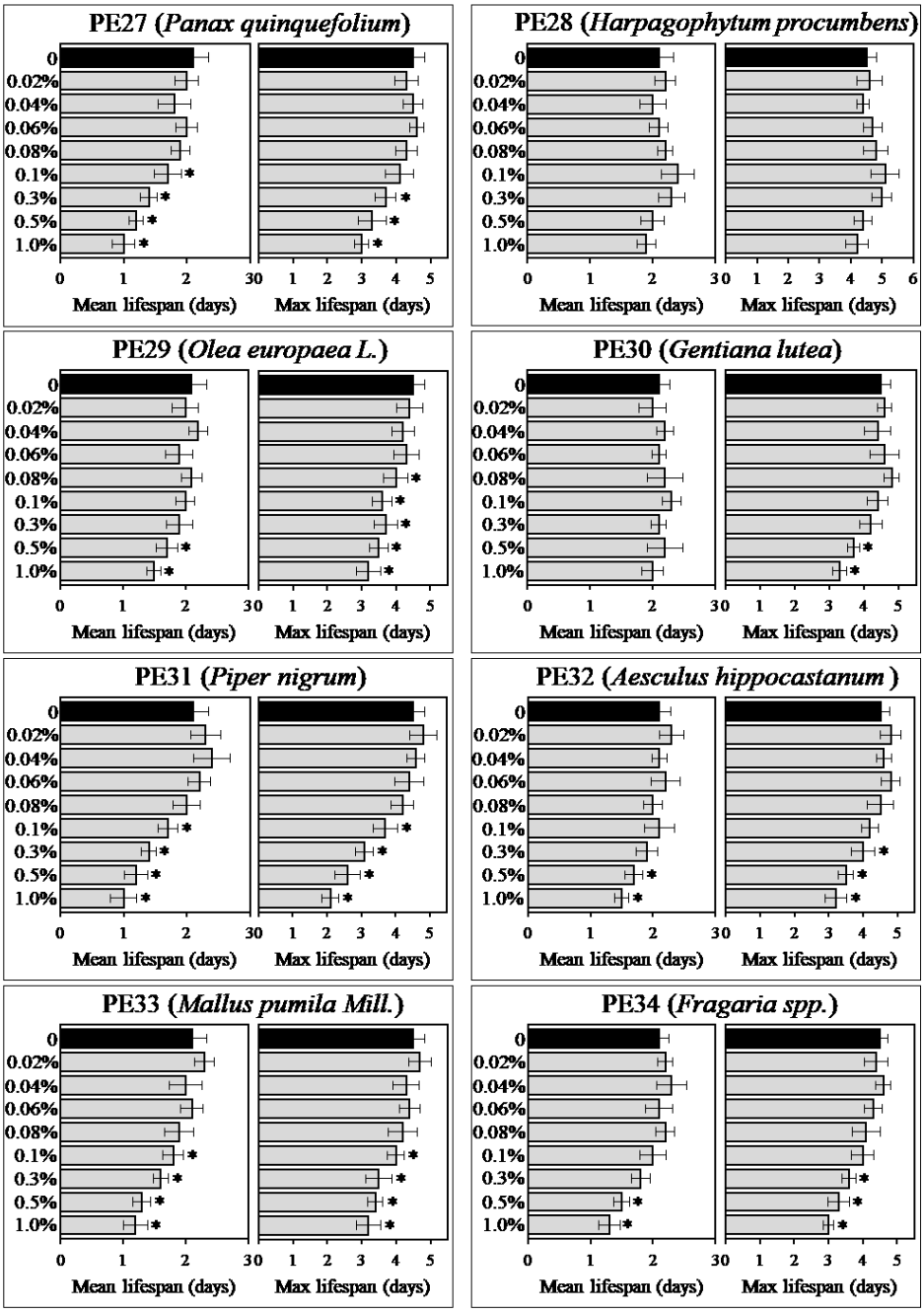

Figure 2.4. PE27, PE28, PE29, PE30, PE31, PE32, PE33 and PE34 do not extend the CLS of WT yeast grown under non-CR conditions. WT cells were grown in synthetic minimal YNB medium initially containing 2% glucose (non-CR conditions), in the presence of a PE or in its absence. The mean and maximum lifespans of a chronologically aging WT strain cultured under non-CR conditions without a PE or with a PE added at various concentrations are shown; data are presented as means ± SEM (n = 5-6; * $p < 0.05$; the p values for comparing the means of two groups were calculated with the help of the GraphPad Prism statistics software using an unpaired two-tailed t test). Note that PE 27, PE29, PE30, PE31, PE32, PE33 and PE34 can shorten the CLS of WT yeast under non-CR conditions if added at high concentrations (n = 6; * $p < 0.05$; the p values for comparing the means of two groups were calculated with the help of the GraphPad Prism statistics software using an unpaired two-tailed t test).

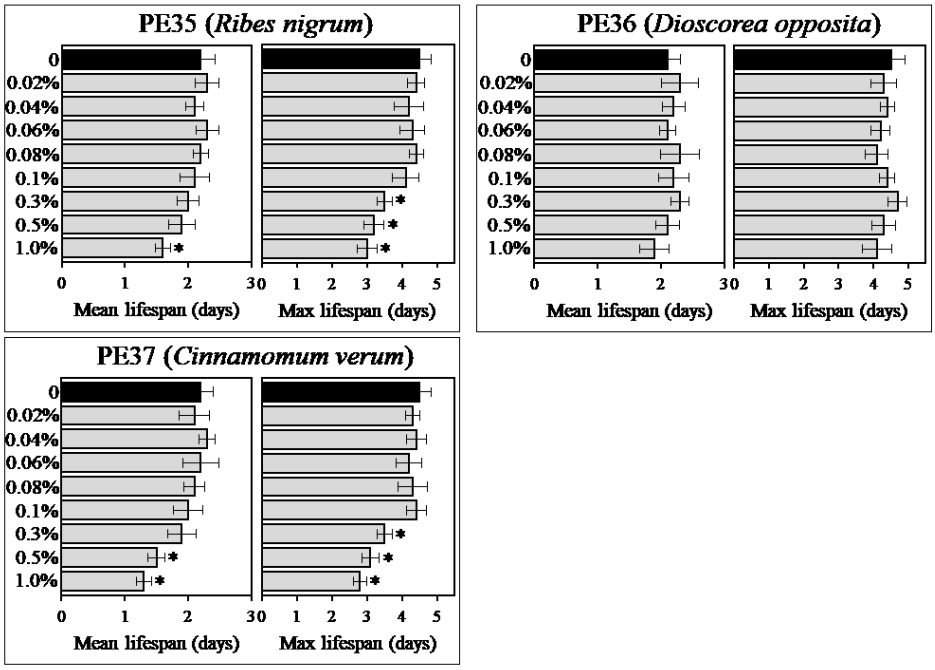

Figure 2.5. PE35, PE36, and PE37 do not extend the CLS of WT yeast grown under non-CR conditions. WT cells were grown in synthetic minimal YNB medium initially containing 2% glucose (non-CR conditions), in the presence of a PE or in its absence. The mean and maximum lifespans of a chronologically aging WT strain cultured under non-CR conditions without a PE or with a PE added at various concentrations are shown; data are presented as means ± SEM (n = 5-6; * $p < 0.05$; the p values for comparing the means of two groups were calculated with the help of the GraphPad Prism statistics software using an unpaired two-tailed t test). Note that PE 35 and PE37 can shorten the CLS of WT yeast under non-CR conditions if added at high concentrations (n = 6; * $p < 0.05$; the p values for comparing the means of two groups were calculated with the help of the GraphPad Prism statistics software using an unpaired two-tailed t test).

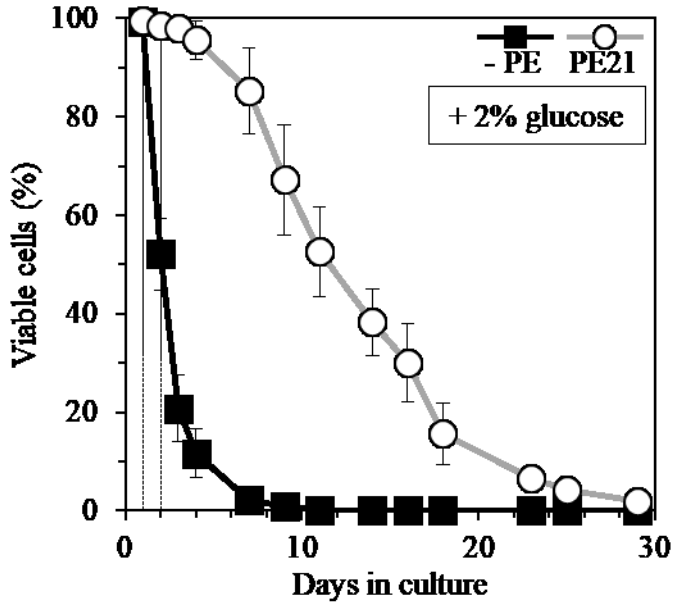

Figure 2.6. PE21 extends the chronological lifespan (CLS) of yeast grown under non-caloric restriction (non-CR) conditions. Wild-type (WT) cells were grown in synthetic minimal YNB medium (0.67% Yeast Nitrogen Base without amino acids) initially containing 2% glucose, in the presence of PE21 or in its absence. Survival curves of chronologically aging WT strain cultured with or without 0.1% PE21 are shown. Data are presented as means ± SEM (n = 21-35). CLS extension was significant for PE21 ($p < 0.05$; the p value for comparing survival curves was calculated with the help of the GraphPad Prism statistics software). Abbreviations: Logarithmic (L), post-diauxic (PD) or stationary (ST) growth phase.

2.3.2 The longevity-extending efficacy of PE21 under CR conditions is significantly lower than that under non-CR conditions

Chronologically aging yeast grown under CR conditions on 0.5% glucose are known to live longer than yeast cultured under non-CR conditions on 2% glucose. Such ability of the CR diet to extend CLS has been reported for yeast cultured in media of various nutrient compositions [2, 5, 7]. We found that, if the CR diet is administered by culturing yeast in YNB medium initially containing 0.5% glucose, it significantly increases both the mean and maximum CLS of *S. cerevisiae* (Figures 2.7A - 2.7C). We discovered that 0.1% PE21 extends the mean CLS of yeast grown under CR conditions (Figures 2.7D and 2.8). We also revealed 0.1% PE21 prolongs the maximum CLS of yeast grown under CR conditions (Figures 2.7D and 2.8). Akin to its effect under non-CR conditions, PE21 did not affect growth rates in L and PD phases or alter the maximum cell density in ST phase of yeast cultures under CR conditions on 0.5% glucose (Figure 2.10). Importantly, PE21 (like the other five lifespan-prolonging PEs) extended both the mean and maximum CLS of yeast cultures under non-CR conditions on 2% glucose to a significantly higher extent than those of yeast under CR at 0.5% glucose (Figure 2.8). This observation indicates that PE21 could mimic the longevity-extending effect of CR.

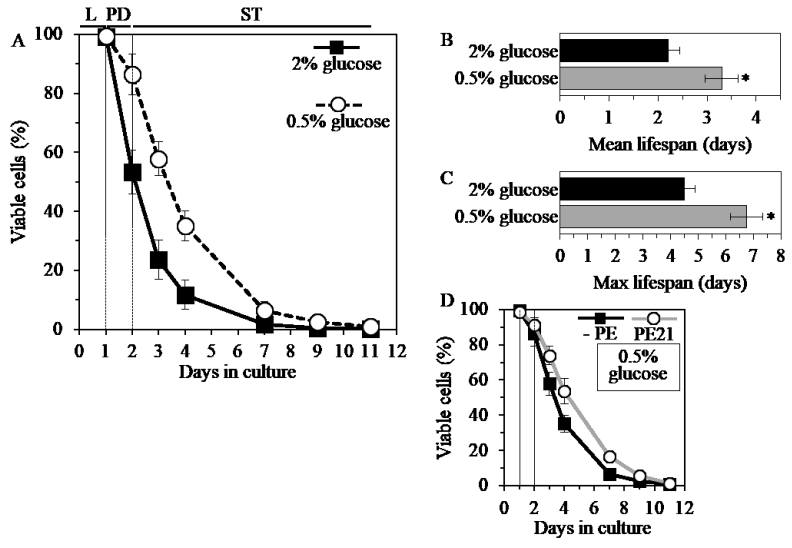

Figure 2.7. PE21 extends the CLS of yeast grown under CR conditions. WT cells were grown in synthetic minimal YNB medium initially containing 0.5% glucose (CR conditions) or 2% glucose (non-CR conditions), in the presence of PE21 or in its absence. Survival curves (**A**), the mean (**B**) and maximum (**C**) lifespans of chronologically aging WT strain cultured under CR or non-CR conditions in the absence of PE21 are shown; data are presented as means ± SEM (n = 5-7). CR caused significant extension of CLS (**A**) ($p < 0.05$; the p value for comparing survival curves were calculated with the help of the GraphPad Prism statistics software). CR extended both the mean (**B**) and maximum (**C**) lifespans (* $p < 0.05$; the p values for comparing the means of two groups were calculated with the help of the GraphPad Prism statistics software using an unpaired two-tailed t test). Survival curves of chronologically aging WT strain cultured under CR on 0.5% glucose with or without 0.1% PE21 (**D**) are shown; data are presented as means ± SEM (n = 5-7). CLS extension under CR on 0.5% glucose was significant for PE21 ($p < 0.05$; the p value for comparing survival curves were calculated with the help of the GraphPad Prism statistics software). Abbreviations: Logarithmic (L), post-diauxic (PD) or stationary (ST) growth phase.

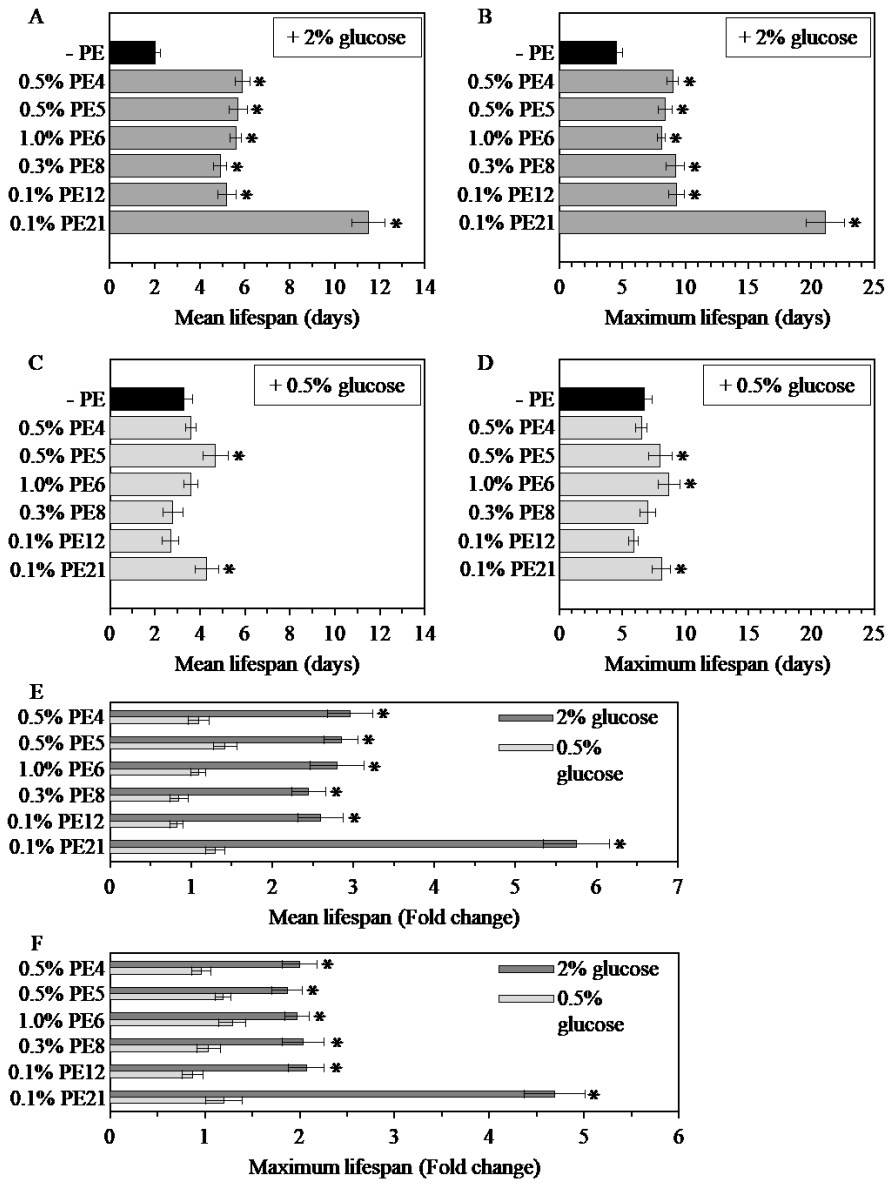

Figure 2.8. The longevity-extending efficiency under non-CR conditions significantly exceeds that under CR conditions for PE21 and the other five lifespan-prolonging PEs. WT cells were grown in synthetic minimal YNB medium initially containing 0.5% glucose (CR conditions) or 2% glucose (non-CR conditions), in the presence of a PE or in its absence. The mean (**A**, **C** and **E**) and maximum (**B**, **D** and **F**) lifespans of chronologically aging WT strain cultured under CR (**C**, **D**, **E** and **F**) or non-CR (**A**, **B**, **E** and **F**) conditions in the absence of a PE or in the presence of 0.5% PE4, 0.5% PE5, 1% PE6, 0.3% PE8, 0.1% PE12 or 0.1% PE21 are shown; data are presented as means ± SEM (n = 5-7; * $p < 0.05$). The extent to which each of the PE tested increases the mean and maximum lifespans under non-CR conditions exceeds that under CR conditions (* $p < 0.05$; the p values for comparing the means of two groups were calculated with the help of the GraphPad Prism statistics software using an unpaired two-tailed t test).

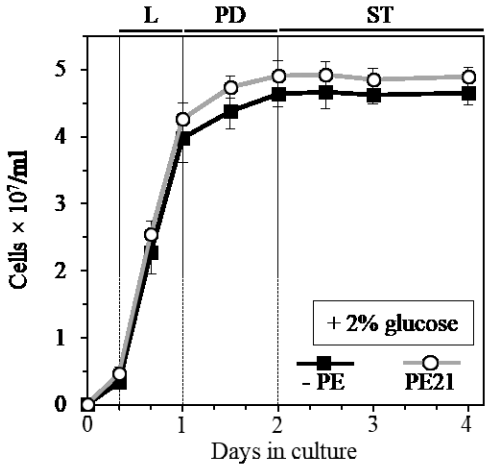

Figure 2.9. PE21 does not cause significant effects on growth of WT yeast under non-CR conditions. WT cells were grown in synthetic minimal YNB medium initially containing 2% glucose (non-CR conditions), in the absence of PE21 or in the presence of 0.1% PE21. Kinetics of cell growth is shown (n = 8-14). Abbreviations: Logarithmic (L), post-diauxic (PD) or stationary (ST) growth phase.

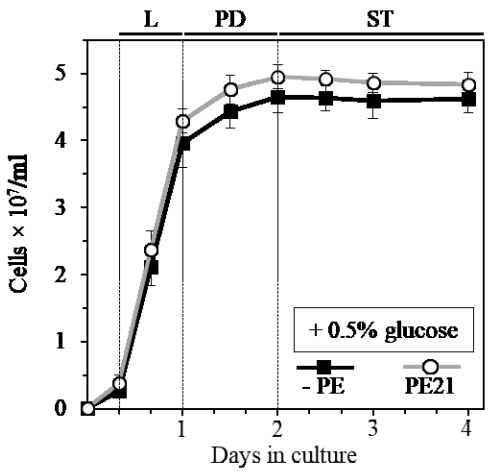

Figure 2.10. PE21 does not cause significant effects on growth of WT yeast under CR conditions. WT cells were grown in synthetic minimal YNB medium initially containing 0.5% glucose (CR conditions), in the absence of PE21 or in the presence of 0.1% PE21. Kinetics of cell growth is shown (n = 6-9). Abbreviations: Logarithmic (L), post-diauxic (PD) or stationary (ST) growth phase.

2.3.3 PE21 is a geroprotector which delays the onset and slows the progression of yeast chronological aging by eliciting a hormetic stress response

As we found, PE21 greatly extends the mean CLS of yeast cultured under non-CR conditions (Figures 2.6 and 2.8). Mean lifespan is believed to be directly proportional to the survival rates of organisms in the population during development and maturity stages of organismal aging; mean lifespan is likely to be under control of certain extrinsic (environmental) factors [60, 465–467]. Thus, it is conceivable that PE21 decreases the extrinsic rate of yeast chronological aging prior to cell entry into quiescence or senescence.

Furthermore, we revealed that PE21 also substantially increases the maximum CLS of yeast grown under non-CR conditions (Figures 2.6 and 2.8). Maximum lifespan is believed to reflect the duration of "healthy" life period (i.e. healthspan) during the quiescence/senescence stage of organismal aging; maximum lifespan is likely to be controlled by certain intrinsic (cellular and organismal) longevity modifiers [60, 465–467]. One could, therefore, conclude that PE21 also decreases the intrinsic rate of yeast chronological aging after cell entry into quiescence or senescence.

Our analysis of the Gompertz mortality function further validated the conclusion that PE21 significantly reduces the rate of yeast chronological aging. Indeed, we found that PE21 causes a substantial decrease in the slope of the Gompertz mortality rate (also known as mortality rate coefficient α) and a considerable increase in the mortality rate doubling time (MRDT) (Figure 2.11). Such changes in the values of α and MRDT are characteristic of interventions that decrease the rate of progression through the process of biological aging [465, 468–471].

Noteworthy, our analyses of how different concentrations of PE21 impact yeast longevity under non-CR conditions revealed that it causes a so-called "hormetic" stress response in chronologically aging yeast with respect to longevity. Indeed, the dose-response curves (i.e. the curves that reflect relationships between PE concentrations and mean or maximum CLS) for PE21 were inverted U-shaped (Figure 2.3). Such nonlinear and biphasic dose-response curves denote a hormetic kind of stress response, in which 1) lower (hormetic) concentrations of a chemical compound increase the survival of a cell or an organism by stimulating biological processes that allow it to maintain cellular or organismal stress at a level which is below a threshold of toxicity; while 2) higher concentrations of this chemical compound decrease the survival of a cell or an organism by creating stress which exceeds such threshold [29, 248, 472–474].

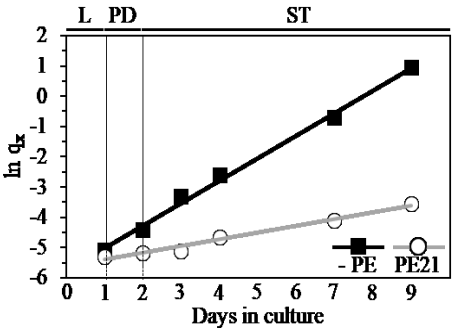

PE	α (Gompertz slope or mortality rate coefficient)	MRDT (mortality rate doubling time)	Rate of aging
- PE	0.74	0.94	
0.1% PE21	0.22	3.15	⬇ decreased

Figure 2.11. Analysis of the Gompertz mortality function indicates that PE21 significantly decreases the rate of chronological aging in yeast. WT cells were grown in synthetic minimal YNB medium initially containing 2% glucose, in the presence of PE21 or in its absence. Survival curves shown in Figure 2.6 were used to calculate the age-specific mortality rates (q_x) of chronologically aging WT yeast populations cultured with or without 0.1% PE21. PE21 caused a substantial decrease in the slope of the Gompertz mortality rate (also known as mortality rate coefficient α) and a considerable increase in the mortality rate doubling time (MRDT). The values of q_x, α and MRDT were calculated as described in Materials and methods. Abbreviations: Logarithmic (L), post-diauxic (PD) or stationary (ST) growth phase.

2.3.4 PE21 alters the age-related chronology of longevity-defining traits of mitochondrial functionality

We hypothesized that PE21 slows yeast chronological aging by influencing certain cellular processes. We sought to identify these longevity-defining processes. Certain aspects of mitochondrial functionality (such as mitochondrial respiration, mitochondrial membrane potential, and mitochondrial reactive oxygen species [ROS] homeostasis) are known to define the rate of chronological aging in yeast [5, 7, 98, 237, 475–483]. We, therefore, assessed how PE21 influences these longevity-defining processes in chronologically aging yeast cultures under non-CR conditions on 2% glucose.

We found that PE21 stimulates coupled mitochondrial respiration, which was monitored by measuring the rate of oxygen consumption by yeast cells. Specifically, PE21 considerably increased the rate of mitochondrial respiration in yeast during PD and ST growth phases (Figure 5.12).

We also found that PE21 sustains healthy populations of functional mitochondria that exhibit high mitochondrial membrane potential ($\Delta\Psi_m$). Indeed, PE21 completely prevented an aging-associated decline in $\Delta\Psi_m$ during PD and ST growth phases (Figure 2.13).

PE21 also caused significant changes in the age-related chronology of intracellular ROS, which in yeast and other organisms are known to be formed mainly as by-products of mitochondrial respiration [475, 476]. We found that PE21 decreased the extent to which the intracellular concentration of mitochondrially generated ROS declined during PD and ST growth phases (Figure 2.14). Of note, on days 3 and 4 of culturing, ROS concentrations in yeast grown with PE21 exceeded those in yeast grown without it (Figure 2.14).

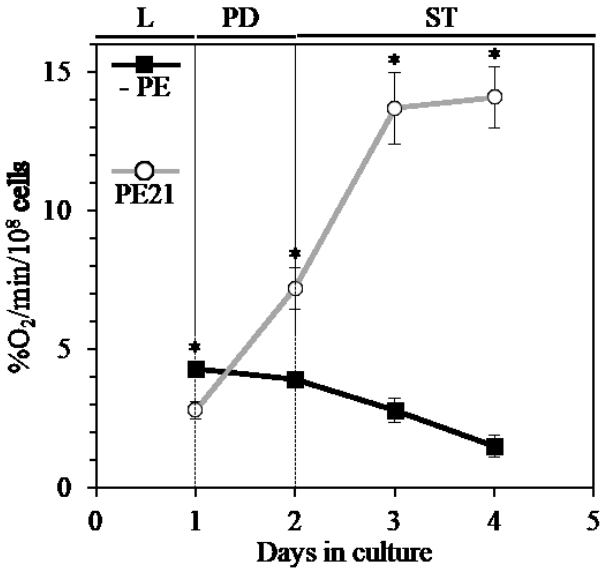

Figure 2.12. PE21 alters the age-related chronology of mitochondrial oxygen consumption by yeast grown under non-CR conditions. WT cells were grown in synthetic minimal YNB medium initially containing 2% glucose, in the presence of PE21 or in its absence. A polarographic assay was used to measure oxygen uptake by live yeast cells, as described in Materials and methods. Age-dependent changes in the rate of mitochondrial oxygen consumption by chronologically aging WT strain cultured under non-CR conditions on 2% glucose with or without 0.1% PE21 are shown; data are presented as means ± SEM (n = 7-9; * $p < 0.05$; the p values for comparing the means of two groups were calculated with the help of the GraphPad Prism statistics software using an unpaired two-tailed t test). Abbreviations: Logarithmic (L), post-diauxic (PD) or stationary (ST) growth phase.

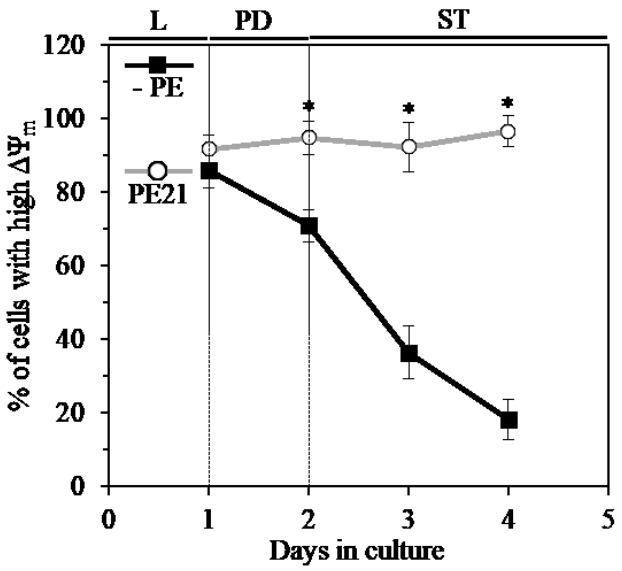

Figure 2.13. PE21 sustains healthy populations of functional mitochondria that exhibit high mitochondrial membrane potential (ΔΨm) in chronologically aging yeast grown under non-CR conditions. WT cells were grown in synthetic minimal YNB medium initially containing 2% glucose, in the presence of PE21 or in its absence. ΔΨm was measured in live yeast by fluorescence microscopy of Rhodamine 123 staining, as described in Materials and methods. Age-dependent changes in the percentage of WT cells displaying high ΔΨm in chronologically aging yeast cultures under non-CR conditions on 2% glucose with or without 0.1% PE21 are shown; data are presented as means ± SEM (n = 3-4; * $p < 0.05$; the p values for comparing the means of two groups were calculated with the help of the GraphPad Prism statistics software using an unpaired two-tailed t test). Abbreviations: Logarithmic (L), post-diauxic (PD) or stationary (ST) growth phase.

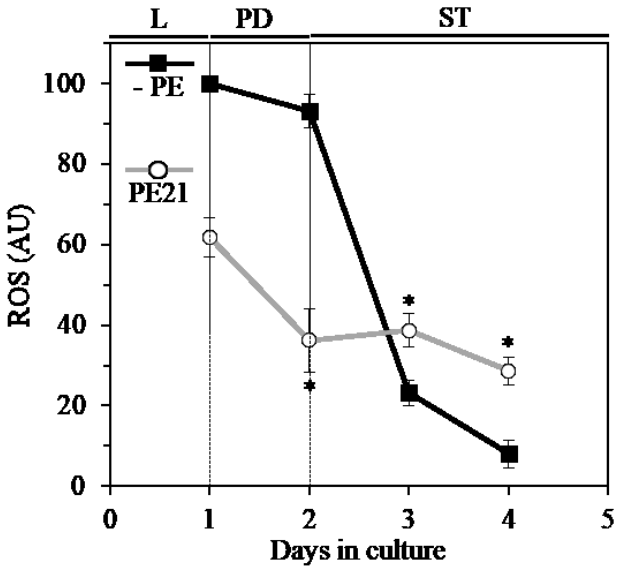

Figure 2.14. In yeast grown under non-CR conditions, PE21 alters the patterns of age-related changes in intracellular reactive oxygen species (ROS) known to be generated mainly as by-products of mitochondrial respiration. WT cells were grown in synthetic minimal YNB medium initially containing 2% glucose, in the presence of PE21 or in its absence. The intracellular concentrations of ROS were measured in live yeast by fluorescence microscopy of dihydrorhodamine 123 staining, as described in Materials and methods. Age-dependent changes in ROS concentrations within chronologically aging WT cells cultured under non-CR conditions on 2% glucose with or without 0.1% PE21 are shown; data are presented as means ± SEM (n = 3-4; * $p < 0.05$; the p values for comparing the means of two groups were calculated with the help of the GraphPad Prism statistics software using an unpaired two-tailed t test). Abbreviations: Logarithmic (L), post-diauxic (PD) or stationary (ST) growth phase.

2.3.5 PE21 decreases the extent of age-related oxidative damage to cellular proteins, membrane lipids, mitochondrial and nuclear genomes

A body of evidence supports the following view on the relationships between cellular ROS, oxidative molecular damage and aging in organisms across phyla: 1) if cellular concentrations of

ROS exceed a threshold of toxicity, ROS cause oxidative damage to proteins, lipids, and DNA; 2) oxidative damage to each kind of these macromolecules accumulates with age; and 3) cumulative oxidative damage to the different kinds of macromolecules is one of the major causes of aging [476–482]. We, therefore, examined how PE21 influences the extent of oxidative damage to proteins, lipids, and DNA in chronologically aging yeast cultured under non-CR conditions on 2% glucose.

We found that PE21 delays an age-dependent rise in the extent of oxidative damage to cellular proteins. PE21 reduced oxidative carbonylation of proteins in yeast cells progressing through the entire ST phase (Figure 2.15A). Furthermore, PE21 caused a significant reduction in the levels of oxidatively damaged membrane lipids; such reduction was observed late in ST phase, on days 3 and/or 4 of culturing (Figure 2.15B).

Moreover, PE21 decreased the frequencies of spontaneous point mutations in the *RIB2* and *RIB3* genes of mitochondrial DNA (mtDNA) (Figure 2.16A) - likely due to a reduced extent of oxidative damage to mtDNA in yeast cells exposed to this PE. Such inhibitory effect of PE21 on oxidative damage to mtDNA was observed late in ST phase, on day 4 of culturing (Figure 2.16A). We also revealed that PE21 causes a significant reduction in the frequencies of spontaneous point mutations in the *CAN1* gene of nuclear DNA (nDNA) (Figure 2.16B) - possibly due to a decreased degree of oxidative damage to nDNA in yeast cells grown in the presence of PE21. Such inhibitory effect of PE21 on oxidative damage to nDNA was also seen late in ST phase, on day 4 of culturing.

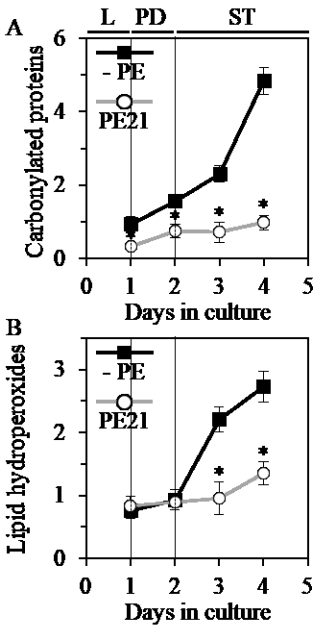

Figure 2.15. PE21 delays an age-dependent rise in the extent of oxidative damage to cellular proteins and membrane lipids in chronologically aging yeast grown under non-CR conditions. WT cells were grown in synthetic minimal YNB medium initially containing 2% glucose, in the presence of PE21 or in its absence. Carbonylated cellular proteins (**A**) and oxidatively damaged membrane lipids (**B**) were determined as described in Materials and methods. Age-dependent changes in the concentrations of these oxidatively damaged macromolecules within chronologically aging WT cells cultured under non-CR conditions on 2% glucose with or without 0.1% PE21 are shown; data are presented as means ± SEM (n = 2-4; * $p < 0.05$; the p values for comparing the means of two groups were calculated with the help of the GraphPad Prism statistics software using an unpaired two-tailed t test). Abbreviations: Logarithmic (L), post-diauxic (PD) or stationary (ST) growth phase.

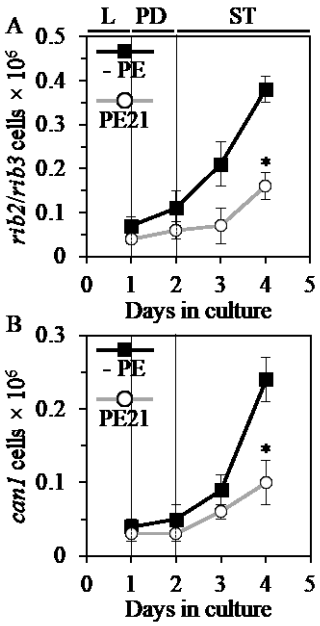

Figure 2.16. PE21 slows down an age-dependent rise in the frequency of spontaneous point mutations in the *rib2* and *rib3* loci of mitochondrial DNA (mtDNA) and in the frequency of spontaneous point mutations in the *CAN1* gene of nuclear DNA (nDNA) in chronologically aging yeast grown under non-CR conditions. WT cells were grown in synthetic minimal YNB medium initially containing 2% glucose, in the presence of PE21 or in its absence. The frequency of spontaneous point mutations in the *rib2* and *rib3* loci of mtDNA (**A**), as well as the frequency of spontaneous point mutations in the *CAN1* gene of nDNA (**B**), were measured as described in Materials and methods. Age-dependent changes in the frequencies of these mtDNA and nDNA mutations in chronologically aging WT cells cultured under non-CR conditions on 2% glucose with or without 0.1% PE21 are shown; data are presented as means ± SEM (n = 3-5; * $p < 0.05$; the p values for comparing the means of two groups were calculated with the help of the GraphPad Prism statistics software using an unpaired two-tailed t test). Abbreviations: Logarithmic (L), post-diauxic (PD) or stationary (ST) growth phase.

2.3.6 PE21 increases the resistance of chronologically aging yeast to chronic oxidative and thermal stresses

A body of evidence implies that the development of resistance to chronic (long-term) oxidative and/or thermal stresses can extend longevity in organisms across phyla, including yeast [1, 2, 5, 7, 11, 84, 248, 473–475, 483–486]. We, therefore, assessed how PE21 influences the abilities of chronologically aging yeast cultured under non-CR conditions to resist chronic oxidative and thermal stresses.

Chronic oxidative stress was administered by recovering yeast cells progressing through L, PD or ST phases of growth/culturing in liquid YNB medium initially containing 2% glucose, spotting these cells on solid YPD medium with 2% glucose and 5 mM hydrogen peroxide, and incubating them for 3 days. We found that PE21, and other longevity-extending PEs discovered in this study significantly increases cell resistance to chronic oxidative stress in yeast cultures progressing through L, PD and ST phases (Figure 2.17).

Chronic thermal stress was administered by recovering yeast cells progressing through L, PD or ST phases of growth/culturing in liquid YNB medium initially containing 2% glucose, spotting these cells on solid YPD medium with 2% glucose and incubating at 60°C for 60 min, and then transferring plates with these cells to 30°C and incubating at this temperature for 3 days. We found that PE21, but not some other longevity-extending PEs discovered in this study increases

cell resistance to chronic thermal stress only in yeast cultures progressing through the ST phase (Figure 2.18).

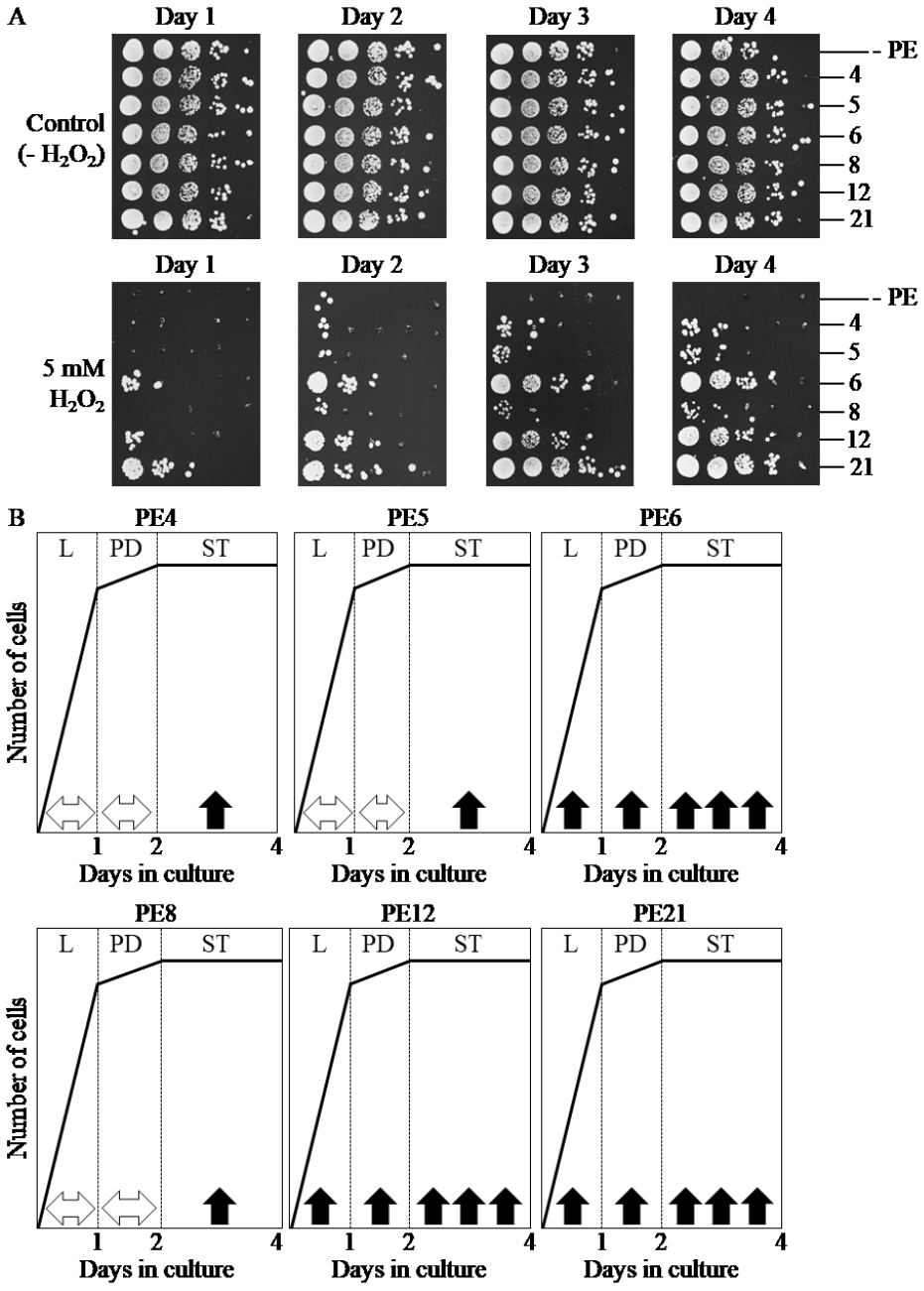

Figure 2.17. PE21 (and other aging-delaying plant extracts) enhances the ability of chronologically aging yeast grown under non-CR conditions to resist chronic oxidative stress. WT cells were grown in synthetic minimal YNB medium initially containing 2% glucose, in the presence of a PE or in its absence. (**A**) Spot assays for monitoring oxidative stress resistance were performed as described in Materials and methods. Serial 10-fold dilutions of cells recovered at different days of culturing were spotted on plates with solid YPD medium containing 2% glucose as carbon source, with or without 5 mM hydrogen peroxide. All pictures were taken after a 3-d incubation at 30ºC. (**B**) A model for how 0.5% PE4, 0.5% PE5, 1% PE6, 0.3% PE8, 0.1% PE12 and 0.1% PE21 influence the resistance of yeast to chronic oxidative stress during logarithmic (L), post-diauxic (PD) or stationary (ST) phases of growth. ⇔ or ⬆ Denote unaltered or enhanced, respectively, cell resistance to chronic oxidative stress during a certain phase of growth. Abbreviations: Logarithmic (L), post-diauxic (PD) or stationary (ST) growth phase.

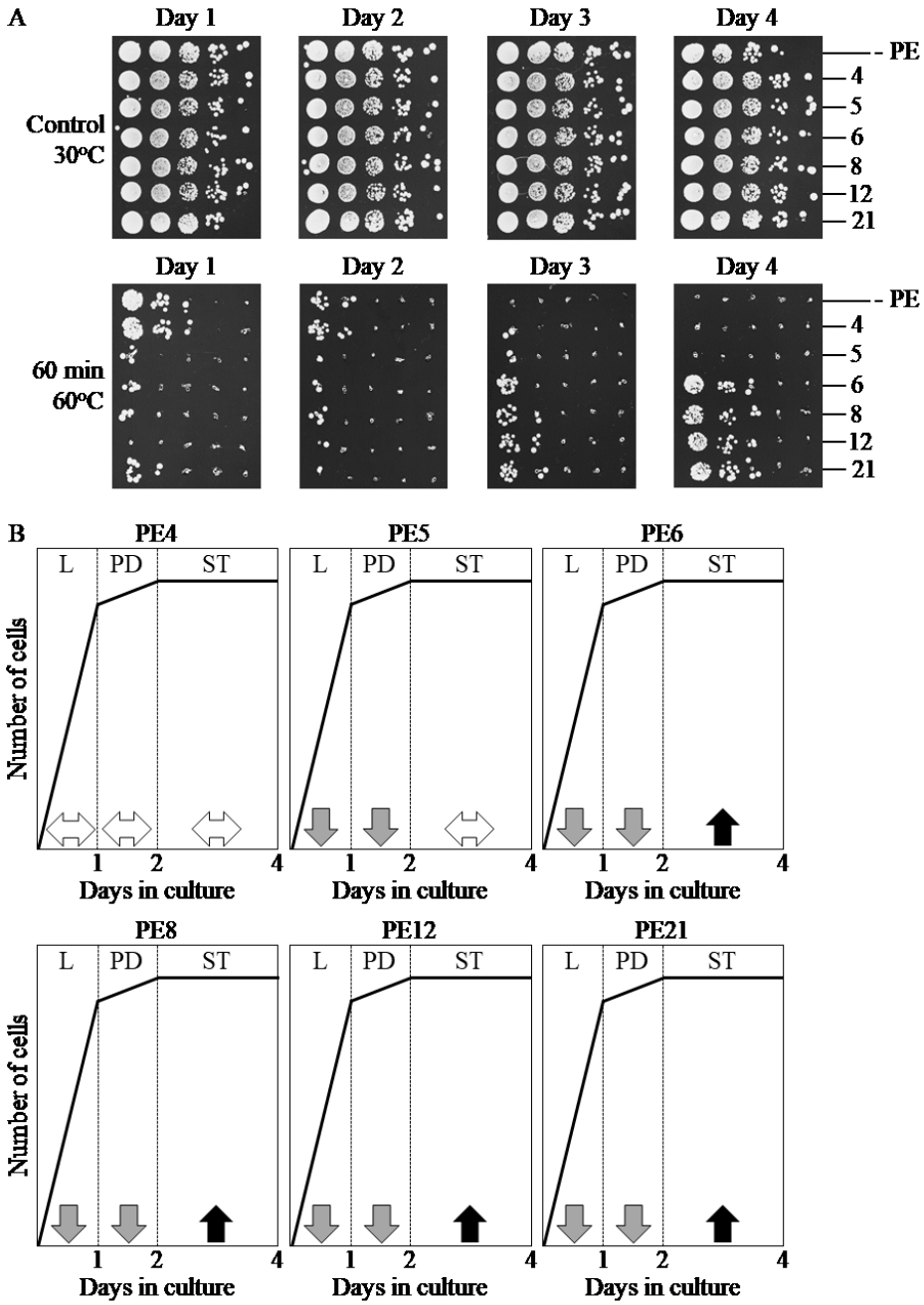

Figure 2.18. PE21 (and other aging-delaying plant extracts) increases cell resistance to chronic thermal stress only in yeast cultures progressing through ST phase. WT cells were grown in synthetic minimal YNB medium initially containing 2% glucose, in the presence of a PE or in its absence. (**A**) Spot assays for monitoring thermal stress resistance were performed as described in Materials and methods. Serial 10-fold dilutions of cells recovered at different days of culturing were spotted on plates with solid YPD medium containing 2% glucose as carbon source. Plates were initially incubated at 30ºC (control) or 60ºC for 60 min and were then transferred to 30ºC. All pictures were taken after a 3-d incubation at 30ºC. (**B**) A model for how 0.5% PE4, 0.5% PE5, 1% PE6, 0.3% PE8, 0.1% PE12 and 0.1% PE21 influence the resistance of yeast to chronic thermal stress during logarithmic (L), post-diauxic (PD) or stationary (ST) phases of growth. ⇔, ⇩ or ⬆ Denote unaltered, reduced or enhanced, respectively, cell resistance to chronic thermal stress during a certain phase of growth. Abbreviations: Logarithmic (L), post-diauxic (PD) or stationary (ST) growth phase.

2.3.7 PE21 causes rapid degradation of neutral lipids deposited in lipid droplets (LDs)

Triacylglycerols and steryl esters are uncharged (and therefore are called “neutral” or “nonpolar”) classes of lipids that can be found in cells of all eukaryotic organisms [173, 292, 487]. After being initially synthesized in the endoplasmic reticulum and then deposited in LDs, these

two highly hydrophobic lipids can undergo lipolytic degradation to provide substrates for the synthesis of phospholipids and sphingolipids [176, 292, 488–490]. Emergent evidence supports the view that the biosynthesis, storage, and lipolysis of neutral lipids are longevity assurance processes; importantly, it has been shown that these processes can be controlled by certain dietary and pharmacological interventions known to delay aging in various eukaryotes, including yeast [7, 53, 98, 110, 237, 246, 490–503]. We, therefore, used live-cell fluorescence microscopy to examine how PE21 influences the age-related dynamics of changes in the intracellular concentrations of neutral lipids confined to LDs in chronologically aging yeast grown under non-CR conditions.

We found that PE21 elicits a rapid age-related decline in the number of yeast cells exhibiting LDs (Figures 2.19 and 2.20). In contrast, no significant changes in the number of cells with LDs were seen in yeast progressing through L, PD and ST phases of culturing in medium without a PE (Figures 2.19 and 2.20). These findings demonstrate that in chronologically aging yeast grown under non-CR conditions, PE21 causes rapid lipolytic degradation of neutral lipids stored in LDs.

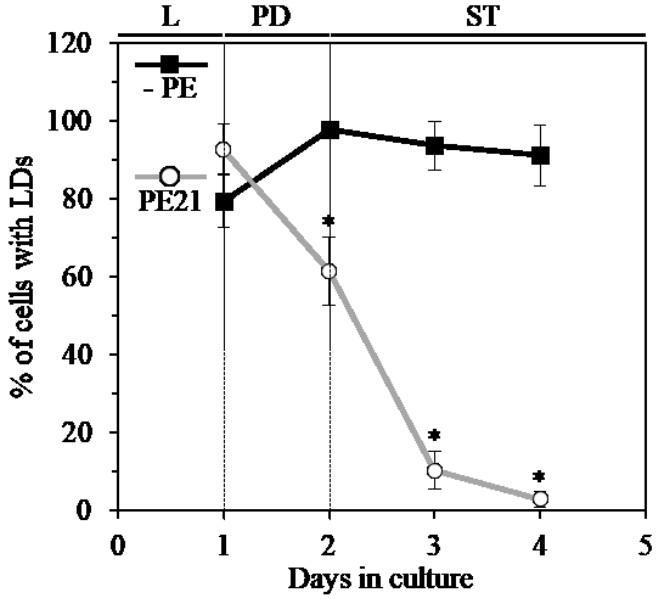

Figure 2.19. PE21 induces rapid consumption of neutral lipids deposited in lipid droplets (LDs) of chronologically aging yeast grown under non-CR conditions. WT cells were grown in synthetic minimal YNB medium initially containing 2% glucose, in the presence of PE21 or in its absence. Neutral lipids deposited in LDs were measured in live yeast by fluorescence microscopy of BODIPY 493/503 staining, as described in Materials and methods. Age-dependent changes in the percentage of WT cells exhibiting LDs in chronologically aging yeast cultures under non-CR conditions on 2% glucose with or without 0.1% PE21 are shown; data are presented as means ± SEM (n = 3-4; * $p < 0.05$; the p values for comparing the means of two groups were calculated with the help of the GraphPad Prism statistics software using an unpaired two-tailed t test). Abbreviations: Logarithmic (L), post-diauxic (PD) or stationary (ST) growth phase.

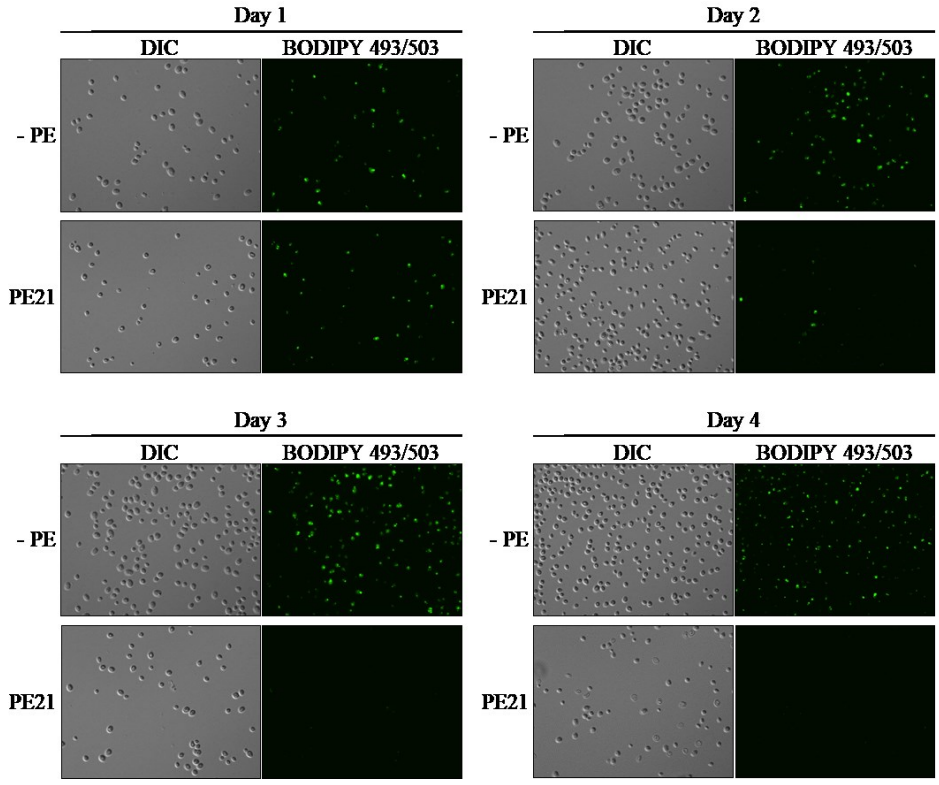

Figure 2.20. PE21 accelerates an age-dependent decline in the number of WT cells that exhibit LDs under non-CR conditions. WT cells were grown in synthetic minimal YNB medium initially containing 2% glucose, in the presence of PE21 or in its absence. Yeast cells were recovered at days 1, 2, 3 and 4 of culturing, stained with BODIPY 493/503 for visualizing cells displaying neutral lipids deposited in LDs, and subjected to live-cell fluorescence microscopy and differential interference contrast (DIC) microscopy as described in Materials and methods.

2.4 Summary

In this study, we performed a screen for PEs capable of extending the longevity of the chronologically aging yeast *S. cerevisiae*. Our screen revealed six PEs (which we call PE4, PE5, PE6, PE8, PE12, and PE21) that can significantly increase yeast CLS. We investigated various properties of one of these longevity-extending PEs, which is called PE21. We demonstrated that PE21 is a geroprotector which delays the onset and slows the progression of yeast chronological aging by eliciting a hormetic stress response. We found that PE21 has the following effects on cellular processes known to define longevity in organisms across phyla: 1) PE21 amplifies mitochondrial respiration and membrane potential; 2) PE21 alters the pattern of age-related changes in the intracellular concentration of ROS; 3) PE21 reduces oxidative damage to cellular proteins, membrane lipids, and mitochondrial and nuclear genomes; 4) PE21 enhances cell resistance to oxidative and thermal stresses; and 5) PE21 accelerates degradation of neutral lipids deposited in LDs (Figure 2.21; this Figure compares the effects of different longevity extending PEs on cellular processes affected by PE21). These findings provide important new insights into mechanisms through which some chemical compounds of plant origin can slow biological aging.

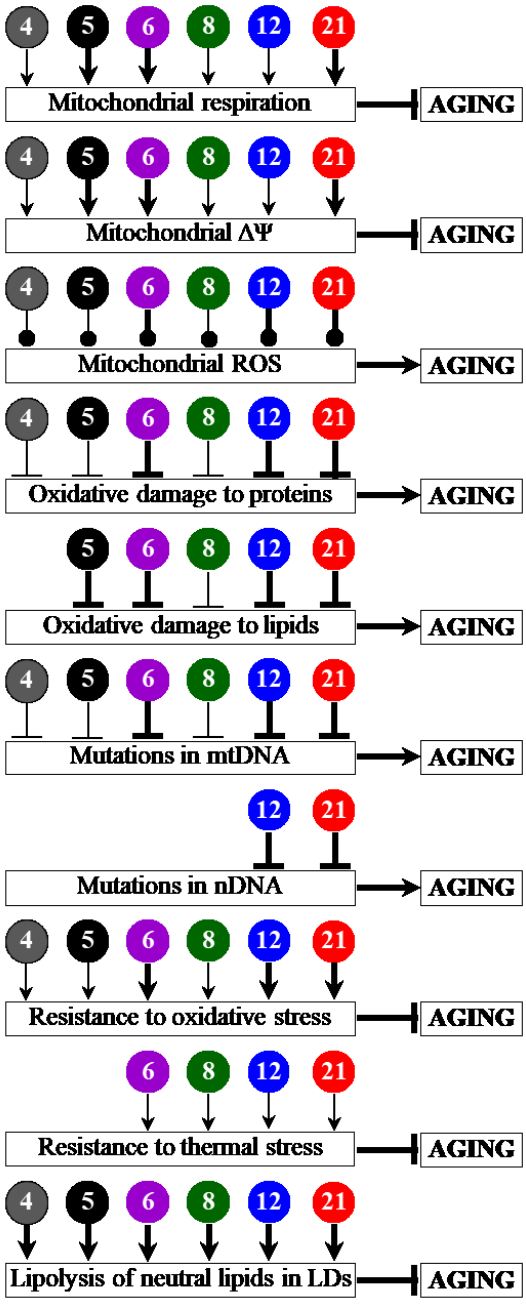

Figure 2.21. PE4, PE5, PE6, PE8, PE12 and PE21 delay yeast chronological aging and have different effects on several longevity-defining cellular processes. Arrows pointing at boxes with the terms of longevity-defining cellular processes denote activation of these processes, T bars denote inhibition of these processes, whereas lines with filled circles denote a change in the age-related chronology of intracellular ROS. The thickness of such arrows, T bars and lines with filled circles correlates with the extent to which a PE activates, inhibits or alters the age-related chronology (respectively) of a certain longevity-defining cellular process. Arrows and T bars pointing at boxes with the term "AGING" denote acceleration or deceleration (respectively) of yeast chronological aging.

2.5 Future perspectives

In the future, it would be important to explore the following key aspects of the mechanisms through which PE21 and the other longevity-extending PEs discovered in this study slow biological aging.

First, it is important to identify the individual chemical compounds responsible for the ability of PE21 and the other longevity-extending PEs to delay the onset and decrease the rate of

yeast chronological aging. Such identification is already underway in our laboratory; of note, it is conceivable that only some combinations of certain chemicals composing these PEs (but not individual chemical compounds *per se*) can be responsible for their extremely high efficiencies as aging-delaying interventions.

Second, it is worthwhile to elucidate how genetic interventions that impair any of the few nutrient- and energy-sensing signaling pathways known to define the longevity of chronologically aging yeast [2, 5, 7, 23, 98] influence the extent to which PE21 and the other longevity-extending PEs can slow aging. These studies may allow identification of protein components of the longevity-defining signaling pathways that are targeted by each of the PEs. These studies may also reveal that certain combinations of these PEs and genetically impaired components of pro-aging signaling pathways exhibit additive or synergistic effects on the efficiencies of lifespan and healthspan extensions.

Third, it is important to investigate how various combinations of the six longevity-extending PEs (including PE21) interact with each other and with known aging-delaying chemical compounds to alter the extent of CLS extension in yeast. These studies may identify such combinations of various pharmacological interventions that impose substantial additive or synergistic effects on the efficiencies with which organismal lifespan and healthspan can be prolonged.

Fourth, our ongoing studies indicate that the six longevity-extending PEs also extend longevities of other eukaryotic model organisms, delay the onset of age-related diseases and/or exhibit anti-tumor effects. In this regard, it needs to be mentioned that genetic, dietary and pharmacological interventions known to delay aging in yeast and other eukaryotes have been shown to selectively kill cultured human cancer cells and/or decrease the incidence of cancer [50, 100, 112, 307, 460, 504–511]. The challenge for the future is to define mechanisms through which the six geroprotective PEs (including PE21) prolong healthy lifespan and decelerate tumorigenesis.

3 The first mechanism by which PE21 slows yeast chronological aging and extends yeast longevity

3.1 Introduction

As described in Chapter 2 of the thesis, PE21 promotes a rapid age-related degradation of neutral lipids deposited in LD. Studies presented in this chapter of the thesis revealed that PE21 also alters the concentrations of other lipid classes and that such alterations occur in an age-related manner. These findings indicated that PE21 causes a specific remodeling of lipid metabolism and transport in chronologically aging yeast. Based on the abilities of PE21 to elicit such remodeling of lipid metabolism and transport (as described in this chapter of the thesis) and to impose changes in certain cellular processes (as outlined in Chapter 2 of the thesis) within yeast cultured under non-CR conditions, we put forward a hypothesis that there may be at least three different mechanisms by which PE21 delays yeast chronological aging and extends yeast CLS. This chapter of the thesis describes studies that confirm the existence of the first proposed mechanism underlying aging delay and longevity extension by PE21. This mechanism consists in the ability of PE21 to decelerate an age-related onset of liponecrotic RCD.

3.2 Materials and methods

3.2.1 Yeast strains, media and growth conditions

The wild-type strain *Saccharomyces cerevisiae* BY4742 (*MATα his3Δ1 leu2Δ0 lys2Δ0 ura3Δ0*) and single-gene-deletion mutant strains in the BY4742 genetic background (all from Thermo Scientific/Open Biosystems) were grown in synthetic minimal YNB medium (0.67% Yeast Nitrogen Base without amino acid) initially containing 2% glucose, 20 mg/l *L*-histidine, 30 mg/l *L*-leucine, 30 mg/l *L*-lysine and 20 mg/l uracil, with 0.1% PE21 (Idunn Technologies Inc.) or without it. PE21 is an ethanol/water extract from the bark of *Salix alba* (see Chapter 2 of the thesis). If added to the growth medium at the time of cell inoculation at a final concentration of 0.1% (w/v), PE21 increases both the mean and maximum CLSs of wild-type strain cultured in medium initially containing 2% glucose (see Chapter 2 of the thesis). A 20% stock solution of PE21 in ethanol was made on the day of adding this PE to cell cultures. The stock solution of PE21 was added to growth medium with 2% glucose immediately following cell inoculation into the

medium. In a culture supplemented with PE21, ethanol was used as a vehicle at the final concentration of 0.5%. In the same experiment, yeast cells were also subjected to ethanol-mock treatment by being cultured in growth medium initially containing 2% glucose and 0.5% ethanol. Cells were cultured at 30ºC with rotational shaking at 200 rpm in Erlenmeyer flasks at a "flask volume/medium volume" ratio of 5:1.

3.2.2 Mass spectrometric identification and quantitation of cellular lipids

A sample of cells was taken from a culture on a certain day of culturing. A fraction of the sample was diluted to determine the total number of cells using a hemocytometer. Yeast cells (5×10^7) were harvested by centrifugation in a Centra CL2 clinical centrifuge for 5 min at 3000 × g at room temperature. The cell pellet was washed once in ice-cold nanopure water and once in ice-cold 155 mM ammonium bicarbonate (pH 8.0), and the cells were harvested by centrifugation at 16000 × g for 1 min at 4°C. The cell pellet was stored at -80°C until lipid extraction. For lipid extraction, the pelleted cells kept at -80°C were thawed on ice before being resuspended in 200 µl of ice-cold nanopure water. The re-suspended sample was transferred to a 15-ml high-strength glass screw-top centrifuge tube with a Teflon lined cap (#0556912; Fisher Scientific). The volume of each sample was topped off to 1 ml with ice-cold nanopure water. To each tube the following was added: 20 µl of the internal standard mix prepared in Chromasolv HPLC (>99.9%) chloroform (Sigma-Aldrich) as described [11], 800 µl of 425-600 µM acid-washed glass beads to break open the cells (#G8772; Sigma-Aldrich) and 3 ml of a Chromasolv HPLC (>99.9%) chloroform-methanol mixture (both from Sigma-Aldrich) at a 17:1 ratio. The samples were then vortexed vigorously for 2 h at 4°C and subjected to centrifugation in a Centra CL2 clinical centrifuge at 3000 × g for 5 min at room temperature. The lower organic phase was then transferred to another 15-ml high-strength glass screw-top centrifuge tube using a glass Pasteur pipette with careful attention not to disrupt the glass beads or upper aqueous phase. 1.5 ml of chloroform-methanol (2:1) solution was added to the remaining upper aqueous phase. The samples were again vortexed vigorously at 4°C for 2 h. The initially separated organic phase was kept at 4°C for the duration of the second vortexing. At the end of 2-h vortexing, the samples were again centrifuged for 5 min at 3000 × g at room temperature; the lower organic phase was then separated and added to the corresponding initial organic phase with a glass Pasteur pipette. With both lower organic phases combined, the solvent was evaporated off by nitrogen gas flow. Once all solvent was evaporated,

the remaining lipid film was dissolved in 100 µl of chloroform-methanol (1:2) and immediately transferred into 2-ml glass vials with Teflon screw tops to avoid evaporation until samples were analyzed by mass spectrometry (MS). Samples were then stored at -80°C and ran on the LTQ Orbitrap Mass Spectrometer within one week of the extraction. Samples were diluted (1:1) with chloroform/methanol (1:2) mixture supplemented with 0.1% ammonium hydroxide. Lipids were resolved by direct injection using a Thermo Orbitrap Velos mass spectrometer equipped with a HESI-II ion source (Thermo Scientific, Waltham, MA, USA) at a flow rate of 5 µl/min. The optimized tune setting and instrument methods for mass spectrometric analysis of lipids were previously described [11]. Mass spectra were converted to open format mzXML using the ProteoWizard MSConvert software (http://proteowizard.sourceforge.net/), the file format used by the Lipid Identification Software LipidXplorer (https://lifs.isas.de/wiki/index.php/) for the automated detection and quantitation of lipid species. Data were normalized by taking the ratio of signal intensity of precursor ions to that of their respective lipid class-specific internal standard (spiked standard), multiplied by the concentration of that standard to give a molar quantity.

3.2.3 CLS assay

A sample of cells was taken from a culture at a certain day following cell inoculation and PE21 addition into the medium. A fraction of the sample was diluted to determine the total number of cells using a hemocytometer. Another fraction of the cell sample was diluted, and serial dilutions of cells were plated in duplicate onto YPD medium (1% yeast extract, 2% peptone) containing 2% glucose as carbon source. After 2 days of incubation at 30ºC, the number of colony-forming units (CFU) per plate was counted. The number of CFU was defined as the number of viable cells in a sample. For each culture, the percentage of viable cells was calculated as follows: (number of viable cells per ml/total number of cells per ml) × 100. The percentage of viable cells in the mid-logarithmic growth phase was set at 100%.

3.2.4 Cell viability assay for monitoring the susceptibility of yeast to a mode of cell death induced by palmitoleic acid (POA)

A sample of cells was taken from a culture on a certain day of culturing. A fraction of the sample was diluted to determine the total number of cells using a hemocytometer. Yeast cells (8×10^7) were harvested by centrifugation for 1 min at 21000 × g at room temperature and resuspended

in 8 ml of YPD medium containing 2% glucose as carbon source. Each cell suspension was divided into 8 equal aliquots. Three pairs of aliquots were supplemented with POA (#P9417; Sigma) from a 50-mM stock solution (in 10% chloroform, 45% hexane and 45% ethanol; #650498, #248878 and #34852, respectively; all from Sigma). The final concentration of POA was 0.05 mM, 0.1 mM or 0.15 mM for each pair of aliquots; in all these aliquots, the final concentrations of chloroform, hexane, and ethanol were 0.03%, 0.135%, and 0.135%, respectively. One pair of aliquots was supplemented only with chloroform, hexane, and ethanol added to the final concentrations of 0.03%, 0.135%, and 0.135%, respectively. All aliquots were then incubated for 2 h at 30°C on a Labquake rotator (#400110; Thermolyne/Barnstead International) set for 360° rotation. Serial dilutions of cells were plated in duplicate onto plates containing YPD medium with 2% glucose as carbon source. After 2 days of incubation at 30°C, the number of colony-forming units (CFU) per plate was counted. The number of CFU was defined as the number of viable cells in a sample. For each aliquot of cells exposed to POA, the % of viable cells was calculated as follows: (number of viable cells per ml in the aliquot exposed to POA/number of viable cells per ml in the control aliquot that was not exposed to POA) × 100.

3.2.5 Fluorescence microscopy

Propidium iodide (PI; #P4170, Sigma) staining for visualizing the extent of plasma membrane permeability for small molecules [357] and Annexin V (#A13201; Thermo Fisher Scientific) staining for visualizing externalized phosphatidylserine [357] were performed according to established procedures. Live imaging was performed on a Leica DM6000B epifluorescence microscope equipped with a high-resolution Hamamatsu Orca ER CCD camera using oil immersion and a 100× objective. Images were acquired with 20-ms exposures using PerkinElmer Volocity software. Image files were exported as TIFFs then opened in ImageJ, where the percentage of PI- and Annexin V-positive cells was calculated.

3.2.6 Statistical analysis

Statistical analysis was performed using Microsoft Excel's Analysis ToolPack-VBA. All data on cell survival are presented as mean ± SEM. The *p* values for comparing the means of two groups using an unpaired two-tailed t-test were calculated with the help of the GraphPad Prism 7 statistics software. The logrank test for comparing each pair of survival curves was performed with

GraphPad Prism 7. Two survival curves were considered statistically different if the *p* value was less than 0.05.

3.3 Results and Discussion

3.3.1 PE21 alters the relative levels of different lipid classes in an age-related manner

The maintenance of lipid homeostasis is indispensable for healthy aging in yeast and metazoans because lipid metabolism and transport are essential contributors to the aging process in unicellular and multicellular eukaryotes [53, 68, 107, 112, 114, 172–176, 193, 201, 206, 208–213, 217, 224, 229, 245, 259, 292, 312, 316, 512–520]. Since PE21 promotes a rapid age-related degradation of neutral lipids deposited in LD (see Chapter 2 of the thesis), we sought to determine whether PE21 may affect the abundance of other lipid classes in chronologically aging yeast under non-CR conditions. We, therefore, used quantitative mass spectrometry to compare the cellular lipidome of wild-type (WT) yeast cultured under non-CR conditions on 2% glucose with 0.1% (w/v) PE21 to the cellular lipidome of WT cells cultured on 2% glucose without PE21. If PE21 is used at the final concentration of 0.1% with ethanol being utilized as a vehicle at the final concentration of 0.5% (v/v), this PE exhibits the highest efficacy of yeast CLS extension under non-CR conditions on 2% glucose; this is in comparison to WT cells subjected to ethanol-mock treatment by being cultured in growth medium initially containing 2% glucose and 0.5% ethanol (see Chapter 2 of the thesis). Cells for lipid extraction and mass spectrometric lipidomics were recovered on days 1, 2, 3 and 4 of culturing on 2% glucose because only 11.7 ± 4.4% (n = 35) of WT cells cultured without PE21 were viable after 4 days of such culturing (see Chapter 2 of the thesis). In contrast, 95.6 ± 3.1% (n = 35) of WT cells cultured with 0.1% PE21 were viable after 4 days of culturing on 2% glucose (see Chapter 2 of the thesis).

PE21 exhibited differential effects on the relative levels of different lipid classes calculated as mol% of all lipids; moreover, these effects of PE21 were age-related. Indeed, we found that 1) PE21 elicits a significant decline in the relative levels of TAG, free (i.e. unesterified) fatty acids (FFA) and the signature mitochondrial membrane lipid cardiolipin (CL); 2) the extent to which PE21 lowers the relative levels of TAG, FFA and CL is gradually increased with the chronological age of WT cells; 3) PE21 causes a significant decline in the relative level of CL in WT cells recovered at L phase (on day 1 of culturing), PD phase (on day 2 of culturing) and ST phase (on

days 3 and 4 of culturing); and 4) PE21 significantly decreases the relative levels of TAG and FFA only in WT cells recovered at PD or ST phase of culturing (Figures 3.1A, 3.1B and 3.1H). Our mass spectrometric identification and quantitation of cellular lipids also revealed that 1) PE21 causes a significant rise in the relative levels of all membrane glycerophospholipids, including phosphatidic acid (PA), phosphatidylserine (PS), phosphatidylethanolamine (PE), phosphatidylcholine (PC) and phosphatidylinositol (PI); 2) the extent of such effect of PE21 on the relative levels of PA, PS, PE, PC and PI is gradually increased with the chronological age of WT cells; 3) PE21 elicits a significant rise in the relative level of PE in WT cells recovered at L phase (on day 1 of culturing), PD phase (on day 2 of culturing) and ST phase (on days 3 and 4 of culturing); 4) PE21 significantly raises the relative levels of PA, PS and PI only in WT cells recovered at PD or ST phase of culturing; and 5) PE21 causes a significant increase in the relative level of PC only in WT cells recovered at ST phase on day 4 of culturing (Figures 3.1C, 3.1D, 3.1E, 3.1F, and 3.1G).

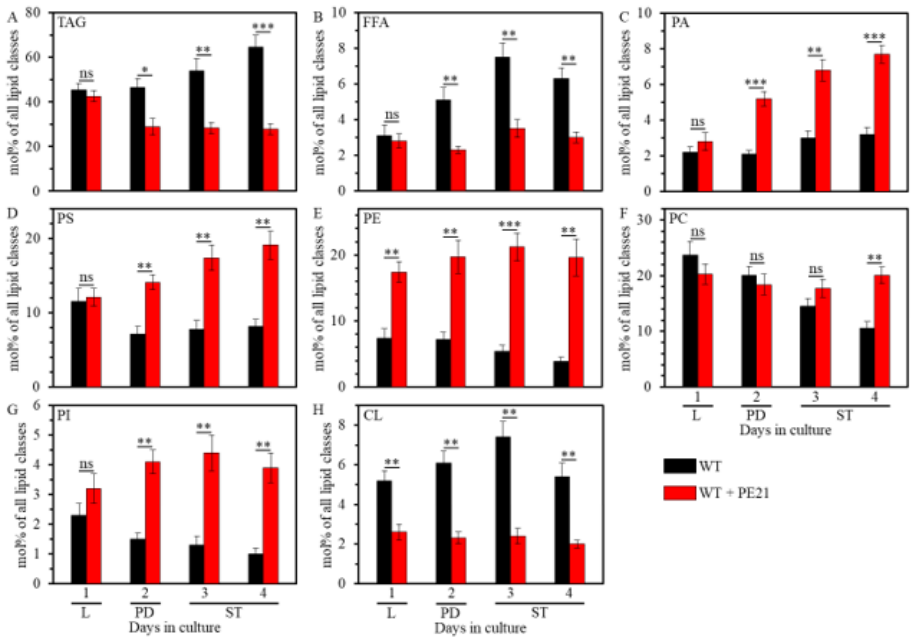

Figure 3.1. PE21 exhibits age-dependent differential effects on the relative levels of different lipid classes. Cells of the wild-type (WT) strain were grown in synthetic minimal YNB medium (0.67% [w/v] Yeast Nitrogen Base without amino acids) initially containing 2% (w/v) glucose, in the presence of 0.1% (w/v) PE21 (ethanol was used as a vehicle at the final concentration of 0.5% [v/v]) or in its absence (cells were subjected to ethanol-mock treatment). Cells were recovered on days 1, 2, 3 and 4 of culturing. Extraction of cellular lipids and mass spectrometric identification and quantitation of different lipid classes were carried out as described in Materials and Methods. Based on these data, the relative levels of different lipid classes were calculated as mol% of all lipid classes in cells recovered on day 1, 2, 3 or 4 of culturing. Data are presented as means ± SEM (n = 4; *$p < 0.05$; **$p < 0.01$; ***$p < 0.001$; ns, not significant). Abbreviations: Logarithmic (L), post-diauxic (PD) or stationary (ST) growth phase.

In sum, these findings indicate that PE21 causes significant age-related changes in the relative levels of different lipid classes in WT cells under non-CR conditions.

3.3.2 PE21 causes a specific remodeling of lipid metabolism and transport in chronologically aging yeast, likely by redirecting the flows of FFA and PA into different classes of lipids

Our findings that PE21 alters the relative levels of FFA, the neutral lipid TAG, the signature mitochondrial membrane lipid CL and all classes of membrane glycerophospholipids suggest that PE21 may instigate a specific remodeling of lipid metabolism and transport in several organelles of chronologically aging yeast. The metabolic and interorganellar transport processes that define the concentrations of all these lipid classes in yeast cells are well known [53, 68, 107, 112, 114, 172–176, 193, 201, 206, 208–213, 217, 224, 229, 245, 259, 292, 312, 316, 512–520]. These processes are catalyzed by enzymes that reside in the cytosol, ER, mitochondria, LD and peroxisomes (Figure 3.2) [53, 68, 107, 112, 114, 172–176, 193, 201, 206, 208–213, 217, 224, 229, 245, 259, 292, 312, 316, 512–520].

Glucose, the only carbon source exogenously added to yeast cultures in this study, is initially converted to pyruvate via the glycolytic pathway in the cytosol (Figure 3.2). The glycolytically produced pyruvate is then used for the synthesis of acetyl-CoA (Ac-CoA) through three consecutive reactions catalyzed by the cytosolic pyruvate decarboxylase isozymes Pdc1, Pdc5 and Pdc6, aldehyde dehydrogenases Ald2-Ald6, and Ac-CoA synthetase isoforms Acs1 and Acs2 (Figure 3.2). After being synthesized in the cytosol, Ac-CoA is used as a substrate for the formation of FFA by the cytosolic Ac-CoA carboxylase Acc1 and FA synthase complex Fas1/Fas2 (Figure 3.2). The cytosolic pool of Ac-CoA used for the formation of FFA by Acc1 and Fas1/Fas2 is also created as the product of peroxisomal β-oxidation of FFA in Fox1-, Fox2- and Fox3-dependent chemical reactions (Figure 3.2). Other sources of FFA are the hydrolysis of TAG by the lipases Tgl1, Tgl3, Tgl4 and Tgl5 confined to LD (Figure 3.2), as well as the lipolytic degradation of TAG-derived diacylglycerols (DAG) and monoacylglycerols (MAG) by the lipases Tgl3 and Yju3 (respectively) in LD (Figure 3.2).

After FFA are formed from Ac-CoA, TAG, DAG or MAG, they are activated to yield fatty acyl-CoA esters (FA-CoA) in reactions catalyzed by the long-chain acyl-CoA synthetases Faa1, Faa4 and Fat1 in the ER (Figure 3.2). These FA-CoA are then used for the *de novo* synthesis of

TAG, glycerophospholipids, and CL by enzymes confined to the ER and mitochondria (Figure 3.2). This *de novo* synthesis begins in the ER where the glycerol-3-phosphate/dihydroxyacetone phosphate acyltransferases Sct1 and Gpt2 catalyze the formation of lysophosphatidic acid (LPA) or acyl-dihydroxyacetone phosphate (ADHAP) from FA-CoA and glycerol-3-phosphate or DHAP, respectively (Figure 3.2). An Ayr1-driven reaction converts ADHAP to LPA (Figure 3.2). The LPA formed in an Sct1-, Gpt2- and Ayr1-dependent manner is then converted to PA in an acyl CoA-dependent reaction catalyzed by the LPA acyl-transferases Slc1, Slc4, Loa1 and Ale1 (Figure 3.2). A Cds1-driven reaction converts PA to cytidine diphosphate (CDP)-DAG, which is then used as a common precursor for the Cho1-dependent synthesis of PS in the ER, transfer of PS from the ER to the outer mitochondrial membrane (OMM) via mitochondria-ER contact sites, Ups2-driven transport of PS from the OMM to the inner mitochondrial membrane (IMM) via the intermediate space (IMS), Psd1-dependent synthesis of PE in the IMM, transfer of PE from the IMM across the IMS to the OMM and then to the ER via mitochondria-ER contact sites, Pis1-dependent synthesis of PI in the ER, and Cho2- and Opi3-dependent synthesis of PC in the ER (Figure 3.2). PA can also be converted to DAG in a reaction catalyzed by the PA phosphatases Pah1, App1, Dpp1 and Lpp1 in the ER (Figure 3.2). The ensuing acylation of DAG to TAG occurs in an FA-CoA-dependent reaction driven by Dga1, Are1 and Are2, and in a PE- and PC-dependent reaction catalyzed by Lro1 (Figure 3.2). After the *de novo* synthesis of TAG in the ER, TAG are deposited in LD (Figure 3.2). In addition, PA can move from the ER to the OMM via mitochondria-ER contact sites and then from the OMM to the IMM in an Ups1-dependent transfer reaction inhibited by CL (Figure 3.2). After the ER-derived PA is delivered to the IMM, it is converted into CDP-DAG, phosphatidylglycerol (PG), CL and monolysocardiolipin (MLCL) in reactions catalyzed by Tam41, Pgs1, Gep4, Crd1, Cld1 and Taz1 (Figure 3.2).

Considering the intensive knowledge of lipid metabolism and interorganellar transport in yeast cells, our data on PE21-dependent changes in the cellular lipidome indicate that PE21 redirects the flows of FFA and PA into different classes of lipids to cause a specific reorganization of lipid metabolism and transport in chronologically aging yeast. A model of such PE21-driven reorganization of lipid metabolism and transport in yeast cells is schematically depicted in Figure 3.3. In this model, PE21 alters the efficiencies with which FFA and PA are incorporated into the synthesis of other lipids as follows: 1) it intensifies FFA incorporation into PA, thus lowering FFA concentration and increasing PA concentration; 2) it decreases the efficiency of PA flow into the

synthesis of TAG in the ER, thereby lowering TAG concentration, decreasing the concentration of FFA derived from TAG lipolysis and raising PA concentration; 3) it intensifies PA entry into the synthesis of glycerophospholipids in the ER and mitochondria, thus increasing the concentrations of PS, PE, PC and PI in the ER and raising PS and PE concentrations in mitochondria; and 4) it lowers the efficiency of PA transport from the ER to the OMM and then to the IMM, thereby decreasing the concentrations of PA-derived CL in mitochondrial membranes (Figure 3.3).

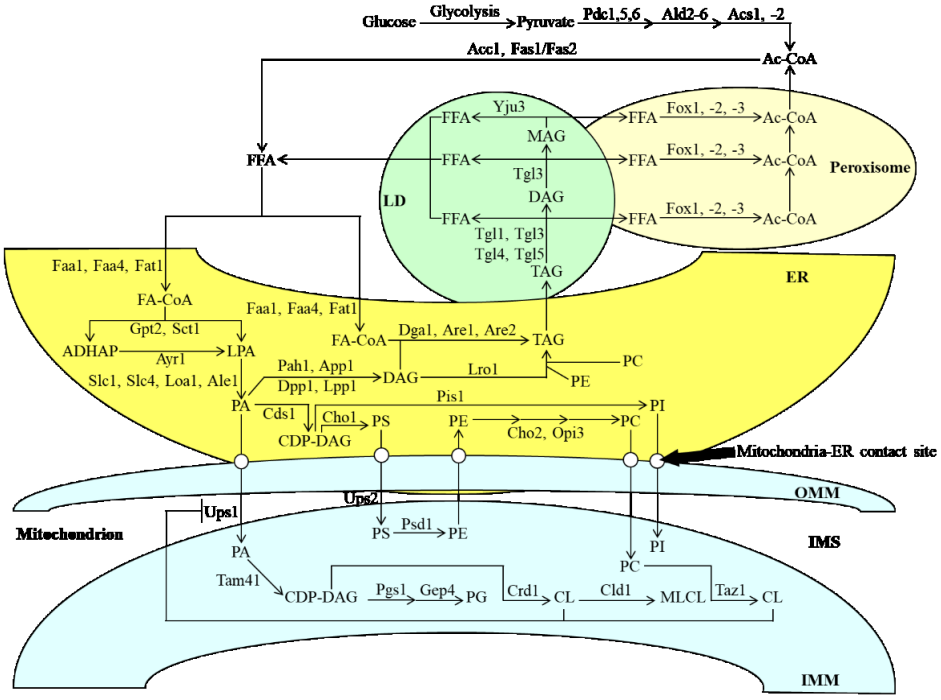

Figure 3.2. The relative concentrations of various lipid classes in yeast cells depend on the metabolic and interorganellar transport processes that are catalyzed by enzymes residing in the cytosol, endoplasmic reticulum (ER), mitochondria, lipid droplets (LD) and peroxisomes. A T bar denotes a cardiolipin (CL)-dependent inhibition of phosphatidic acid (PA) transfer from the outer mitochondrial membrane (OMM) across the intermediate space (IMS) to the inner mitochondrial membrane (IMM). See text for more details. Other abbreviations: Acc1, acetyl-CoA carboxylase 1; Ac-CoA, acetyl-CoA; Acs1 and Acs2, acetyl CoA synthetases 1 and 2; ADHAP, acyl-dihydroxyacetone phosphate; Ale1, acyltransferase for lysophosphatidylethanolamine 1; Ald2-6, aldehyde dehydrogenases 2 to 6; App1, actin patch protein 1; Are1/2, acyl-coenzyme A: cholesterol acyl transferase-related enzymes 1 and 2; Ayr1, acyl-dihydroxyacetone-phosphate reductase 1; CDP, cytidine diphosphate; Cds1, CDP-diacylglycerol synthase 1; Cho1/2, choline requiring 1 and 2; CL, cardiolipin; Cld1, cardiolipin-specific deacylase 1; Crd1, cardiolipin synthase 1; DAG, diacylglycerol; Dga1, diacylglycerol acyltransferase 1; Dpp1, diacylglycerol pyrophosphate phosphatase 1; Faa1 and Faa4, fatty acid activation proteins 1 and 4; FA-CoA, fatty acyl-CoA ester; Fas1 and Fas2, fatty acid synthetases 1 and 2; Fat1, fatty acid transporter 1; FFA, free fatty acid; Fox1, Fox2 and Fox3, fatty acid oxidation proteins 1, 2 and 3; Gep4, genetic interactor of prohibitins protein 4; Gpt2, glycerol-3-phosphate acyltransferase; Loa1, lysophosphatidic acid: oleoyl-CoA acyltransferase 1; Lpp1, lipid phosphate phosphatase 1; LPA, lysophosphatidic acid; Lro1, lecithin cholesterol acyl transferase related open reading frame 1; MAG, monoacylglycerol; MLCL, monolysocardiolipin; Opi3, overproducer of inositol 3; PA, phosphatidic acid; Pah1, phosphatidic acid phosphohydrolase 1; PC, phosphatidylcholine; Pdc1, Pdc5 and Pdc6, pyruvate decarboxylases 1, 5 and 6; PE, phosphatidylethanolamine; PG, phosphatidylglycerol; Pgs1, phosphatidylglycerolphosphate synthase 1; PI, phosphatidylinositol; Pis1, phosphatidylinositol synthase 1; PS, phosphatidylserine; Psd1, phosphatidylserine decarboxylase 1; Sct1, suppressor of choline-transport mutants 1; Slc1 and Slc4, sphingolipid compensation proteins 1 and 4; Tam41, translocator assembly and maintenance protein 41; TAG, triacylglycerol; Taz1, tafazzin protein 1;

Tgl1, Tgl3, Tgl4, Tgl5, triglyceride lipases 1, 3, 4 and 5; Ups1 and Ups2, unprocessed proteins 1 and 2; Yju3, monoglyceride lipase.

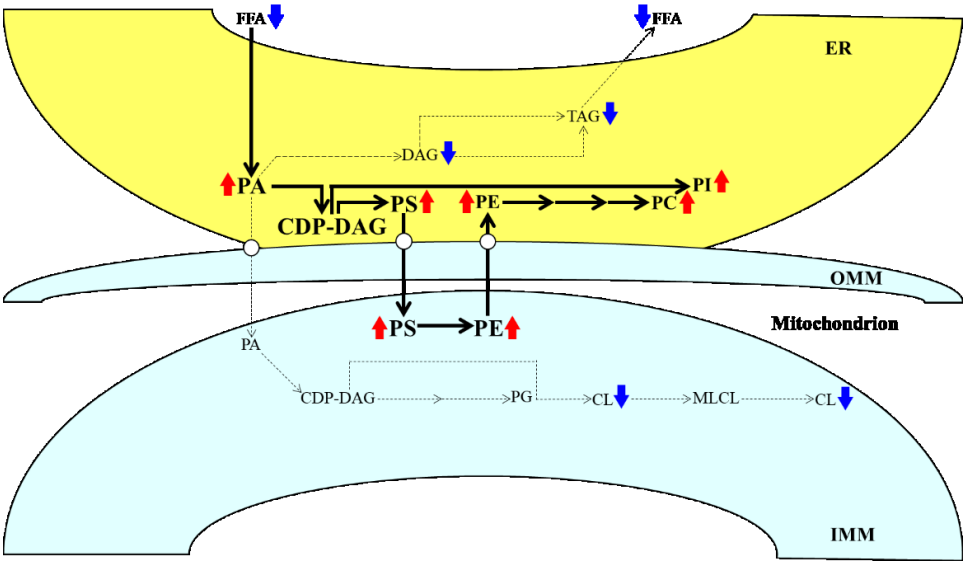

Figure 3.3. A model for a PE21-dependent reorganization of lipid metabolism and transport in yeast cells. PE21 alters the efficiencies with which free fatty acids (FFA) and phosphatidic acid (PA) are included in the synthesis of other lipid classes in the endoplasmic reticulum (ER) and mitochondria. Arrows next to the names of lipid classes denote those of them whose concentrations are increased (red arrows) or decreased (blue arrows) in yeast cells cultured in the presence of PE21. The thickness of black arrows is proportional to the efficiency with which FFA and PA are included in the synthesis of other lipid classes. See text for more details. Other abbreviations: CL, cardiolipin; CDP, cytidine diphosphate; DAG, diacylglycerol; IMM, inner mitochondrial membrane; MLCL, monolysocardiolipin; OMM, outer mitochondrial membrane; PC, phosphatidylcholine; PE, phosphatidylethanolamine; PG, phosphatidylglycerol; PI, phosphatidylinositol; PS, phosphatidylserine; TAG, triacylglycerol.

3.3.3 Our hypothesis on three possible mechanisms through which PE21 may delay yeast chronological aging and extend yeast longevity

Based on the abilities of PE21 to cause a specific remodeling of lipid metabolism and transport (see above) and to impose changes in certain cellular processes (see Chapter 2 of the thesis) within yeast cultured under non-CR conditions, we put forward a hypothesis that there may be at least three different mechanisms by which PE21 delays yeast chronological aging and extends yeast CLS. These possible mechanisms are outlined below and schematically depicted in Figure 3.4.

First mechanism: the present study demonstrates that PE21 lowers FFA concentration, likely because it intensifies FFA incorporation into PA (Figures 3.1B and 3.1C; Figure 3.3). The present study also reveals that PE21 decreases the concentration of TAG (Figure 3.1A; Figure 3.3), the major form of FFA storage [53, 68, 107, 172, 174, 211, 212, 292, 517]; this may further contribute to the PE21-driven decline in FFA concentration because the lipolysis of TAG in chronologically aging yeast is known to be a source of the bulk quantities of FFA [53, 68, 107,

172, 174, 211, 212, 292, 517]. Exposure of yeast cells to exogenous FFA has been shown to promote a "liponecrotic" form of RCD in an age-related manner [68, 98, 610, 623-628]. Such exposure elicits the incorporation of FFA into membrane glycerophospholipids and TAG, thereby reorganizing lipid metabolism and transfer in the ER, mitochondria, LD and the plasma membrane (PM) [68, 98, 110, 112, 246, 521–524]. Certain aspects of the FFA-driven reorganization of lipid metabolism and transfer are essential contributors to the commitment of yeast to liponecrosis or to the execution of this mode of RCD [68, 98, 110, 112, 246, 521–524]. These aspects include the following: 1) an excessive rise in PM permeability for small molecules; 2) a decline in mitochondrial functionality; 3) an excessive production of ROS in mitochondria; 4) oxidative damage to various cellular organelles, which promotes massive autophagic degradation of these organelles; and 5) oxidative impairment of the bulk quantities of cellular proteins, which disturbs cellular proteostasis by eliciting a build-up of dysfunctional, unfolded and aggregated proteins in the cytosol [68, 98, 110, 112, 246, 521–524]. Because the accumulation of excessive quantities of FFA actively increases the risk of liponecrotic cell death and decreases the chance of cell survival throughout the chronological lifespan, FFA accumulation in quantities exceeding a toxic threshold shortens the longevity of chronologically aging yeast [68, 98, 110, 112, 246, 521–524]. It needs to be emphasized that PE21 not only extends yeast longevity but also affects some of those aspects of the FFA-driven reorganization of the cellular lipidome that contribute to the commitment or execution of liponecrotic RCD (see Chapter 2 of this thesis). Indeed, PE21 slows an age-related decline in mitochondrial functionality, alters the pattern of age-related changes in mitochondrially produced ROS and decreases the extent of oxidative damage to cellular proteins (see Chapter 2 of this thesis). Taken together, these findings suggest that the first mechanism through which PE21 may delay yeast chronological aging and extend yeast CLS consists in the ability of PE21 to lower FFA concentration, thus maintaining FFA concentration below the toxic threshold and weakening an age-related form of FFA-driven liponecrotic RCD (Figure 3.4).

Second mechanism: the present study shows that PE21 causes significant perturbations in the relative levels of membrane lipids within the ER by weakening TAG formation and strengthening glycerophospholipid synthesis in this organelle (Figures 3.1B and 3.1C-3.1G; Figure 3.3). Such perturbations in the relative levels of ER membrane lipids are known to stimulate the unfolded protein response in the ER (UPR^{ER}) in yeast and metazoans, either by weakening the folding of ER proteins and eliciting their accumulation in the ER or without causing unfolded

protein stress within this organelle [111, 525, 526, 527–547]. When activated, the UPR^{ER} system allows to reinstate protein and lipid homeostasis in the ER by slowing down protein synthesis in the ER, stimulating *N*-linked protein glycosylation of ER proteins, promoting a refolding of some improperly folded ER proteins, directing other improperly folded proteins accumulated in the ER for the removal by ER-associated degradation or autophagy, enhancing vesicular traffic from the ER throughout the secretory pathway, and activating the synthesis of membrane lipids in the ER [544, 548–554]. A body of evidence indicates that the UPR^{ER} system of protein and lipid homeostasis restoration within the ER is indispensable for preventing an age-related decline in protein and lipid homeostasis maintenance within the entire cell; this is because the UPR^{ER} system slows protein synthesis, weakens oxidative and thermal protein damage, promotes protein folding and vesicular transport, stimulates autophagic and proteasomal degradation of improperly folded proteins, and controls lipid metabolism within the entire cell [530, 534, 539, 542–544, 546, 549, 553–568]. As such, the UPR^{ER} system is commonly perceived as a process that is essential for delaying cellular and organismal aging and slowing down the onset of aging-associated disorders [111, 529, 532, 549, 553–568]. Of note, the ability of PE21 to extend the longevity of chronologically aging yeast coincides with its ability to decrease the extent of oxidative damage to cellular proteins, lipids and nucleic acids, and to increase cell resistance to chronic oxidative stress (see Chapter 2 of this thesis). In sum, the above findings suggest that the second mechanism by which PE21 may delay yeast chronological aging and extend yeast CLS consists in its ability to alter the ER lipidome, thus activating the UPR^{ER} (Figure 3.4). Our hypothesis posits that such PE21-driven activation of the UPR^{ER} system may be responsible for the observed abilities of PE21 to slow down an age-related decline in protein, lipid and nucleic acid homeostasis and to decelerate an aging-associated weakening of cell resistance to oxidative and thermal stresses (see Chapter 2 of this thesis).

Third mechanism: the present study reveals that PE21 alters the membrane lipidome of mitochondria by raising PS and PE concentrations and lowering CL concentration in these organelles (Figures 3.1D, 3.1E and 3.1H; Figure 3.3). A body of evidence supports the notion that the composition of mitochondrial membrane lipids is an essential contributor to mitochondrial functionality and as such, the mitochondrial membrane lipidome defines the longevity of yeast and multicellular eukaryotes [63, 68, 72, 251, 254–257, 507, 569–573]. Notable, PE21 not only prolongs yeast longevity but also amends the pattern of age-related changes in several key aspects

of mitochondrial functionality, including mitochondrial respiration, mitochondrial membrane potential, and mitochondrial ROS production (see chapter 2 of this thesis). These findings suggest that the third mechanism by which PE21 may delay yeast chronological aging and extend yeast longevity consists in its ability to reorganize some processes confined to mitochondria, thus altering mitochondrial functionality (Figure 3.4).

In a series of experiments outlined below in this chapter, we assessed how the first proposed mechanism contributes to the extension of yeast CLS by PE21.

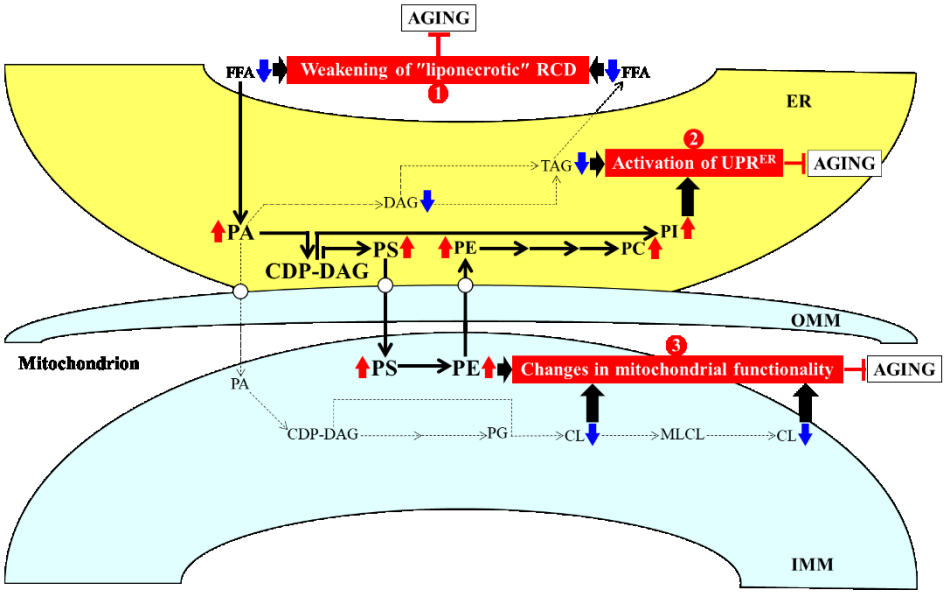

Figure 3.4. Possible mechanisms through which PE21 may delay yeast chronological aging. Arrows next to the names of lipid classes denote those of them whose concentrations are increased (red arrows) or decreased (blue arrows) in yeast cells cultured in the presence of PE21. The thickness of black arrows is proportional to the efficiency with which free fatty acids (FFA) and phosphatidic acid (PA) are included in the synthesis of other lipid classes. There may be at least three different mechanisms by which PE21 delays yeast chronological aging. These mechanisms are numbered. Mechanism 1: PE21 maintains FFA concentration below a toxic threshold, thus weakening an age-related form of FFA-driven liponecrotic regulated cell death (RCD). Mechanism 2: PE21 suppresses TAG formation and promotes glycerophospholipid synthesis in the endoplasmic reticulum (ER), thereby activating the unfolded protein response in the ER (UPR^{ER}). Mechanism 3: PE21 increases phosphatidylserine (PS) and phosphatidylethanolamine (PE) concentrations and lower cardiolipin (CL) concentration in mitochondria, thus altering mitochondrial functionality. See text for more details. Other abbreviations: CDP, cytidine diphosphate; DAG, diacylglycerol; IMM, inner mitochondrial membrane; MLCL, monolysocardiolipin; OMM, outer mitochondrial membrane; PC, phosphatidylcholine; PG, phosphatidylglycerol; PI, phosphatidylinositol; TAG, triacylglycerol.

3.3.4 PE21 extends the longevity of chronologically aging yeast in part because it delays the age-related onset of FFA-dependent liponecrotic RCD

Our hypothesis on the first mechanism through which PE21 may extend the longevity of chronologically aging yeast predicts that mutations capable of increasing cellular FFA concentration will weaken the longevity-extending efficiency of PE21 (Figure 3.4). To test this

prediction, we examined how a single-gene-deletion mutation eliminating the Faa1, Faa4, Ale1 or Slc1 protein affects the efficiency of yeast CLS extension by PE21 and how it influences the cellular concentration of FFA. Faa1, Faa4, Ale1 and Slc1 catalyze reactions of the incorporation of FFA into PA within the ER (Figure 3.2) [68, 175, 176, 513]. A single-gene-deletion mutation eliminating either of these four proteins is known to increase the concentration of FFA in yeast cultured in the nutrient-rich YPD (1% yeast extract and 2% peptone) medium initially containing 2% glucose [177, 186, 189, 574, 575]. It was unknown, however, if any of these mutations have a similar effect on FFA concentration in yeast cultured in synthetic minimal YNB medium (0.67% yeast nitrogen base) initially containing 2% glucose (i.e. under culturing conditions used in the present study). We found that the *faa1Δ*, *faa4Δ*, *ale1Δ* and *slc1Δ* mutations cause a significant decline in the efficiency with which PE21 can prolong both the mean and maximum CLS of *S. cerevisiae*, although the extent of such decline was different for each of these single-gene-deletion mutations (Figures 3.5A-3.5D and 3.5F-3.5I for *faa1Δ* and *faa4Δ*, respectively; Figures 3.6A-3.6D and 3.6F-3.6I for *ale11Δ* and *slc1Δ*, respectively). We also revealed that all of these single-gene-deletion mutations substantially increase cellular FFA concentration; however, the extent of such rise in cellular FFA concentration was different for each of them (Figures 3.5E and 3.5J for *faa1Δ* and *faa4Δ*, respectively; Figures 3.6E and 3.6J for *ale11Δ* and *slc1Δ*, respectively). In sum, the above findings support our prediction that mutations increasing cellular FFA concentration can weaken the efficiency with which PE21 prolongs the longevity of chronologically aging yeast.

In our hypothesis on the first mechanism, mutations that decrease cellular FFA concentration are expected to enhance the longevity-extending efficiency of PE21 (Figure 3.4). We, therefore, investigated how a single-gene-deletion mutation eliminating the Tgl1, Tgl3, Tgl4 or Tgl5 protein influences the efficiency of yeast CLS extension by PE21 and how it affects the cellular concentration of FFA. Tgl1, Tgl3, Tgl4 and Tgl5 catalyze reactions of the formation of FFA as products of TAG lipolysis in LD (Figure 3.2) [53, 68, 172–174, 201, 211, 212, 512]. A knock-out mutation removing any of these four proteins has been shown to increase the concentration of FFA in yeast cultured in the nutrient-rich YPD medium initially supplemented with 2% glucose [198, 199, 576]. However, it remained unknown if any of these mutations have a similar effect on FFA concentration in yeast cultured in a synthetic minimal YNB medium initially supplemented with 2% glucose, i.e. under conditions yeast were cultured in the present study. We found that the *tgl1Δ*, *tgl3Δ*, *tgl4Δ* and *tgl5Δ* mutations increase the efficiency with which PE21

can extend yeast CLS and that the extent of such increase is different for each of these mutations (Figures 3.7A-3.7D and 3.7F-3.7I for *tgl1Δ* and *tgl3Δ*, respectively; Figures 3.8A-3.8D and 3.8F-3.8I for *tgl4Δ* and *tgl5Δ*, respectively). We also noted that all of these mutations decrease cellular FFA concentration and that the extent of such decrease is different for each of them (Figures 3.7E and 3.7J for *tgl1Δ* and *tgl3Δ*, respectively; Figures 3.8E and 3.8J for *tgl3Δ* and *tgl4Δ*, respectively). Together, these data confirm that mutations decreasing cellular FFA concentration can enhance the longevity-extending efficiency of PE21.

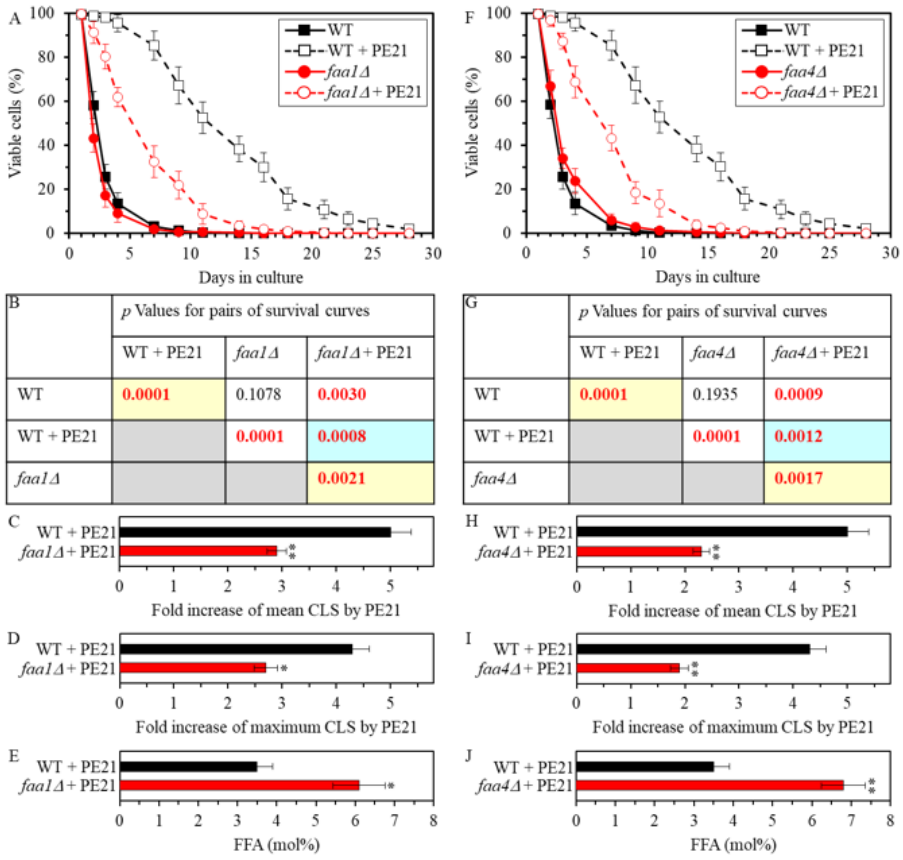

Figure 3.5. The *faa1Δ* and *faa4Δ* mutations eliminate enzymes involved in the incorporation of FFA into PA. These mutations increase cellular FFA concentration and decrease the efficiency with which PE21 prolongs yeast chronological lifespan (CLS). WT cells and mutant cells carrying a single-gene-deletion mutation eliminating either Faa1 or Faa4 were cultured in the synthetic minimal YNB medium initially containing 2% glucose with 0.1% PE21 or without it. (**A**, **F**) Survival curves of the chronologically aging WT and *faa1Δ* (**A**) or WT and *faa4Δ* (**F**) strains are shown. Data are presented as means ± SEM (n = 3). (**B**, **G**) *p* Values for different pairs of survival curves of the WT and *faa1Δ* (**B**) or WT and *faa4Δ* (**G**) strains cultured with or without PE21. Survival curves are shown in **A** or **F** (respectively) were compared. Two survival curves were considered statistically different if the *p* value was less than 0.05. The *p* values for comparing pairs of survival curves using the logrank test were calculated as described in Materials and Methods. The *p* values displayed on a yellow color background indicate that PE21 statistically significantly prolongs the CLS of the WT, *faa1Δ* (**B**) and *faa4Δ* (**G**) strains. The *p* values displayed on a blue color background indicate that PE21 prolongs the CLS of the *faa1Δ* (**B**) and *faa4Δ* (**G**) strains to a lower extent than that of the WT strain. (**C**, **D**, **H**, **I**) Survival curves shown in (**A**, **F**) were used to calculate the fold of increase of the mean (**C**, **H**) and maximum (**D**, **I**) CLS by PE21 for the WT and *faa1Δ* (**C**, **D**) and WT and *faa4Δ* (**H**, **I**) strains. Data are presented as means ± SEM (n = 3; **p* < 0.05; ***p* < 0.01). (**E**, **J**) The maximum concentration of free fatty acids (FFA), which was observed in WT and *faa1Δ* (**E**) or WT and *faa4Δ* (**J**) cells recovered on day 3 of culturing with PE21, is shown. Data are presented as means ± SEM (n = 4; **p* < 0.05; ***p* < 0.01).

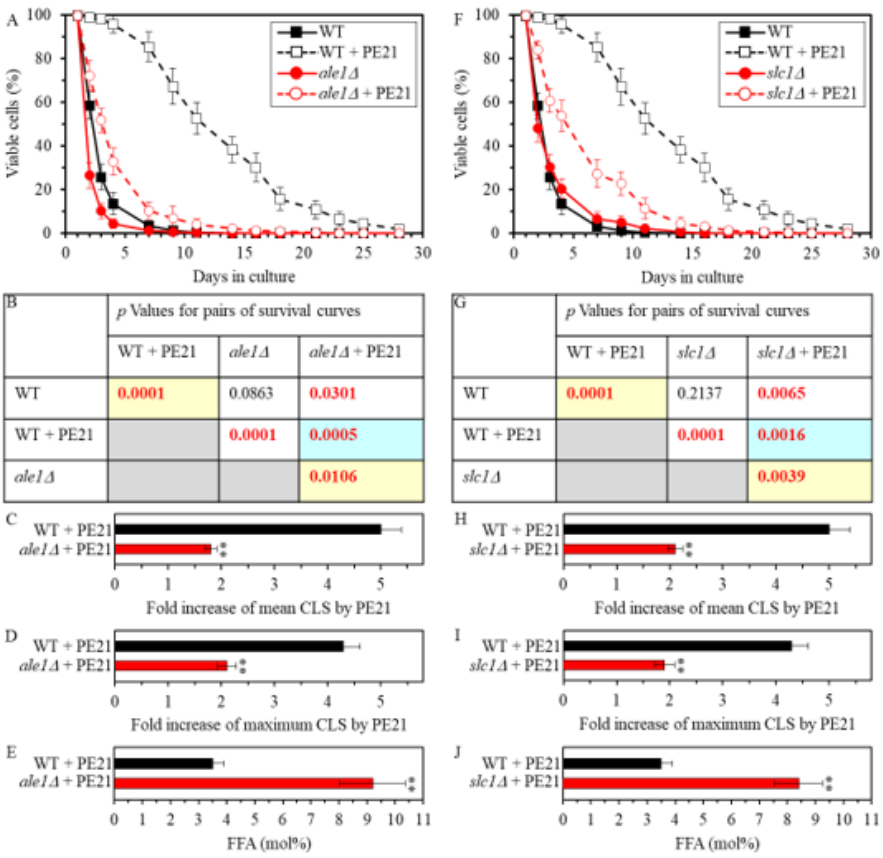

Figure 3.6. The *ale1Δ* and *slc1Δ* mutations eliminate enzymes involved in the incorporation of FFA into PA. These mutations increase cellular FFA concentration and decrease the efficiency with which PE21 prolongs yeast CLS. WT cells and mutant cells carrying a single-gene-deletion mutation eliminating either Ale1 or Slc1 were cultured in the synthetic minimal YNB medium initially containing 2% glucose with 0.1% PE21 or without it. (**A**, **F**) Survival curves of the chronologically aging WT and *ale1Δ* (**A**) or WT and *slc1Δ* (**F**) strains are shown. Data are presented as means ± SEM (n = 3). (**B**, **G**) *p* Values for different pairs of survival curves of the WT and *ale1Δ* (**B**) or WT and *slc1Δ* (**G**) strains cultured with or without PE21. Survival curves are shown in **A** or **F** (respectively) were compared. Two survival curves were considered statistically different if the *p* value was less than 0.05. The *p* values for comparing pairs of survival curves using the logrank test were calculated as described in Materials and Methods. The *p* values displayed on a yellow color background indicate that PE21 statistically significantly prolongs the CLS of the WT, *ale1Δ* (**B**) and *slc1Δ* (**G**) strains. The *p* values displayed on a blue color background indicate that PE21 prolongs the CLS of the *ale1Δ* (**B**) and *slc1Δ* (**G**) strains to a lower extent than that of the WT strain. (**C**, **D**, **H**, **I**) Survival curves shown in (**A**, **F**) were used to calculate the fold of increase of the mean (**C**, **H**) and maximum (**D**, **I**) CLS by PE21 for the WT and *ale1Δ* (**C**, **D**) and WT and *slc1Δ* (**H**, **I**) strains. Data are presented as means ± SEM (n = 3; $^{**}p < 0.01$). (**E**, **J**) The maximum concentration of free fatty acids (FFA), which was observed in WT and *ale1Δ* (**E**) or WT and *slc1Δ* (**J**) cells recovered on day 3 of culturing with PE21, is shown. Data are presented as means ± SEM (n = 4; $^{*}p < 0.05$; $^{**}p < 0.01$).

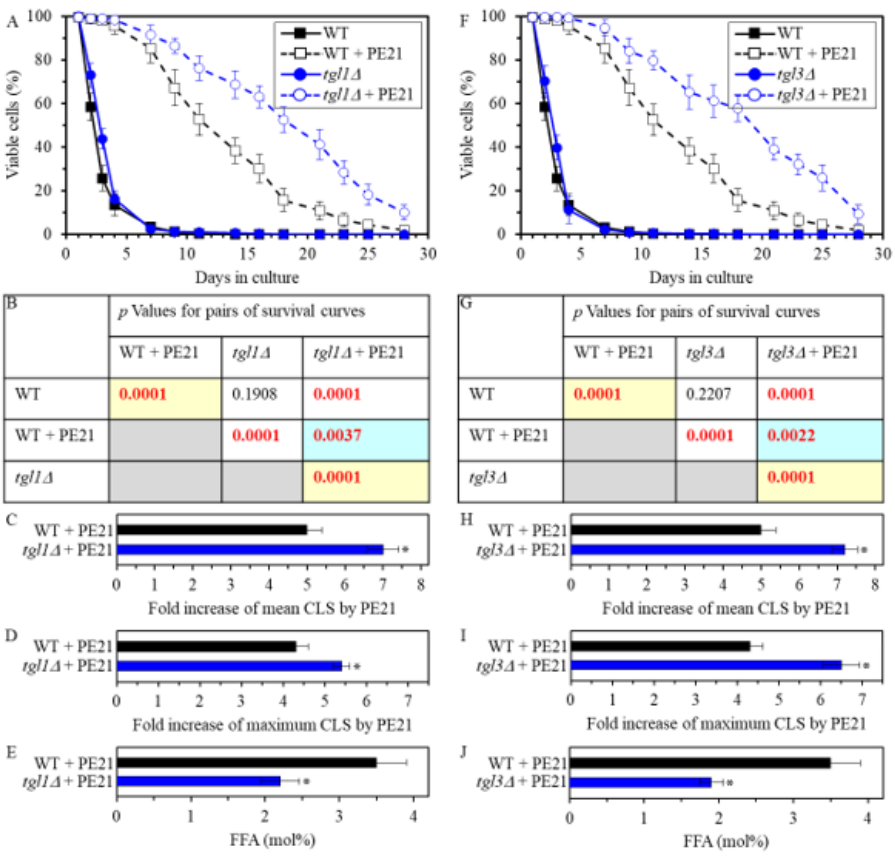

Figure 3.7. The *tgl1Δ* and *tgl3Δ* mutations eliminate enzymes involved in the formation of FFA as products of TAG lipolysis. These mutations cause a decline in cellular FFA concentration and elicit a rise in the efficiency of yeast CLS extension by PE21. WT cells and mutant cells carrying a single-gene-deletion mutation eliminating either Tgl1 or Tgl3 were cultured in the synthetic minimal YNB medium initially containing 2% glucose with 0.1% PE21 or without it. (**A**, **F**) Survival curves of the chronologically aging WT and *tgl1Δ* (**A**) or WT and *tgl3Δ* (**F**) strains are shown. Data are presented as means ± SEM (n = 3). (**B**, **G**) *p* Values for different pairs of survival curves of the WT and *tgl1Δ* (**B**) or WT and *tgl3Δ* (**G**) strains cultured with or without PE21. Survival curves are shown in **A** or **F** (respectively) were compared. Two survival curves were considered statistically different if the *p* value was less than 0.05. The *p* values for comparing pairs of survival curves using the logrank test were calculated as described in Materials and Methods. The *p* values displayed on a yellow color background indicate that PE21 statistically significantly prolongs the CLS of the WT, *tgl1Δ* (**B**) and *tgl3Δ* (**G**) strains. The *p* values displayed on a blue color background indicate that PE21 prolongs the CLS of the *tgl1Δ* (**B**) and *tgl3Δ* (**G**) strains to a higher extent than that of the WT strain. (**C**, **D**, **H**, **I**) Survival curves shown in (**A**, **F**) were used to calculate the fold of increase of the mean (**C**, **H**) and maximum (**D**, **I**) CLS by PE21 for the WT and *tgl1Δ* (**C**, **D**) and WT and *tgl3Δ* (**H**, **I**) strains. Data are presented as means ± SEM (n = 3; $*p < 0.05$). (**E**, **J**) The maximum concentration of free fatty acids (FFA), which was observed in WT and *tgl1Δ* (**E**) or WT and *tgl3Δ* (**J**) cells recovered on day 3 of culturing with PE21, is shown. Data are presented as means ± SEM (n = 4; $*p < 0.05$; $**p < 0.01$).

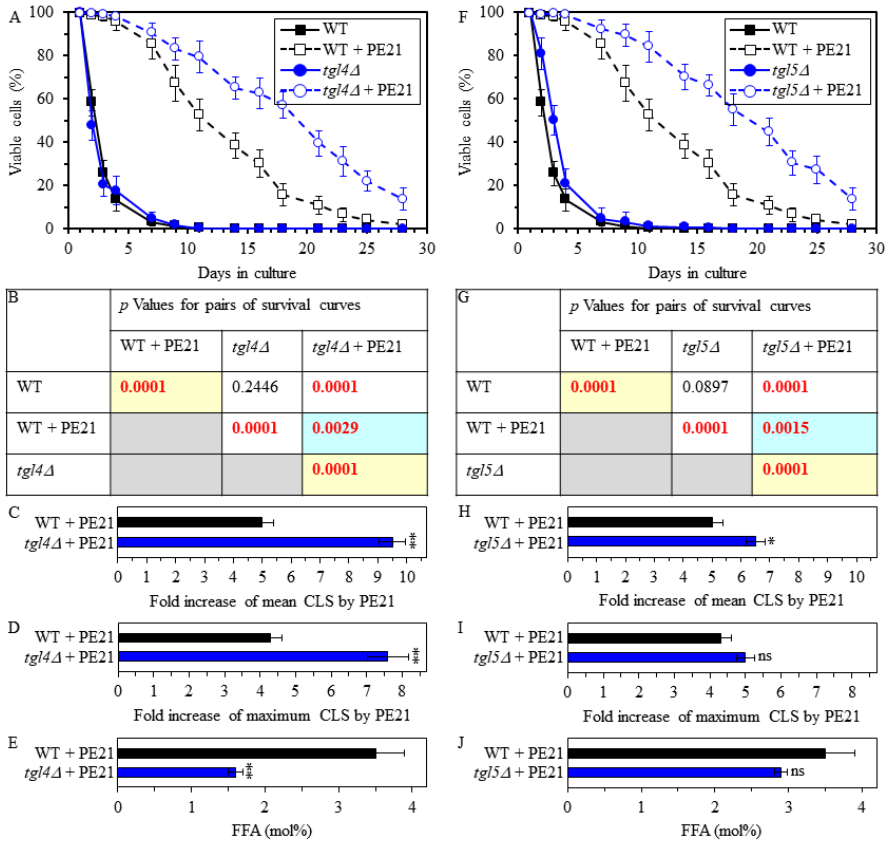

Figure 3.8. The *tgl4Δ* and *tgl5Δ* mutations eliminate enzymes that catalyze the formation of FFA as products of TAG lipolysis. These mutations cause a decline in cellular FFA concentration and elicit a rise in the efficiency of yeast CLS extension by PE21. WT cells and mutant cells carrying a single-gene-deletion mutation eliminating either Tgl4 or Tgl5 were cultured in the synthetic minimal YNB medium initially containing 2% glucose with 0.1% PE21 or without it. (**A**, **F**) Survival curves of the chronologically aging WT and *tgl4Δ* (**A**) or WT and *tgl5Δ* (**F**) strains are shown. Data are presented as means ± SEM (n = 3). (**B**, **G**) *p* Values for different pairs of survival curves of the WT and *tgl4Δ* (**B**) or WT and *tgl5Δ* (**G**) strains cultured with or without PE21. Survival curves are shown in **A** or **F** (respectively) were compared. Two survival curves were considered statistically different if the *p* value was less than 0.05. The *p* values for comparing pairs of survival curves using the logrank test were calculated as described in Materials and Methods. The *p* values displayed on a yellow color background indicate that PE21 statistically significantly extends the CLS of the WT, *tgl4Δ* (**B**) and *tgl5Δ* (**G**) strains. The *p* values displayed on a blue color background indicate that PE21 extends the CLS of the *tgl4Δ* (**B**) and *tgl5Δ* (**G**) strains to a higher extent than that of the WT strain. (**C**, **D**, **H**, **I**) Survival curves shown in (**A**, **F**) were used to calculate the fold of increase of the mean (**C**, **H**) and maximum (**D**, **I**) CLS by PE21 for the WT and *tgl4Δ* (**C**, **D**) and WT and *tgl5Δ* (**H**, **I**) strains. Data are presented as means ± SEM (n = 3; $^{**}p < 0.01$; ns, not significant). (**E**, **J**) The maximum concentration of free fatty acids (FFA), which was observed in WT and *tgl4Δ* (**E**) or WT and *tgl5Δ* (**J**) cells recovered on day 3 of culturing with PE21, is shown. Data are presented as means ± SEM (n = 4; $^{*}p < 0.05$; $^{**}p < 0.01$).

Using the above data on the values of CLS and cellular FFA concentrations for WT and mutant strains, we compared the PE21-dependent fold increase of mean or maximum CLS and the highest intracellular concentration of FFA in yeast cells cultured with PE21; FFA concentration was the highest in WT, *faa1Δ*, *faa4Δ*, *ale1Δ*, *slc1Δ*, *tgl1Δ*, *tgl3Δ*, *tgl4Δ* and *tgl5Δ* cells recovered on day 3 of culturing. We revealed that the Pearson's correlation coefficient (r) values for the correlation between these two compared variables are less than - 0.9 for both possible pairwise combinations of the mean or maximum CLS and the highest intracellular concentration of FFA (Figure 3.9). Because a Pearson's r value ranging from -0.9 to -1.0 is considered a very high

negative correlation between the two variables [577], we concluded that the PE21-dependent fold increase of mean or maximum CLS has a very high negative correlation with FFA concentration in the yeast cell. This observation confirms that, as predicted by our hypothesis on the first mechanism of PE21-dependent longevity extension, the efficiency of such extension inversely correlates with the intracellular concentration of FFA. Thus, PE21 delays yeast chronological aging and prolongs yeast CLS in part because it decreases FFA concentration in the yeast cell.

Our hypothesis on the first mechanism suggests that, because PE21 maintains FFA concentration below the toxic threshold, it may weaken an age-related form of FFA-driven liponecrotic RCD (Figure 3.4). To test this suggestion, we first used live-cell fluorescence microscopy with propidium iodide (PI) to examine if PE21 can influence the age-related onset and/or progression of this mode of necrotic RCD in WT and mutant strains. PI-positive staining is characteristic of necrotic RCD because PI is a stain used to visualize the loss of PM integrity, a hallmark event of necrotic RCD in yeast [25, 91, 110, 353, 521–524]. We found the following: 1) in WT cells, PE21 postpones the onset of necrosis as of day 2 of culturing and decelerates the progression of necrotic RCD after that (Figures 3.10A and 3.10B); 2) as of day 3 of culturing with PE21, the *faa1Δ*, *faa4Δ*, *ale1Δ* and *slc1Δ* mutations significantly increase the percentage of cells displaying PI-positive staining typical of necrotic RCD (Figures 3.11A-3.11D and 3.11J); and 3) as of day 3 of culturing with PE21, the *tgl1Δ*, *tgl3Δ*, *tgl4Δ* and *tgl5Δ* mutations decrease the percentage of cells exhibiting PI-positive staining characteristic of necrotic RCD (Supplementary Figures 3.11E-3.11H and 3.11J). Our comparison of the maximum percentage of cells displaying PI-positive staining (which was observed in WT, *faa1Δ*, *faa4Δ*, *ale1Δ*, *slc1Δ*, *tgl1Δ*, *tgl3Δ*, *tgl4Δ* and *tgl5Δ* cells recovered on day 4 of culturing with PE21) and the highest intracellular concentration of FFA in these cells has revealed that the Pearson's r value for the correlation between these two compared variables is more than 0.9 (Figure 3.11I). Hence, the percentage of cells undergoing necrotic RCD has a very high positive correlation [577] and, therefore, directly correlates with FFA concentration in the yeast cell. This finding supports our assumption that PE21 delays the age-related onset of necrotic RCD and slows down the progression of this mode of RCD because it allows to sustain FFA concentration below the toxic threshold.

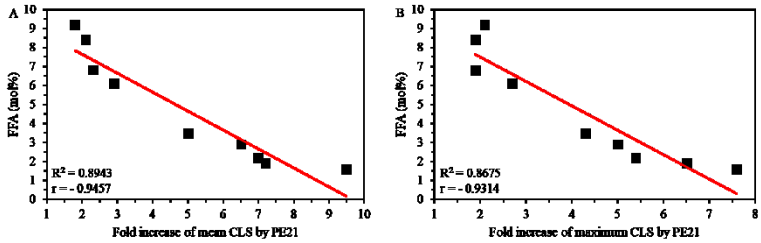

C

Genetic background	Fold increase of mean CLS by PE21	Fold increase of maximum CLS by PE21	FFA concentration (mol%)
tgl4Δ	9.5 ± 0.5	7.6 ± 0.6	1.6 ± 0.1
tgl3Δ	7.2 ± 0.3	6.5 ± 0.4	1.9 ± 0.2
tgl1Δ	7.0 ± 0.4	5.4 ± 0.2	2.2 ± 0.3
tgl5Δ	6.5 ± 0.3	5.0 ± 0.2	2.9 ± 0.1
WT	5.0 ± 0.4	4.3 ± 0.3	3.5 ± 0.4
faa1Δ	2.9 ± 0.2	2.7 ± 0.2	6.1 ± 0.7
faa4Δ	2.3 ± 0.2	1.9 ± 0.1	6.8 ± 0.6
slc1Δ	2.1 ± 0.1	1.9 ± 0.2	8.4 ± 0.9
ale1Δ	1.8 ± 0.1	2.1 ± 0.2	9.2 ± 1.2

Figure 3.9. The efficiency with which PE21 extends yeast longevity inversely correlates with the intracellular concentration of FFA. WT cells and mutant cells that carry a single-gene-deletion mutation eliminating either Faa1, Faa4, Ale1, Slc1, Tgl1, Tgl3, Tgl4 or Tgl5 were cultured in the synthetic minimal YNB medium initially containing 2% glucose with 0.1% PE21. Survival curves shown in Figures 3A, 3F, 4A, 4F, 5A, 5F, 6A, and 6F were used to calculate the folds of increase of the mean and maximum CLS by PE21 for the WT, *faa1Δ*, *faa4Δ*, *ale1Δ*, *slc1Δ*, *tgl1Δ*, *tgl3Δ*, *tgl4Δ* and *tgl5Δ* strains, as shown in Figures 3C, 3D, 3H, 3I, 4C, 4D, 4H, 4I, 5C, 5D, 5H, 5I, 6C, 6D, 6H and 6I. (**A**, **B**) Plots comparing the folds increase of mean (**A**) or maximum (**B**) CLS and the highest intracellular concentration of FFA (which was observed in WT and mutant cells recovered on day 3 of culturing with PE21). Different points show the data for WT, *faa1Δ*, *faa4Δ*, *ale1Δ*, *slc1Δ*, *tgl1Δ*, *tgl3Δ*, *tgl4Δ* or *tgl5Δ* cells. Linear trendlines and the R-squared values are displayed; these values demonstrate a good fit of the line to the data. The Pearson's correlation coefficient (r) values are also shown; because the r value less than - 0.9 is considered a very high negative correlation between the two variables, the fold increase of the mean (**A**) or maximum (**B**) CLS has a very high negative correlation with the intracellular concentration of FFA. (**C**) The experimental data used to create plots shown in (**A** and **B**). Genetic backgrounds of strains, the folds of increase of the mean and maximum CLS by PE21, and the highest concentration of FFA (which was observed in WT and mutant cells recovered on day 3 of culturing with PE21) are shown. Data are presented as means ± SEM (n = 4). Abbreviation: FFA, free fatty acids.

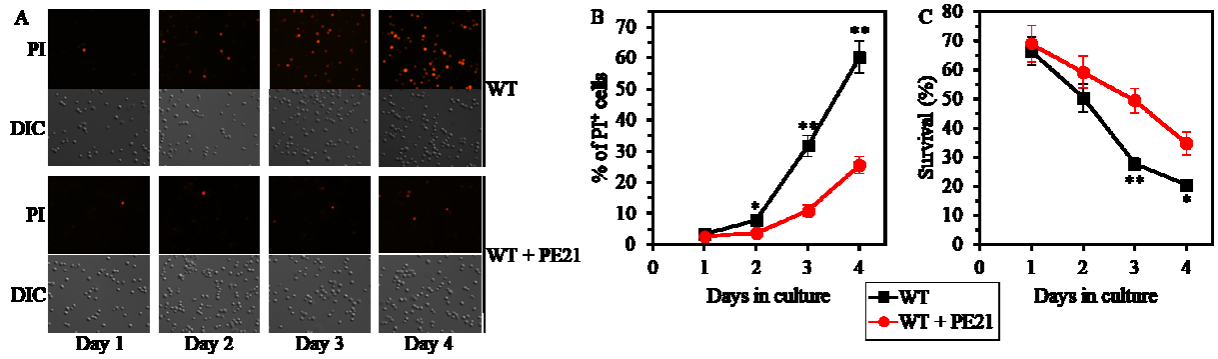

Figure 3.10. PE21 delays an age-related onset of necrotic death in yeast cells, decelerates the progression of the necrotic cell death process, and makes yeast less susceptible to a liponecrotic mode of regulated cell death (RCD). WT cells were cultured in the synthetic minimal YNB medium initially containing 2% glucose with 0.1% PE21 or without it. (**A**) Cells recovered on different days of culturing with or without PE21 were visualized using the differential interference contrast (DIC) microscopy and stained with propidium iodide (PI) as described in Materials and Methods. PI-positive staining identifies cells that are permeable to PI because their plasma membranes have been damaged. Such loss of plasma membrane integrity is characteristic of necrotic cell death. (**B**) Percentage of cells displaying PI-positive staining, a hallmark event of necrotic cell death. Images like the representative images shown in (**A**) were quantitated. Data are presented as means ± SEM (n = 3; *p < 0.05; **p < 0.01). (**C**) Clonogenic survival of cells recovered on different days of culturing with or without PE21 and then exposed for 2 h to 0.1 mM palmitoleic acid (POA) as described in Materials and Methods. POA is a monounsaturated form of FFA that triggers a liponecrotic mode of RCD. Data are presented as means ± SEM (n = 3; *p < 0.05; **p < 0.01).

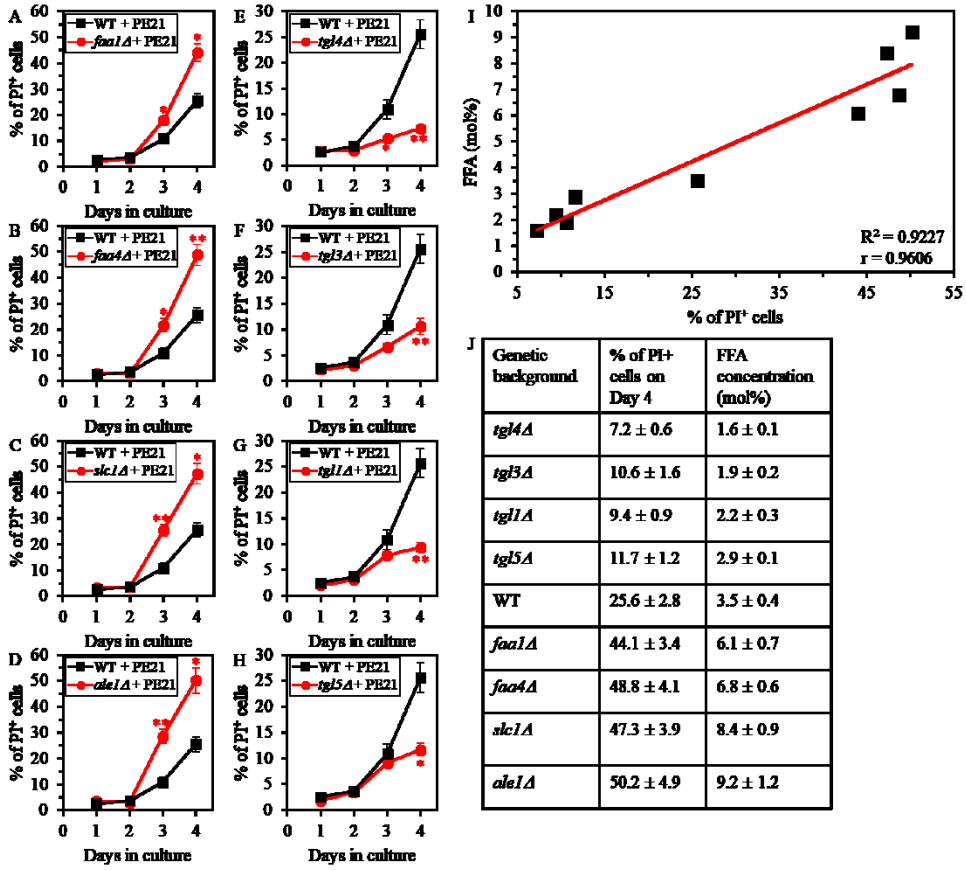

J

Genetic background	% of PI+ cells on Day 4	FFA concentration (mol%)
tgl4Δ	7.2 ± 0.6	1.6 ± 0.1
tgl3Δ	10.6 ± 1.6	1.9 ± 0.2
tgl1Δ	9.4 ± 0.9	2.2 ± 0.3
tgl5Δ	11.7 ± 1.2	2.9 ± 0.1
WT	25.6 ± 2.8	3.5 ± 0.4
faa1Δ	44.1 ± 3.4	6.1 ± 0.7
faa4Δ	48.8 ± 4.1	6.8 ± 0.6
slc1Δ	47.3 ± 3.9	8.4 ± 0.9
ale1Δ	50.2 ± 4.9	9.2 ± 1.2

Figure 3.11. The percentage of cells undergoing necrotic death directly correlates with FFA concentration in the yeast cell. WT cells and mutant cells carrying a single-gene-deletion mutation eliminating either Faa1, Faa4, Ale1, Slc1, Tgl1, Tgl3, Tgl4 or Tgl5 were cultured in the synthetic minimal YNB medium initially containing 2% glucose with 0.1% PE21. (**A-H**) Cells recovered on different days of culturing were stained with propidium iodide (PI) as described in Materials and Methods. PI-positive staining identifies cells that are permeable to PI because their plasma membranes have been damaged. Such loss of plasma membrane integrity is a hallmark event of necrotic cell death. Percentage of cells exhibiting PI-positive staining is shown. Data are presented as means ± SEM (n = 3; *p < 0.05; **p < 0.01). (**I**) Plot comparing the maximum percentage of cells exhibiting PI-positive staining (which was observed in WT and mutant cells recovered on day 4 of culturing with PE21) and the highest intracellular concentration of FFA (which was observed in WT and mutant cells recovered on day 3 of culturing with PE21). Different points show the data for WT, *faa1Δ*, *faa4Δ*, *ale1Δ*, *slc1Δ*, *tgl1Δ*, *tgl3Δ*, *tgl4Δ* or *tgl5Δ* cells. Linear trendline and the R-squared value are displayed; the R-squared value demonstrates a good fit of the line to the data. Pearson's correlation coefficient (r) value is also shown. Because the r value more than 0.9 is considered a very high positive correlation between the two variables, the percentage of cells exhibiting PI-positive staining has a very high positive correlation with the intracellular concentration of FFA. (**J**) The experimental data used to create the plot shown in (**I**). Genetic backgrounds of strains, the percentage of cells exhibiting PI-positive staining on day 4 of culturing with PE21, and the highest intracellular concentration of FFA observed on day 3 of culturing with PE21 are shown. Data are presented as means ± SEM (n = 3). Abbreviation: FFA, free fatty acids.

We then investigated if PE21 can affect the susceptibilities of WT and mutant strains to liponecrotic RCD. This mode of age-related RCD is known to be initiated in response to brief exposure of yeast cells to exogenous FFA [98, 110, 246, 522]. The extent of liponecrotic RCD was measured as a decline in clonogenic survival of yeast cells that were treated for 2 h with a monounsaturated form of FFA called palmitoleic acid (POA). We found the following: 1) PE21 decreases the susceptibility of WT cells to liponecrotic RCD as of day 2 of culturing (Figure 3.10C); 2) as of day 2 of culturing with PE21, the *faa1Δ*, *faa4Δ*, *ale1Δ* and *slc1Δ* mutations make

yeast cells more sensitive to liponecrotic RCD (Figures 3.12A-3.12D and 3.12J); and 3) as of day 3 of culturing with PE21, the *tgl1Δ*, *tgl3Δ*, *tgl4Δ* and *tgl5Δ* mutations make yeast cells more resistant to liponecrotic RCD (Figures 3.12E-3.12H and 3.12J). Our comparison of the minimum percentage of clonogenic survival of POA-treated cells (which was observed in WT, *faa1Δ*, *faa4Δ*, *ale1Δ*, *slc1Δ*, *tgl1Δ*, *tgl3Δ*, *tgl4Δ* and *tgl5Δ* cells recovered on day 4 of culturing with PE21) and the highest intracellular concentration of FFA in these cells has shown that the Pearson's r value for the correlation between these two compared variables is less than - 0.9 (Figure 3.12I). We, therefore, have inferred that the resistance of yeast cells to liponecrotic RCD has a very high negative correlation [577] and, thus, inversely correlates with the intracellular concentration of FFA in the yeast cell. This observation indicates that PE21 makes yeast cells less vulnerable to liponecrotic RCD by allowing to lower FFA concentration.

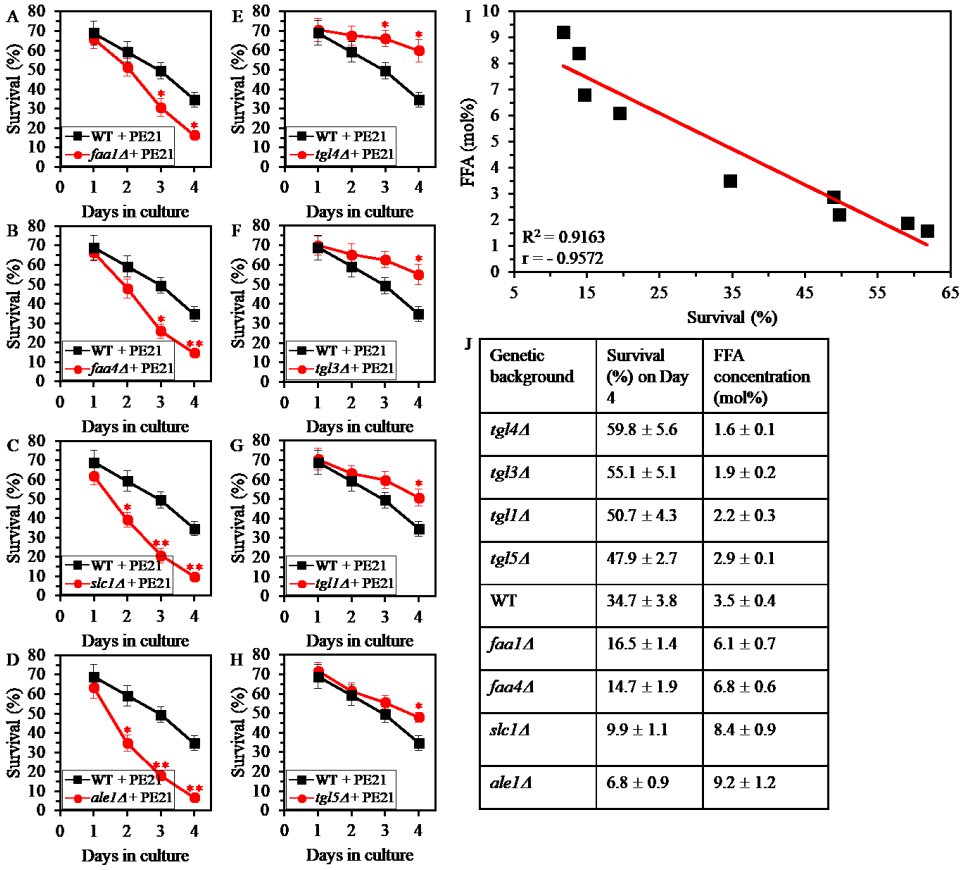

J

Genetic background	Survival (%) on Day 4	FFA concentration (mol%)
tgl4Δ	59.8 ± 5.6	1.6 ± 0.1
tgl3Δ	55.1 ± 5.1	1.9 ± 0.2
tgl1Δ	50.7 ± 4.3	2.2 ± 0.3
tgl5Δ	47.9 ± 2.7	2.9 ± 0.1
WT	34.7 ± 3.8	3.5 ± 0.4
faa1Δ	16.5 ± 1.4	6.1 ± 0.7
faa4Δ	14.7 ± 1.9	6.8 ± 0.6
slc1Δ	9.9 ± 1.1	8.4 ± 0.9
ale1Δ	6.8 ± 0.9	9.2 ± 1.2

Figure 3.12. The resistance of yeast cells to liponecrotic RCD inversely correlates with FFA concentration in the yeast cell. WT cells and mutant cells carrying a single-gene-deletion mutation eliminating either Faa1, Faa4, Ale1, Slc1, Tgl1, Tgl3, Tgl4 or Tgl5 were cultured in the synthetic minimal YNB medium initially containing 2% glucose with 0.1% PE21. (**A-H**) Clonogenic survival of cells recovered on different days of culturing and then treated for 2 h with 0.1 mM POA (a monounsaturated form of FFA) to elicit a liponecrotic mode of RCD as described in Materials and Methods. Data are presented as means ± SEM (n = 3; *p < 0.05; **p < 0.01). (**I**) Plot comparing the minimum percentage of clonogenic survival of POA-treated cells (which was observed in WT and mutant cells that were recovered on day 4 of culturing with PE21 and then treated with POA) and the highest intracellular concentration of FFA (which was observed in WT and mutant cells recovered on day 3 of culturing with PE21). Different points show the data for WT, *faa1Δ*, *faa4Δ*, *ale1Δ*, *slc1Δ*, *tgl1Δ*, *tgl3Δ*, *tgl4Δ* or *tgl5Δ* cells. Linear

trendline and the R-squared value are displayed; the R-squared value demonstrates a good fit of the line to the data. Pearson's correlation coefficient (r) value is also shown. Because the r value less than - 0.9 is considered a very high negative correlation between the two variables, the resistance of yeast cells to liponecrotic RCD has a very high negative correlation with FFA concentration in the yeast cell. (**J**) The experimental data used to create the plot shown in (**I**). Genetic backgrounds of strains, the minimum percentage of clonogenic survival of cells that were recovered on day 4 of culturing with PE21 and then treated with POA, and the highest intracellular concentration of FFA observed on day 3 of culturing with PE21 are shown. Data are presented as means ± SEM (n = 3). Abbreviation: FFA, free fatty acids.

3.4 Summary

Altogether, the findings described in Chapter 3 of the thesis validate our hypothesis on the first mechanism through which PE21 decelerates yeast chronological aging and prolongs yeast CLS (Figure 3.4). In this mechanism, PE21 decreases the risk of aging-associated liponecrotic RCD and increases the chance of elderly cells to survive because PE21 enables yeast cells to maintain FFA concentrations below the toxic threshold.

4 The second mechanism by which PE21 slows yeast chronological aging and extends yeast longevity

4.1 Introduction

To make a first step towards testing our hypothesis on the second and third mechanisms of yeast longevity extension by PE21 (this hypothesis is described in chapter 3 of the thesis), we wanted to get a broader view of cellular processes that are affected by PE21 in yeast. We, therefore, used quantitative mass spectrometry to compare the cellular proteomes of yeast cultured in the presence of PE21 or in its absence. We found that PE21 prompts the establishment of a distinct cellular proteome profile in yeast and that the efficiency with which PE21 changes this profile is gradually increased with the chronological age of yeast cells. We assessed how single-gene-deletion mutations eliminating proteins that are up- or downregulated by PE21 influence the geroprotective efficiency of PE21. This assessment validated our hypothesis on the second mechanism by which PE21 delays yeast chronological aging and extends yeast CLS. In this mechanism, PE21 stimulates the UPR^{ER} system, thus slowing an age-related decline in protein and lipid homeostasis and decelerating an aging-associated deterioration of cell resistance to oxidative and thermal stresses.

4.2 Materials and Methods

4.2.1 Yeast strains, media and growth conditions

The wild-type strain *Saccharomyces cerevisiae* BY4742 (*MATα his3Δ1 leu2Δ0 lys2Δ0 ura3Δ0*) and single-gene-deletion mutant strains in the BY4742 genetic background (all from Thermo Scientific/Open Biosystems) were grown in synthetic minimal YNB medium (0.67% Yeast Nitrogen Base without amino acid) initially containing 2% glucose, 20 mg/l *L*-histidine, 30 mg/l *L*-leucine, 30 mg/l *L*-lysine and 20 mg/l uracil, with 0.1% PE21 (Idunn Technologies Inc.) or without it. PE21 is an ethanol/water extract from the bark of *Salix alba* (see Chapter 2 of the thesis). If added to the growth medium at the time of cell inoculation at a final concentration of 0.1% (w/v), PE21 increases both the mean and maximum CLSs of wild-type strain cultured in medium initially containing 2% glucose (see Chapter 2 of the thesis). A 20% stock solution of PE21 in ethanol was made on the day of adding this PE to cell cultures. The stock solution of PE21 was

added to growth medium with 2% glucose immediately following cell inoculation into the medium. In a culture supplemented with PE21, ethanol was used as a vehicle at the final concentration of 0.5%. In the same experiment, yeast cells were also subjected to ethanol-mock treatment by being cultured in growth medium initially containing 2% glucose and 0.5% ethanol. Cells were cultured at 30^{o}C with rotational shaking at 200 rpm in Erlenmeyer flasks at a "flask volume/medium volume" ratio of 5:1.

4.2.2 Total cell lysates preparation

Cells were pelleted by centrifugation at 3000 x rpm for 7 minutes. The pellets were washed with 500 µL of a solution of 25 mM Tris/HCl (pH 8.5) + 4% CHAPS The cells were pelleted again at 16000 x g for 1 minute. The washing step is done twice. Following that, total cell lysates were obtained by disrupting the cells in ice-cold 25 mM Tris/HCl (pH 8.5) + 4% CHAPS with glass beads using a Fisher Scientific Disruptor Genie (#15567345) for 10 minutes. The resulting suspension was centrifuged for 5 minutes in 4 °C for at 16000 x g. The supernatant was transferred to a clean tube and used for protein precipitation.

4.2.3 Protein precipitation with TCA

The protein concentration of each sample was determined using Bradford assay and 10 µg/sample was precipitated by mixing 4 volumes of sample with 1 volume of 50% TCA and incubating on ice for 30 minutes. The mixture was then centrifuged at 16000 x g for 10 minutes at 4 °C. The pellet was washed with 80% cold acetone (stored at – 20 °C) twice, each time incubating on ice for 10 minutes then centrifuging at 16000 x g for 10 minutes. After washing, the pellet was resuspended in 10 µL of buffer (96.7% 1X Sample Buffer and 3.3% 2M Tris/HCl at pH 8.8). The mixture was then incubated at room temperature for 1 hour used for SDS-PAGE.

4.2.4 Mass spectrometric identification and quantitation of cellular proteins

SDS-PAGE of cellular proteins was performed as previously described [63]. Protein gels were fixed for 15 minutes with 50 mL of fixing solution (10% glacial acetic acid, 40% ethanol, 50% nanopure water). The fixing solution was discarded, and the gel was washed with plenty nanopure water. Following that, the gel was stained with QC Colloidal Coomassie Blue for an hour and then destained with nanopure for an hour. Protein gel bands were cut with a razor blade

and transferred to a new Eppendorf tube. These bands were then incubated in a solution of 50 mM NH_4HCO_3 + 10 mM DTT for 30 mins to reduce thiol groups in peptides. DTT was discarded and the bands were incubated in 50 µl of 50 mM NH_4HCO_3 with 50 mM iodoacetamide (IAA) for 30 min in the dark to remove the residual DTT. The IAA solution was discarded, and the gel pieces were washed in three different solutions. First, they were washed for 15 minutes with a 50 mM NH_4HCO_3 solution. Then solution is discarded, and the gel pieces are washed with a 25 mM NH_4HCO_3 + 5% ACN solution for 15 minutes. This solution is then discarded, and the gel pieces are washed twice with a solution of 25 mM NH_4HCO_3 + 50% ACN for 30 minutes. Finally, the gel pieces are washed with 100% ACN for 10 minutes and dried in a Speed Vac at 43 °C. The gels are then rehydrated with just enough digest solution (0.01 µg/µL trypsin in 25 mM NH_4HCO_3) and incubated overnight at 30 °C. The following day, the samples were spun down and the supernatants containing peptides were transferred to new Eppendorf tubes. To extract more peptides, the gel pieces were subjected to three washes with a solution of 60% ACN + 0.5% formic acid. The samples were then dried in a Speed Vac at 43 °C and stored in -20 °C until MS analysis. The gel pieces were no longer used and discarded. Before MS analysis, the dried peptides were resuspended in a solution of 2% ACN + 1% formic acid. Individual proteins composing each band were then identified by reverse- phase high- performance liquid chromatography coupled to mass spectrometry (RP-HPLC/MS) using an LTQ Orbitrap. 3-µl aliquots of peptides were separated in ACN gradient using a 100-µm capillary column packed with C18 stationary phase. Once acquiring time was completed using the LTQ Orbitrap, the raw mass spectrometry data file obtained by Xcalibur were analyzed using the Thermo Scientific Proteome Discoverer application (version 2.3) hereafter referred to as the Proteome Discoverer. The Proteome Discoverer was used to identify individual proteins by comparing the raw data of mass spectra of digested fragments to the mass spectra of peptides within the Uniprot FASTA database. The analysis by the Proteome Discoverer coupled to the FASTA database was enabled by using the peak-finding search engine SEQUEST. The SEQUEST engine processes MS data using a peak-finding algorithm to search the raw data for generating a peak probability list with relative protein abundances. The ″Proteome Discoverer″ software was used to calculate the exponentially modified protein abundance index (emPAI), a measure of the relative abundance of cellular proteins in a pair of analyzed datasets.

4.2.5 CLS assay

A sample of cells was taken from a culture at a certain day following cell inoculation and PE21 addition into the medium. A fraction of the sample was diluted to determine the total number of cells using a hemocytometer. Another fraction of the cell sample was diluted, and serial dilutions of cells were plated in duplicate onto YPD medium (1% yeast extract, 2% peptone) containing 2% glucose as carbon source. After 2 days of incubation at 30^{o}C, the number of colony-forming units (CFU) per plate was counted. The number of CFU was defined as the number of viable cells in a sample. For each culture, the percentage of viable cells was calculated as follows: (number of viable cells per ml/total number of cells per ml) × 100. The percentage of viable cells in the mid-logarithmic growth phase was set at 100%.

4.2.6 Statistical analysis

Statistical analysis was performed using Microsoft Excel's Analysis ToolPack-VBA. All data on cell survival are presented as mean ± SEM. The *p* values for comparing the means of two groups using an unpaired two-tailed *t* test were calculated with the help of the GraphPad Prism 7 statistics software. The logrank test for comparing each pair of survival curves was performed with GraphPad Prism 7. Two survival curves were considered statistically different if the *p* value was less than 0.05.

4.3 Results and Discussion

4.3.1 PE21 causes global remodeling of the cellular proteome in an age-related manner

To make a first step towards testing our hypothesis on the second and third mechanisms of yeast longevity extension by PE21, we wanted to get a broader view of cellular processes that are affected by PE21 in yeast. We, therefore, used quantitative mass spectrometry to compare the cellular proteomes of WT yeast cultured in the presence of PE21 or in its absence.

We found that PE21 causes changes in the relative concentrations of many cellular proteins in WT yeast (Figures 4.1A-4.1D). We also noticed that the total number of proteins upregulated or downregulated in WT cells in response to PE21 exposure is increased with the chronological age of these cells (Figure 4.1E).

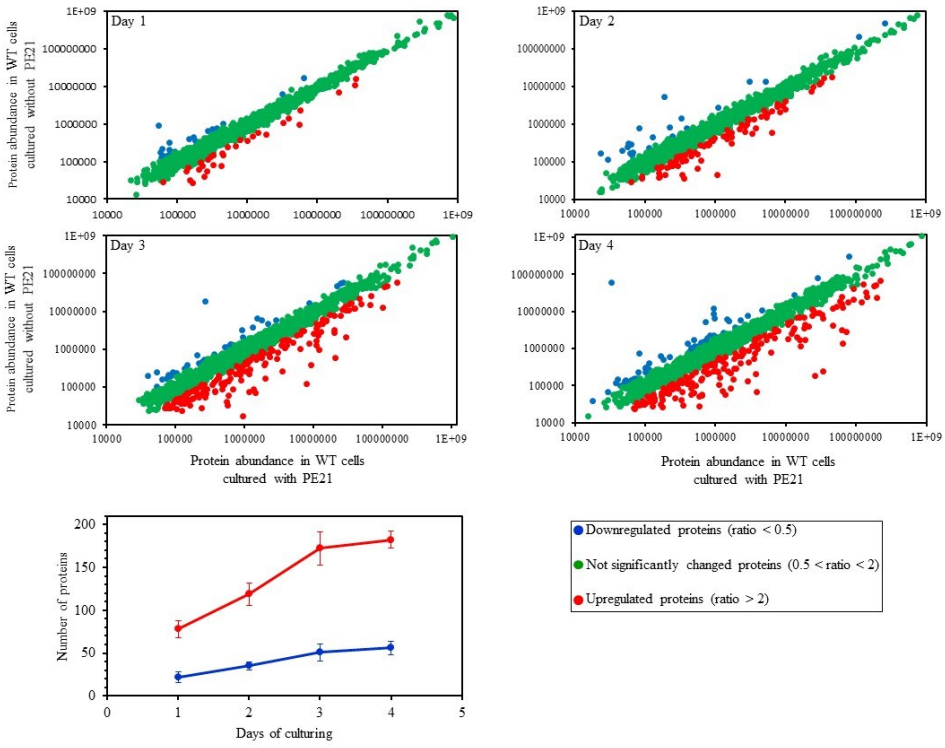

Figure 4.1. PE21 causes changes in the relative concentrations of many cellular proteins in an age-related manner. WT cells were cultured in the synthetic minimal YNB medium initially containing 2% glucose with 0.1% PE21 or without it. Cells were recovered on days 1, 2, 3 and 4 of culturing. Mass spectrometry-based identification and quantitation of proteins recovered from these cells, and the calculation of the relative abundance of cellular proteins in a pair of analyzed datasets (i.e. in the datasets of age-matched WT cells cultured with or without PE21), were performed as described in Materials and Methods. (**A**-**D**) Scatter plots comparing the relative abundance of cellular proteins between specified datasets were plotted on a log-log scale spanning six orders of magnitude. (**E**) The total number of proteins upregulated or downregulated in response to the treatment with PE21. Data are presented as means ± SEM (n = 2).

We used principal component analysis (PCA) to compare the proteome of WT cells cultured in the presence of PE21 to the proteome of age-matched WT cells cultured in the absence of PE21; the cells were recovered on days 1, 2, 3 or 4 of culturing. Our PCA revealed that PE21 elicits a distinct cellular proteome profile in WT yeast that significantly differs from a profile of the cellular proteome in WT yeast cultured in the absence of PE21 (Figures 4.2A-4.2D). This distinct PE21-driven cellular proteome profile was observed in WT cells recovered on any of the four days of culturing (Figures 4.2A-4.2D). The sample with PE21 and the reference without PE21 were separated farthest from each other (i.e. 30 and 55 units of distance between final cluster centers along the PC1 and PC2 axes, respectively) in case of the cellular proteomes of chronologically old WT cells recovered on day 4 of culturing (Figure 4.2D). Although the sample with PE21 and the reference without PE21 were also separated from each other in case of the cellular proteomes of chronologically young WT cells recovered on day 1 of culturing, they were clustered much closer to each other (i.e. 12 and 4 units of distance between final cluster centers

along the PC1 and PC2 axes, respectively) than those of chronologically old WT cells recovered on day 4 (compare Figures 4.2A and 4.2D).

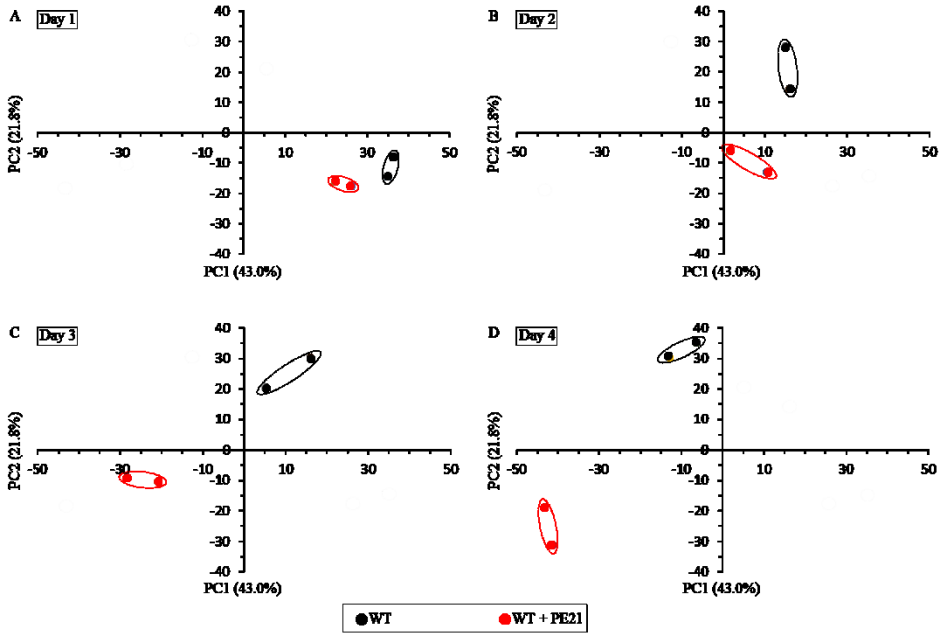

Figure 4.2. Principal component analysis (PCA) for the comparison of cellular proteins identified in yeast cultured in the presence of PE21 or in its absence. WT cells were cultured in the synthetic minimal YNB medium initially containing 2% glucose with 0.1% PE21 or without it. Cells were recovered on days 1, 2, 3 and 4 of culturing. Mass spectrometry-based identification and quantitation of proteins recovered from these cells was performed as described in Materials and Methods. (**A**-**D**) PCA was performed for proteins identified in cells that were cultured with or without PE21 and recovered on day 1 (**A**), day 2 (**B**), day 3 (**C**) or day 4 (**D**) of culturing. Data of 2 independent experiments are presented. Partitional clustering of quantitative data was performed using the *k*-means clustering algorithm.

4.3.2 PE21 prolongs the longevity of chronologically aging yeast in part because it promotes UPR^{ER}

Our hypothesis on the second mechanism through which PE21 may extend longevity of chronologically aging yeast assumes that, because PE21 alters the ER lipidome, it stimulates the UPR^{ER} system (Figure 3.4); such PE21-driven stimulation of UPR^{ER} may be responsible, in part, for the observed abilities of PE21 to slow down an age-related decline in protein, lipid, and nucleic acid homeostasis and to decelerate an aging-associated weakening of cell resistance to oxidative and thermal stresses (see chapter 2 of this thesis). In support of this assumption, we found that in WT yeast PE21 alters the relative concentrations of various cellular proteins whose upregulation or downregulation is indispensable for the restoration and maintenance of cellular homeostasis because it is essential for proper control of the UPR^{ER} system.

We noticed that PE21 increases the abundance of many cellular proteins known to be upregulated during the UPR^{ER} response in yeast [528, 530, 533, 549, 557, 561, 566, 578, 579].

The cellular proteins upregulated by PE21 included the following ones: 1) chaperones involved in protein folding and assembly in the ER or the cytosol (Figure 4.3A); 2) proteins that catalyze *N*-linked protein glycosylation or *O*-linked protein mannosylation in the ER (Figure 4.3B); 3) stress response proteins that prevent and/or repair an oxidative or thermal damage to proteins and/or lipids in the ER, mitochondria, cytosol and/or PM (Figure 4.3C); 4) protein components of the ubiquitin-proteasome system involved in the degradation of improperly folded proteins that are accumulated in the ER and then exported to the cytosol (Figure 4.3D); 5) proteins implicated in vesicular traffic from the ER throughout the secretory pathway (Figure 4.3E); and 6) proteins that catalyze the synthesis of some lipids in the ER and mitochondria (Figure 4.3F). Of note, the PE21-dependent increase in the abundance of enzymes catalyzing the synthesis of PA (i.e. Faa1, Faa4, Fat1, Slc1 and Slc4), PS (i.e. Cho1), PE (i.e. Psd1), PC (i.e. Cho2 and Opi3) and PI (i.e. Pis1) in the ER and mitochondria (Figure 4.3F and Figure 3.2) can satisfactorily explain the PE21-dependent rise in the concentrations of these glycerophospholipids (Figures 3.1C, 3.1D, 3.1E, 3.1F and 3.1G). It needs to be emphasized that, as we found, a single-gene-deletion mutation eliminating Faa1, Faa4 or Slc1 causes a significant decline in longevity-extending efficiency of PE21 (Figures 3.5A-3.5D, 3.5F-3.5I and 3.6F-3.6I). Thus, PE21 extends the longevity of chronologically aging yeast in part because it stimulates a branch of the UPR^{ER} network responsible for glycerophospholipid synthesis in the ER. As discussed below in this section, the PE21-driven upregulation of other UPR^{ER} network branches also contributes to the PE21-dependent extension of yeast CLS.

We also found that PE21 decreases the abundance of cellular proteins known to be downregulated during the UPR^{ER} response in yeast [528, 530, 533, 549, 557, 561, 566, 578, 579]. These proteins have been implicated in ribosome assembly, tRNA synthesis and protein translation in the cytosol (Figure 4.4).

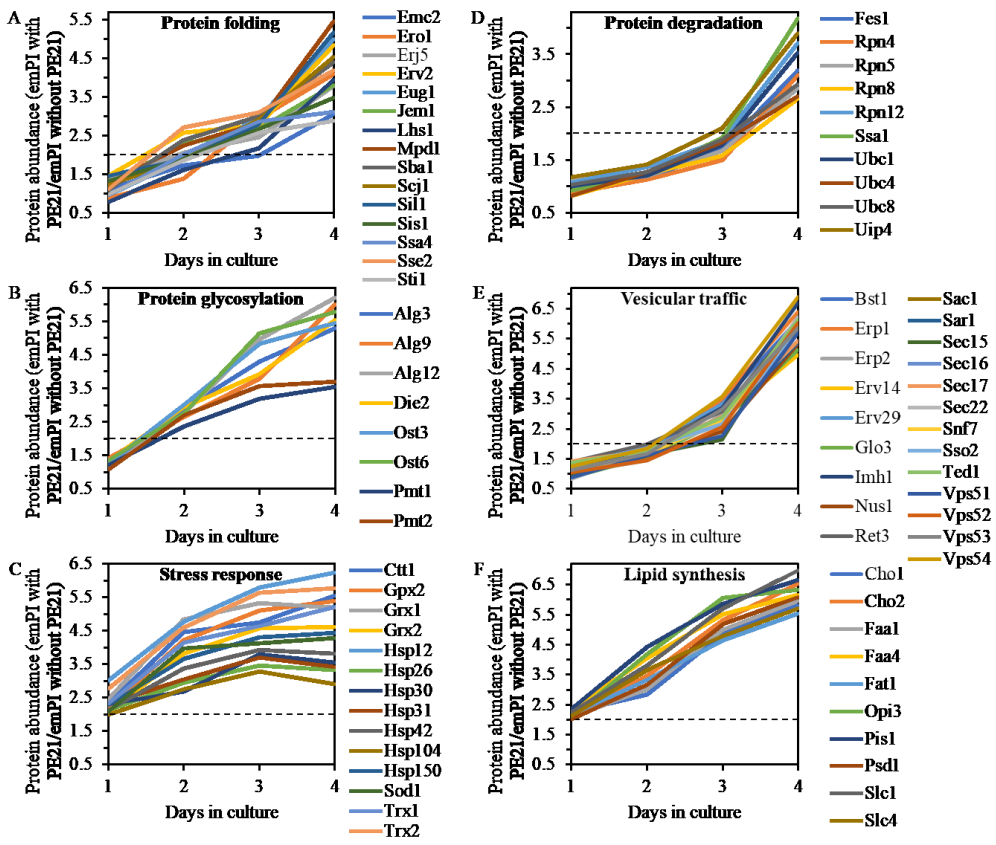

Figure 4.3. PE21 increases the abundance of six classes of cellular proteins known to be upregulated during the UPR^{ER} response in yeast. WT cells were cultured in the synthetic minimal YNB medium initially containing 2% glucose with 0.1% PE21 or without it. Cells were recovered on days 1, 2, 3 and 4 of culturing. Mass spectrometry-based identification and quantitation of proteins recovered from these cells, and the calculation of the relative abundance of cellular proteins in a pair of analyzed datasets (i.e. in the datasets of age-matched WT cells cultured with or without PE21), were performed as described in Materials and Methods. (**A**-**F**) Relative levels of proteins in WT cells cultured with PE21 (fold difference relative to those in WT cells cultured without PE21) are shown. These proteins include the following ones: chaperones involved in protein folding and assembly in the endoplasmic reticulum or the cytosol (**A**), proteins that catalyze *N*-linked protein glycosylation or *O*-linked protein mannosylation in the endoplasmic reticulum (**B**), stress response proteins that prevent and/or repair an oxidative or thermal damage to proteins in the endoplasmic reticulum, cytosol and plasma membrane (**C**), proteins involved in the degradation of improperly folded proteins accumulated in the endoplasmic reticulum via the ubiquitin-proteasome pathway (**D**), proteins implicated in vesicular traffic from the endoplasmic reticulum throughout the secretory pathway (**E**), and proteins that catalyze the synthesis of some lipids in the endoplasmic reticulum and mitochondria (**F**). The 2-fold increase in the ratio "protein abundance with PE21/protein abundance without PE21" is shown by a dotted line. Data are presented as mean values of 2 independent experiments. Abbreviation: emPAI, the exponentially modified protein abundance index, a measure of the relative abundance of cellular proteins in a pair of analyzed datasets.

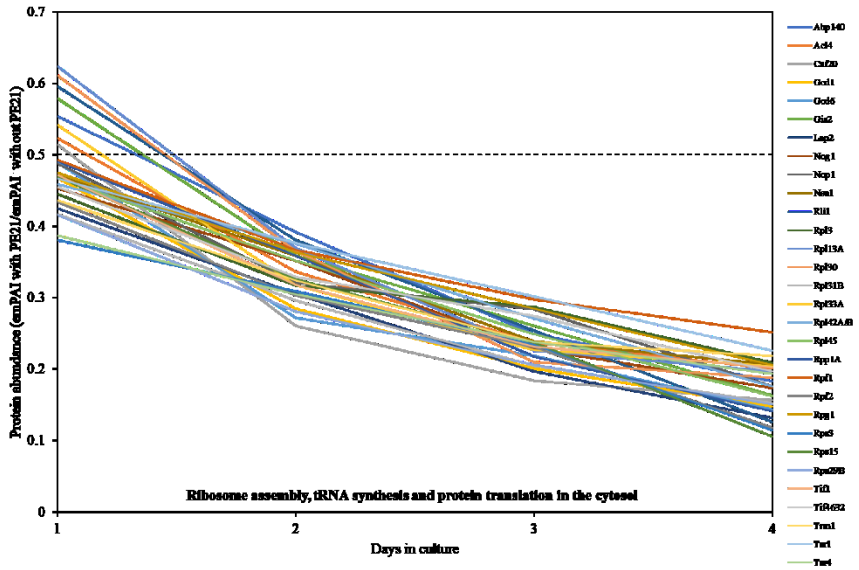

Figure 4.4. PE21 decreases the abundance of cellular proteins known to be downregulated during the UPR^{ER} response in yeast. These proteins are involved in ribosome assembly, tRNA synthesis and protein translation in the cytosol. WT cells were cultured in the synthetic minimal YNB medium initially containing 2% glucose with 0.1% PE21 or without it. Cells were recovered on days 1, 2, 3 and 4 of culturing. Mass spectrometry-based identification and quantitation of proteins recovered from these cells, and the calculation of the relative abundance of cellular proteins in a pair of analyzed datasets (i.e. in the datasets of age-matched WT cells cultured with or without PE21), were performed as described in Materials and Methods. Relative levels of proteins in WT cells cultured with PE21 (fold difference relative to those in WT cells cultured without PE21) are shown. The 2-fold decrease in the ratio "protein abundance with PE21/protein abundance without PE21" is shown by a dotted line. Data are presented as mean values of 2 independent experiments. Abbreviation: emPAI, the exponentially modified protein abundance index, a measure of the relative abundance of cellular proteins in a pair of analyzed datasets.

We thought that some cellular proteins upregulated by both PE21 and UPR^{ER} stimuli may play essential roles in enabling aging delay by PE21. We, therefore, hypothesized that single-gene-deletion mutations eliminating such proteins may decrease the aging-delaying (geroprotective) efficiency of PE21. In support of our hypothesis, yeast mutants that lack the following proteins upregulated in a PE21- and UPR^{ER}-dependent manner exhibited a statistically significant decline in the geroprotective efficiency of PE21: 1) Emc2, Erj5, Erv2 and Eug1, all of which are chaperones assisting in the folding and assembly of other proteins within the ER (Figures 4.5A, 4.5E, 4.5I and 4.5J for the *emc2Δ* mutant; Figures 4.6A and 4.6B for the *erj5Δ*, *erv2Δ* and *eug1Δ* mutants); 2) Alg3, Alg12, Ost3 and Ost6, all of which are enzymes catalyzing *N*-linked protein glycosylation within the ER (Figures 4.5B, 4.5F, 4.5I and 4.5J for the *alg3Δ* mutant; Figures 4.6C and 4.6D for the *alg12Δ*, *ost3Δ* and *ost6Δ* mutants); 3) Ctt1, Gpx2, Grx1 and Grx2, all of which are stress response proteins preventing and/or repairing an oxidative damage to proteins and/or lipids in the cytosol and mitochondria (Figures 4.5C, 4.5G, 4.5I and 4.5J for the *ctt1Δ* mutant; Figures 4.6E and 4.6F for the *gpx2Δ*, *grx1Δ* and *grx2Δ* mutants); 4) Fes1, Rpn4, Ssa1 and Ubc8, all of which are components of the ubiquitin-proteasome pathway for the degradation of improperly folded proteins that amass in the ER (Figures 4.5D, 4.5H, 4.5I and 4.5J for the *fes1Δ*

mutant; Figures 4.6G and 4.6H for the *rpn4Δ*, *ssa1Δ* and *ubc8Δ* mutants); 5) Bst1, Erp1, Erp2 and Erv29, all of which are proteins involved in vesicular traffic from the ER to the Golgi apparatus (Figures 4.7A, 4.7D, 4.7G and 4.7H for the *bst1Δ* mutant; Figures 4.6I and 4.6J for the *erp1Δ*, *erp2Δ* and *erv29Δ* mutants); and 6) Fat1 and Opi3, both being implicated in glycerophospholipid synthesis within the ER (Figures 4.7B, 4.7E, 4.7G and 4.7H for the *fat1Δ* mutant; Figures 4.6K and 4.6L for the *opi3Δ* mutant; as indicated above and as shown in Figures 3.5A-3.5D, 3.5F-3.5I and 3.6F-3.6I, the geroprotective efficiency of PE21 is also decreased in yeast mutants lacking other glycerophospholipid synthesis enzymes that are upregulated in a PE21- and UPR^{ER}-dependent manner).

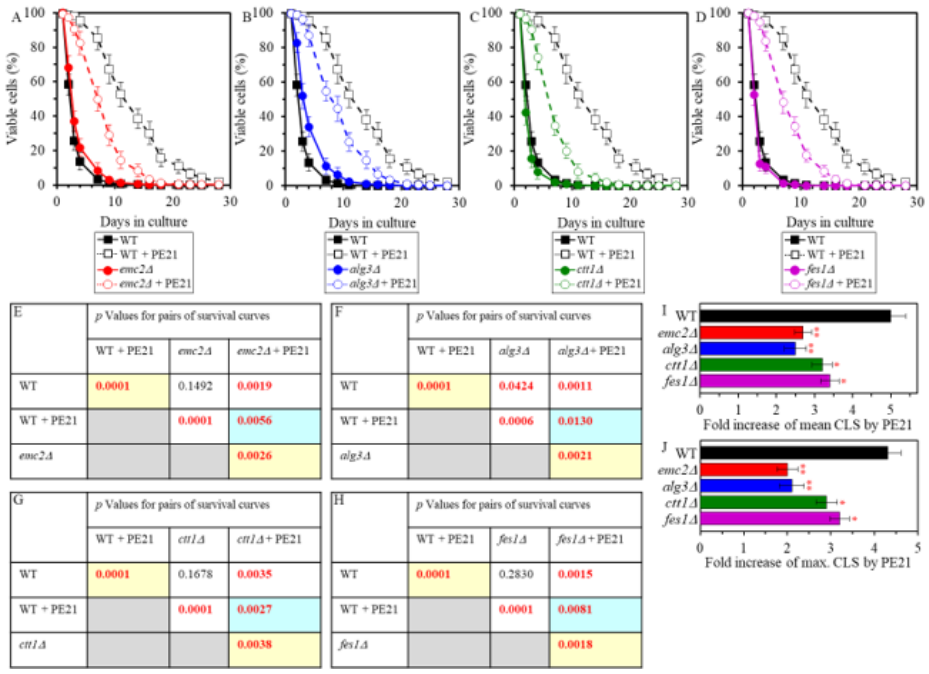

E — *p* Values for pairs of survival curves

	WT + PE21	*emc2Δ*	*emc2Δ* + PE21
WT	0.0001	0.1492	0.0019
WT + PE21		0.0001	0.0056
emc2Δ			0.0026

F — *p* Values for pairs of survival curves

	WT + PE21	*alg3Δ*	*alg3Δ* + PE21
WT	0.0001	0.0424	0.0011
WT + PE21		0.0006	0.0130
alg3Δ			0.0021

G — *p* Values for pairs of survival curves

	WT + PE21	*ctt1Δ*	*ctt1Δ* + PE21
WT	0.0001	0.1678	0.0035
WT + PE21		0.0001	0.0027
ctt1Δ			0.0038

H — *p* Values for pairs of survival curves

	WT + PE21	*fes1Δ*	*fes1Δ* + PE21
WT	0.0001	0.2830	0.0015
WT + PE21		0.0001	0.0081
fes1Δ			0.0018

Figure 4.5. Single-gene-deletion mutations eliminating proteins that are upregulated by both PE21 and UPR^{ER} stimuli decrease the efficiency with which PE21 extends yeast longevity. WT cells and mutant cells carrying a single-gene-deletion mutation eliminating either Emc2, Alg3, Ctt1 or Fes1 were cultured in the synthetic minimal YNB medium initially containing 2% glucose with 0.1% PE21 or without it. (**A-D**) Survival curves of the chronologically aging WT and *emc2Δ* (**A**), WT and *alg3Δ* (**B**), WT and *ctt1Δ* (**C**) or WT and *fes1Δ* (**D**) strains are shown. Data are presented as means ± SEM (n = 3). (**E-H**) *p* Values for different pairs of survival curves of the WT and *emc2Δ* (**E**), WT and *alg3Δ* (**F**), WT and *ctt1Δ* (**G**) or WT and *fes1Δ* (**H**) strains cultured with or without PE21. Survival curves shown in **A-D** (respectively) were compared. Two survival curves were considered statistically different if the *p* value was less than 0.05. The *p* values for comparing pairs of survival curves using the logrank test were calculated as described in Materials and Methods. The *p* values displayed on a yellow color background indicate that PE21 statistically significantly prolongs the CLS of the WT (**E-H**), *emc2Δ* (**E**), *alg3Δ* (**F**), *ctt1Δ* (**G**) and *fes1Δ* (**H**) strains. The *p* values displayed on a blue color background indicate that PE21 prolongs the CLS of the *emc2Δ* (**E**), *alg3Δ* (**F**), *ctt1Δ* (**G**) and *fes1Δ* (**H**) strains to a lower extent than that of the WT strain. (**I**, **J**) Survival curves shown in (**A-D**) were used to calculate the fold of increase of the mean (**I**) and maximum (**J**) CLS by PE21 for the WT, *emc2Δ*, *alg3Δ*, *ctt1Δ* and *fes1Δ* strains. Data are presented as means ± SEM (n = 3; **p* < 0.05; ***p* < 0.01).

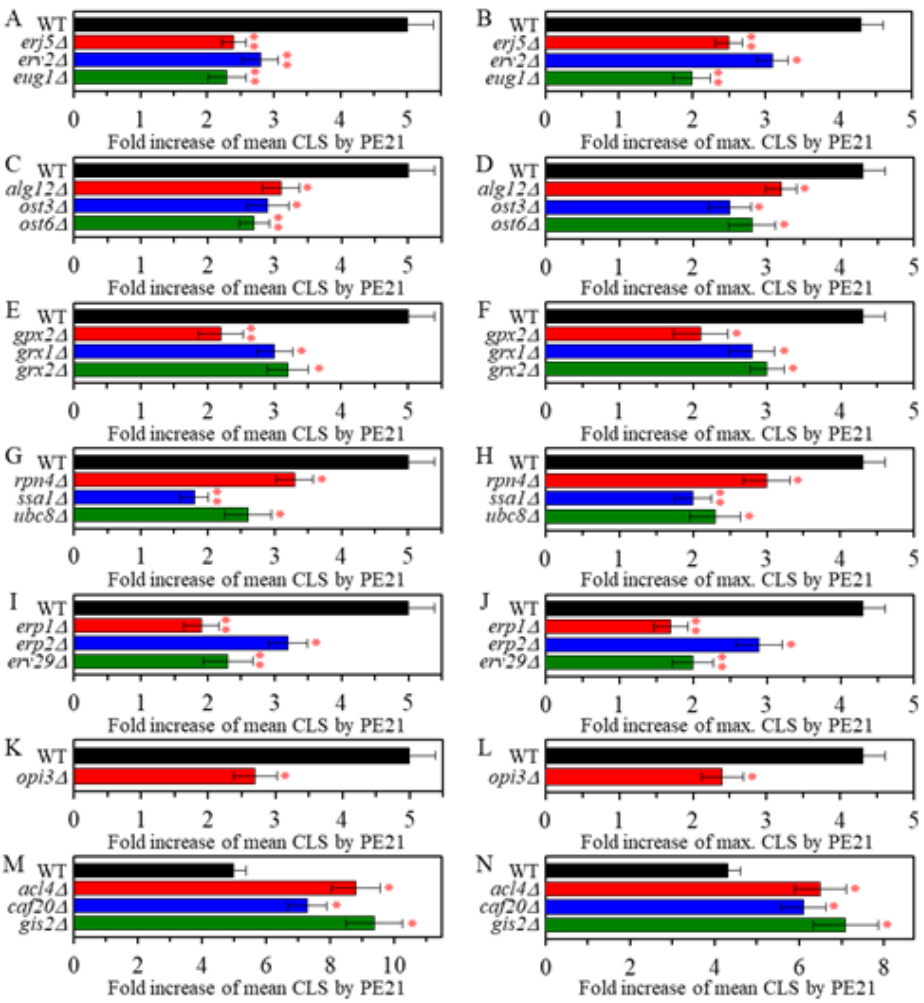

Figure 4.6. Single-gene-deletion mutations eliminating proteins that are upregulated by both PE21 and UPR^{ER} stimuli decrease the efficiency with which PE21 extends yeast longevity, whereas single-gene-deletion mutations eliminating proteins that are downregulated by both PE21 and UPR^{ER} stimuli increase such efficiency. WT cells and mutant cells carrying a single-gene-deletion mutation eliminating a protein upregulated or downregulated by both PE21 and UPR^{ER} stimuli were cultured in the synthetic minimal YNB medium initially containing 2% glucose with 0.1% PE21 or without it. Survival curves of chronologically aging WT and mutant strains were used to calculate the fold of increase of the mean (**A**, **C**, **E**, **G**, **I**, **K**, **M**) and maximum (**B**, **D**, **F**, **H**, **J**, **L**, **N**) CLS by PE21 for the WT and mutant strains. Data are presented as means ± SEM (n = 3; *$p < 0.05$; **$p < 0.01$).

We also thought that some cellular proteins downregulated by both PE21 and UPR^{ER} stimuli may be important for impeding aging delay by PE21. Therefore, our hypothesis was that single-gene-deletion mutations eliminating such proteins may increase the geroprotective efficiency of PE21. In support of our hypothesis, yeast mutants that lack Abp140, Acl4, Caf20, and Gis2 displayed a statistically significant rise in the geroprotective efficiency of PE21 (Figures 4.7C, 4.7F, 4.7G and 4.7H for the *abp140Δ* mutant; Figures 4.6M and 4.6N for the *acl4Δ*, *caf20Δ* and *gis2Δ* mutants). These proteins play essential roles in ribosome assembly, tRNA synthesis and protein translation in the cytosol [696-703] and are downregulated by both PE21 (Figure 4.4) and UPR^{ER} stimuli [528, 530, 533, 549, 557, 561, 566, 578, 579].

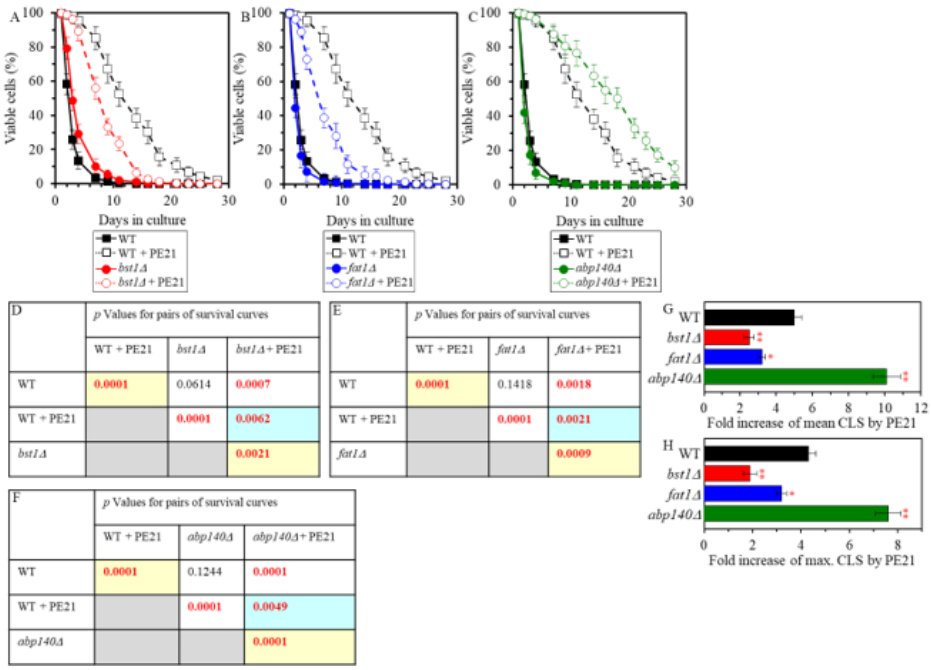

Figure 4.7. Single-gene-deletion mutations eliminating proteins that are upregulated by both PE21 and UPR^{ER} stimuli decrease the efficiency with which PE21 extends yeast longevity, while a single-gene-deletion mutation eliminating a protein that is downregulated by both PE21 and UPR^{ER} stimuli increases such efficiency. WT cells and mutant cells carrying a single-gene-deletion mutation eliminating either Bst1, Fat1 or Abp140 were cultured in the synthetic minimal YNB medium initially containing 2% glucose with 0.1% PE21 or without it. (**A**-**C**) Survival curves of the chronologically aging WT and *bst1Δ* (**A**), WT and *fat1Δ* (**B**) or WT and *abp140Δ* (**C**) strains are shown. Data are presented as means ± SEM (n = 3). (**D**-**F**) *p* Values for different pairs of survival curves of the WT and *bst1Δ* (**D**), WT and *fat1Δ* (**E**) or WT and *abp140Δ* (**F**) strains cultured with or without PE21. Survival curves shown in **A**-**C** (respectively) were compared. Two survival curves were considered statistically different if the *p* value was less than 0.05. The *p* values for comparing pairs of survival curves using the logrank test were calculated as described in Materials and Methods. The *p* values displayed on a yellow color background indicate that PE21 statistically significantly prolongs the CLS of the WT (**D**-**F**), *bst1Δ* (**D**), *fat1Δ* (**E**) and *abp140Δ* (**F**) strains. The *p* values displayed on a blue color background indicate the following: 1) PE21 prolongs the CLS of the *bst11Δ* (**D**) and *fat1Δ* (**E**) strains to a lower extent than that of the WT strain; and 2) PE21 prolongs the CLS of the *fat1Δ* strain (**F**) to a higher extent than that of the WT strain. (**G**, **H**) Survival curves shown in (**A**-**C**) were used to calculate the fold of increase of the mean (**G**) and maximum (**H**) CLS by PE21 for the WT, *bst1Δ*, *fat1Δ* and *abp140Δ* strains. Data are presented as means ± SEM (n = 3; **p* < 0.05; ***p* < 0.01).

4.4 Summary

Taken together, the findings described in chapter 4 of the thesis validate our hypothesis on the second mechanism by which PE21 delays yeast chronological aging and extends yeast CLS (Figure 3.4). In this mechanism, PE21 stimulates the UPR^{ER} system, thus slowing an age-related decline in protein and lipid homeostasis and decelerating an aging-associated deterioration of cell resistance to oxidative and thermal stresses.

5 The third mechanism through which PE21 delays yeast chronological aging and prolongs yeast longevity

5.1 Introduction

In our hypothesis on the third mechanism by which PE21 may prolong the longevity of chronologically aging yeast, the PE21-dependent changes in the membrane lipidome of mitochondria may remodel certain processes taking place in these organelles, thus altering mitochondrial functionality. Our hypothesis posits such PE21-dependent alterations in mitochondrial functionality may be responsible, in part, for the observed ability of PE21 to amend the temporal dynamics of age-related alterations in mitochondrial respiration, mitochondrial membrane potential, and mitochondrial ROS production. In studies described in this chapter of the thesis, we found that PE21 causes changes in the concentrations of many mitochondrial proteins. We examined how single-gene-deletion mutations eliminating mitochondrial proteins that are up- or downregulated by PE21 influence the geroprotective efficiency of PE21. This examination validated our hypothesis on the third mechanism by which PE21 delays yeast chronological aging and prolongs yeast CLS.

5.2 Materials and Methods

5.2.1 Yeast strains, media and growth conditions

The wild-type strain *Saccharomyces cerevisiae* BY4742 (*MATα his3Δ1 leu2Δ0 lys2Δ0 ura3Δ0*) and single-gene-deletion mutant strains in the BY4742 genetic background (all from Thermo Scientific/Open Biosystems) were grown in synthetic minimal YNB medium (0.67% Yeast Nitrogen Base without amino acid) initially containing 2% glucose, 20 mg/l *L*-histidine, 30 mg/l *L*-leucine, 30 mg/l *L*-lysine and 20 mg/l uracil, with 0.1% PE21 (Idunn Technologies Inc.) or without it. PE21 is an ethanol/water extract from the bark of *Salix alba* (see Chapter 2 of the thesis). If added to the growth medium at the time of cell inoculation at a final concentration of 0.1% (w/v), PE21 increases both the mean and maximum CLSs of wild-type strain cultured in medium initially containing 2% glucose (see Chapter 2 of the thesis). A 20% stock solution of PE21 in ethanol was made on the day of adding this PE to cell cultures. The stock solution of PE21 was added to growth medium with 2% glucose immediately following cell inoculation into the

medium. In a culture supplemented with PE21, ethanol was used as a vehicle at the final concentration of 0.5%. In the same experiment, yeast cells were also subjected to ethanol-mock treatment by being cultured in growth medium initially containing 2% glucose and 0.5% ethanol. Cells were cultured at 30ºC with rotational shaking at 200 rpm in Erlenmeyer flasks at a "flask volume/medium volume" ratio of 5:1.

5.2.2 Total cell lysates preparation

Cells were pelleted by centrifugation at 3000 x rpm for 7 minutes. The pellets were washed with 500 µL of a solution of 25 mM Tris/HCl (pH 8.5) + 4% CHAPS The cells were pelleted again at 16000 x g for 1 minute. The washing step is done twice. Following that, total cell lysates were obtained by disrupting the cells in ice-cold 25 mM Tris/HCl (pH 8.5) + 4% CHAPS with glass beads using a Fisher Scientific Disruptor Genie (#15567345) for 10 minutes. The resulting suspension was centrifuged for 5 minutes in 4 °C for at 16000 x g. The supernatant was transferred to a clean tube and used for protein precipitation.

5.2.3 Protein precipitation with TCA

The protein concentration of each sample was determined using Bradford assay and 10 µg/sample was precipitated by mixing 4 volumes of sample with 1 volume of 50% TCA and incubating on ice for 30 minutes. The mixture was then centrifuged at 16000 x g for 10 minutes at 4 °C. The pellet was washed with 80% cold acetone (stored at – 20 °C) twice, each time incubating on ice for 10 minutes then centrifuging at 16000 x g for 10 minutes. After washing, the pellet was resuspended in 10 µL of buffer (96.7% 1X Sample Buffer and 3.3% 2M Tris/HCl at pH 8.8). The mixture was then incubated at room temperature for 1 hour used for SDS-PAGE.

5.2.4 Mass spectrometric identification and quantitation of cellular proteins

SDS-PAGE of cellular proteins was performed as previously described [63]. Protein gels were fixed for 15 minutes with 50 mL of fixing solution (10% glacial acetic acid, 40% ethanol, 50% nanopure water). The fixing solution was discarded, and the gel was washed with plenty nanopure water. Following that, the gel was stained with QC Colloidal Coomassie Blue for an hour and then destained with nanopure for an hour. Protein gel bands were cut with a razor blade and transferred to a new Eppendorf tube. These bands were then incubated in a solution of 50 mM

NH_4HCO_3 + 10 mM DTT for 30 mins to reduce thiol groups in peptides. DTT was discarded and the bands were incubated in 50 µl of 50 mM NH_4HCO_3 with 50 mM iodoacetamide (IAA) for 30 min in the dark to remove the residual DTT. The IAA solution was discarded, and the gel pieces were washed in three different solutions. First, they were washed for 15 minutes with a 50 mM NH_4HCO_3 solution. Then solution is discarded, and the gel pieces are washed with a 25 mM NH_4HCO_3 + 5% ACN solution for 15 minutes. This solution is then discarded, and the gel pieces are washed twice with a solution of 25 mM NH_4HCO_3 + 50% ACN for 30 minutes. Finally, the gel pieces are washed with 100% ACN for 10 minutes and dried in a Speed Vac at 43 °C. The gels are then rehydrated with just enough digest solution (0.01 µg/µL trypsin in 25 mM NH_4HCO_3) and incubated overnight at 30 °C. The following day, the samples were spun down and the supernatants containing peptides were transferred to new Eppendorf tubes. To extract more peptides, the gel pieces were subjected to three washes with a solution of 60% ACN + 0.5% formic acid. The samples were then dried in a Speed Vac at 43 °C and stored in -20 °C until MS analysis. The gel pieces were no longer used and discarded. Before MS analysis, the dried peptides were resuspended in a solution of 2% ACN + 1% formic acid. Individual proteins composing each band were then identified by reverse- phase high- performance liquid chromatography coupled to mass spectrometry (RP-HPLC/MS) using an LTQ Orbitrap. 3-µl aliquots of peptides were separated in ACN gradient using a 100-µm capillary column packed with C18 stationary phase. Once acquiring time was completed using the LTQ Orbitrap, the raw mass spectrometry data file obtained by Xcalibur were analyzed using the Thermo Scientific Proteome Discoverer application (version 2.3) hereafter referred to as the Proteome Discoverer. The Proteome Discoverer was used to identify individual proteins by comparing the raw data of mass spectra of digested fragments to the mass spectra of peptides within the Uniprot FASTA database. The analysis by the Proteome Discoverer coupled to the FASTA database was enabled by using the peak-finding search engine SEQUEST. The SEQUEST engine processes MS data using a peak-finding algorithm to search the raw data for generating a peak probability list with relative protein abundances. The ″Proteome Discoverer″ software was used to calculate the exponentially modified protein abundance index (emPAI), a measure of the relative abundance of cellular proteins in a pair of analyzed datasets.

5.2.5 CLS assay

A sample of cells was taken from a culture at a certain day following cell inoculation and PE21 addition into the medium. A fraction of the sample was diluted to determine the total number of cells using a hemocytometer. Another fraction of the cell sample was diluted, and serial dilutions of cells were plated in duplicate onto YPD medium (1% yeast extract, 2% peptone) containing 2% glucose as carbon source. After 2 days of incubation at 30^{o}C, the number of colony-forming units (CFU) per plate was counted. The number of CFU was defined as the number of viable cells in a sample. For each culture, the percentage of viable cells was calculated as follows: (number of viable cells per ml/total number of cells per ml) × 100. The percentage of viable cells in the mid-logarithmic growth phase was set at 100%.

5.2.6 Statistical analysis

Statistical analysis was performed using Microsoft Excel's Analysis ToolPack-VBA. All data on cell survival are presented as mean ± SEM. The *p* values for comparing the means of two groups using an unpaired two-tailed *t* test were calculated with the help of the GraphPad Prism 7 statistics software. The logrank test for comparing each pair of survival curves was performed with GraphPad Prism 7. Two survival curves were considered statistically different if the *p* value was less than 0.05.

5.3 Results and Discussion

5.3.1 PE21 causes changes in the abundance of many mitochondrial proteins involved in essential functions of mitochondria

Our hypothesis on the third mechanism through which PE21 may extend the longevity of chronologically aging yeast posits that, because PE21 alters the membrane lipidome of mitochondria, it may reorganize some processes within these organelles to change mitochondrial functionality (Figure 3.4). In our hypothesis, such PE21-dependent change in mitochondrial functionality may be responsible, in part, for the observed ability of PE21 to amend the temporal dynamics of age-related alterations in mitochondrial respiration, mitochondrial membrane potential, and mitochondrial ROS production (see section 2 of this thesis). In support of our

hypothesis, we found that in WT yeast, PE21 elicits changes in the relative concentrations of various mitochondrial proteins implicated in some key aspects of mitochondrial functionality.

Specifically, we noted that PE21 increases the abundance of proteins involved in the following mitochondrial processes: 1) the electron transport chain (ETC) and oxidative phosphorylation (OXPHOS) system in mitochondria (Figures 5.1A and 5.1B); 2) the mitochondrial tricarboxylic acid (TCA) cycle, glyoxylate cycle, synthesis of NADPH and formation of glutamate (which is a common precursor for the synthesis of other amino acids, folates and glutathione in mitochondria and the cytosol [580]) (Figures 5.1C and 5.1D); 3) ROS detoxification and oxidative stress protection (Figure 5.2A); 4) the synthesis of heme and its attachment to proteins (Figure 5.2B); 5) protein folding and refolding (Figure 5.2C); and 6) protein import into mitochondria (Figure 5.2D).

We also noted that PE21 decreases the abundance of mitochondrial proteins implicated in the division (fission) of mitochondria as well as in RNA synthesis, processing, and translation within these organelles (Figure 5.3).

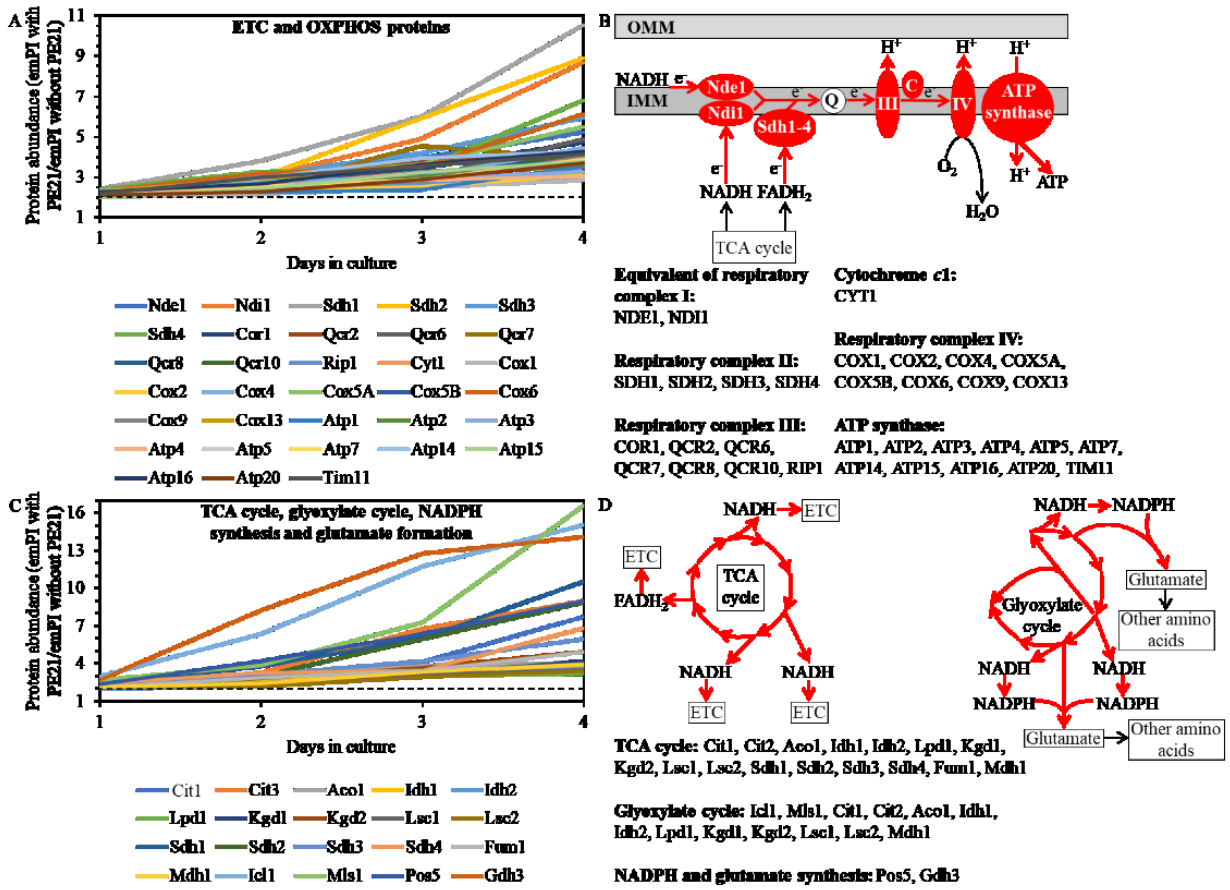

Figure 5.1. PE21 increases the abundance of proteins involved in the mitochondrial electron transport chain (ETC), oxidative phosphorylation (OXPHOS) system, tricarboxylic acid (TCA) cycle (TCA), glyoxylate cycle, NADPH synthesis, and glutamate formation. WT cells were cultured in the synthetic minimal YNB medium initially containing 2% glucose with 0.1% PE21 or without it. Cells were recovered on days 1, 2, 3 and 4 of culturing. Mass spectrometry-based identification and quantitation of proteins recovered from these cells, and the calculation of the relative abundance of cellular proteins in a pair of analyzed datasets (i.e. in the datasets of age-matched WT cells cultured with or without PE21), were performed as described in Materials and Methods. (**A**, **C**) Relative levels of proteins in WT cells cultured with PE21 (fold difference relative to those in WT cells cultured without PE21) are shown. The 2-fold increase in the ratio "protein abundance with PE21/protein abundance without PE21" is shown by a dotted line. Data are presented as mean values of 2 independent experiments. (**B**) Protein components of the mitochondrial ETC and OXPHOS system whose concentrations are increased in yeast cells cultured in the presence of PE21 are displayed in red color. The names of these protein components are provided. Red arrows denote the reactions of electron transport, proton transfer across the inner mitochondrial membrane (IMM) and ATP synthesis that are accelerated due to a PE21-dependent upregulation of protein components of the mitochondrial ETC and OXPHOS system. (**D**) Red arrows indicate the reactions of the TCA cycle, glyoxylate cycle, NADPH synthesis and glutamate formation that are accelerated because of a PE21-dependent upregulation of protein components involved in these metabolic processes within mitochondria. The names of these protein components are provided. Other abbreviations: C, cytochrome *c*; emPAI, the exponentially modified protein abundance index, a measure of the relative abundance of cellular proteins in a pair of analyzed datasets; OMM, outer mitochondrial membrane; Q, ubiquinone (coenzyme Q); III and IV, respiratory complexes III and IV of the mitochondrial ETC.

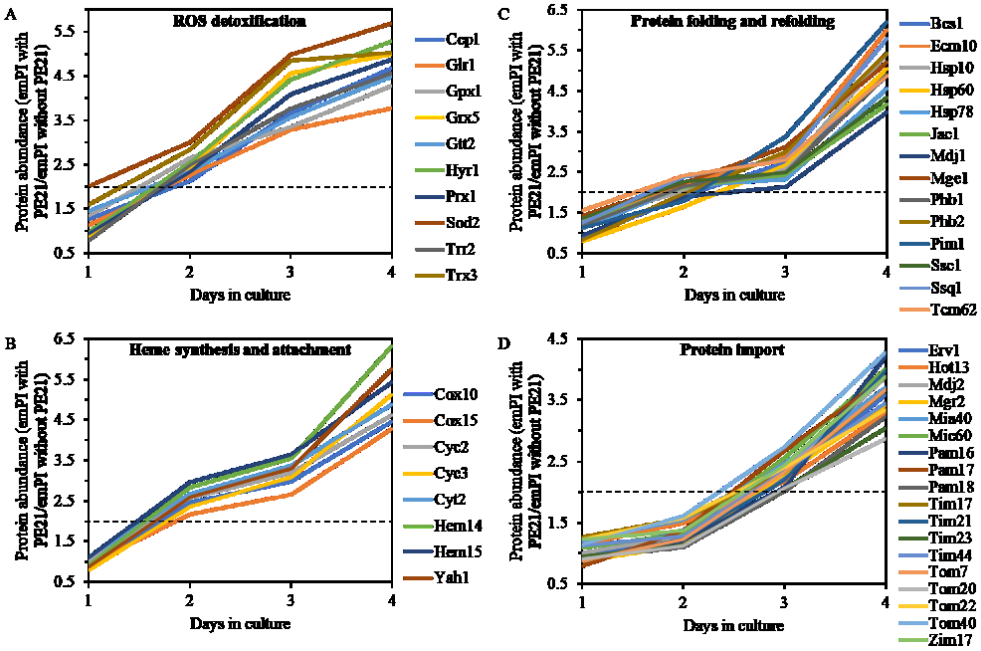

Figure 5.2. PE21 increases the abundance of mitochondrial proteins implicated in ROS detoxification, heme synthesis, and protein attachment, protein folding and refolding, and protein import into mitochondria. WT cells were cultured in the synthetic minimal YNB medium initially containing 2% glucose with 0.1% PE21 or without it. Cells were recovered on days 1, 2, 3 and 4 of culturing. Mass spectrometry-based identification and quantitation of proteins recovered from these cells, and the calculation of the relative abundance of cellular proteins in a pair of analyzed datasets (i.e. in the datasets of age-matched WT cells cultured with or without PE21), were performed as described in Materials and Methods. Relative levels of proteins in WT cells cultured with PE21 (fold difference relative to those in WT cells cultured without PE21) are shown. These proteins include the following ones: mitochondrial proteins involved in ROS detoxification and oxidative stress protection (**A**), enzymes catalyzing heme synthesis and proteins facilitating heme attachment to other proteins (**B**), chaperones assisting in the folding and refolding of other mitochondrial proteins (**C**), components of the mitochondrial protein import machinery (**D**). The 2-fold increase in the ratio "protein abundance with PE21/protein abundance without PE21" is shown by a dotted line. Data are presented as mean values of 2 independent experiments. Abbreviation: emPAI, the exponentially modified protein abundance index, a measure of the relative abundance of cellular proteins in a pair of analyzed datasets.

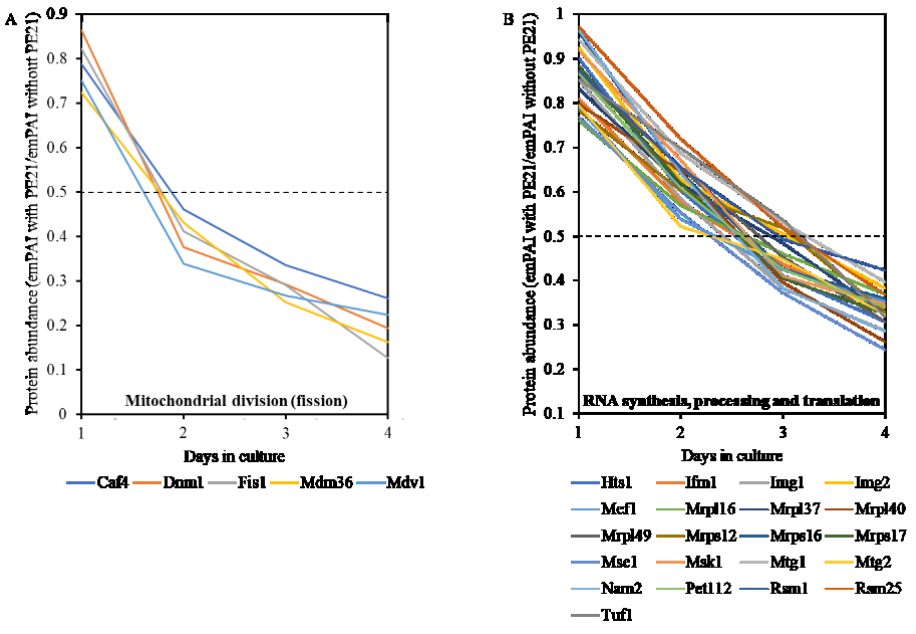

Figure 5.3. PE21 decreases the abundance of two classes of mitochondrial proteins. WT cells were cultured in the synthetic minimal YNB medium initially containing 2% glucose with 0.1% PE21 or without it. Cells were recovered on days 1, 2, 3 and 4 of culturing. Mass spectrometry-based identification and quantitation of proteins recovered from these cells, and the calculation of the relative abundance of cellular proteins in a pair of analyzed datasets (i.e. in the datasets of age-

matched WT cells cultured with or without PE21), were performed as described in Materials and Methods. Relative levels of proteins in WT cells cultured with PE21 (fold difference relative to those in WT cells cultured without PE21) are shown. These proteins include the following ones: components of the mitochondrial division (fission) machinery (**A**), and proteins that catalyze RNA synthesis, processing, and translation within mitochondria (**B**). The 2-fold decrease in the ratio "protein abundance with PE21/protein abundance without PE21" is shown by a dotted line. Data are presented as mean values of 2 independent experiments. Abbreviation: emPAI, the exponentially modified protein abundance index, a measure of the relative abundance of cellular proteins in a pair of analyzed datasets.

5.3.2 PE21 extends the longevity of chronologically aging yeast in part because it rearranges some processes within mitochondria, thus changing the functionality of these organelles

It is conceivable that those mitochondrial proteins that are upregulated by PE21 may be essential contributors to a PE21-dependent delay of yeast chronological aging. If this assumption is correct, then single-gene-deletion mutations that eliminate such mitochondrial proteins may reduce the geroprotective potential of PE21. We found that this assumption holds true, as PE21 is a significantly less efficient geroprotective agent for single-gene-deletion mutants that lack the following PE21-inducible mitochondrial proteins: 1) components of the ETC and OXPHOS system in mitochondria (Figures 5.4A, 5.4E, 5.4I and 5.4J for the *nde1Δ* mutant; Figures 5.5A and 5.5B for the *ndi1Δ*, *sdh1Δ* and *sdh2Δ* mutants); 2) enzymes of the TCA and glyoxylate cycles in mitochondria (Figures 5.4B, 5.4F, 5.4I and 5.4J for the *cit1Δ* mutant; Figures 5.5C and 5.5D for the *cit3Δ*, *idh1Δ* and *idh2Δ* mutants); 3) enzymes implicated in ROS detoxification and oxidative stress protection in mitochondria (Figures 5.4C, 5.4G, 5.4I and 5.4J for the *ccp1Δ* mutant; Figures 5.5E and 5.5F for the *glr1Δ*, *gpx1Δ* and *gtt2Δ* mutants); 4) proteins involved in the formation of heme and its attachment to other proteins in mitochondria (Figures 5.4D, 5.4H, 5.4I and 5.4J for the *cox10Δ* mutant; Figures 5.5G and 5.5H for the *cox15Δ*, *cyc2Δ* and *cyc3Δ* mutants); 5) chaperones assisting in the folding and refolding of proteins within mitochondria (Figures 5.6A, 5.6E, 5.6I and 5.6J for the *bcs1Δ* mutant; Figures 5.5I and 5.5J for the *ecm10Δ*, *hsp78Δ* and *mdj1Δ* mutants); and 6) components of the mitochondrial protein import machinery (Figures 5.6B, 5.6F, 5.6I and 5.6J for the *hot13Δ* mutant; Figures 5.5K and 5.50L for the *mdj2Δ*, *mgr2Δ* and *mic60Δ* mutants).

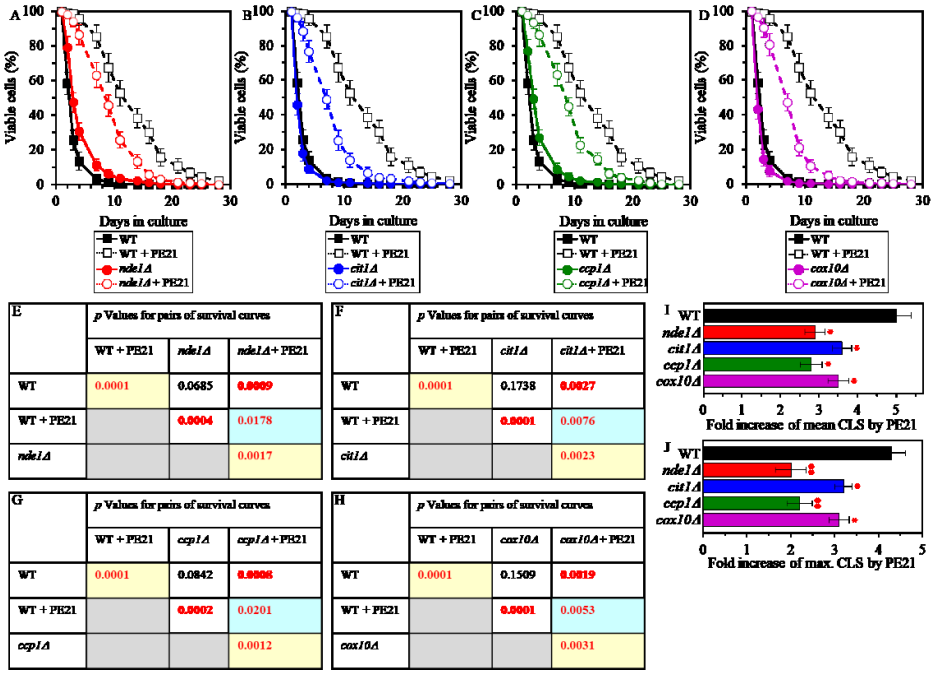

Figure 5.4. Single-gene-deletion mutations eliminating mitochondrial proteins that are upregulated by PE21 reduce the geroprotective potential of PE21. WT cells and mutant cells carrying a single-gene-deletion mutation eliminating either Nde1, Cit1, Ccp1 or Cox10 were cultured in the synthetic minimal YNB medium initially containing 2% glucose with 0.1% PE21 or without it. (**A**-**D**) Survival curves of the chronologically aging WT and *nde1Δ* (**A**), WT and *cit1Δ* (**B**), WT and *ccp1Δ* (**C**) or WT and *cox10Δ* (**D**) strains are shown. Data are presented as means ± SEM (n = 3). (**E**-**H**) *p* Values for different pairs of survival curves of the WT and *nde1Δ* (**E**), WT and *cit1Δ* (**F**), WT and *ccp1Δ* (**G**) or WT and *cox10Δ* (**H**) strains cultured with or without PE21. Survival curves shown in **A**-**D** (respectively) were compared. Two survival curves were considered statistically different if the *p* value was less than 0.05. The *p* values for comparing pairs of survival curves using the logrank test were calculated as described in Materials and Methods. The *p* values displayed on a yellow color background indicate that PE21 statistically significantly prolongs the CLS of the WT (**E**-**H**), *nde1Δ* (**E**), *cit1Δ* (**F**), *ccp1Δ* (**G**) and *cox10Δ* (**H**) strains. The *p* values displayed on a blue color background indicate that PE21 prolongs the CLS of the *nde1Δ* (**E**), *cit1Δ* (**F**), *ccp1Δ* (**G**) and *cox10Δ* (**H**) strains to a lower extent than that of the WT strain. (**I**, **J**) Survival curves shown in (**A**-**D**) were used to calculate the fold of increase of the mean (**I**) and maximum (**J**) CLS by PE21 for the WT, *nde1Δ*, *cit1Δ*, *ccp1Δ* and *cox10Δ* strains. Data are presented as means ± SEM (n = 3; **p* < 0.05; ***p* < 0.01).

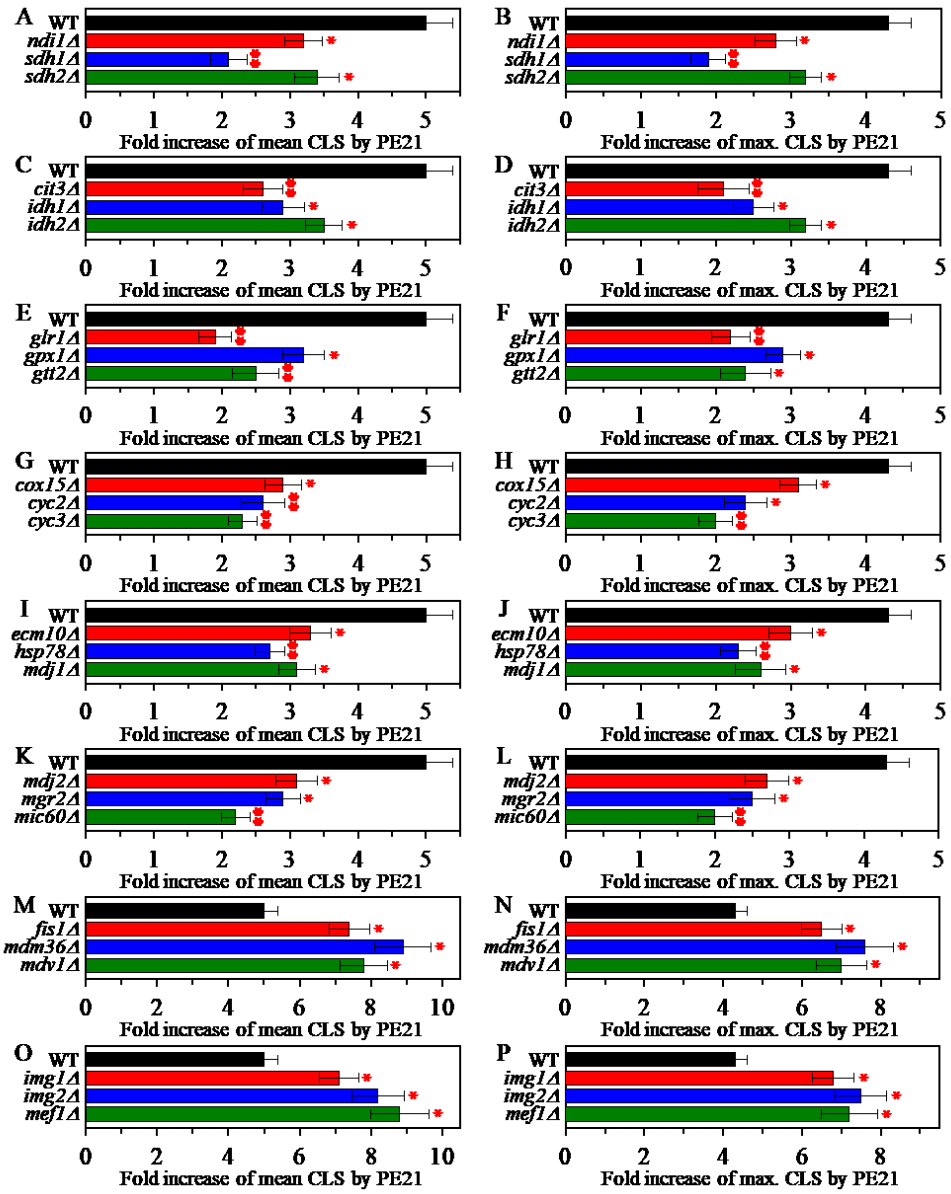

Figure 5.5. Single-gene-deletion mutations eliminating mitochondrial proteins that are upregulated by PE21 decrease the geroprotective efficiency of PE21, while single-gene-deletion mutations eliminating mitochondrial proteins that are downregulated by PE21 increases such efficiency. WT cells and mutant cells carrying a single-gene-deletion mutation eliminating a mitochondrial protein upregulated or downregulated by PE21 were cultured in the synthetic minimal YNB medium initially containing 2% glucose with 0.1% PE21 or without it. Survival curves of chronologically aging WT and mutant strains were used to calculate the fold of increase of the mean (**A**, **C**, **E**, **G**, **I**, **K**, **M**, **O**) and maximum (**B**, **D**, **F**, **H**, **J**, **L**, **N**, **P**) CLS by PE21 for the WT and mutant strains. Data are presented as means ± SEM (n = 3; *$p < 0.05$; **$p < 0.01$).

It is also plausible that those mitochondrial proteins that are downregulated by PE21 may have important contributions to the suppression of a geroprotective action of PE21. One could, therefore, assume that single-gene-deletion mutations that eliminate such mitochondrial proteins may enhance the geroprotective potential of PE21. This assumption holds true, as we observed that PE21 is a significantly more efficient geroprotector for single-gene-deletion mutants that lack the following PE21-suppressible mitochondrial proteins: 1) components of the mitochondrial division (fission) machinery (Figures 5.6C, 5.6G, 5.6I and 5.6J for the *dnm1Δ* mutant; Figures

5.5M and 5.5N for the *fis1Δ*, *mdm36Δ* and *mdv1Δ* mutants); and 2) proteins involved in RNA synthesis, processing and translation within mitochondria (Figures 5.6D, 5.6H, 5.6I and 5.6J for the *ifm1Δ* mutant; Figures 5.5O and 5.5P for the *img1Δ*, *img2Δ* and *mef1Δ* mutants).

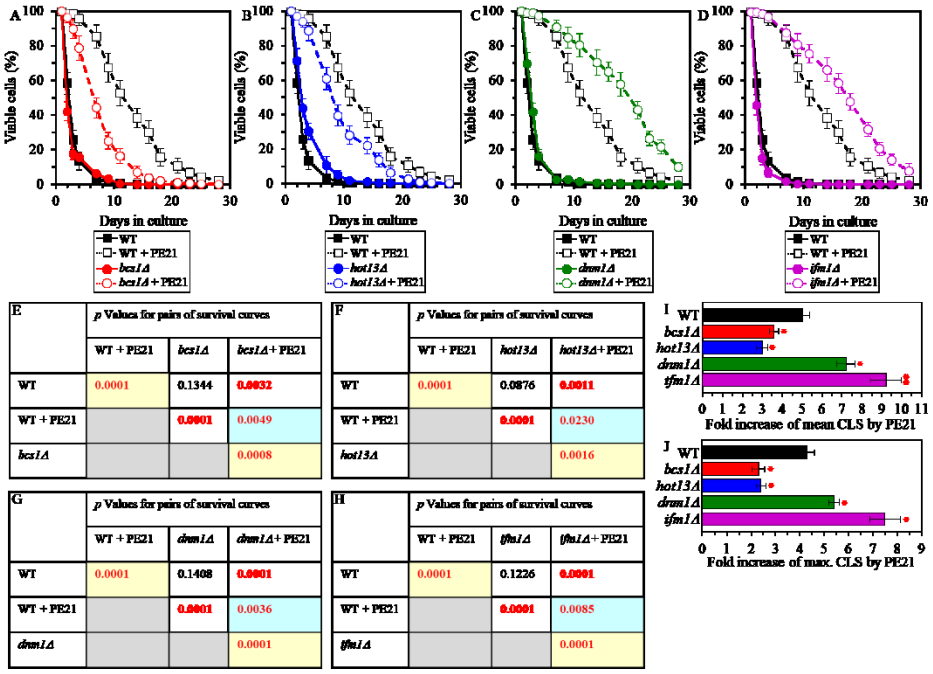

Figure 5.6. Single-gene-deletion mutations eliminating mitochondrial proteins that are upregulated by PE21 decrease the geroprotective potential of PE21, whereas single-gene-deletion mutations eliminating mitochondrial proteins that are downregulated by PE21 increases such potential. WT cells and mutant cells carrying a single-gene-deletion mutation eliminating either Bcs1, Hot13, Dnm1 or Ifm1 were cultured in the synthetic minimal YNB medium initially containing 2% glucose with 0.1% PE21 or without it. (**A**-**D**) Survival curves of the chronologically aging WT and *bcs1Δ* (**A**), WT and *hot13Δ* (**B**), WT and *dnm1Δ* (**C**) or WT and *ifm1Δ* (**D**) strains are shown. Data are presented as means ± SEM (n = 3). (**E**-**H**) *p* Values for different pairs of survival curves of the WT and *bcs1Δ* (**E**), WT and *hot13Δ* (**F**), WT and *dnm1Δ* (**G**) or WT and *ifm1Δ* (**H**) strains cultured with or without PE21. Survival curves shown in **A**-**D** (respectively) were compared. Two survival curves were considered statistically different if the *p* value was less than 0.05. The *p* values for comparing pairs of survival curves using the logrank test were calculated as described in Materials and Methods. The *p* values displayed on a yellow color background indicate that PE21 statistically significantly prolongs the CLS of the WT (**E**-**H**), *bcs1Δ* (**E**), *hot13Δ* (**F**), *dnm1Δ* (**G**) and *ifm1Δ* (**H**) strains. The *p* values displayed on a blue color background indicate that PE21 prolongs the CLS 1) to a lower extent for the *bcs1Δ* (**E**), *hot13Δ* (**F**) strains; and 2) to a higher extent for the *dnm1Δ* (**G**) and *ifm1Δ* (**H**) strains; than that of the WT strain. (**I**, **J**) Survival curves shown in (**A**-**D**) were used to calculate the fold of increase of the mean (**I**) and maximum (**J**) CLS by PE21 for the WT, *bcs1Δ*, *hot13Δ*, *dnm1Δ* and *ifm1Δ* strains. Data are presented as means ± SEM (n = 3; **p* < 0.05; ***p* < 0.01).

5.4 Summary

In sum, the above findings confirm our hypothesis on the third mechanism through which PE21 decelerates yeast chronological aging and prolongs yeast longevity (Figure 3.4). This mechanism consists in a PE21-driven remodeling of certain processes taking place within mitochondria and the resulting changes in functionality of these organelles.

6 General discussion

Studies presented in this thesis validate our hypothesis on the existence of three different mechanisms through which PE21 can delay yeast chronological aging and extend yeast longevity. This hypothesis is described in the Results section and schematically depicted in Figure 3.4.

We found that PE21 activates these three different mechanisms of aging delay and longevity extension because it instigates specific changes in the concentrations of several lipid classes, as summarized below.

The first mechanism by which PE21 slows aging and extends longevity consists in the ability of PE21 to decrease the intracellular concentration of FFA (Figure 3.4). This allows PE21 to sustain FFA concentration below the toxic threshold, thus postponing the age-related onset of a FFA-dependent mode of liponecrotic RCD (Figure 3.4). The commitment of yeast to this mode of RCD in response to excessive FFA concentrations is caused by an augmentation of PM permeability for small molecules, a weakening of mitochondrial functionality, a significant increase in mitochondrial ROS production, an oxidative damage to different types of cellular organelles and the ensuing *en masse* autophagic degradation of these organelles, and an oxidative impairment of many cytosolic proteins that leads to a build-up of the dysfunctional, unfolded and aggregated forms of these proteins [68, 98, 110, 112, 246, 521–524]. Because PE21 decreases the risk of aging-associated liponecrotic RCD and increases the chance of elderly cells to survive, it decelerates chronological aging and prolongs the longevity of *S. cerevisiae*.

The second mechanism through which PE21 delays aging and extends longevity consists in its ability to decrease the concentration of TAG and to increase the concentrations of all glycerophospholipid classes (i.e. PA, PC, PE, PI, and PS) within the ER membrane (Figure 3.4). These PE21-dependent perturbations in the abundance of ER membrane lipids activate the UPR^{ER} system (Figure 3.4). After being activated by PE21, the UPR^{ER} system promotes protein folding and assembly assisted by certain chaperones within the ER, *N*-linked protein glycosylation aided by mannosyltransferases and oligosaccharyltransferases in the ER, the ubiquitin-proteasome pathway for the degradation of improperly folded proteins that amass in the ER, vesicular protein traffic from the ER to the Golgi apparatus, an enzymatic machinery for glycerophospholipid synthesis within the ER, and stress response proteins that prevent and repair oxidative damage to proteins and lipids in the cytosol and mitochondria. The PE21-dependent activation of the UPR^{ER} system also suppresses ribosome assembly, tRNA synthesis and protein translation in the cytosol;

such suppression is known to delay aging and extend longevity in evolutionarily distant eukaryotes [37, 62, 66, 81, 581–603]. All cellular processes that are promoted or suppressed by the PE21-inducible UPR^{ER} system are indispensable for the ability of PE21 to slow yeast chronological aging because they allow to decelerate an age-related decline in protein and lipid homeostasis and to delay an aging-associated deterioration of cell resistance to oxidative and thermal stresses.

The third mechanisms underlying aging delay and longevity extension by PE21 consists in the ability of PE21 to increase PS and PE concentrations and to decrease CL concentration in the mitochondrial membranes (Figure 3.4). These PE21-driven changes in the mitochondrial membrane lipidome alter mitochondrial functionality because they cause an upregulation or downregulation of many mitochondrial proteins, thereby reorganizing some vital processes confined to mitochondria. Mitochondrial proteins that are upregulated in response to PE21 include components of the ETC and OXPHOS, enzymes that catalyze the TCA and glyoxylate cycles, proteins involved in ROS detoxification and oxidative stress protection, proteins implicated in the synthesis of heme and its attachment to other proteins, chaperones that assist in the folding and refolding of other proteins, and components of the mitochondrial protein import machinery. Among mitochondrial proteins that are downregulated in response to PE21 are components of the mitochondrial division (fission) apparatus as well as proteins implicated in mitochondrial RNA synthesis, processing, and translation. As we found, all mitochondrial processes that are upregulated or downregulated by PE21 play essential roles in the PE21-dependent delay of yeast chronological aging because they allow to amend the pattern of age-related changes in mitochondrial respiration, mitochondrial membrane potential, and mitochondrial ROS production.

The challenge for the future is to define mechanisms underlying the PE21-dependent remodeling of the ER and mitochondrial membrane lipidomes in chronologically aging yeast. Because PE21 slows aging by inhibiting a form of the pro-aging protein kinase Sch9 that is activated by the pro-aging PKH1/2 signaling pathway [604], one could envision that these mechanisms may involve certain changes in the reversible phosphorylation of some proteins implicated in lipid metabolism and transport in the ER and mitochondria. The ongoing studies in the Titorenko laboratory address the validity of this assumption.

REFERENCES

1. Fontana L, Partridge L, Longo VD. Extending healthy life span--from yeast to humans. Science. United States; 2010; 328: 321–6.
2. Kaeberlein M. Lessons on longevity from budding yeast. Nature. England; 2010; 464: 513–9.
3. Weissman J, Guthrie C, Fink G. Guide to Yeast Genetics: Functional Genomics, Proteomics and Other Systems Analysis - 2nd Edition - ISBN: 9780123751713, 9780123848864 Guide to Yeast Genetics: Functional Genomics, Proteomics and Other Systems Analysis, Volume 470 2nd Edition. 2010. 944 p.
4. Botstein D, Fink GR. Yeast: an experimental organism for 21st Century biology. Genetics. United States; 2011; 189: 695–704.
5. Longo VD, Shadel GS, Kaeberlein M, Kennedy B. Replicative and chronological aging in Saccharomyces cerevisiae. Cell Metab. United States; 2012; 16: 18–31.
6. Sutphin GL, Olsen BA, Kennedy BK, Kaeberlein M. Genome-wide analysis of yeast aging. Subcell Biochem. United States; 2012; 57: 251–89.
7. Arlia-Ciommo A, Leonov A, Piano A, Svistkova V, Titorenko V. Cell-autonomous mechanisms of chronological aging in the yeast Saccharomyces cerevisiae. Microb Cell. 2014; 1: 163–78.
8. Denoth Lippuner A, Julou T, Barral Y. Budding yeast as a model organism to study the effects of age. FEMS Microbiol Rev. England; 2014; 38: 300–25.
9. Duina AA, Miller ME, Keeney JB. Budding yeast for budding geneticists: a primer on the Saccharomyces cerevisiae model system. Genetics. United States; 2014; 197: 33–48.
10. Garay E, Campos SE, Gonzalez de la Cruz J, Gaspar AP, Jinich A, Deluna A. High-resolution profiling of stationary-phase survival reveals yeast longevity factors and their genetic interactions. PLoS Genet. United States; 2014; 10: e1004168.
11. Richard VR, Bourque SD, Titorenko VI. Metabolomic and lipidomic analyses of chronologically aging yeast. Methods Mol Biol. United States; 2014; 1205: 359–73.
12. Bilinski T, Bylak A, Zadrag-Tecza R. The budding yeast Saccharomyces cerevisiae as a model organism: possible implications for gerontological studies. Biogerontology. Netherlands; 2017; 18: 631–40.
13. He C, Zhou C, Kennedy BK. The yeast replicative aging model. Biochim Biophys acta Mol basis Dis. Netherlands; 2018; 1864: 2690–6.
14. Strynatka KA, Gurrola-Gal MC, Berman JN, McMaster CR. How Surrogate and Chemical Genetics in Model Organisms Can Suggest Therapies for Human Genetic Diseases. Genetics. United States; 2018; 208: 833–51.

15. Zimmermann A, Hofer S, Pendl T, Kainz K, Madeo F, Carmona-Gutierrez D. Yeast as a tool to identify anti-aging compounds. FEMS Yeast Res. England; 2018; 18.

16. Vachova L, Cap M, Palkova Z. Yeast colonies: a model for studies of aging, environmental adaptation, and longevity. Oxid Med Cell Longev. United States; 2012; 2012: 601836.

17. Nystrom T, Liu B. Protein quality control in time and space - links to cellular aging. FEMS Yeast Res. England; 2014; 14: 40–8.

18. Pitt JN, Kaeberlein M. Why is aging conserved and what can we do about it? PLoS Biol. United States; 2015; 13: e1002131.

19. Smith J, Wright J, Schneider BL. A budding yeast's perspective on aging: the shape I'm in. Exp Biol Med (Maywood). England; 2015; 240: 701–10.

20. Kaeberlein M. The Biology of Aging: Citizen Scientists and Their Pets as a Bridge Between Research on Model Organisms and Human Subjects. Vet Pathol. United States; 2016; 53: 291–8.

21. Sontag EM, Samant RS, Frydman J. Mechanisms and Functions of Spatial Protein Quality Control. Annu Rev Biochem. United States; 2017; 86: 97–122.

22. Crane MM, Kaeberlein M. The paths of mortality: how understanding the biology of aging can help explain systems behavior of single cells. Curr Opin Syst Biol. England; 2018; 8: 25–31.

23. Mair W, Dillin A. Aging and survival: the genetics of life span extension by dietary restriction. Annu Rev Biochem. United States; 2008; 77: 727–54.

24. de Cabo R, Carmona-Gutierrez D, Bernier M, Hall MN, Madeo F. The search for antiaging interventions: from elixirs to fasting regimens. Cell. United States; 2014; 157: 1515–26.

25. Eisenberg T, Knauer H, Schauer A, Buttner S, Ruckenstuhl C, Carmona-Gutierrez D, Ring J, Schroeder S, Magnes C, Antonacci L, Fussi H, Deszcz L, Hartl R, et al. Induction of autophagy by spermidine promotes longevity. Nat Cell Biol. England; 2009; 11: 1305–14.

26. Hubbard BP, Sinclair DA. Small molecule SIRT1 activators for the treatment of aging and age- related diseases. Trends Pharmacol Sci. England; 2014; 35: 146–54.

27. Sinclair DA, Guarente L. Small-molecule allosteric activators of sirtuins. Annu Rev Pharmacol Toxicol. United States; 2014; 54: 363–80.

28. Madeo F, Pietrocola F, Eisenberg T, Kroemer G. Caloric restriction mimetics: towards a molecular definition. Nature reviews. Drug discovery. England; 2014. p. 727–40.

29. Leonov A, Arlia-Ciommo A, Piano A, Svistkova V, Lutchman V, Medkour Y, Titorenko VI. Longevity extension by phytochemicals. Molecules. Switzerland; 2015; 20: 6544–72.

30. Moskalev A, Chernyagina E, de Magalhaes JP, Barardo D, Thoppil H, Shaposhnikov M, Budovsky A, Fraifeld VE, Garazha A, Tsvetkov V, Bronovitsky E, Bogomolov V, Scerbacov A, et al. Geroprotectors.org: a new, structured and curated database of current therapeutic interventions in aging and age-related disease. Aging (Albany NY). United States; 2015; 7: 616–28.

31. Moskalev A, Chernyagina E, Tsvetkov V, Fedintsev A, Shaposhnikov M, Krut'ko V, Zhavoronkov A, Kennedy BK. Developing criteria for evaluation of geroprotectors as a key stage toward translation to the clinic. Aging Cell. England; 2016; 15: 407–15.

32. Moskalev A, Chernyagina E, Kudryavtseva A, Shaposhnikov M. Geroprotectors: A Unified Concept and Screening Approaches. Aging Dis. United States; 2017; 8: 354–63.

33. Madeo F, Carmona-Gutierrez D, Kepp O, Kroemer G. Spermidine delays aging in humans. Aging (Albany NY). United States; 2018; 10: 2209–11.

34. Madeo F, Eisenberg T, Pietrocola F, Kroemer G. Spermidine in health and disease. Science. United States; 2018; 359.

35. Steinkraus KA, Kaeberlein M, Kennedy BK. Replicative aging in yeast: the means to the end. Annu Rev Cell Dev Biol. United States; 2008; 24: 29–54.

36. Steffen KK, Kennedy BK, Kaeberlein M. Measuring replicative life span in the budding yeast. J Vis Exp. United States; 2009; .

37. Smith ED, Tsuchiya M, Fox LA, Dang N, Hu D, Kerr EO, Johnston ED, Tchao BN, Pak DN, Welton KL, Promislow DEL, Thomas JH, Kaeberlein M, et al. Quantitative evidence for conserved longevity pathways between divergent eukaryotic species. Genome Res. United States; 2008; 18: 564–70.

38. Ghavidel A, Baxi K, Ignatchenko V, Prusinkiewicz M, Arnason TG, Kislinger T, Carvalho CE, Harkness TAA. A Genome Scale Screen for Mutants with Delayed Exit from Mitosis: Ire1-Independent Induction of Autophagy Integrates ER Homeostasis into Mitotic Lifespan. PLoS Genet. 2015; 11: e1005429.

39. McCormick MA, Delaney JR, Tsuchiya M, Tsuchiyama S, Shemorry A, Sim S, Chou AC-Z, Ahmed U, Carr D, Murakami CJ, Schleit J, Sutphin GL, Wasko BM, et al. A Comprehensive Analysis of Replicative Lifespan in 4,698 Single-Gene Deletion Strains Uncovers Conserved Mechanisms of Aging. Cell Metab. 2015; 22: 895–906.

40. Janssens GE, Veenhoff LM. Evidence for the hallmarks of human aging in replicatively aging yeast. Microb cell (Graz, Austria). Austria; 2016; 3: 263–74.

41. Fabrizio P, Longo VD. The chronological life span of Saccharomyces cerevisiae. Methods Mol Biol. United States; 2007; 371: 89–95.

42. Longo VD, Fabrizio P. Chronological aging in Saccharomyces cerevisiae. Subcell Biochem. United States; 2012; 57: 101–21.

43. Burtner CR, Murakami CJ, Kennedy BK, Kaeberlein M. A molecular mechanism of chronological aging in yeast. Cell Cycle. United States; 2009; 8: 1256–70.

44. Longo VD, Kennedy BK. Sirtuins in aging and age-related disease. Cell. United States; 2006; 126: 257–68.

45. Murakami C, Delaney JR, Chou A, Carr D, Schleit J, Sutphin GL, An EH, Castanza AS, Fletcher M, Goswami S, Higgins S, Holmberg M, Hui J, et al. pH neutralization protects against reduction in replicative lifespan following chronological aging in yeast. Cell Cycle.

2012; 11: 3087–96.

46. Delaney JR, Murakami C, Chou A, Carr D, Schleit J, Sutphin GL, An EH, Castanza AS, Fletcher M, Goswami S, Higgins S, Holmberg M, Hui J, et al. Dietary restriction and mitochondrial function link replicative and chronological aging in Saccharomyces cerevisiae. Exp Gerontol. 2013; 48: 1006–13.

47. Molon M, Zadrag-Tecza R, Bilinski T. The longevity in the yeast Saccharomyces cerevisiae: A comparison of two approaches for assessment the lifespan. Biochem Biophys Res Commun. United States; 2015; 460: 651–6.

48. Guarente LP, Partridge L, Douglas WC. Molecular Biology of Aging. Cold Spring Harbor: Cold Spring Harbor Laboratory Press; 2008. 610 p.

49. J ME, N AS. Handbook of the Biology of Aging. 7th Editio. Amsterdam: Academic Press; 2011.

50. Lopez-Otin C, Blasco MA, Partridge L, Serrano M, Kroemer G. The hallmarks of aging. Cell. United States; 2013; 153: 1194–217.

51. Jay OS, M MG, L KJ. Aging: The Longevity Dividend. Cold Spring Harbor: Cold Spring Harbor Laboratory Press; 2016. 243 p.

52. Greer EL, Brunet A. Signaling networks in aging. J Cell Sci. England; 2008; 121: 407–12.

53. Goldberg AA, Bourque SD, Kyryakov P, Boukh-Viner T, Gregg C, Beach A, Burstein MT, Machkalyan G, Richard V, Rampersad S, Titorenko VI. A novel function of lipid droplets in regulating longevity. Biochem Soc Trans. England; 2009; 37: 1050–5.

54. Kenyon CJ. The genetics of ageing. Nature. England; 2010; 464: 504–12.

55. Kyryakov P, Beach A, Richard VR, Burstein MT, Leonov A, Levy S, Titorenko VI. Caloric restriction extends yeast chronological lifespan by altering a pattern of age-related changes in trehalose concentration. Front Physiol. Switzerland; 2012; 3: 256.

56. Ahlqvist KJ, Suomalainen A, Hamalainen RH. Stem cells, mitochondria and aging. Biochim Biophys Acta. Netherlands; 2015; 1847: 1380–6.

57. Beach A, Leonov A, Arlia-Ciommo A, Svistkova V, Lutchman V, Titorenko VI. Mechanisms by which different functional states of mitochondria define yeast longevity. Int J Mol Sci. Switzerland; 2015; 16: 5528–54.

58. Goodell MA, Rando TA. Stem cells and healthy aging. Science. United States; 2015; 350: 1199–204.

59. Chandel NS, Jasper H, Ho TT, Passegue E. Metabolic regulation of stem cell function in tissue homeostasis and organismal ageing. Nat Cell Biol. England; 2016; 18: 823–32.

60. Medkour Y, Svistkova V, Titorenko VI. Cell-Nonautonomous Mechanisms Underlying Cellular and Organismal Aging. Int Rev Cell Mol Biol. Netherlands: Elsevier Inc.; 2016; 321: 259–97.

61. Ocampo A, Reddy P, Belmonte JCI. Anti-Aging Strategies Based on Cellular

Reprogramming. Trends Mol Med. England; 2016; 22: 725–38.

62. Steffen KK, Dillin A. A Ribosomal Perspective on Proteostasis and Aging. Cell Metab. United States; 2016; 23: 1004–12.

63. Leonov A, Arlia-Ciommo A, Bourque SD, Koupaki O, Kyryakov P, Dakik P, McAuley M, Medkour Y, Mohammad K, Di Maulo T, Titorenko VI. Specific changes in mitochondrial lipidome alter mitochondrial proteome and increase the geroprotective efficiency of lithocholic acid in chronologically aging yeast. Oncotarget. 2017; 8: 30672–91.

64. Ren R, Ocampo A, Liu G-H, Izpisua Belmonte JC. Regulation of Stem Cell Aging by Metabolism and Epigenetics. Cell Metab. United States; 2017; 26: 460–74.

65. Revuelta M, Matheu A. Autophagy in stem cell aging. Aging Cell. England; 2017; 16: 912–5.

66. Anisimova AS, Alexandrov AI, Makarova NE, Gladyshev VN, Dmitriev SE. Protein synthesis and quality control in aging. Aging (Albany NY). United States; 2018; 10: 4269–88.

67. Hansen M, Rubinsztein DC, Walker DW. Autophagy as a promoter of longevity: insights from model organisms. Nat Rev Mol Cell Biol. England; 2018; 19: 579–93.

68. Mitrofanova D, Dakik P, McAuley M, Medkour Y, Mohammad K, Titorenko VI. Lipid metabolism and transport define longevity of the yeast Saccharomyces cerevisiae. Front Biosci. United States; 2017; 23: 1166–94.

69. Panel M, Ghaleh B, Morin D. Mitochondria and aging: A role for the mitochondrial transition pore? Aging Cell. England; 2018; 17: e12793.

70. So W-K, Cheung TH. Molecular Regulation of Cellular Quiescence: A Perspective from Adult Stem Cells and Its Niches. Methods Mol Biol. United States; 2018; 1686: 1–25.

71. Barbosa MC, Grosso RA, Fader CM. Hallmarks of Aging: An Autophagic Perspective. Front Endocrinol (Lausanne). Switzerland; 2018; 9: 790.

72. Dakik PP, Medkour Y, Mohammad K, Titorenko VI. Mechanisms Through Which Some Mitochondria-Generated Metabolites Act as Second Messengers That Are Essential Contributors to the Aging Process in Eukaryotes Across Phyla. Front Physiol. Switzerland; 2019; 10: 461.

73. Escobar KA, Cole NH, Mermier CM, VanDusseldorp TA. Autophagy and aging: Maintaining the proteome through exercise and caloric restriction. Aging Cell. England; 2019; 18: e12876.

74. Wagner W. The Link Between Epigenetic Clocks for Aging and Senescence. Front Genet. Switzerland; 2019; 10: 303.

75. Riera CE, Merkwirth C, De Magalhaes Filho CD, Dillin A. Signaling Networks Determining Life Span. Annu Rev Biochem. United States; 2016; 85: 35–64.

76. Salminen A, Kaarniranta K, Kauppinen A. Age-related changes in AMPK activation: Role for AMPK phosphatases and inhibitory phosphorylation by upstream signaling pathways.

Ageing Res Rev. England; 2016; 28: 15–26.

77. Bettedi L, Foukas LC. Growth factor, energy and nutrient sensing signalling pathways in metabolic ageing. Biogerontology. Netherlands; 2017; 18: 913–29.

78. Pan H, Finkel T. Key proteins and pathways that regulate lifespan. J Biol Chem. United States; 2017; 292: 6452–60.

79. Slack C, Tullet J. Signal Transduction Pathways in Ageing. Subcell Biochem. United States; 2018; 90: 323–50.

80. Lin SS, Manchester JK, Gordon JI. Sip2, an N-myristoylated beta subunit of Snf1 kinase, regulates aging in Saccharomyces cerevisiae by affecting cellular histone kinase activity, recombination at rDNA loci, and silencing. J Biol Chem. 2003; 278: 13390–7.

81. Kaeberlein M, Powers RW 3rd, Steffen KK, Westman EA, Hu D, Dang N, Kerr EO, Kirkland KT, Fields S, Kennedy BK. Regulation of yeast replicative life span by TOR and Sch9 in response to nutrients. Science. United States; 2005; 310: 1193–6.

82. Powers RW 3rd, Kaeberlein M, Caldwell SD, Kennedy BK, Fields S. Extension of chronological life span in yeast by decreased TOR pathway signaling. Genes Dev. United States; 2006; 20: 174–84.

83. Urban J, Soulard A, Huber A, Lippman S, Mukhopadhyay D, Deloche O, Wanke V, Anrather D, Ammerer G, Riezman H, Broach JR, De Virgilio C, Hall MN, et al. Sch9 is a major target of TORC1 in Saccharomyces cerevisiae. Mol Cell. United States; 2007; 26: 663–74.

84. Wei M, Fabrizio P, Hu J, Ge H, Cheng C, Li L, Longo VD. Life span extension by calorie restriction depends on Rim15 and transcription factors downstream of Ras/PKA, Tor, and Sch9. PLoS Genet. United States; 2008; 4: e13.

85. Alvers AL, Fishwick LK, Wood MS, Hu D, Chung HS, Dunn WAJ, Aris JP. Autophagy and amino acid homeostasis are required for chronological longevity in Saccharomyces cerevisiae. Aging Cell. England; 2009; 8: 353–69.

86. Alvers AL, Wood MS, Hu D, Kaywell AC, Dunn WAJ, Aris JP. Autophagy is required for extension of yeast chronological life span by rapamycin. Autophagy. United States; 2009; 5: 847–9.

87. Morselli E, Galluzzi L, Kepp O, Criollo A, Maiuri MC, Tavernarakis N, Madeo F, Kroemer G. Autophagy mediates pharmacological lifespan extension by spermidine and resveratrol. Aging (Albany NY). United States; 2009; 1: 961–70.

88. Lu J-Y, Lin Y-Y, Sheu J-C, Wu J-T, Lee F-J, Chen Y, Lin M-I, Chiang F-T, Tai T-Y, Berger SL, Zhao Y, Tsai K-S, Zhu H, et al. Acetylation of yeast AMPK controls intrinsic aging independently of caloric restriction. Cell. United States; 2011; 146: 969–79.

89. De Virgilio C. The essence of yeast quiescence. FEMS Microbiol Rev. England; 2012; 36: 306–39.

90. Liu J, Huang X, Withers BR, Blalock E, Liu K, Dickson RC. Reducing sphingolipid

synthesis orchestrates global changes to extend yeast lifespan. Aging Cell. England; 2013; 12: 833–41.

91. Richard VR, Leonov A, Beach A, Burstein MT, Koupaki O, Gomez-Perez A, Levy S, Pluska L, Mattie S, Rafesh R, Iouk T, Sheibani S, Greenwood M, et al. Macromitophagy is a longevity assurance process that in chronologically aging yeast limited in calorie supply sustains functional mitochondria and maintains cellular lipid homeostasis. Aging (Albany NY). 2013; 5: 234–69.

92. Conrad M, Schothorst J, Kankipati HN, Van Zeebroeck G, Rubio-Texeira M, Thevelein JM. Nutrient sensing and signaling in the yeast Saccharomyces cerevisiae. FEMS Microbiol Rev. England; 2014; 38: 254–99.

93. Huang X, Withers BR, Dickson RC. Sphingolipids and lifespan regulation. Biochim Biophys Acta. Netherlands; 2014; 1841: 657–64.

94. Swinnen E, Ghillebert R, Wilms T, Winderickx J. Molecular mechanisms linking the evolutionary conserved TORC1-Sch9 nutrient signalling branch to lifespan regulation in Saccharomyces cerevisiae. FEMS Yeast Res. England; 2014; 14: 17–32.

95. Jiao R, Postnikoff S, Harkness TA, Arnason TG. The SNF1 Kinase Ubiquitin-associated Domain Restrains Its Activation, Activity, and the Yeast Life Span. J Biol Chem. United States; 2015; 290: 15393–404.

96. Teixeira V, Costa V. Unraveling the role of the Target of Rapamycin signaling in sphingolipid metabolism. Prog Lipid Res. England; 2016; 61: 109–33.

97. Fabrizio P, Pozza F, Pletcher SD, Gendron CM, Longo VD. Regulation of longevity and stress resistance by Sch9 in yeast. Science. United States; 2001; 292: 288–90.

98. Goldberg AA, Richard VR, Kyryakov P, Bourque SD, Beach A, Burstein MT, Glebov A, Koupaki O, Boukh-Viner T, Gregg C, Juneau M, English AM, Thomas DY, et al. Chemical genetic screen identifies lithocholic acid as an anti-aging compound that extends yeast chronological life span in a TOR-independent manner, by modulating housekeeping longevity assurance processes. Aging (Albany NY). 2010; 2: 393–414.

99. Minois N, Carmona-Gutierrez D, Madeo F. Polyamines in aging and disease. Aging (Albany NY). United States; 2011; 3: 716–32.

100. Arlia-Ciommo A, Piano A, Svistkova V, Mohtashami S, Titorenko VI. Mechanisms underlying the anti-aging and anti-tumor effects of lithocholic bile acid. Int J Mol Sci. Switzerland; 2014; 15: 16522–43.

101. van Meer G, Voelker DR, Feigenson GW. Membrane lipids: where they are and how they behave. Nat Rev Mol Cell Biol. England; 2008; 9: 112–24.

102. Bou Khalil M, Hou W, Zhou H, Elisma F, Swayne LA, Blanchard AP, Yao Z, Bennett SAL, Figeys D. Lipidomics era: accomplishments and challenges. Mass Spectrom Rev. United States; 2010; 29: 877–929.

103. Shevchenko A, Simons K. Lipidomics: coming to grips with lipid diversity. Nature reviews. Molecular cell biology. England; 2010. p. 593–8.

104. Brugger B. Lipidomics: analysis of the lipid composition of cells and subcellular organelles by electrospray ionization mass spectrometry. Annu Rev Biochem. United States; 2014; 83: 79–98.

105. Holthuis JCM, Menon AK. Lipid landscapes and pipelines in membrane homeostasis. Nature. England; 2014; 510: 48–57.

106. Kai S. The Biology of Lipids: Trafficking, Regulation, and Function. Cold Spring Harbor: Cold Spring Harbor Laboratory Press; 2011. 334 p.

107. Zechner R, Zimmermann R, Eichmann TO, Kohlwein SD, Haemmerle G, Lass A, Madeo F. FAT SIGNALS--lipases and lipolysis in lipid metabolism and signaling. Cell Metab. United States; 2012; 15: 279–91.

108. Bogdanov M, Dowhan W, Vitrac H. Lipids and topological rules governing membrane protein assembly. Biochim Biophys Acta. Netherlands; 2014; 1843: 1475–88.

109. Eisenberg T, Buttner S. Lipids and cell death in yeast. FEMS Yeast Res. England; 2014; 14: 179–97.

110. Richard VR, Beach A, Piano A, Leonov A, Feldman R, Burstein MT, Kyryakov P, Gomez-Perez A, Arlia-Ciommo A, Baptista S, Campbell C, Goncharov D, Pannu S, et al. Mechanism of liponecrosis, a distinct mode of programmed cell death. Cell Cycle. 2014; 13: 3707–26.

111. Volmer R, Ron D. Lipid-dependent regulation of the unfolded protein response. Curr Opin Cell Biol. England; 2015; 33: 67–73.

112. Arlia-Ciommo A, Svistkova V, Mohtashami S, Titorenko VI. A novel approach to the discovery of anti-tumor pharmaceuticals: searching for activators of liponecrosis. Oncotarget. United States; 2016; 7: 5204–25.

113. Jackson CL, Walch L, Verbavatz J-M. Lipids and Their Trafficking: An Integral Part of Cellular Organization. Dev Cell. United States; 2016; 39: 139–53.

114. Martensson CU, Doan KN, Becker T. Effects of lipids on mitochondrial functions. Biochim Biophys acta Mol cell Biol lipids. Netherlands; 2017; 1862: 102–13.

115. Hansen M, Flatt T, Aguilaniu H. Reproduction, fat metabolism, and life span: what is the connection? Cell Metab. United States; 2013; 17: 10–9.

116. Hanada K. Serine palmitoyltransferase, a key enzyme of sphingolipid metabolism. Biochim Biophys Acta. Netherlands; 2003; 1632: 16–30.

117. Dickson RC. Thematic review series: sphingolipids. New insights into sphingolipid metabolism and function in budding yeast. J Lipid Res. United States; 2008; 49: 909–21.

118. Dickson RC. Roles for sphingolipids in Saccharomyces cerevisiae. Adv Exp Med Biol. United States; 2010; 688: 217–31.

119. Fujita T, Inoue K, Yamamoto S, Ikumoto T, Sasaki S, Toyama R, Chiba K, Hoshino Y, Okumoto T. Fungal metabolites. Part 11. A potent immunosuppressive activity found in Isaria sinclairii metabolite. J Antibiot (Tokyo). Japan; 1994; 47: 208–15.

120. Miyake Y, Kozutsumi Y, Nakamura S, Fujita T, Kawasaki T. Serine palmitoyltransferase is the primary target of a sphingosine-like immunosuppressant, ISP-1/myriocin. Biochem Biophys Res Commun. United States; 1995; 211: 396–403.

121. Beeler T, Bacikova D, Gable K, Hopkins L, Johnson C, Slife H, Dunn T. The Saccharomyces cerevisiae TSC10/YBR265w gene encoding 3-ketosphinganine reductase is identified in a screen for temperature-sensitive suppressors of the Ca2+-sensitive csg2Delta mutant. J Biol Chem. 1998; 273: 30688–94.

122. Grilley MM, Stock SD, Dickson RC, Lester RL, Takemoto JY. Syringomycin action gene SYR2 is essential for sphingolipid 4-hydroxylation in Saccharomyces cerevisiae. J Biol Chem. United States; 1998; 273: 11062–8.

123. D'mello NP, Childress AM, Franklin DS, Kale SP, Pinswasdi C, Jazwinski SM. Cloning and characterization of LAG1, a longevity-assurance gene in yeast. J Biol Chem. United States; 1994; 269: 15451–9.

124. Haak D, Gable K, Beeler T, Dunn T. Hydroxylation of Saccharomyces cerevisiae ceramides requires Sur2p and Scs7p. J Biol Chem. United States; 1997; 272: 29704–10.

125. Guillas I, Kirchman PA, Chuard R, Pfefferli M, Jiang JC, Jazwinski SM, Conzelmann A. C26-CoA-dependent ceramide synthesis of Saccharomyces cerevisiae is operated by Lag1p and Lac1p. EMBO J. England; 2001; 20: 2655–65.

126. Schorling S, Vallee B, Barz WP, Riezman H, Oesterhelt D. Lag1p and Lac1p are essential for the Acyl-CoA-dependent ceramide synthase reaction in Saccharomyces cerevisae. Mol Biol Cell. United States; 2001; 12: 3417–27.

127. Vallee B, Riezman H. Lip1p: a novel subunit of acyl-CoA ceramide synthase. EMBO J. England; 2005; 24: 730–41.

128. Merrill AHJ, Sullards MC, Wang E, Voss KA, Riley RT. Sphingolipid metabolism: roles in signal transduction and disruption by fumonisins. Environ Health Perspect. United States; 2001; 109 Suppl: 283–9.

129. Mandala SM, Thornton RA, Frommer BR, Curotto JE, Rozdilsky W, Kurtz MB, Giacobbe RA, Bills GF, Cabello MA, Martín I. The discovery of australifungin, a novel inhibitor of sphinganine N-acyltransferase from Sporormiella australis. Producing organism, fermentation, isolation, and biological activity. J Antibiot (Tokyo). 1995; 48: 349–56.

130. Funato K, Riezman H. Vesicular and nonvesicular transport of ceramide from ER to the Golgi apparatus in yeast. J Cell Biol. United States; 2001; 155: 949–59.

131. Kajiwara K, Ikeda A, Aguilera-Romero A, Castillon GA, Kagiwada S, Hanada K, Riezman H, Muniz M, Funato K. Osh proteins regulate COPII-mediated vesicular transport of ceramide from the endoplasmic reticulum in budding yeast. J Cell Sci. England; 2014; 127: 376–87.

132. Liu L-K, Choudhary V, Toulmay A, Prinz WA. An inducible ER-Golgi tether facilitates ceramide transport to alleviate lipotoxicity. J Cell Biol. United States; 2017; 216: 131–47.

133. Nagiec MM, Nagiec EE, Baltisberger JA, Wells GB, Lester RL, Dickson RC. Sphingolipid

synthesis as a target for antifungal drugs. Complementation of the inositol phosphorylceramide synthase defect in a mutant strain of Saccharomyces cerevisiae by the AUR1 gene. J Biol Chem. 1997; 272: 9809–17.

134. Sato K, Noda Y, Yoda K. Kei1: a novel subunit of inositolphosphorylceramide synthase, essential for its enzyme activity and Golgi localization. Mol Biol Cell. United States; 2009; 20: 4444–57.

135. Heidler SA, Radding JA. The AUR1 gene in Saccharomyces cerevisiae encodes dominant resistance to the antifungal agent aureobasidin A (LY295337). Antimicrob Agents Chemother. United States; 1995; 39: 2765–9.

136. Hashida-Okado T, Ogawa A, Endo M, Yasumoto R, Takesako K, Kato I. AUR1, a novel gene conferring aureobasidin resistance on Saccharomyces cerevisiae: a study of defective morphologies in Aur1p-depleted cells. Mol Gen Genet. Germany; 1996; 251: 236–44.

137. Okamoto Y, Vaena De Avalos S, Hannun YA. Structural requirements for selective binding of ISC1 to anionic phospholipids. J Biol Chem. United States; 2002; 277: 46470–7.

138. Vaena de Avalos S, Okamoto Y, Hannun YA. Activation and localization of inositol phosphosphingolipid phospholipase C, Isc1p, to the mitochondria during growth of Saccharomyces cerevisiae. J Biol Chem. United States; 2004; 279: 11537–45.

139. Kitagaki H, Cowart LA, Matmati N, Montefusco D, Gandy J, de Avalos SV, Novgorodov SA, Zheng J, Obeid LM, Hannun YA. ISC1-dependent metabolic adaptation reveals an indispensable role for mitochondria in induction of nuclear genes during the diauxic shift in Saccharomyces cerevisiae. J Biol Chem. 2009; 284: 10818–30.

140. Nagiec MM, Skrzypek M, Nagiec EE, Lester RL, Dickson RC. The LCB4 (YOR171c) and LCB5 (YLR260w) genes of Saccharomyces encode sphingoid long chain base kinases. J Biol Chem. United States; 1998; 273: 19437–42.

141. Saba JD, Nara F, Bielawska A, Garrett S, Hannun YA. The BST1 gene of Saccharomyces cerevisiae is the sphingosine-1-phosphate lyase. J Biol Chem. United States; 1997; 272: 26087–90.

142. Jiang JC, Kirchman PA, Allen M, Jazwinski SM. Suppressor analysis points to the subtle role of the LAG1 ceramide synthase gene in determining yeast longevity. Exp Gerontol. England; 2004; 39: 999–1009.

143. Aerts AM, François IEJA, Bammens L, Cammue BPA, Smets B, Winderickx J, Accardo S, De Vos DE, Thevissen K. Level of M(IP)2C sphingolipid affects plant defensin sensitivity, oxidative stress resistance and chronological life-span in yeast. FEBS Lett. 2006; 580: 1903–7.

144. Dickson RC, Nagiec EE, Wells GB, Nagiec MM, Lester RL. Synthesis of mannose-(inositol-P)2-ceramide, the major sphingolipid in Saccharomyces cerevisiae, requires the IPT1 (YDR072c) gene. J Biol Chem. United States; 1997; 272: 29620–5.

145. Thevissen K, Idkowiak-Baldys J, Im Y-J, Takemoto J, François IEJA, Ferket KKA, Aerts AM, Meert EMK, Winderickx J, Roosen J, Cammue BPA. SKN1, a novel plant defensin-sensitivity gene in Saccharomyces cerevisiae, is implicated in sphingolipid biosynthesis.

FEBS Lett. 2005; 579: 1973–7.

146. Almeida T, Marques M, Mojzita D, Amorim MA, Silva RD, Almeida B, Rodrigues P, Ludovico P, Hohmann S, Moradas-Ferreira P, Côrte-Real M, Costa V. Isc1p plays a key role in hydrogen peroxide resistance and chronological lifespan through modulation of iron levels and apoptosis. Mol Biol Cell. 2008; 19: 865–76.

147. Barbosa AD, Osório H, Sims KJ, Almeida T, Alves M, Bielawski J, Amorim MA, Moradas-Ferreira P, Hannun YA, Costa V. Role for Sit4p-dependent mitochondrial dysfunction in mediating the shortened chronological lifespan and oxidative stress sensitivity of Isc1p-deficient cells. Mol Microbiol. 2011; 81: 515–27.

148. Barbosa AD, Graça J, Mendes V, Chaves SR, Amorim MA, Mendes MV, Moradas-Ferreira P, Côrte-Real M, Costa V. Activation of the Hog1p kinase in Isc1p-deficient yeast cells is associated with mitochondrial dysfunction, oxidative stress sensitivity and premature aging. Mech Ageing Dev. 2012; 133: 317–30.

149. Teixeira V, Medeiros TC, Vilaca R, Moradas-Ferreira P, Costa V. Reduced TORC1 signaling abolishes mitochondrial dysfunctions and shortened chronological lifespan of Isc1p-deficient cells. Microb cell (Graz, Austria). Austria; 2014; 1: 21–36.

150. Spincemaille P, Cammue BP, Thevissen K. Sphingolipids and mitochondrial function, lessons learned from yeast. Microb cell (Graz, Austria). Austria; 2014; 1: 210–24.

151. Spincemaille P, Matmati N, Hannun YA, Cammue BPA, Thevissen K. Sphingolipids and mitochondrial function in budding yeast. Biochim Biophys Acta. Netherlands; 2014; 1840: 3131–7.

152. Jazwinski SM. Mitochondria to nucleus signaling and the role of ceramide in its integration into the suite of cell quality control processes during aging. Ageing Res Rev. England; 2015; 23: 67–74.

153. Eltschinger S, Loewith R. TOR Complexes and the Maintenance of Cellular Homeostasis. Trends Cell Biol. England; 2016; 26: 148–59.

154. Woodacre A, Lone MA, Jablonowski D, Schneiter R, Giorgini F, Schaffrath R. A novel Sit4 phosphatase complex is involved in the response to ceramide stress in yeast. Oxid Med Cell Longev. United States; 2013; 2013: 129645.

155. Berchtold D, Piccolis M, Chiaruttini N, Riezman I, Riezman H, Roux A, Walther TC, Loewith R. Plasma membrane stress induces relocalization of Slm proteins and activation of TORC2 to promote sphingolipid synthesis. Nat Cell Biol. England; 2012; 14: 542–7.

156. Swinnen E, Wilms T, Idkowiak-Baldys J, Smets B, De Snijder P, Accardo S, Ghillebert R, Thevissen K, Cammue B, De Vos D, Bielawski J, Hannun YA, Winderickx J. The protein kinase Sch9 is a key regulator of sphingolipid metabolism in Saccharomyces cerevisiae. Mol Biol Cell. 2014; 25: 196–211.

157. Yi JK, Xu R, Jeong E, Mileva I, Truman J-P, Lin C-L, Wang K, Snider J, Wen S, Obeid LM, Hannun YA, Mao C. Aging-related elevation of sphingoid bases shortens yeast chronological life span by compromising mitochondrial function. Oncotarget. 2016; 7: 21124–44.

158. Huang X, Liu J, Dickson RC. Down-regulating sphingolipid synthesis increases yeast lifespan. PLoS Genet. United States; 2012; 8: e1002493.

159. Liu K, Zhang X, Lester RL, Dickson RC. The sphingoid long chain base phytosphingosine activates AGC-type protein kinases in Saccharomyces cerevisiae including Ypk1, Ypk2, and Sch9. J Biol Chem. United States; 2005; 280: 22679–87.

160. Han S, Lone MA, Schneiter R, Chang A. Orm1 and Orm2 are conserved endoplasmic reticulum membrane proteins regulating lipid homeostasis and protein quality control. Proc Natl Acad Sci U S A. United States; 2010; 107: 5851–6.

161. Breslow DK, Collins SR, Bodenmiller B, Aebersold R, Simons K, Shevchenko A, Ejsing CS, Weissman JS. Orm family proteins mediate sphingolipid homeostasis. Nature. England; 2010; 463: 1048–53.

162. Roelants FM, Breslow DK, Muir A, Weissman JS, Thorner J. Protein kinase Ypk1 phosphorylates regulatory proteins Orm1 and Orm2 to control sphingolipid homeostasis in Saccharomyces cerevisiae. Proc Natl Acad Sci U S A. United States; 2011; 108: 19222–7.

163. Liu M, Huang C, Polu SR, Schneiter R, Chang A. Regulation of sphingolipid synthesis through Orm1 and Orm2 in yeast. J Cell Sci. England; 2012; 125: 2428–35.

164. Shimobayashi M, Oppliger W, Moes S, Jeno P, Hall MN. TORC1-regulated protein kinase Npr1 phosphorylates Orm to stimulate complex sphingolipid synthesis. Mol Biol Cell. United States; 2013; 24: 870–81.

165. Niles BJ, Mogri H, Hill A, Vlahakis A, Powers T. Plasma membrane recruitment and activation of the AGC kinase Ypk1 is mediated by target of rapamycin complex 2 (TORC2) and its effector proteins Slm1 and Slm2. Proc Natl Acad Sci U S A. United States; 2012; 109: 1536–41.

166. Sun Y, Miao Y, Yamane Y, Zhang C, Shokat KM, Takematsu H, Kozutsumi Y, Drubin DG. Orm protein phosphoregulation mediates transient sphingolipid biosynthesis response to heat stress via the Pkh-Ypk and Cdc55-PP2A pathways. Mol Biol Cell. 2012; 23: 2388–98.

167. Aronova S, Wedaman K, Aronov PA, Fontes K, Ramos K, Hammock BD, Powers T. Regulation of ceramide biosynthesis by TOR complex 2. Cell Metab. United States; 2008; 7: 148–58.

168. Muir A, Ramachandran S, Roelants FM, Timmons G, Thorner J. TORC2-dependent protein kinase Ypk1 phosphorylates ceramide synthase to stimulate synthesis of complex sphingolipids. Elife. England; 2014; 3.

169. Kobayashi SD, Nagiec MM. Ceramide/long-chain base phosphate rheostat in Saccharomyces cerevisiae: regulation of ceramide synthesis by Elo3p and Cka2p. Eukaryot Cell. United States; 2003; 2: 284–94.

170. Fresques T, Niles B, Aronova S, Mogri H, Rakhshandehroo T, Powers T. Regulation of ceramide synthase by casein kinase 2-dependent phosphorylation in Saccharomyces cerevisiae. J Biol Chem. United States; 2015; 290: 1395–403.

171. Voordeckers K, Kimpe M, Haesendonckx S, Louwet W, Versele M, Thevelein JM. Yeast 3-phosphoinositide-dependent protein kinase-1 (PDK1) orthologs Pkh1-3 differentially regulate phosphorylation of protein kinase A (PKA) and the protein kinase B (PKB)/S6K ortholog Sch9. J Biol Chem. 2011; 286: 22017–27.

172. Kohlwein SD. Triacylglycerol homeostasis: insights from yeast. J Biol Chem. United States; 2010; 285: 15663–7.

173. Koch B, Schmidt C, Daum G. Storage lipids of yeasts: a survey of nonpolar lipid metabolism in Saccharomyces cerevisiae, Pichia pastoris, and Yarrowia lipolytica. FEMS Microbiol Rev. England; 2014; 38: 892–915.

174. Kohlwein SD. Obese and anorexic yeasts: experimental models to understand the metabolic syndrome and lipotoxicity. Biochim Biophys Acta. Netherlands; 2010; 1801: 222–9.

175. Henry SA, Kohlwein SD, Carman GM. Metabolism and regulation of glycerolipids in the yeast Saccharomyces cerevisiae. Genetics. United States; 2012; 190: 317–49.

176. Klug L, Daum G. Yeast lipid metabolism at a glance. FEMS Yeast Res. England; 2014; 14: 369–88.

177. Athenstaedt K, Daum G. Biosynthesis of phosphatidic acid in lipid particles and endoplasmic reticulum of Saccharomyces cerevisiae. J Bacteriol. United States; 1997; 179: 7611–6.

178. Zheng Z, Zou J. The initial step of the glycerolipid pathway: identification of glycerol 3-phosphate/dihydroxyacetone phosphate dual substrate acyltransferases in Saccharomyces cerevisiae. J Biol Chem. United States; 2001; 276: 41710–6.

179. Stoops JK, Wakil SJ. The isolation of the two subunits of yeast fatty acid synthetase. Biochem Biophys Res Commun. United States; 1978; 84: 225–31.

180. Wieland F, Renner L, Verfurth C, Lynen F. Studies on the multi-enzyme complex of yeast fatty-acid synthetase. Reversible dissociation and isolation of two polypeptide chains. Eur J Biochem. England; 1979; 94: 189–97.

181. Mohamed AH, Chirala SS, Mody NH, Huang WY, Wakil SJ. Primary structure of the multifunctional alpha subunit protein of yeast fatty acid synthase derived from FAS2 gene sequence. J Biol Chem. United States; 1988; 263: 12315–25.

182. Hasslacher M, Ivessa AS, Paltauf F, Kohlwein SD. Acetyl-CoA carboxylase from yeast is an essential enzyme and is regulated by factors that control phospholipid metabolism. J Biol Chem. United States; 1993; 268: 10946–52.

183. Fichtlscherer F, Wellein C, Mittag M, Schweizer E. A novel function of yeast fatty acid synthase. Subunit alpha is capable of self-pantetheinylation. Eur J Biochem. England; 2000; 267: 2666–71.

184. Leibundgut M, Maier T, Jenni S, Ban N. The multienzyme architecture of eukaryotic fatty acid synthases. Curr Opin Struct Biol. England; 2008; 18: 714–25.

185. Athenstaedt K, Daum G. 1-Acyldihydroxyacetone-phosphate reductase (Ayr1p) of the yeast

Saccharomyces cerevisiae encoded by the open reading frame YIL124w is a major component of lipid particles. J Biol Chem. United States; 2000; 275: 235–40.

186. Benghezal M, Roubaty C, Veepuri V, Knudsen J, Conzelmann A. SLC1 and SLC4 encode partially redundant acyl-coenzyme A 1-acylglycerol-3-phosphate O-acyltransferases of budding yeast. J Biol Chem. United States; 2007; 282: 30845–55.

187. Chen Q, Kazachkov M, Zheng Z, Zou J. The yeast acylglycerol acyltransferase LCA1 is a key component of Lands cycle for phosphatidylcholine turnover. FEBS Lett. England; 2007; 581: 5511–6.

188. Jain S, Stanford N, Bhagwat N, Seiler B, Costanzo M, Boone C, Oelkers P. Identification of a novel lysophospholipid acyltransferase in Saccharomyces cerevisiae. J Biol Chem. United States; 2007; 282: 30562–9.

189. Riekhof WR, Wu J, Jones JL, Voelker DR. Identification and characterization of the major lysophosphatidylethanolamine acyltransferase in Saccharomyces cerevisiae. J Biol Chem. United States; 2007; 282: 28344–52.

190. Ayciriex S, Le Guédard M, Camougrand N, Velours G, Schoene M, Leone S, Wattelet-Boyer V, Dupuy J-W, Shevchenko A, Schmitter J-M, Lessire R, Bessoule J-J, Testet E. YPR139c/LOA1 encodes a novel lysophosphatidic acid acyltransferase associated with lipid droplets and involved in TAG homeostasis. Mol Biol Cell. 2012; 23: 233–46.

191. Shen H, Heacock PN, Clancey CJ, Dowhan W. The CDS1 gene encoding CDP-diacylglycerol synthase in Saccharomyces cerevisiae is essential for cell growth. J Biol Chem. United States; 1996; 271: 789–95.

192. Han G-S, Wu W-I, Carman GM. The Saccharomyces cerevisiae Lipin homolog is a Mg2+-dependent phosphatidate phosphatase enzyme. J Biol Chem. United States; 2006; 281: 9210–8.

193. Carman GM, Han G-S. Phosphatidic acid phosphatase, a key enzyme in the regulation of lipid synthesis. J Biol Chem. United States; 2009; 284: 2593–7.

194. Chae M, Han G-S, Carman GM. The Saccharomyces cerevisiae actin patch protein App1p is a phosphatidate phosphatase enzyme. J Biol Chem. United States; 2012; 287: 40186–96.

195. Oelkers P, Cromley D, Padamsee M, Billheimer JT, Sturley SL. The DGA1 gene determines a second triglyceride synthetic pathway in yeast. J Biol Chem. United States; 2002; 277: 8877–81.

196. Sorger D, Daum G. Synthesis of triacylglycerols by the acyl-coenzyme A:diacyl-glycerol acyltransferase Dga1p in lipid particles of the yeast Saccharomyces cerevisiae. J Bacteriol. United States; 2002; 184: 519–24.

197. Oelkers P, Tinkelenberg A, Erdeniz N, Cromley D, Billheimer JT, Sturley SL. A lecithin cholesterol acyltransferase-like gene mediates diacylglycerol esterification in yeast. J Biol Chem. United States; 2000; 275: 15609–12.

198. Athenstaedt K, Daum G. YMR313c/TGL3 encodes a novel triacylglycerol lipase located in lipid particles of Saccharomyces cerevisiae. J Biol Chem. United States; 2003; 278: 23317–

23.

199. Athenstaedt K, Daum G. Tgl4p and Tgl5p, two triacylglycerol lipases of the yeast Saccharomyces cerevisiae are localized to lipid particles. J Biol Chem. United States; 2005; 280: 37301–9.

200. Jandrositz A, Petschnigg J, Zimmermann R, Natter K, Scholze H, Hermetter A, Kohlwein SD, Leber R. The lipid droplet enzyme Tgl1p hydrolyzes both steryl esters and triglycerides in the yeast, Saccharomyces cerevisiae. Biochim Biophys Acta. 2005; 1735: 50–8.

201. Kurat CF, Natter K, Petschnigg J, Wolinski H, Scheuringer K, Scholz H, Zimmermann R, Leber R, Zechner R, Kohlwein SD. Obese yeast: triglyceride lipolysis is functionally conserved from mammals to yeast. J Biol Chem. United States; 2006; 281: 491–500.

202. Ploier B, Scharwey M, Koch B, Schmidt C, Schatte J, Rechberger G, Kollroser M, Hermetter A, Daum G. Screening for hydrolytic enzymes reveals Ayr1p as a novel triacylglycerol lipase in Saccharomyces cerevisiae. J Biol Chem. United States; 2013; 288: 36061–72.

203. Heier C, Taschler U, Rengachari S, Oberer M, Wolinski H, Natter K, Kohlwein SD, Leber R, Zimmermann R. Identification of Yju3p as functional orthologue of mammalian monoglyceride lipase in the yeast Saccharomycescerevisiae. Biochim Biophys Acta. 2010; 1801: 1063–71.

204. Huh W-K, Falvo J V, Gerke LC, Carroll AS, Howson RW, Weissman JS, O'Shea EK. Global analysis of protein localization in budding yeast. Nature. England; 2003; 425: 686–91.

205. Natter K, Leitner P, Faschinger A, Wolinski H, McCraith S, Fields S, Kohlwein SD. The spatial organization of lipid synthesis in the yeast Saccharomyces cerevisiae derived from large scale green fluorescent protein tagging and high resolution microscopy. Mol Cell Proteomics. 2005; 4: 662–72.

206. Black PN, DiRusso CC. Yeast acyl-CoA synthetases at the crossroads of fatty acid metabolism and regulation. Biochim Biophys Acta. Netherlands; 2007; 1771: 286–98.

207. Binns D, Januszewski T, Chen Y, Hill J, Markin VS, Zhao Y, Gilpin C, Chapman KD, Anderson RGW, Goodman JM. An intimate collaboration between peroxisomes and lipid bodies. J Cell Biol. United States; 2006; 173: 719–31.

208. Titorenko VI, Terlecky SR. Peroxisome metabolism and cellular aging. Traffic. England; 2011; 12: 252–9.

209. Beach A, Burstein MT, Richard VR, Leonov A, Levy S, Titorenko VI. Integration of peroxisomes into an endomembrane system that governs cellular aging. Front Physiol. Switzerland; 2012; 3: 283.

210. Leonov A, Titorenko VI. A network of interorganellar communications underlies cellular aging. IUBMB Life. England; 2013; 65: 665–74.

211. Gao Q, Goodman JM. The lipid droplet-a well-connected organelle. Front cell Dev Biol. Switzerland; 2015; 3: 49.

212. Hashemi HF, Goodman JM. The life cycle of lipid droplets. Curr Opin Cell Biol. England; 2015; 33: 119–24.

213. Dakik P, Titorenko VI. Communications between Mitochondria, the Nucleus, Vacuoles, Peroxisomes, the Endoplasmic Reticulum, the Plasma Membrane, Lipid Droplets, and the Cytosol during Yeast Chronological Aging. Front Genet. Switzerland; 2016; 7: 177.

214. Kurat CF, Wolinski H, Petschnigg J, Kaluarachchi S, Andrews B, Natter K, Kohlwein SD. Cdk1/Cdc28-dependent activation of the major triacylglycerol lipase Tgl4 in yeast links lipolysis to cell-cycle progression. Mol Cell. United States; 2009; 33: 53–63.

215. Chauhan N, Visram M, Cristobal-Sarramian A, Sarkleti F, Kohlwein SD. Morphogenesis checkpoint kinase Swe1 is the executor of lipolysis- dependent cell-cycle progression. Proc Natl Acad Sci U S A. United States; 2015; 112: E1077-85.

216. Yang P-L, Hsu T-H, Wang C-W, Chen R-H. Lipid droplets maintain lipid homeostasis during anaphase for efficient cell separation in budding yeast. Mol Biol Cell. United States; 2016; 27: 2368–80.

217. Barbosa AD, Siniossoglou S. Function of lipid droplet-organelle interactions in lipid homeostasis. Biochim Biophys acta Mol cell Res. Netherlands; 2017; 1864: 1459–68.

218. van Zutphen T, Todde V, de Boer R, Kreim M, Hofbauer HF, Wolinski H, Veenhuis M, van der Klei IJ, Kohlwein SD. Lipid droplet autophagy in the yeast Saccharomyces cerevisiae. Mol Biol Cell. United States; 2014; 25: 290–301.

219. Barbosa AD, Savage DB, Siniossoglou S. Lipid droplet-organelle interactions: emerging roles in lipid metabolism. Curr Opin Cell Biol. England; 2015; 35: 91–7.

220. Shpilka T, Welter E, Borovsky N, Amar N, Mari M, Reggiori F, Elazar Z. Lipid droplets and their component triglycerides and steryl esters regulate autophagosome biogenesis. EMBO J. England; 2015; 34: 2117–31.

221. Vevea JD, Garcia EJ, Chan RB, Zhou B, Schultz M, Di Paolo G, McCaffery JM, Pon LA. Role for Lipid Droplet Biogenesis and Microlipophagy in Adaptation to Lipid Imbalance in Yeast. Dev Cell. United States; 2015; 35: 584–99.

222. Eisenberg-Bord M, Shai N, Schuldiner M, Bohnert M. A Tether Is a Tether Is a Tether: Tethering at Membrane Contact Sites. Dev Cell. United States; 2016; 39: 395–409.

223. Wong LH, Levine TP. Lipid transfer proteins do their thing anchored at membrane contact sites... but what is their thing? Biochem Soc Trans. England; 2016; 44: 517–27.

224. Dimmer KS, Rapaport D. Mitochondrial contact sites as platforms for phospholipid exchange. Biochim Biophys acta Mol cell Biol lipids. Netherlands; 2017; 1862: 69–80.

225. Schuldiner M, Bohnert M. A different kind of love - lipid droplet contact sites. Biochim Biophys acta Mol cell Biol lipids. Netherlands; 2017; 1862: 1188–96.

226. Santos-Rosa H, Leung J, Grimsey N, Peak-Chew S, Siniossoglou S. The yeast lipin Smp2 couples phospholipid biosynthesis to nuclear membrane growth. EMBO J. England; 2005; 24: 1931–41.

227. Choi H-S, Su W-M, Morgan JM, Han G-S, Xu Z, Karanasios E, Siniossoglou S, Carman GM. Phosphorylation of phosphatidate phosphatase regulates its membrane association and physiological functions in Saccharomyces cerevisiae: identification of SER(602), THR(723), AND SER(744) as the sites phosphorylated by CDC28 (CDK1)-encoded cyclin-dependen. J Biol Chem. 2011; 286: 1486–98.

228. Choi H-S, Su W-M, Han G-S, Plote D, Xu Z, Carman GM. Pho85p-Pho80p phosphorylation of yeast Pah1p phosphatidate phosphatase regulates its activity, location, abundance, and function in lipid metabolism. J Biol Chem. United States; 2012; 287: 11290–301.

229. Pascual F, Carman GM. Phosphatidate phosphatase, a key regulator of lipid homeostasis. Biochim Biophys Acta. Netherlands; 2013; 1831: 514–22.

230. Shirra MK, Patton-Vogt J, Ulrich A, Liuta-Tehlivets O, Kohlwein SD, Henry SA, Arndt KM. Inhibition of acetyl coenzyme A carboxylase activity restores expression of the INO1 gene in a snf1 mutant strain of Saccharomyces cerevisiae. Mol Cell Biol. 2001; 21: 5710–22.

231. Su W-M, Han G-S, Casciano J, Carman GM. Protein kinase A-mediated phosphorylation of Pah1p phosphatidate phosphatase functions in conjunction with the Pho85p-Pho80p and Cdc28p-cyclin B kinases to regulate lipid synthesis in yeast. J Biol Chem. 2012; 287: 33364–76.

232. Xu Z, Su W-M, Carman GM. Fluorescence spectroscopy measures yeast PAH1-encoded phosphatidate phosphatase interaction with liposome membranes. J Lipid Res. United States; 2012; 53: 522–8.

233. Madeira JB, Masuda CA, Maya-Monteiro CM, Matos GS, Montero-Lomeli M, Bozaquel-Morais BL. TORC1 inhibition induces lipid droplet replenishment in yeast. Mol Cell Biol. United States; 2015; 35: 737–46.

234. Handee W, Li X, Hall KW, Deng X, Li P, Benning C, Williams BL, Kuo M-H. An Energy-Independent Pro-longevity Function of Triacylglycerol in Yeast. PLoS Genet. United States; 2016; 12: e1005878.

235. Li X, Handee W, Kuo M-H. The slim, the fat, and the obese: guess who lives the longest? Curr Genet. United States; 2017; 63: 43–9.

236. Sinclair DA. Toward a unified theory of caloric restriction and longevity regulation. Mech Ageing Dev. Ireland; 2005; 126: 987–1002.

237. Goldberg AA, Bourque SD, Kyryakov P, Gregg C, Boukh-Viner T, Beach A, Burstein MT, Machkalyan G, Richard V, Rampersad S, Cyr D, Milijevic S, Titorenko VI. Effect of calorie restriction on the metabolic history of chronologically aging yeast. Exp Gerontol. 2009; 44: 555–71.

238. Colman RJ, Anderson RM, Johnson SC, Kastman EK, Kosmatka KJ, Beasley TM, Allison DB, Cruzen C, Simmons HA, Kemnitz JW, Weindruch R. Caloric restriction delays disease onset and mortality in rhesus monkeys. Science. United States; 2009; 325: 201–4.

239. Colman RJ, Beasley TM, Kemnitz JW, Johnson SC, Weindruch R, Anderson RM. Caloric restriction reduces age-related and all-cause mortality in rhesus monkeys. Nat Commun.

England; 2014; 5: 3557.

240. Lee C, Longo V. Dietary restriction with and without caloric restriction for healthy aging. F1000Research. England; 2016; 5.

241. Fabrizio P, Gattazzo C, Battistella L, Wei M, Cheng C, McGrew K, Longo VD. Sir2 blocks extreme life-span extension. Cell. United States; 2005; 123: 655–67.

242. Hiltunen JK, Mursula AM, Rottensteiner H, Wierenga RK, Kastaniotis AJ, Gurvitz A. The biochemistry of peroxisomal beta-oxidation in the yeast Saccharomyces cerevisiae. FEMS Microbiol Rev. England; 2003; 27: 35–64.

243. van der Klei IJ, Yurimoto H, Sakai Y, Veenhuis M. The significance of peroxisomes in methanol metabolism in methylotrophic yeast. Biochim Biophys Acta. Netherlands; 2006; 1763: 1453–62.

244. Beach A, Titorenko VI. In search of housekeeping pathways that regulate longevity. Cell cycle (Georgetown, Tex.). United States; 2011. p. 3042–4.

245. Beach A, Titorenko VI. Essential roles of peroxisomally produced and metabolized biomolecules in regulating yeast longevity. Subcell Biochem. United States; 2013; 69: 153–67.

246. Sheibani S, Richard VR, Beach A, Leonov A, Feldman R, Mattie S, Khelghatybana L, Piano A, Greenwood M, Vali H, Titorenko VI. Macromitophagy, neutral lipids synthesis, and peroxisomal fatty acid oxidation protect yeast from “liponecrosis”, a previously unknown form of programmed cell death. Cell Cycle. 2014; 13: 138–47.

247. Lefebvre P, Cariou B, Lien F, Kuipers F, Staels B. Role of bile acids and bile acid receptors in metabolic regulation. Physiol Rev. United States; 2009; 89: 147–91.

248. Goldberg AA, Kyryakov P, Bourque SD, Titorenko VI. Xenohormetic, hormetic and cytostatic selective forces driving longevity at the ecosystemic level. Aging (Albany NY). United States; 2010; 2: 461–70.

249. Gomez-Perez A, Kyryakov P, Burstein MT, Asbah N, Noohi F, Iouk T, Titorenko VI. Empirical Validation of a Hypothesis of the Hormetic Selective Forces Driving the Evolution of Longevity Regulation Mechanisms. Front Genet. Switzerland; 2016; 7: 216.

250. Kyryakov P, Gomez-Perez A, Glebov A, Asbah N, Bruno L, Meunier C, Iouk T, Titorenko VI. Empirical verification of evolutionary theories of aging. Aging (Albany NY). United States; 2016; 8: 2568–89.

251. Beach A, Richard VR, Leonov A, Burstein MT, Bourque SD, Koupaki O, Juneau M, Feldman R, Iouk T, Titorenko VI. Mitochondrial membrane lipidome defines yeast longevity. Aging (Albany NY). United States; 2013; 5: 551–74.

252. Burstein MT, Kyryakov P, Beach A, Richard VR, Koupaki O, Gomez-Perez A, Leonov A, Levy S, Noohi F, Titorenko VI. Lithocholic acid extends longevity of chronologically aging yeast only if added at certain critical periods of their lifespan. Cell Cycle. 2012; 11: 3443–62.

253. Beach A, Richard VR, Bourque S, Boukh-Viner T, Kyryakov P, Gomez-Perez A, Arlia-Ciommo A, Feldman R, Leonov A, Piano A, Svistkova V, Titorenko VI. Lithocholic bile acid accumulated in yeast mitochondria orchestrates a development of an anti-aging cellular pattern by causing age-related changes in cellular proteome. Cell Cycle. 2015; 14: 1643–56.

254. Vögtle F-N, Keller M, Taskin AA, Horvath SE, Guan XL, Prinz C, Opalińska M, Zorzin C, van der Laan M, Wenk MR, Schubert R, Wiedemann N, Holzer M, et al. The fusogenic lipid phosphatidic acid promotes the biogenesis of mitochondrial outer membrane protein Ugo1. J Cell Biol. 2015; 210: 951–60.

255. Burstein MT, Titorenko VI. A mitochondrially targeted compound delays aging in yeast through a mechanism linking mitochondrial membrane lipid metabolism to mitochondrial redox biology. Redox Biol. Netherlands; 2014; 2: 305–7.

256. Medkour Y, Titorenko VI. Mitochondria operate as signaling platforms in yeast aging. Aging (Albany NY). United States; 2016; 8: 212–3.

257. Medkour Y, Dakik P, McAuley M, Mohammad K, Mitrofanova D, Titorenko VI. Mechanisms Underlying the Essential Role of Mitochondrial Membrane Lipids in Yeast Chronological Aging. Oxid Med Cell Longev. United States; 2017; 2017: 1–15.

258. Jarsch IK, Daste F, Gallop JL. Membrane curvature in cell biology: An integration of molecular mechanisms. J Cell Biol. United States; 2016; 214: 375–87.

259. Tatsuta T, Langer T. Intramitochondrial phospholipid trafficking. Biochim Biophys acta Mol cell Biol lipids. Netherlands; 2017; 1862: 81–9.

260. McMahon HT, Boucrot E. Membrane curvature at a glance. J Cell Sci. England; 2015; 128: 1065–70.

261. Galluzzi L, Vitale I, Abrams JM, Alnemri ES, Baehrecke EH, Blagosklonny M V, Dawson TM, Dawson VL, El-Deiry WS, Fulda S, Gottlieb E, Green DR, Hengartner MO, et al. Molecular definitions of cell death subroutines: recommendations of the Nomenclature Committee on Cell Death 2012. Cell Death Differ. 2012; 19: 107–20.

262. Fuchs Y, Steller H. Live to die another way: modes of programmed cell death and the signals emanating from dying cells. Nat Rev Mol Cell Biol. England; 2015; 16: 329–44.

263. Galluzzi L, Bravo-San Pedro JM, Kepp O, Kroemer G. Regulated cell death and adaptive stress responses. Cell Mol Life Sci. Switzerland; 2016; 73: 2405–10.

264. Ke B, Tian M, Li J, Liu B, He G. Targeting Programmed Cell Death Using Small-Molecule Compounds to Improve Potential Cancer Therapy. Med Res Rev. United States; 2016; 36: 983–1035.

265. Wallach D, Kang T-B, Dillon CP, Green DR. Programmed necrosis in inflammation: Toward identification of the effector molecules. Science. United States; 2016; 352: aaf2154.

266. Shi J, Gao W, Shao F. Pyroptosis: Gasdermin-Mediated Programmed Necrotic Cell Death. Trends Biochem Sci. England; 2017; 42: 245–54.

267. Green DR, Victor B. The pantheon of the fallen: why are there so many forms of cell death? Trends Cell Biol. England; 2012; 22: 555–6.

268. Stratford M, Anslow PA. Comparison of the inhibitory action on Saccharomyces cerevisiae of weak- acid preservatives, uncouplers, and medium-chain fatty acids. FEMS Microbiol Lett. England; 1996; 142: 53–8.

269. Mitsui K, Nakagawa D, Nakamura M, Okamoto T, Tsurugi K. Valproic acid induces apoptosis dependent of Yca1p at concentrations that mildly affect the proliferation of yeast. FEBS Lett. England; 2005; 579: 723–7.

270. Sun Q, Bi L, Su X, Tsurugi K, Mitsui K. Valproate induces apoptosis by inducing accumulation of neutral lipids which was prevented by disruption of the SIR2 gene in Saccharomyces cerevisiae. FEBS Lett. England; 2007; 581: 3991–5.

271. Garbarino J, Padamsee M, Wilcox L, Oelkers PM, D'Ambrosio D, Ruggles K V, Ramsey N, Jabado O, Turkish A, Sturley SL. Sterol and diacylglycerol acyltransferase deficiency triggers fatty acid- mediated cell death. J Biol Chem. United States; 2009; 284: 30994–1005.

272. Petschnigg J, Wolinski H, Kolb D, Zellnig G, Kurat CF, Natter K, Kohlwein SD. Good fat, essential cellular requirements for triacylglycerol synthesis to maintain membrane homeostasis in yeast. J Biol Chem. United States; 2009; 284: 30981–93.

273. Rockenfeller P, Ring J, Muschett V, Beranek A, Buettner S, Carmona-Gutierrez D, Eisenberg T, Khoury C, Rechberger G, Kohlwein SD, Kroemer G, Madeo F. Fatty acids trigger mitochondrion-dependent necrosis. Cell Cycle. United States; 2010; 9: 2836–42.

274. Carmona-Gutierrez D, Reisenbichler A, Heimbucher P, Bauer MA, Braun RJ, Ruckenstuhl C, Büttner S, Eisenberg T, Rockenfeller P, Fröhlich K-U, Kroemer G, Madeo F. Ceramide triggers metacaspase-independent mitochondrial cell death in yeast. Cell Cycle. 2011; 10: 3973–8.

275. Fakas S, Qiu Y, Dixon JL, Han G-S, Ruggles K V, Garbarino J, Sturley SL, Carman GM. Phosphatidate phosphatase activity plays key role in protection against fatty acid-induced toxicity in yeast. J Biol Chem. United States; 2011; 286: 29074–85.

276. Galluzzi L, Vitale I, Senovilla L, Eisenberg T, Carmona-Gutierrez D, Vacchelli E, Robert T, Ripoche H, Jägemann N, Paccard C, Servant N, Hupé P, Lazar V, et al. Independent transcriptional reprogramming and apoptosis induction by cisplatin. Cell Cycle. 2012; 11: 3472–80.

277. Kitagaki H, Cowart LA, Matmati N, Vaena de Avalos S, Novgorodov SA, Zeidan YH, Bielawski J, Obeid LM, Hannun YA. Isc1 regulates sphingolipid metabolism in yeast mitochondria. Biochim Biophys Acta. Netherlands; 2007; 1768: 2849–61.

278. Aerts AM, Zabrocki P, François IEJA, Carmona-Gutierrez D, Govaert G, Mao C, Smets B, Madeo F, Winderickx J, Cammue BPA, Thevissen K. Ydc1p ceramidase triggers organelle fragmentation, apoptosis and accelerated ageing in yeast. Cell Mol Life Sci. 2008; 65: 1933–42.

279. Bener Aksam E, Jungwirth H, Kohlwein SD, Ring J, Madeo F, Veenhuis M, van der Klei

IJ. Absence of the peroxiredoxin Pmp20 causes peroxisomal protein leakage and necrotic cell death. Free Radic Biol Med. United States; 2008; 45: 1115–24.

280. Jungwirth H, Ring J, Mayer T, Schauer A, Buttner S, Eisenberg T, Carmona-Gutierrez D, Kuchler K, Madeo F. Loss of peroxisome function triggers necrosis. FEBS Lett. England; 2008; 582: 2882–6.

281. Tulha J, Faria-Oliveira F, Lucas C, Ferreira C. Programmed cell death in Saccharomyces cerevisiae is hampered by the deletion of GUP1 gene. BMC Microbiol. England; 2012; 12: 80.

282. Zaremberg V, Gajate C, Cacharro LM, Mollinedo F, McMaster CR. Cytotoxicity of an anti-cancer lysophospholipid through selective modification of lipid raft composition. J Biol Chem. United States; 2005; 280: 38047–58.

283. Zhang H, Gajate C, Yu L-P, Fang Y-X, Mollinedo F. Mitochondrial-derived ROS in edelfosine-induced apoptosis in yeasts and tumor cells. Acta Pharmacol Sin. United States; 2007; 28: 888–94.

284. Cerantola V, Guillas I, Roubaty C, Vionnet C, Uldry D, Knudsen J, Conzelmann A. Aureobasidin A arrests growth of yeast cells through both ceramide intoxication and deprivation of essential inositolphosphorylceramides. Mol Microbiol. England; 2009; 71: 1523–37.

285. Kajiwara K, Muneoka T, Watanabe Y, Karashima T, Kitagaki H, Funato K. Perturbation of sphingolipid metabolism induces endoplasmic reticulum stress-mediated mitochondrial apoptosis in budding yeast. Mol Microbiol. England; 2012; 86: 1246–61.

286. Czyz O, Bitew T, Cuesta-Marbán A, McMaster CR, Mollinedo F, Zaremberg V. Alteration of plasma membrane organization by an anticancer lysophosphatidylcholine analogue induces intracellular acidification and internalization of plasma membrane transporters in yeast. J Biol Chem. 2013; 288: 8419–32.

287. Rego A, Trindade D, Chaves SR, Manon S, Costa V, Sousa MJ, Corte-Real M. The yeast model system as a tool towards the understanding of apoptosis regulation by sphingolipids. FEMS Yeast Res. England; 2014; 14: 160–78.

288. Ruggles K V, Garbarino J, Liu Y, Moon J, Schneider K, Henneberry A, Billheimer J, Millar JS, Marchadier D, Valasek MA, Joblin-Mills A, Gulati S, Munkacsi AB, et al. A functional, genome-wide evaluation of liposensitive yeast identifies the “ARE2 required for viability” (ARV1) gene product as a major component of eukaryotic fatty acid resistance. J Biol Chem. 2014; 289: 4417–31.

289. Valachovic M, Garaiova M, Holic R, Hapala I. Squalene is lipotoxic to yeast cells defective in lipid droplet biogenesis. Biochem Biophys Res Commun. United States; 2016; 469: 1123–8.

290. Kohlwein SD, Petschnigg J. SLipid-induced cell dysfunction and cell death: lessons from yeast. Curr Hypertens Rep. United States; 2007; 9: 455–61.

291. Rockenfeller P, Madeo F. Ageing and eating. Biochim Biophys Acta. Netherlands; 2010; 1803: 499–506.

292. Kohlwein SD, Veenhuis M, van der Klei IJ. Lipid droplets and peroxisomes: key players in cellular lipid homeostasis or a matter of fat--store 'em up or burn 'em down. Genetics. United States; 2013; 193: 1–50.

293. Natter K, Kohlwein SD. Yeast and cancer cells - common principles in lipid metabolism. Biochim Biophys Acta. Netherlands; 2013; 1831: 314–26.

294. Kopelman PG. Obesity as a medical problem. Nature. England; 2000; 404: 635–43.

295. Unger RH. Lipotoxic diseases. Annu Rev Med. United States; 2002; 53: 319–36.

296. Schaffer JE. Lipotoxicity: when tissues overeat. Curr Opin Lipidol. England; 2003; 14: 281–7.

297. Unger RH. Longevity, lipotoxicity and leptin: the adipocyte defense against feasting and famine. Biochimie. France; 2005; 87: 57–64.

298. Brookheart RT, Michel CI, Schaffer JE. As a matter of fat. Cell Metab. United States; 2009; 10: 9–12.

299. Garbarino J, Sturley SL. Saturated with fat: new perspectives on lipotoxicity. Curr Opin Clin Nutr Metab Care. England; 2009; 12: 110–6.

300. Kusminski CM, Shetty S, Orci L, Unger RH, Scherer PE. Diabetes and apoptosis: lipotoxicity. Apoptosis. Netherlands; 2009; 14: 1484–95.

301. Lopez S, Bermudez B, Abia R, Muriana FJG. The influence of major dietary fatty acids on insulin secretion and action. Curr Opin Lipidol. England; 2010; 21: 15–20.

302. Unger RH, Scherer PE. Gluttony, sloth and the metabolic syndrome: a roadmap to lipotoxicity. Trends Endocrinol Metab. United States; 2010; 21: 345–52.

303. Currie E, Schulze A, Zechner R, Walther TC, Farese RVJ. Cellular fatty acid metabolism and cancer. Cell Metab. United States; 2013; 18: 153–61.

304. Galluzzi L, Kepp O, Vander Heiden MG, Kroemer G. Metabolic targets for cancer therapy. Nature reviews. Drug discovery. England; 2013. p. 829–46.

305. Zadra G, Photopoulos C, Loda M. The fat side of prostate cancer. Biochim Biophys Acta. Netherlands; 2013; 1831: 1518–32.

306. Park J, Morley TS, Kim M, Clegg DJ, Scherer PE. Obesity and cancer--mechanisms underlying tumour progression and recurrence. Nat Rev Endocrinol. England; 2014; 10: 455–65.

307. Piano A, Titorenko VI. The Intricate Interplay between Mechanisms Underlying Aging and Cancer. Aging Dis. United States; 2015; 6: 56–75.

308. Carrasco S, Meyer T. STIM proteins and the endoplasmic reticulum-plasma membrane junctions. Annu Rev Biochem. United States; 2011; 80: 973–1000.

309. Friedman JR, Voeltz GK. The ER in 3D: a multifunctional dynamic membrane network. Trends Cell Biol. England; 2011; 21: 709–17.

310. Rowland AA, Voeltz GK. Endoplasmic reticulum-mitochondria contacts: function of the junction. Nat Rev Mol Cell Biol. 2012; 13: 607–25.

311. Tavassoli S, Chao JT, Young BP, Cox RC, Prinz WA, de Kroon AIPM, Loewen CJR. Plasma membrane--endoplasmic reticulum contact sites regulate phosphatidylcholine synthesis. EMBO Rep. England; 2013; 14: 434–40.

312. Horvath SE, Daum G. Lipids of mitochondria. Prog Lipid Res. England; 2013; 52: 590–614.

313. Aaltonen MJ, Friedman JR, Osman C, Salin B, di Rago J-P, Nunnari J, Langer T, Tatsuta T. MICOS and phospholipid transfer by Ups2-Mdm35 organize membrane lipid synthesis in mitochondria. J Cell Biol. United States; 2016; 213: 525–34.

314. Miyata N, Watanabe Y, Tamura Y, Endo T, Kuge O. Phosphatidylserine transport by Ups2-Mdm35 in respiration-active mitochondria. J Cell Biol. United States; 2016; 214: 77–88.

315. Connerth M, Tatsuta T, Haag M, Klecker T, Westermann B, Langer T. Intramitochondrial transport of phosphatidic acid in yeast by a lipid transfer protein. Science. United States; 2012; 338: 815–8.

316. Baile MG, Lu Y-W, Claypool SM. The topology and regulation of cardiolipin biosynthesis and remodeling in yeast. Chem Phys Lipids. Ireland; 2014; 179: 25–31.

317. Babst M, Katzmann DJ, Estepa-Sabal EJ, Meerloo T, Emr SD. Escrt-III: an endosome-associated heterooligomeric protein complex required for mvb sorting. Dev Cell. United States; 2002; 3: 271–82.

318. Lamb TM, Mitchell AP. The transcription factor Rim101p governs ion tolerance and cell differentiation by direct repression of the regulatory genes NRG1 and SMP1 in Saccharomyces cerevisiae. Mol Cell Biol. United States; 2003; 23: 677–86.

319. Xu W, Smith FJJ, Subaran R, Mitchell AP. Multivesicular body-ESCRT components function in pH response regulation in Saccharomyces cerevisiae and Candida albicans. Mol Biol Cell. United States; 2004; 15: 5528–37.

320. Barwell KJ, Boysen JH, Xu W, Mitchell AP. Relationship of DFG16 to the Rim101p pH response pathway in Saccharomyces cerevisiae and Candida albicans. Eukaryot Cell. United States; 2005; 4: 890–9.

321. Hayashi M, Fukuzawa T, Sorimachi H, Maeda T. Constitutive activation of the pH-responsive Rim101 pathway in yeast mutants defective in late steps of the MVB/ESCRT pathway. Mol Cell Biol. United States; 2005; 25: 9478–90.

322. Weiss P, Huppert S, Kolling R. Analysis of the dual function of the ESCRT-III protein Snf7 in endocytic trafficking and in gene expression. Biochem J. England; 2009; 424: 89–97.

323. Shukla AK, Xiao K, Lefkowitz RJ. Emerging paradigms of beta-arrestin-dependent seven transmembrane receptor signaling. Trends Biochem Sci. England; 2011; 36: 457–69.

324. Maeda T. The signaling mechanism of ambient pH sensing and adaptation in yeast and fungi. FEBS J. England; 2012; 279: 1407–13.

325. Obara K, Yamamoto H, Kihara A. Membrane protein Rim21 plays a central role in sensing ambient pH in Saccharomyces cerevisiae. J Biol Chem. United States; 2012; 287: 38473–81.

326. Kato U, Emoto K, Fredriksson C, Nakamura H, Ohta A, Kobayashi T, Murakami-Murofushi K, Kobayashi T, Umeda M. A novel membrane protein, Ros3p, is required for phospholipid translocation across the plasma membrane in Saccharomyces cerevisiae. J Biol Chem. 2002; 277: 37855–62.

327. Kihara A, Igarashi Y. Identification and characterization of a Saccharomyces cerevisiae gene, RSB1, involved in sphingoid long-chain base release. J Biol Chem. United States; 2002; 277: 30048–54.

328. Kihara A, Igarashi Y. Cross talk between sphingolipids and glycerophospholipids in the establishment of plasma membrane asymmetry. Mol Biol Cell. United States; 2004; 15: 4949–59.

329. Ikeda M, Kihara A, Denpoh A, Igarashi Y. The Rim101 pathway is involved in Rsb1 expression induced by altered lipid asymmetry. Mol Biol Cell. United States; 2008; 19: 1922–31.

330. Reggiori F, Klionsky DJ. Autophagic processes in yeast: mechanism, machinery and regulation. Genetics. United States; 2013; 194: 341–61.

331. Feng Y, He D, Yao Z, Klionsky DJ. The machinery of macroautophagy. Cell Res. England; 2014; 24: 24–41.

332. Klionsky DJ, Abdelmohsen K, Abe A, Abedin MJ, Abeliovich H, Acevedo Arozena A, Adachi H, Adams CM, Adams PD, Adeli K, Adhihetty PJ, Adler SG, Agam G, et al. Guidelines for the use and interpretation of assays for monitoring autophagy (3rd edition). Autophagy. United States; 2016; 12: 1–222.

333. Carmona-Gutierrez D, Eisenberg T, Buttner S, Meisinger C, Kroemer G, Madeo F. Apoptosis in yeast: triggers, pathways, subroutines. Cell Death Differ. England; 2010; 17: 763–73.

334. Madeo F, Carmona-Gutierrez D, Ring J, Buttner S, Eisenberg T, Kroemer G. Caspase-dependent and caspase-independent cell death pathways in yeast. Biochem Biophys Res Commun. United States; 2009; 382: 227–31.

335. Bialik S, Zalckvar E, Ber Y, Rubinstein AD, Kimchi A. Systems biology analysis of programmed cell death. Trends Biochem Sci. England; 2010; 35: 556–64.

336. Madeo F, Herker E, Maldener C, Wissing S, Lachelt S, Herlan M, Fehr M, Lauber K, Sigrist SJ, Wesselborg S, Frohlich KU. A caspase-related protease regulates apoptosis in yeast. Mol Cell. United States; 2002; 9: 911–7.

337. Fahrenkrog B, Sauder U, Aebi U. The S. cerevisiae HtrA-like protein Nma111p is a nuclear serine protease that mediates yeast apoptosis. J Cell Sci. England; 2004; 117: 115–26.

338. Zalckvar E, Bialik S, Kimchi A. The road not taken: a systems level strategy for analyzing the cell death network. Autophagy. United States; 2010; 6: 813–5.

339. Khan MAS, Chock PB, Stadtman ER. Knockout of caspase-like gene, YCA1, abrogates apoptosis and elevates oxidized proteins in Saccharomyces cerevisiae. Proc Natl Acad Sci U S A. United States; 2005; 102: 17326–31.

340. Lee REC, Brunette S, Puente LG, Megeney LA. Metacaspase Yca1 is required for clearance of insoluble protein aggregates. Proc Natl Acad Sci U S A. United States; 2010; 107: 13348–53.

341. Lefevre S, Sliwa D, Auchere F, Brossas C, Ruckenstuhl C, Boggetto N, Lesuisse E, Madeo F, Camadro J-M, Santos R. The yeast metacaspase is implicated in oxidative stress response in frataxin-deficient cells. FEBS Lett. England; 2012; 586: 143–8.

342. Shrestha A, Puente LG, Brunette S, Megeney LA. The role of Yca1 in proteostasis. Yca1 regulates the composition of the insoluble proteome. J Proteomics. Netherlands; 2013; 81: 24–30.

343. Hill SM, Hao X, Liu B, Nystrom T. Life-span extension by a metacaspase in the yeast Saccharomyces cerevisiae. Science. United States; 2014; 344: 1389–92.

344. Hill SM, Nystrom T. The dual role of a yeast metacaspase: What doesn't kill you makes you stronger. Bioessays. United States; 2015; 37: 525–31.

345. Longo V, Zdralevic M, Guaragnella N, Giannattasio S, Zolla L, Timperio AM. Proteome and metabolome profiling of wild-type and YCA1-knock-out yeast cells during acetic acid-induced programmed cell death. J Proteomics. Netherlands; 2015; 128: 173–88.

346. Ždralević M, Longo V, Guaragnella N, Giannattasio S, Timperio AM, Zolla L. Differential proteome-metabolome profiling of YCA1-knock-out and wild type cells reveals novel metabolic pathways and cellular processes dependent on the yeast metacaspase. Mol Biosyst. 2015; 11: 1573–83.

347. Walter D, Wissing S, Madeo F, Fahrenkrog B. The inhibitor-of-apoptosis protein Bir1p protects against apoptosis in S. cerevisiae and is a substrate for the yeast homologue of Omi/HtrA2. J Cell Sci. England; 2006; 119: 1843–51.

348. Wilkinson D, Ramsdale M. Proteases and caspase-like activity in the yeast Saccharomyces cerevisiae. Biochem Soc Trans. England; 2011; 39: 1502–8.

349. Falcone C, Mazzoni C. External and internal triggers of cell death in yeast. Cell Mol Life Sci. Switzerland; 2016; 73: 2237–50.

350. Kourtis N, Tavernarakis N. Autophagy and cell death in model organisms. Cell Death Differ. England; 2009; 16: 21–30.

351. Shen H-M, Codogno P. Autophagic cell death: Loch Ness monster or endangered species? Autophagy. United States; 2011; 7: 457–65.

352. Denton D, Nicolson S, Kumar S. Cell death by autophagy: facts and apparent artefacts. Cell Death Differ. England; 2012; 19: 87–95.

353. Eisenberg T, Carmona-Gutierrez D, Buttner S, Tavernarakis N, Madeo F. Necrosis in yeast. Apoptosis. Netherlands; 2010; 15: 257–68.

354. Vandenabeele P, Galluzzi L, Vanden Berghe T, Kroemer G. Molecular mechanisms of necroptosis: an ordered cellular explosion. Nat Rev Mol Cell Biol. England; 2010; 11: 700–14.

355. Zalckvar E, Yosef N, Reef S, Ber Y, Rubinstein AD, Mor I, Sharan R, Ruppin E, Kimchi A. A systems level strategy for analyzing the cell death network: implication in exploring the apoptosis/autophagy connection. Cell Death Differ. England; 2010; 17: 1244–53.

356. Rubinstein AD, Kimchi A. Life in the balance - a mechanistic view of the crosstalk between autophagy and apoptosis. J Cell Sci. England; 2012; 125: 5259–68.

357. Madeo F, Frohlich E, Frohlich KU. A yeast mutant showing diagnostic markers of early and late apoptosis. J Cell Biol. United States; 1997; 139: 729–34.

358. Zhao Y, Gilliat AF, Ziehm M, Turmaine M, Wang H, Ezcurra M, Yang C, Phillips G, McBay D, Zhang WB, Partridge L, Pincus Z, Gems D. Two forms of death in ageing Caenorhabditis elegans. Nat Commun. England; 2017; 8: 15458.

359. Abudugupur A, Mitsui K, Yokota S, Tsurugi K. An ARL1 mutation affected autophagic cell death in yeast, causing a defect in central vacuole formation. Cell Death Differ. England; 2002; 9: 158–68.

360. Harborne J. Introduction to Ecological Biochemistry. 4th Editio. London, UK: Elsevier Inc.; 1993. 316 p.

361. J G. The cost of plant chemical defense against herbivory: A biochemical perspective. In: EA B, editor. Insect-plant interactions. Boca Raton, USA: CRC Press; 1994. p. 105–73.

362. Reymond P, Weber H, Damond M, Farmer EE. Differential gene expression in response to mechanical wounding and insect feeding in Arabidopsis. Plant Cell. United States; 2000; 12: 707–20.

363. Hermsmeier D, Schittko U, Baldwin IT. Molecular interactions between the specialist herbivore Manduca sexta (Lepidoptera, Sphingidae) and its natural host Nicotiana attenuata. I. Large-scale changes in the accumulation of growth- and defense-related plant mRNAs. Plant Physiol. 2001; 125: 683–700.

364. Kennedy DO, Wightman EL. Herbal extracts and phytochemicals: plant secondary metabolites and the enhancement of human brain function. Adv Nutr. United States; 2011; 2: 32–50.

365. Strobel G, Daisy B, Castillo U, Harper J. Natural products from endophytic microorganisms. J Nat Prod. United States; 2004; 67: 257–68.

366. Verma VC, Kharwar RN, Strobel GA. Chemical and functional diversity of natural products from plant associated endophytic fungi. Nat Prod Commun. United States; 2009; 4: 1511–32.

367. Yu H, Zhang L, Li L, Zheng C, Guo L, Li W, Sun P, Qin L. Recent developments and future prospects of antimicrobial metabolites produced by endophytes. Microbiol Res. Germany; 2010; 165: 437–49.

368. Bascom-Slack CA, Arnold AE, Strobel SA. IBI series winner. Student-directed discovery of the plant microbiome and its products. Science. United States; 2012; 338: 485–6.

369. Aly AH, Debbab A, Proksch P. Fungal endophytes - secret producers of bioactive plant metabolites. Pharmazie. Germany; 2013; 68: 499–505.

370. Mousa WK, Raizada MN. The diversity of anti-microbial secondary metabolites produced by fungal endophytes: an interdisciplinary perspective. Front Microbiol. Switzerland; 2013; 4: 65.

371. Hansen BG, Halkier BA. New insight into the biosynthesis and regulation of indole compounds in Arabidopsis thaliana. Planta. Germany; 2005; 221: 603–6.

372. Higdon J, Drake V. An evidence-based approach to phytochemicals and other dietary factors. Edition 2nd, editor. New York, USA: Thieme; 2012. 328 p.

373. Menendez JA, Joven J, Aragones G, Barrajon-Catalan E, Beltran-Debon R, Borras-Linares I, Camps J, Corominas-Faja B, Cufi S, Fernandez-Arroyo S, Garcia-Heredia A, Hernandez-Aguilera A, Herranz-Lopez M, et al. Xenohormetic and anti-aging activity of secoiridoid polyphenols present in extra virgin olive oil: a new family of gerosuppressant agents. Cell Cycle. United States; 2013; 12: 555–78.

374. Si H, Liu D. Dietary antiaging phytochemicals and mechanisms associated with prolonged survival. J Nutr Biochem. United States; 2014; 25: 581–91.

375. Wu Z, Song L, Liu SQ, Huang D. Tanshinones extend chronological lifespan in budding yeast Saccharomyces cerevisiae. Appl Microbiol Biotechnol. Germany; 2014; 98: 8617–28.

376. Somani SJ, Modi KP, Majumdar AS, Sadarani BN. Phytochemicals and their potential usefulness in inflammatory bowel disease. Phytother Res. England; 2015; 29: 339–50.

377. Hooper PL, Hooper PL, Tytell M, Vigh L. Xenohormesis: health benefits from an eon of plant stress response evolution. Cell Stress Chaperones. Netherlands; 2010; 15: 761–70.

378. Wink M. Evolution of secondary metabolites from an ecological and molecular phylogenetic perspective. Phytochemistry. England; 2003; 64: 3–19.

379. Tahara S. A journey of twenty-five years through the ecological biochemistry of flavonoids. Biosci Biotechnol Biochem. England; 2007; 71: 1387–404.

380. Murakami A. Modulation of protein quality control systems by food phytochemicals. J Clin Biochem Nutr. Japan; 2013; 52: 215–27.

381. Adrian M, Jeandet P, Veneau J, Weston LA, Bessis R. Biological Activity of Resveratrol, a Stilbenic Compound from Grapevines, Against Botrytis cinerea, the Causal Agent for Gray Mold. J Chem Ecol. 1997; 23: 1689–702.

382. Heath MC. Hypersensitive response-related death. Plant Mol Biol. Netherlands; 2000; 44: 321–34.

383. Arimura G, Kost C, Boland W. Herbivore-induced, indirect plant defences. Biochim Biophys Acta. Netherlands; 2005; 1734: 91–111.

384. Brencic A, Winans SC. Detection of and response to signals involved in host-microbe interactions by plant-associated bacteria. Microbiol Mol Biol Rev. United States; 2005; 69: 155–94.

385. Mattson MP, Son TG, Camandola S. Viewpoint: mechanisms of action and therapeutic potential of neurohormetic phytochemicals. Dose Response. United States; 2007; 5: 174–86.

386. Santiago R, Malvar RA. Role of dehydrodiferulates in maize resistance to pests and diseases. Int J Mol Sci. Switzerland; 2010; 11: 691–703.

387. Tang K, Zhan J-C, Yang H-R, Huang W-D. Changes of resveratrol and antioxidant enzymes during UV-induced plant defense response in peanut seedlings. J Plant Physiol. Germany; 2010; 167: 95–102.

388. Arimura G-I, Ozawa R, Maffei ME. Recent advances in plant early signaling in response to herbivory. Int J Mol Sci. Switzerland; 2011; 12: 3723–39.

389. Barros-Rios J, Malvar RA, Jung H-JG, Santiago R. Cell wall composition as a maize defense mechanism against corn borers. Phytochemistry. England; 2011; 72: 365–71.

390. Bednarek P. Sulfur-containing secondary metabolites from Arabidopsis thaliana and other Brassicaceae with function in plant immunity. Chembiochem. Germany; 2012; 13: 1846–59.

391. Nwachukwu ID, Slusarenko AJ, Gruhlke MCH. Sulfur and sulfur compounds in plant defence. Nat Prod Commun. United States; 2012; 7: 395–400.

392. Huot OB, Nachappa P, Tamborindeguy C. The evolutionary strategies of plant defenses have a dynamic impact on the adaptations and interactions of vectors and pathogens. Insect Sci. Australia; 2013; 20: 297–306.

393. Kazan K, Lyons R. Intervention of Phytohormone Pathways by Pathogen Effectors. The Plant cell. United States; 2014. p. 2285–309.

394. Porras-Alfaro A, Bayman P. Hidden fungi, emergent properties: endophytes and microbiomes. Annu Rev Phytopathol. United States; 2011; 49: 291–315.

395. Zhao J, Shan T, Mou Y, Zhou L. Plant-derived bioactive compounds produced by endophytic fungi. Mini Rev Med Chem. Netherlands; 2011; 11: 159–68.

396. Kusari S, Hertweck C, Spiteller M. Chemical ecology of endophytic fungi: origins of secondary metabolites. Chem Biol. United States; 2012; 19: 792–8.

397. Nath A, Raghunatha P, Joshi SR. Diversity and Biological Activities of Endophytic Fungi of Emblica officinalis, an Ethnomedicinal Plant of India. Mycobiology. Korea (South); 2012; 40: 8–13.

398. Zhang Y, Han T, Ming Q, Wu L, Rahman K, Qin L. Alkaloids produced by endophytic fungi: a review. Nat Prod Commun. United States; 2012; 7: 963–8.

399. Lebeis SL. The potential for give and take in plant-microbiome relationships. Front Plant Sci. Switzerland; 2014; 5: 287.

400. Harikumar KB, Aggarwal BB. Resveratrol: a multitargeted agent for age-associated chronic diseases. Cell Cycle. United States; 2008; 7: 1020–35.

401. Pan W, Jiang S, Luo P, Wu J, Gao P. Isolation, purification and structure identification of antioxidant compound from the roots of Incarvillea younghusbandii Sprague and its life span prolonging effect in Drosophila melanogaster. Nat Prod Res. 2008; 22: 719–25.

402. Moriguchi T, Takashina K, Chu PJ, Saito H, Nishiyama N. Prolongation of life span and improved learning in the senescence accelerated mouse produced by aged garlic extract. Biol Pharm Bull. Japan; 1994; 17: 1589–94.

403. Moriguchi T, Saito H, Nishiyama N. Anti-ageing effect of aged garlic extract in the inbred brain atrophy mouse model. Clin Exp Pharmacol Physiol. Australia; 1997; 24: 235–42.

404. Nishiyama N, Moriguchi T, Saito H. Beneficial effects of aged garlic extract on learning and memory impairment in the senescence-accelerated mouse. Exp Gerontol. England; 1997; 32: 149–60.

405. Howitz KT, Bitterman KJ, Cohen HY, Lamming DW, Lavu S, Wood JG, Zipkin RE, Chung P, Kisielewski A, Zhang L-L, Scherer B, Sinclair DA. Small molecule activators of sirtuins extend Saccharomyces cerevisiae lifespan. Nature. England; 2003; 425: 191–6.

406. Pietsch K, Saul N, Chakrabarti S, Sturzenbaum SR, Menzel R, Steinberg CEW. Hormetins, antioxidants and prooxidants: defining quercetin-, caffeic acid- and rosmarinic acid-mediated life extension in C. elegans. Biogerontology. Netherlands; 2011; 12: 329–47.

407. Wanke V, Cameroni E, Uotila A, Piccolis M, Urban J, Loewith R, De Virgilio C. Caffeine extends yeast lifespan by targeting TORC1. Mol Microbiol. England; 2008; 69: 277–85.

408. Rallis C, Codlin S, Bahler J. TORC1 signaling inhibition by rapamycin and caffeine affect lifespan, global gene expression, and cell proliferation of fission yeast. Aging Cell. England; 2013; 12: 563–73.

409. Lublin A, Isoda F, Patel H, Yen K, Nguyen L, Hajje D, Schwartz M, Mobbs C. FDA-approved drugs that protect mammalian neurons from glucose toxicity slow aging dependent on cbp and protect against proteotoxicity. PLoS One. United States; 2011; 6: e27762.

410. Sutphin GL, Bishop E, Yanos ME, Moller RM, Kaeberlein M. Caffeine extends life span, improves healthspan, and delays age- associated pathology in Caenorhabditis elegans. Longev Heal. England; 2012; 1: 9.

411. Saul N, Pietsch K, Menzel R, Sturzenbaum SR, Steinberg CEW. Catechin induced longevity in C. elegans: from key regulator genes to disposable soma. Mech Ageing Dev. Ireland; 2009; 130: 477–86.

412. Kiaei M, Kipiani K, Petri S, Chen J, Calingasan NY, Beal MF. Celastrol blocks neuronal cell death and extends life in transgenic mouse model of amyotrophic lateral sclerosis. Neurodegener Dis. Switzerland; 2005; 2: 246–54.

413. Liao VH-C, Yu C-W, Chu Y-J, Li W-H, Hsieh Y-C, Wang T-T. Curcumin-mediated lifespan extension in Caenorhabditis elegans. Mech Ageing Dev. Ireland; 2011; 132: 480–

7.

414. Lee K-S, Lee B-S, Semnani S, Avanesian A, Um C-Y, Jeon H-J, Seong K-M, Yu K, Min K-J, Jafari M. Curcumin extends life span, improves health span, and modulates the expression of age-associated aging genes in Drosophila melanogaster. Rejuvenation Res. 2010; 13: 561–70.

415. Shen L-R, Xiao F, Yuan P, Chen Y, Gao Q-K, Parnell LD, Meydani M, Ordovas JM, Li D, Lai C-Q. Curcumin-supplemented diets increase superoxide dismutase activity and mean lifespan in Drosophila. Age (Dordr). Netherlands; 2013; 35: 1133–42.

416. Caesar I, Jonson M, Nilsson KPR, Thor S, Hammarstrom P. Curcumin promotes A-beta fibrillation and reduces neurotoxicity in transgenic Drosophila. PLoS One. United States; 2012; 7: e31424.

417. Bakshi HA, Sam S, Feroz A, Ravesh Z, Shah GA, Sharma M. Crocin from Kashmiri saffron (Crocus sativus) induces in vitro and in vivo xenograft growth inhibition of Dalton's lymphoma (DLA) in mice. Asian Pac J Cancer Prev. Thailand; 2009; 10: 887–90.

418. Choi MJ, Kim BK, Park KY, Yokozawa T, Song YO, Cho EJ. Anti-aging Effects of Cyanidin under a Stress-Induced Premature Senescence Cellular System. Biol Pharm Bull. 2010; 33: 421–6.

419. Powolny AA, Singh S V, Melov S, Hubbard A, Fisher AL. The garlic constituent diallyl trisulfide increases the lifespan of C. elegans via skn-1 activation. Exp Gerontol. England; 2011; 46: 441–52.

420. Saul N, Pietsch K, Sturzenbaum SR, Menzel R, Steinberg CEW. Diversity of polyphenol action in Caenorhabditis elegans: between toxicity and longevity. J Nat Prod. United States; 2011; 74: 1713–20.

421. Abbas S, Wink M. Epigallocatechin gallate from green tea (Camellia sinensis) increases lifespan and stress resistance in Caenorhabditis elegans. Planta Med. Germany; 2009; 75: 216–21.

422. Abbas S, Wink M. Epigallocatechin gallate inhibits beta amyloid oligomerization in Caenorhabditis elegans and affects the daf-2/insulin-like signaling pathway. Phytomedicine. Germany; 2010; 17: 902–9.

423. Si H, Fu Z, Babu PVA, Zhen W, Leroith T, Meaney MP, Voelker KA, Jia Z, Grange RW, Liu D. Dietary epicatechin promotes survival of obese diabetic mice and Drosophila melanogaster. J Nutr. United States; 2011; 141: 1095–100.

424. Sayed AAR. Ferulsinaic acid attenuation of advanced glycation end products extends the lifespan of Caenorhabditis elegans. J Pharm Pharmacol. England; 2011; 63: 423–8.

425. Kampkötter A, Gombitang Nkwonkam C, Zurawski RF, Timpel C, Chovolou Y, Wätjen W, Kahl R. Effects of the flavonoids kaempferol and fisetin on thermotolerance, oxidative stress and FoxO transcription factor DAF-16 in the model organism Caenorhabditis elegans. Arch Toxicol. 2007; 81: 849–58.

426. Zarse K, Bossecker A, Müller-Kuhrt L, Siems K, Hernandez MA, Berendsohn WG,

Birringer M, Ristow M. The phytochemical glaucarubinone promotes mitochondrial metabolism, reduces body fat, and extends lifespan of Caenorhabditis elegans. Horm Metab Res. 2011; 43: 241–3.

427. Wang P, Zhang Z, Ma X, Huang Y, Liu X, Tu P, Tong T. HDTIC-1 and HDTIC-2, two compounds extracted from Astragali Radix, delay replicative senescence of human diploid fibroblasts. Mech Ageing Dev. Ireland; 2003; 124: 1025–34.

428. Cai W-J, Huang J-H, Zhang S-Q, Wu B, Kapahi P, Zhang X-M, Shen Z-Y. Icariin and its derivative icariside II extend healthspan via insulin/IGF-1 pathway in C. elegans. PLoS One. United States; 2011; 6: e28835.

429. Grunz G, Haas K, Soukup S, Klingenspor M, Kulling SE, Daniel H, Spanier B. Structural features and bioavailability of four flavonoids and their implications for lifespan-extending and antioxidant actions in C. elegans. Mech Ageing Dev. Ireland; 2012; 133: 1–10.

430. West M, Mhatre M, Ceballos A, Floyd RA, Grammas P, Gabbita SP, Hamdheydari L, Mai T, Mou S, Pye QN, Stewart C, West S, Williamson KS, et al. The arachidonic acid 5-lipoxygenase inhibitor nordihydroguaiaretic acid inhibits tumor necrosis factor alpha activation of microglia and extends survival of G93A-SOD1 transgenic mice. J Neurochem. 2004; 91: 133–43.

431. Strong R, Miller RA, Astle CM, Floyd RA, Flurkey K, Hensley KL, Javors MA, Leeuwenburgh C, Nelson JF, Ongini E, Nadon NL, Warner HR, Harrison DE. Nordihydroguaiaretic acid and aspirin increase lifespan of genetically heterogeneous male mice. Aging Cell. 2008; 7: 641–50.

432. Buu-Hoi NP, Ratsimamanga AR. Retarding action of nordihydroguiaiaretic acid on aging in the rat. C R Seances Soc Biol Fil. 1959; 153: 1180–2. Available from http://www.ncbi.nlm.nih.gov/pubmed/13806555

433. Miquel J, Fleming J, Economos AC. Antioxidants, metabolic rate and aging in Drosophila. Arch Gerontol Geriatr. Netherlands; 1982; 1: 159–65.

434. Richie JPJ, Mills BJ, Lang CA. Dietary nordihydroguaiaretic acid increases the life span of the mosquito. Proc Soc Exp Biol Med. United States; 1986; 183: 81–5.

435. Katsiki M, Chondrogianni N, Chinou I, Rivett AJ, Gonos ES. The olive constituent oleuropein exhibits proteasome stimulatory properties in vitro and confers life span extension of human embryonic fibroblasts. Rejuvenation Res. United States; 2007; 10: 157–72.

436. Xiang L, Sun K, Lu J, Weng Y, Taoka A, Sakagami Y, Qi J. Anti-aging effects of phloridzin, an apple polyphenol, on yeast via the SOD and Sir2 genes. Biosci Biotechnol Biochem. England; 2011; 75: 854–8.

437. Belinha I, Amorim MA, Rodrigues P, de Freitas V, Moradas-Ferreira P, Mateus N, Costa V. Quercetin increases oxidative stress resistance and longevity in Saccharomyces cerevisiae. J Agric Food Chem. United States; 2007; 55: 2446–51.

438. Kampkotter A, Nkwonkam CG, Zurawski RF, Timpel C, Chovolou Y, Watjen W, Kahl R. Investigations of protective effects of the flavonoids quercetin and rutin on stress resistance

in the model organism Caenorhabditis elegans. Toxicology. Ireland; 2007; 234: 113–23.

439. Kampkotter A, Timpel C, Zurawski RF, Ruhl S, Chovolou Y, Proksch P, Watjen W. Increase of stress resistance and lifespan of Caenorhabditis elegans by quercetin. Comp Biochem Physiol B Biochem Mol Biol. England; 2008; 149: 314–23.

440. Pietsch K, Saul N, Menzel R, Sturzenbaum SR, Steinberg CEW. Quercetin mediated lifespan extension in Caenorhabditis elegans is modulated by age-1, daf-2, sek-1 and unc-43. Biogerontology. Netherlands; 2009; 10: 565–78.

441. Chondrogianni N, Kapeta S, Chinou I, Vassilatou K, Papassideri I, Gonos ES. Anti-ageing and rejuvenating effects of quercetin. Exp Gerontol. England; 2010; 45: 763–71.

442. Xue Y-L, Ahiko T, Miyakawa T, Amino H, Hu F, Furihata K, Kita K, Shirasawa T, Sawano Y, Tanokura M. Isolation and Caenorhabditis elegans lifespan assay of flavonoids from onion. J Agric Food Chem. United States; 2011; 59: 5927–34.

443. Srivastava D, Arya U, SoundaraRajan T, Dwivedi H, Kumar S, Subramaniam JR. Reserpine can confer stress tolerance and lifespan extension in the nematode C. elegans. Biogerontology. Netherlands; 2008; 9: 309–16.

444. Arya U, Dwivedi H, Subramaniam JR. Reserpine ameliorates Abeta toxicity in the Alzheimer's disease model in Caenorhabditis elegans. Exp Gerontol. England; 2009; 44: 462–6.

445. Wood JG, Rogina B, Lavu S, Howitz K, Helfand SL, Tatar M, Sinclair D. Sirtuin activators mimic caloric restriction and delay ageing in metazoans. Nature. England; 2004; 430: 686–9.

446. Valenzano DR, Terzibasi E, Genade T, Cattaneo A, Domenici L, Cellerino A. Resveratrol prolongs lifespan and retards the onset of age-related markers in a short-lived vertebrate. Curr Biol. England; 2006; 16: 296–300.

447. Rascon B, Hubbard BP, Sinclair DA, Amdam G V. The lifespan extension effects of resveratrol are conserved in the honey bee and may be driven by a mechanism related to caloric restriction. Aging (Albany NY). United States; 2012; 4: 499–508.

448. Baur JA, Pearson KJ, Price NL, Jamieson HA, Lerin C, Kalra A, Prabhu V V, Allard JS, Lopez-Lluch G, Lewis K, Pistell PJ, Poosala S, Becker KG, et al. Resveratrol improves health and survival of mice on a high-calorie diet. Nature. England; 2006; 444: 337–42.

449. Morselli E, Maiuri MC, Markaki M, Megalou E, Pasparaki A, Palikaras K, Criollo A, Galluzzi L, Malik SA, Vitale I, Michaud M, Madeo F, Tavernarakis N, et al. Caloric restriction and resveratrol promote longevity through the Sirtuin-1-dependent induction of autophagy. Cell Death Dis. 2010; 1: e10.

450. Minois N, Carmona-Gutierrez D, Bauer MA, Rockenfeller P, Eisenberg T, Brandhorst S, Sigrist SJ, Kroemer G, Madeo F. Spermidine promotes stress resistance in Drosophila melanogaster through autophagy-dependent and -independent pathways. Cell Death Dis. 2012; 3: e401.

451. Minois N, Rockenfeller P, Smith TK, Carmona-Gutierrez D. Spermidine feeding decreases

age-related locomotor activity loss and induces changes in lipid composition. PLoS One. United States; 2014; 9: e102435.

452. Saul N, Pietsch K, Menzel R, Sturzenbaum SR, Steinberg CEW. The longevity effect of tannic acid in Caenorhabditis elegans: Disposable Soma meets hormesis. J Gerontol A Biol Sci Med Sci. United States; 2010; 65: 626–35.

453. Moriguchi T, Saito H, Nishiyama N. Aged garlic extract prolongs longevity and improves spatial memory deficit in senescence-accelerated mouse. Biol Pharm Bull. Japan; 1996; 19: 305–7.

454. Strong R, Miller RA, Astle CM, Baur JA, de Cabo R, Fernandez E, Guo W, Javors M, Kirkland JL, Nelson JF, Sinclair DA, Teter B, Williams D, et al. Evaluation of resveratrol, green tea extract, curcumin, oxaloacetic acid, and medium-chain triglyceride oil on life span of genetically heterogeneous mice. J Gerontol A Biol Sci Med Sci. 2013; 68: 6–16.

455. Cañuelo A, Gilbert-López B, Pacheco-Liñán P, Martínez-Lara E, Siles E, Miranda-Vizuete A. Tyrosol, a main phenol present in extra virgin olive oil, increases lifespan and stress resistance in Caenorhabditis elegans. Mech Ageing Dev. 2012; 133: 563–74.

456. Dong Y, Guha S, Sun X, Cao M, Wang X, Zou S. Nutraceutical interventions for promoting healthy aging in invertebrate models. Oxid Med Cell Longev. United States; 2012; 2012: 718491.

457. Guarente L. Aging research-where do we stand and where are we going? Cell. United States; 2014; 159: 15–9.

458. Kennedy BK, Berger SL, Brunet A, Campisi J, Cuervo AM, Epel ES, Franceschi C, Lithgow GJ, Morimoto RI, Pessin JE, Rando TA, Richardson A, Schadt EE, et al. Geroscience: linking aging to chronic disease. Cell. United States; 2014; 159: 709–13.

459. Labbadia J, Morimoto RI. Proteostasis and longevity: when does aging really begin? F1000Prime Rep. England; 2014; 6: 7.

460. Partridge L. Intervening in ageing to prevent the diseases of ageing. Trends Endocrinol Metab. United States; 2014; 25: 555–7.

461. Harel I, Benayoun BA, Machado B, Singh PP, Hu C-K, Pech MF, Valenzano DR, Zhang E, Sharp SC, Artandi SE, Brunet A. A platform for rapid exploration of aging and diseases in a naturally short-lived vertebrate. Cell. 2015; 160: 1013–26.

462. Lee D, Hwang W, Artan M, Jeong D-E, Lee S-J. Effects of nutritional components on aging. Aging Cell. England; 2015; 14: 8–16.

463. Argyropoulou A, Aligiannis N, Trougakos IP, Skaltsounis A-L. Natural compounds with anti-ageing activity. Nat Prod Rep. England; 2013; 30: 1412–37.

464. Lutchman V, Medkour Y, Samson E, Arlia-Ciommo A, Dakik P, Cortes B, Feldman R, Mohtashami S, McAuley M, Chancharoen M, Rukundo B, Simard É, Titorenko VI. Discovery of plant extracts that greatly delay yeast chronological aging and have different effects on longevity-defining cellular processes. Oncotarget. 2016; 7.

465. McDonald RB. Biology of Aging. New York, USA: Garland Science; 2014. p. 1–54.

466. Abrams PA. Evolutionary biology: mortality and lifespan. Nature. England; 2004. p. 1048.

467. Kirkwood TBL. Understanding the odd science of aging. Cell. United States; 2005; 120: 437–47.

468. de Magalhaes JP, Cabral JAS, Magalhaes D. The influence of genes on the aging process of mice: a statistical assessment of the genetics of aging. Genetics. United States; 2005; 169: 265–74.

469. Finch C. Longevity, senescence, and the genome. Chicago: University of Chicago Press; 1990.

470. Gavrilov L, NS G. The biology of life span: a quantitative approach. Chur, Switzerland/New York, Harwood Academic; 1991.

471. Lashmanova E, Proshkina E, Zhikrivetskaya S, Shevchenko O, Marusich E, Leonov S, Melerzanov A, Zhavoronkov A, Moskalev A. Fucoxanthin increases lifespan of Drosophila melanogaster and Caenorhabditis elegans. Pharmacol Res. Netherlands; 2015; 100: 228–41.

472. Burstein MT, Beach A, Richard VR, Koupaki O, Gomez-Perez A, Goldberg AA, Kyryakov P, Bourque SD, Glebov A, Titorenko VI. Interspecies Chemical Signals Released into the Environment May Create Xenohormetic, Hormetic and Cytostatic Selective Forces that Drive the Ecosystemic Evolution of Longevity Regulation Mechanisms. Dose Response. 2012; 10: 75–82.

473. Calabrese V, Cornelius C, Dinkova-Kostova AT, Iavicoli I, Di Paola R, Koverech A, Cuzzocrea S, Rizzarelli E, Calabrese EJ. Cellular stress responses, hormetic phytochemicals and vitagenes in aging and longevity. Biochim Biophys Acta. Netherlands; 2012; 1822: 753–83.

474. Calabrese EJ, Mattson MP. Hormesis provides a generalized quantitative estimate of biological plasticity. J Cell Commun Signal. Netherlands; 2011; 5: 25–38.

475. Giorgio M, Trinei M, Migliaccio E, Pelicci PG. Hydrogen peroxide: a metabolic by-product or a common mediator of ageing signals? Nat Rev Mol Cell Biol. England; 2007; 8: 722–8.

476. Ristow M, Schmeisser K. Mitohormesis: Promoting Health and Lifespan by Increased Levels of Reactive Oxygen Species (ROS). Dose Response. United States; 2014; 12: 288–341.

477. Shadel GS, Horvath TL. Mitochondrial ROS signaling in organismal homeostasis. Cell. United States; 2015; 163: 560–9.

478. Wang Y, Hekimi S. Mitochondrial dysfunction and longevity in animals: Untangling the knot. Science. United States; 2015; 350: 1204–7.

479. Cui H, Kong Y, Zhang H. Oxidative stress, mitochondrial dysfunction, and aging. J Signal Transduct. United States; 2012; 2012: 646354.

480. Gladyshev VN. The origin of aging: imperfectness-driven non-random damage defines the

aging process and control of lifespan. Trends Genet. England; 2013; 29: 506–12.

481. Ray PD, Huang B-W, Tsuji Y. Reactive oxygen species (ROS) homeostasis and redox regulation in cellular signaling. Cell Signal. England; 2012; 24: 981–90.

482. Schieber M, Chandel NS. ROS function in redox signaling and oxidative stress. Curr Biol. England; 2014; 24: R453-62.

483. Calabrese V, Cornelius C, Cuzzocrea S, Iavicoli I, Rizzarelli E, Calabrese EJ. Hormesis, cellular stress response and vitagenes as critical determinants in aging and longevity. Mol Aspects Med. England; 2011; 32: 279–304.

484. D'Autreaux B, Toledano MB. ROS as signalling molecules: mechanisms that generate specificity in ROS homeostasis. Nat Rev Mol Cell Biol. England; 2007; 8: 813–24.

485. Gems D, Partridge L. Stress-response hormesis and aging: "that which does not kill us makes us stronger". Cell Metab. United States; 2008; 7: 200–3.

486. Veal E, Day A. Hydrogen peroxide as a signaling molecule. Antioxid Redox Signal. United States; 2011; 15: 147–51.

487. Walther TC, Farese RVJ. Lipid droplets and cellular lipid metabolism. Annu Rev Biochem. United States; 2012; 81: 687–714.

488. Ohsaki Y, Suzuki M, Fujimoto T. Open questions in lipid droplet biology. Chem Biol. United States; 2014; 21: 86–96.

489. Pol A, Gross SP, Parton RG. Review: biogenesis of the multifunctional lipid droplet: lipids, proteins, and sites. J Cell Biol. United States; 2014; 204: 635–46.

490. Wang C-W. Lipid droplet dynamics in budding yeast. Cell Mol Life Sci. Switzerland; 2015; 72: 2677–95.

491. Bluher M. Fat tissue and long life. Obes Facts. Switzerland; 2008; 1: 176–82.

492. Bluher M, Kahn BB, Kahn CR. Extended longevity in mice lacking the insulin receptor in adipose tissue. Science. United States; 2003; 299: 572–4.

493. Chiu C-H, Lin W-D, Huang S-Y, Lee Y-H. Effect of a C/EBP gene replacement on mitochondrial biogenesis in fat cells. Genes Dev. United States; 2004; 18: 1970–5.

494. Greenberg AS, Coleman RA, Kraemer FB, McManaman JL, Obin MS, Puri V, Yan Q-W, Miyoshi H, Mashek DG. The role of lipid droplets in metabolic disease in rodents and humans. J Clin Invest. United States; 2011; 121: 2102–10.

495. Gronke S, Mildner A, Fellert S, Tennagels N, Petry S, Muller G, Jackle H, Kuhnlein RP. Brummer lipase is an evolutionary conserved fat storage regulator in Drosophila. Cell Metab. United States; 2005; 1: 323–30.

496. Haemmerle G, Lass A, Zimmermann R, Gorkiewicz G, Meyer C, Rozman J, Heldmaier G, Maier R, Theussl C, Eder S, Kratky D, Wagner EF, Klingenspor M, et al. Defective lipolysis and altered energy metabolism in mice lacking adipose triglyceride lipase. Science. 2006; 312: 734–7.

497. Krahmer N, Farese RVJ, Walther TC. Balancing the fat: lipid droplets and human disease. EMBO Mol Med. England; 2013; 5: 973–83.

498. Narbonne P, Roy R. Caenorhabditis elegans dauers need LKB1/AMPK to ration lipid reserves and ensure long-term survival. Nature. England; 2009; 457: 210–4.

499. Picard F, Kurtev M, Chung N, Topark-Ngarm A, Senawong T, Machado De Oliveira R, Leid M, McBurney MW, Guarente L. Sirt1 promotes fat mobilization in white adipocytes by repressing PPAR- gamma. Nature. England; 2004; 429: 771–6.

500. Rambold AS, Cohen S, Lippincott-Schwartz J. Fatty acid trafficking in starved cells: regulation by lipid droplet lipolysis, autophagy, and mitochondrial fusion dynamics. Dev Cell. United States; 2015; 32: 678–92.

501. Russell SJ, Kahn CR. Endocrine regulation of ageing. Nat Rev Mol Cell Biol. England; 2007; 8: 681–91.

502. Wang MC, O'Rourke EJ, Ruvkun G. Fat metabolism links germline stem cells and longevity in C. elegans. Science. United States; 2008; 322: 957–60.

503. Welte MA. Expanding roles for lipid droplets. Curr Biol. England; 2015; 25: R470-81.

504. Blagosklonny M V. Aging and immortality: quasi-programmed senescence and its pharmacologic inhibition. Cell Cycle. United States; 2006; 5: 2087–102.

505. Blagosklonny M V, Hall MN. Growth and aging: a common molecular mechanism. Aging (Albany NY). United States; 2009; 1: 357–62.

506. Campisi J. Aging, cellular senescence, and cancer. Annu Rev Physiol. United States; 2013; 75: 685–705.

507. Goldberg AA, Beach A, Davies GF, Harkness TAA, Leblanc A, Titorenko VI. Lithocholic bile acid selectively kills neuroblastoma cells, while sparing normal neuronal cells. Oncotarget. United States; 2011; 2: 761–82.

508. Hanahan D, Weinberg RA. Hallmarks of cancer: the next generation. Cell. United States; 2011; 144: 646–74.

509. Kaeberlein M. Longevity and aging. F1000Prime Rep. England; 2013; 5: 5.

510. Niccoli T, Partridge L. Ageing as a risk factor for disease. Curr Biol. England; 2012; 22: R741-52.

511. Rodier F, Campisi J. Four faces of cellular senescence. J Cell Biol. United States; 2011; 192: 547–56.

512. Rajakumari S, Grillitsch K, Daum G. Synthesis and turnover of non-polar lipids in yeast. Prog Lipid Res. England; 2008; 47: 157–71.

513. Carman GM, Han G-S. Regulation of phospholipid synthesis in the yeast Saccharomyces cerevisiae. Annu Rev Biochem. United States; 2011; 80: 859–83.

514. Fernandez-Murray JP, McMaster CR. Lipid synthesis and membrane contact sites: a crossroads for cellular physiology. J Lipid Res. United States; 2016; 57: 1789–805.

515. Elbaz-Alon Y. Mitochondria-organelle contact sites: the plot thickens. Biochem Soc Trans. England; 2017; 45: 477–88.

516. Csordas G, Weaver D, Hajnoczky G. Endoplasmic Reticulum-Mitochondrial Contactology: Structure and Signaling Functions. Trends Cell Biol. England; 2018; 28: 523–40.

517. Graef M. Lipid droplet-mediated lipid and protein homeostasis in budding yeast. FEBS Lett. England; 2018; 592: 1291–303.

518. Renne MF, de Kroon AIPM. The role of phospholipid molecular species in determining the physical properties of yeast membranes. FEBS Lett. England; 2018; 592: 1330–45.

519. Simmen T, Herrera-Cruz MS. Plastic mitochondria-endoplasmic reticulum (ER) contacts use chaperones and tethers to mould their structure and signaling. Curr Opin Cell Biol. England; 2018; 53: 61–9.

520. Tamura Y, Kawano S, Endo T. Organelle contact zones as sites for lipid transfer. J Biochem. England; 2019; 165: 115–23.

521. Carmona-Gutierrez D, Bauer MA, Zimmermann A, Aguilera A, Austriaco N, Ayscough K, Balzan R, Bar-Nun S, Barrientos A, Belenky P, Blondel M, Braun RJ, Breitenbach M, et al. Guidelines and recommendations on yeast cell death nomenclature. Microb cell (Graz, Austria). Austria; 2018; 5: 4–31.

522. Mohammad K, Dakik P, Medkour Y, McAuley M, Mitrofanova D, Titorenko VI. Yeast Cells Exposed to Exogenous Palmitoleic Acid Either Adapt to Stress and Survive or Commit to Regulated Liponecrosis and Die. Oxid Med Cell Longev. United States; 2018; 2018: 1–11.

523. Rockenfeller P, Gourlay CW. Lipotoxicty in yeast: a focus on plasma membrane signalling and membrane contact sites. FEMS Yeast Res. England; 2018; 18.

524. Rockenfeller P, Smolnig M, Diessl J, Bashir M, Schmiedhofer V, Knittelfelder O, Ring J, Franz J, Foessl I, Khan MJ, Rost R, Graier WF, Kroemer G, et al. Diacylglycerol triggers Rim101 pathway-dependent necrosis in yeast: a model for lipotoxicity. Cell Death Differ. England; 2018; 25: 767–83.

525. Borradaile NM, Han X, Harp JD, Gale SE, Ory DS, Schaffer JE. Disruption of endoplasmic reticulum structure and integrity in lipotoxic cell death. J Lipid Res. United States; 2006; 47: 2726–37.

526. Deguil J, Pineau L, Rowland Snyder EC, Dupont S, Beney L, Gil A, Frapper G, Ferreira T. Modulation of lipid-induced ER stress by fatty acid shape. Traffic. England; 2011; 12: 349–62.

527. Fu S, Yang L, Li P, Hofmann O, Dicker L, Hide W, Lin X, Watkins SM, Ivanov AR, Hotamisligil GS. Aberrant lipid metabolism disrupts calcium homeostasis causing liver endoplasmic reticulum stress in obesity. Nature. England; 2011; 473: 528–31.

528. Promlek T, Ishiwata-Kimata Y, Shido M, Sakuramoto M, Kohno K, Kimata Y. Membrane aberrancy and unfolded proteins activate the endoplasmic reticulum stress sensor Ire1 in different ways. Mol Biol Cell. United States; 2011; 22: 3520–32.

529. Fu S, Watkins SM, Hotamisligil GS. The role of endoplasmic reticulum in hepatic lipid homeostasis and stress signaling. Cell Metab. United States; 2012; 15: 623–34.

530. Thibault G, Shui G, Kim W, McAlister GC, Ismail N, Gygi SP, Wenk MR, Ng DTW. The membrane stress response buffers lethal effects of lipid disequilibrium by reprogramming the protein homeostasis network. Mol Cell. United States; 2012; 48: 16–27.

531. Cui W, Ma J, Wang X, Yang W, Zhang J, Ji Q. Free fatty acid induces endoplasmic reticulum stress and apoptosis of beta-cells by Ca2+/calpain-2 pathways. PLoS One. United States; 2013; 8: e59921.

532. Lagace TA, Ridgway ND. The role of phospholipids in the biological activity and structure of the endoplasmic reticulum. Biochim Biophys Acta. Netherlands; 2013; 1833: 2499–510.

533. Surma MA, Klose C, Peng D, Shales M, Mrejen C, Stefanko A, Braberg H, Gordon DE, Vorkel D, Ejsing CS, Farese R, Simons K, Krogan NJ, et al. A lipid E-MAP identifies Ubx2 as a critical regulator of lipid saturation and lipid bilayer stress. Mol Cell. 2013; 51: 519–30.

534. Volmer R, van der Ploeg K, Ron D. Membrane lipid saturation activates endoplasmic reticulum unfolded protein response transducers through their transmembrane domains. Proc Natl Acad Sci U S A. United States; 2013; 110: 4628–33.

535. Wu H, Ng BSH, Thibault G. Endoplasmic reticulum stress response in yeast and humans. Biosci Rep. England; 2014; 34.

536. Covino R, Ballweg S, Stordeur C, Michaelis JB, Puth K, Wernig F, Bahrami A, Ernst AM, Hummer G, Ernst R. A Eukaryotic Sensor for Membrane Lipid Saturation. Mol Cell. United States; 2016; 63: 49–59.

537. Akoumi A, Haffar T, Mousterji M, Kiss RS, Bousette N. Palmitate mediated diacylglycerol accumulation causes endoplasmic reticulum stress, Plin2 degradation, and cell death in H9C2 cardiomyoblasts. Exp Cell Res. United States; 2017; 354: 85–94.

538. Chen E, Tsai TH, Li L, Saha P, Chan L, Chang BH-J. PLIN2 is a Key Regulator of the Unfolded Protein Response and Endoplasmic Reticulum Stress Resolution in Pancreatic beta Cells. Sci Rep. England; 2017; 7: 40855.

539. Halbleib K, Pesek K, Covino R, Hofbauer HF, Wunnicke D, Hanelt I, Hummer G, Ernst R. Activation of the Unfolded Protein Response by Lipid Bilayer Stress. Mol Cell. United States; 2017; 67: 673-684.e8.

540. Covino R, Hummer G, Ernst R. Integrated Functions of Membrane Property Sensors and a Hidden Side of the Unfolded Protein Response. Mol Cell. United States; 2018; 71: 458–67.

541. Ho N, Xu C, Thibault G. From the unfolded protein response to metabolic diseases - lipids under the spotlight. J Cell Sci. England; 2018; 131.

542. Koh JH, Wang L, Beaudoin-Chabot C, Thibault G. Lipid bilayer stress-activated IRE-1 modulates autophagy during endoplasmic reticulum stress. J Cell Sci. England; 2018; 131.

543. Shyu PJ, Wong XFA, Crasta K, Thibault G. Dropping in on lipid droplets: insights into

cellular stress and cancer. Biosci Rep. England; 2018; 38.

544. Almanza A, Carlesso A, Chintha C, Creedican S, Doultsinos D, Leuzzi B, Luís A, McCarthy N, Montibeller L, More S, Papaioannou A, Püschel F, Sassano ML, et al. Endoplasmic reticulum stress signalling - from basic mechanisms to clinical applications. FEBS J. 2019; 286: 241–78.

545. Cho H, Stanzione F, Oak A, Kim GH, Yerneni S, Qi L, Sum AK, Chan C. Intrinsic Structural Features of the Human IRE1alpha Transmembrane Domain Sense Membrane Lipid Saturation. Cell Rep. United States; 2019; 27: 307-320.e5.

546. Fun XH, Thibault G. Lipid bilayer stress and proteotoxic stress-induced unfolded protein response deploy divergent transcriptional and non-transcriptional programmes. Biochim Biophys acta Mol cell Biol lipids. Netherlands; 2019; .

547. Hariri H, Speer N, Bowerman J, Rogers S, Fu G, Reetz E, Datta S, Feathers JR, Ugrankar R, Nicastro D, Henne WM. Mdm1 maintains endoplasmic reticulum homeostasis by spatially regulating lipid droplet biogenesis. J Cell Biol. United States; 2019; 218: 1319–34.

548. Ron D, Walter P. Signal integration in the endoplasmic reticulum unfolded protein response. Nat Rev Mol Cell Biol. England; 2007; 8: 519–29.

549. Jonikas MC, Collins SR, Denic V, Oh E, Quan EM, Schmid V, Weibezahn J, Schwappach B, Walter P, Weissman JS, Schuldiner M. Comprehensive characterization of genes required for protein folding in the endoplasmic reticulum. Science. United States; 2009; 323: 1693–7.

550. Walter P, Ron D. The unfolded protein response: from stress pathway to homeostatic regulation. Science. United States; 2011; 334: 1081–6.

551. Araki K, Nagata K. Protein folding and quality control in the ER. Cold Spring Harb Perspect Biol. United States; 2011; 3: a007526.

552. Gardner BM, Pincus D, Gotthardt K, Gallagher CM, Walter P. Endoplasmic reticulum stress sensing in the unfolded protein response. Cold Spring Harb Perspect Biol. United States; 2013; 5: a013169.

553. Higuchi-Sanabria R, Frankino PA, Paul JW 3rd, Tronnes SU, Dillin A. A Futile Battle? Protein Quality Control and the Stress of Aging. Dev Cell. United States; 2018; 44: 139–63.

554. Karagoz GE, Acosta-Alvear D, Walter P. The Unfolded Protein Response: Detecting and Responding to Fluctuations in the Protein-Folding Capacity of the Endoplasmic Reticulum. Cold Spring Harb Perspect Biol. United States; 2019; 11.

555. Salminen A, Kaarniranta K. ER stress and hormetic regulation of the aging process. Ageing Res Rev. England; 2010; 9: 211–7.

556. Hou J, Tang H, Liu Z, Osterlund T, Nielsen J, Petranovic D. Management of the endoplasmic reticulum stress by activation of the heat shock response in yeast. FEMS Yeast Res. England; 2014; 14: 481–94.

557. Beaupere C, Labunskyy VM. (Un)folding mechanisms of adaptation to ER stress: lessons from aneuploidy. Curr Genet. United States; 2019; 65: 467–71.

558. Cui H-J, Liu X-G, McCormick M, Wasko BM, Zhao W, He X, Yuan Y, Fang B-X, Sun X-R, Kennedy BK, Suh Y, Zhou Z-J, Kaeberlein M, et al. PMT1 deficiency enhances basal UPR activity and extends replicative lifespan of Saccharomyces cerevisiae. Age (Dordr). 2015; 37: 9788.

559. Weindling E, Bar-Nun S. Sir2 links the unfolded protein response and the heat shock response in a stress response network. Biochem Biophys Res Commun. United States; 2015; 457: 473–8.

560. Piperi C, Adamopoulos C, Papavassiliou AG. XBP1: A Pivotal Transcriptional Regulator of Glucose and Lipid Metabolism. Trends Endocrinol Metab. United States; 2016; 27: 119–22.

561. Cohen N, Breker M, Bakunts A, Pesek K, Chas A, Argemí J, Orsi A, Gal L, Chuartzman S, Wigelman Y, Jonas F, Walter P, Ernst R, et al. Iron affects Ire1 clustering propensity and the amplitude of endoplasmic reticulum stress signaling. J Cell Sci. 2017; 130: 3222–33.

562. Guzel E, Arlier S, Guzeloglu-Kayisli O, Tabak MS, Ekiz T, Semerci N, Larsen K, Schatz F, Lockwood CJ, Kayisli UA. Endoplasmic Reticulum Stress and Homeostasis in Reproductive Physiology and Pathology. Int J Mol Sci. Switzerland; 2017; 18.

563. Martinez G, Duran-Aniotz C, Cabral-Miranda F, Vivar JP, Hetz C. Endoplasmic reticulum proteostasis impairment in aging. Aging Cell. England; 2017; 16: 615–23.

564. Postnikoff SDL, Johnson JE, Tyler JK. The integrated stress response in budding yeast lifespan extension. Microb cell (Graz, Austria). Austria; 2017; 4: 368–75.

565. Remondelli P, Renna M. The Endoplasmic Reticulum Unfolded Protein Response in Neurodegenerative Disorders and Its Potential Therapeutic Significance. Front Mol Neurosci. Switzerland; 2017; 10: 187.

566. Moon HW, Han HG, Jeon YJ. Protein Quality Control in the Endoplasmic Reticulum and Cancer. Int J Mol Sci. Switzerland; 2018; 19.

567. Chadwick SR, Lajoie P. Endoplasmic Reticulum Stress Coping Mechanisms and Lifespan Regulation in Health and Diseases. Front cell Dev Biol. Switzerland; 2019; 7: 84.

568. Lehrbach NJ, Ruvkun G. Endoplasmic reticulum-associated SKN-1A/Nrf1 mediates a cytoplasmic unfolded protein response and promotes longevity. Elife. England; 2019; 8.

569. Ha EE-J, Frohman MA. Regulation of mitochondrial morphology by lipids. Biofactors. Netherlands; 2014; 40: 419–24.

570. Valencak TG, Azzu V. Making heads or tails of mitochondrial membranes in longevity and aging: a role for comparative studies. Longev Heal. England; 2014; 3: 3.

571. Kim H-E, Grant AR, Simic MS, Kohnz RA, Nomura DK, Durieux J, Riera CE, Sanchez M, Kapernick E, Wolff S, Dillin A. Lipid Biosynthesis Coordinates a Mitochondrial-to-Cytosolic Stress Response. Cell. United States; 2016; 166: 1539-1552.e16.

572. Ademowo OS, Dias HKI, Burton DGA, Griffiths HR. Lipid (per) oxidation in mitochondria: an emerging target in the ageing process? Biogerontology. Netherlands; 2017; 18: 859–79.

573. Pollard AK, Ortori CA, Stoger R, Barrett DA, Chakrabarti L. Mouse mitochondrial lipid composition is defined by age in brain and muscle. Aging (Albany NY). United States; 2017; 9: 986–98.

574. Johnson DR, Knoll LJ, Levin DE, Gordon JI. Saccharomyces cerevisiae contains four fatty acid activation (FAA) genes: an assessment of their role in regulating protein N-myristoylation and cellular lipid metabolism. J Cell Biol. United States; 1994; 127: 751–62.

575. Athenstaedt K, Daum G. Phosphatidic acid, a key intermediate in lipid metabolism. Eur J Biochem. England; 1999; 266: 1–16.

576. Koffel R, Tiwari R, Falquet L, Schneiter R. The Saccharomyces cerevisiae YLL012/YEH1, YLR020/YEH2, and TGL1 genes encode a novel family of membrane-anchored lipases that are required for steryl ester hydrolysis. Mol Cell Biol. United States; 2005; 25: 1655–68.

577. Mukaka MM. Statistics corner: A guide to appropriate use of correlation coefficient in medical research. Malawi Med J. Malawi; 2012; 24: 69–71.

578. Schmidt RM, Schessner JP, Borner GH, Schuck S. The proteasome biogenesis regulator Rpn4 cooperates with the unfolded protein response to promote ER stress resistance. Elife. England; 2019; 8.

579. Jesch SA, Liu P, Zhao X, Wells MT, Henry SA. Multiple endoplasmic reticulum-to-nucleus signaling pathways coordinate phospholipid metabolism with gene expression by distinct mechanisms. J Biol Chem. United States; 2006; 281: 24070–83.

580. Fraenkel D. Yeast intermediary metabolism. Cold Spring Harbor: Cold Spring Harbor Laboratory Press; 2011.

581. Stearns SC, Kaiser M. The effects of enhanced expression of elongation factor EF-1 alpha on lifespan in Drosophila melanogaster. IV. A summary of three experiments. Genetica. Netherlands; 1993; 91: 167–82.

582. Shikama N, Ackermann R, Brack C. Protein synthesis elongation factor EF-1 alpha expression and longevity in Drosophila melanogaster. Proc Natl Acad Sci U S A. United States; 1994; 91: 4199–203.

583. Hamilton B, Dong Y, Shindo M, Liu W, Odell I, Ruvkun G, Lee SS. A systematic RNAi screen for longevity genes in C. elegans. Genes Dev. United States; 2005; 19: 1544–55.

584. Teleman AA, Chen Y-W, Cohen SM. 4E-BP functions as a metabolic brake used under stress conditions but not during normal growth. Genes Dev. United States; 2005; 19: 1844–8.

585. Henderson ST, Bonafe M, Johnson TE. daf-16 protects the nematode Caenorhabditis elegans during food deprivation. J Gerontol A Biol Sci Med Sci. United States; 2006; 61: 444–60.

586. Chen D, Pan KZ, Palter JE, Kapahi P. Longevity determined by developmental arrest genes in Caenorhabditis elegans. Aging Cell. England; 2007; 6: 525–33.

587. Curran SP, Ruvkun G. Lifespan regulation by evolutionarily conserved genes essential for viability. PLoS Genet. United States; 2007; 3: e56.

588. Hansen M, Taubert S, Crawford D, Libina N, Lee S-J, Kenyon C. Lifespan extension by conditions that inhibit translation in Caenorhabditis elegans. Aging Cell. England; 2007; 6: 95–110.

589. Hipkiss AR. On why decreasing protein synthesis can increase lifespan. Mech Ageing Dev. Ireland; 2007; 128: 412–4.

590. Pan KZ, Palter JE, Rogers AN, Olsen A, Chen D, Lithgow GJ, Kapahi P. Inhibition of mRNA translation extends lifespan in Caenorhabditis elegans. Aging Cell. England; 2007; 6: 111–9.

591. Syntichaki P, Troulinaki K, Tavernarakis N. eIF4E function in somatic cells modulates ageing in Caenorhabditis elegans. Nature. England; 2007; 445: 922–6.

592. Steffen KK, MacKay VL, Kerr EO, Tsuchiya M, Hu D, Fox LA, Dang N, Johnston ED, Oakes JA, Tchao BN, Pak DN, Fields S, Kennedy BK, et al. Yeast life span extension by depletion of 60s ribosomal subunits is mediated by Gcn4. Cell. United States; 2008; 133: 292–302.

593. Tavernarakis N. Ageing and the regulation of protein synthesis: a balancing act? Trends Cell Biol. England; 2008; 18: 228–35.

594. Tohyama D, Yamaguchi A, Yamashita T. Inhibition of a eukaryotic initiation factor (eIF2Bdelta/F11A3.2) during adulthood extends lifespan in Caenorhabditis elegans. FASEB J. United States; 2008; 22: 4327–37.

595. Kennedy BK, Kaeberlein M. Hot topics in aging research: protein translation, 2009. Aging Cell. England; 2009; 8: 617–23.

596. Demontis F, Perrimon N. FOXO/4E-BP signaling in Drosophila muscles regulates organism-wide proteostasis during aging. Cell. United States; 2010; 143: 813–25.

597. Rogers AN, Chen D, McColl G, Czerwieniec G, Felkey K, Gibson BW, Hubbard A, Melov S, Lithgow GJ, Kapahi P. Life span extension via eIF4G inhibition is mediated by posttranscriptional remodeling of stress response gene expression in C. elegans. Cell Metab. 2011; 14: 55–66.

598. Pestov DG, Shcherbik N. Rapid cytoplasmic turnover of yeast ribosomes in response to rapamycin inhibition of TOR. Mol Cell Biol. United States; 2012; 32: 2135–44.

599. Leprivier G, Remke M, Rotblat B, Dubuc A, Mateo A-RF, Kool M, Agnihotri S, El-Naggar A, Yu B, Somasekharan SP, Faubert B, Bridon G, Tognon CE, et al. The eEF2 kinase confers resistance to nutrient deprivation by blocking translation elongation. Cell. United States; 2013; 153: 1064–79.

600. Cattie DJ, Richardson CE, Reddy KC, Ness-Cohn EM, Droste R, Thompson MK, Gilbert

W V, Kim DH. Mutations in Nonessential eIF3k and eIF3l Genes Confer Lifespan Extension and Enhanced Resistance to ER Stress in Caenorhabditis elegans. PLoS Genet. 2016; 12: e1006326.

601. Gonskikh Y, Polacek N. Alterations of the translation apparatus during aging and stress response. Mech Ageing Dev. Ireland; 2017; 168: 30–6.

602. Mathis AD, Naylor BC, Carson RH, Evans E, Harwell J, Knecht J, Hexem E, Peelor FF, Miller BF, Hamilton KL, Transtrum MK, Bikman BT, Price JC. Mechanisms of In Vivo Ribosome Maintenance Change in Response to Nutrient Signals. Mol Cell Proteomics. 2017; 16: 243–54.

603. Solis GM, Kardakaris R, Valentine ER, Bar-Peled L, Chen AL, Blewett MM, McCormick MA, Williamson JR, Kennedy B, Cravatt BF, Petrascheck M. Translation attenuation by minocycline enhances longevity and proteostasis in old post-stress-responsive organisms. Elife. 2018; 7.

604. Lutchman V, Dakik P, McAuley M, Cortes B, Ferraye G, Gontmacher L, Graziano D, Moukhariq F-Z, Simard E, Titorenko VI. Six plant extracts delay yeast chronological aging through different signaling pathways. Oncotarget. United States; 2016; 7: 50845–63.